LEABHARLANN CHOLÁISTE NA TRÍONÓIDE, BAILE ÁTHA CLIATH | TRINITY COLLEGE LIBRARY DUBLIN
Ollscoil Átha Cliath | The University of Dublin

Terms and Conditions of Use of Digitised Theses from Trinity College Library Dublin

Copyright statement

All material supplied by Trinity College Library is protected by copyright (under the Copyright and Related Rights Act, 2000 as amended) and other relevant Intellectual Property Rights. By accessing and using a Digitised Thesis from Trinity College Library you acknowledge that all Intellectual Property Rights in any Works supplied are the sole and exclusive property of the copyright and/or other IPR holder. Specific copyright holders may not be explicitly identified. Use of materials from other sources within a thesis should not be construed as a claim over them.

A non-exclusive, non-transferable licence is hereby granted to those using or reproducing, in whole or in part, the material for valid purposes, providing the copyright owners are acknowledged using the normal conventions. Where specific permission to use material is required, this is identified and such permission must be sought from the copyright holder or agency cited.

Liability statement

By using a Digitised Thesis, I accept that Trinity College Dublin bears no legal responsibility for the accuracy, legality or comprehensiveness of materials contained within the thesis, and that Trinity College Dublin accepts no liability for indirect, consequential, or incidental, damages or losses arising from use of the thesis for whatever reason. Information located in a thesis may be subject to specific use constraints, details of which may not be explicitly described. It is the responsibility of potential and actual users to be aware of such constraints and to abide by them. By making use of material from a digitised thesis, you accept these copyright and disclaimer provisions. Where it is brought to the attention of Trinity College Library that there may be a breach of copyright or other restraint, it is the policy to withdraw or take down access to a thesis while the issue is being resolved.

Access Agreement

By using a Digitised Thesis from Trinity College Library you are bound by the following Terms & Conditions. Please read them carefully.

I have read and I understand the following statement: All material supplied via a Digitised Thesis from Trinity College Library is protected by copyright and other intellectual property rights, and duplication or sale of all or part of any of a thesis is not permitted, except that material may be duplicated by you for your research use or for educational purposes in electronic or print form providing the copyright owners are acknowledged using the normal conventions. You must obtain permission for any other use. Electronic or print copies may not be offered, whether for sale or otherwise to anyone. This copy has been supplied on the understanding that it is copyright material and that no quotation from the thesis may be published without proper acknowledgement.

TRINITY COLLEGE
05 AUG 2008
LIBRARY DUBLIN
THOSIS
8504

On the ejection of high velocity massive stars from star clusters

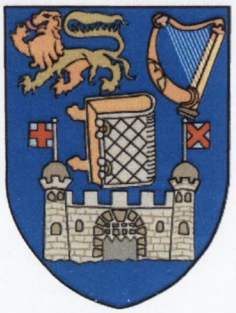
by

Cóilín Ó Maoiléidigh

A Thesis submitted to
The University of Dublin
for the degree of

Doctor of Philosophy

Dublin Institute for Advanced Studies
School of Cosmic Physics
Dunsink Observatory
and
University of Dublin
Trinity College
School of Physics



2008



Declaration

This thesis has not been submitted as an exercise for a degree at any other University. Except where otherwise stated, the work described herein has been carried out by the author alone. This thesis may be borrowed or copied upon request with the permission of the Librarian, University of Dublin, Trinity College. The copyright belongs jointly to the college and Cóilín Ó Maoiléidigh.

Signature of Author .....

Cóilín Ó Maoiléidigh

April, 2008

Summary

OB[1] runaways are massive, early-type, high velocity stars which have been ejected from their parent birthplaces. Some of which have velocities above 200km/s. Two mechanisms are plausible explanations for these objects: A supernova occurring in a binary system can often result in the system becoming unbound and the companion star being released from the system with a velocity comparable to its orbital velocity (SuperNova in a Binary scenario (SNB)); Close gravitational interactions between two or more stars can result in one or more of the stars being flung from the system with a high velocity (Dynamical Ejection scenario (DE)). Both of these mechanisms have been shown to exist in nature, however, which mechanism dominates the production of OB runaways is still unknown.

The goals of this thesis are to investigate the production of runaways via both mechanisms in detail and to compare and contrast the relative number of ejections from various cluster environments with different initial conditions. Thus we seek to determine the fraction of runaways ejected by both mechanisms and compare these results to observations.

In Chapter 2 we investigate the dynamical ejection mechanism using a sophisticated N-body code which simulates gravitational encounters between stars in a realistic cluster environment including many other cluster properties and details relating to stellar evolution. Not only are the initial conditions of star clusters in general unknown but there exist a wide variety of clusters with different properties, such as, mass, size, density etc. Hence we study a range of cluster conditions and how the rate of ejection of massive stars is altered within these varying environments. We consider the effects of: low, intermediate and high stellar densities; initial binary populations; initial binary binding energies; primordial mass segregation; gas expulsion; population size; and stellar mass distributions.

In Chapter 3 we use a set of population synthesis routines in order to study the supernova in a binary ejection mechanism is detail. We discuss the implications of the natal kick velocity given to the exploding core of a neutron star on our runaway population. We show how the number of ejections change as a result of different initial binary separation ranges. From the velocity dispersion of binaries ejected via this the SNB mechanism we give evidence that the applied natal kick velocity distribution is bimodal, with lower kicks being applied to binaries which subsequently become Be/X-ray binaries and higher kicks to binaries which become OB-supergiant X-ray binaries. From a consideration of mass transfer

[1]OB indicates O and B spectral type stars, typically earlier than B5

from the primary star to the companion prior to the supernova explosion we calculate that nearly all O and only ~30% of B star runaways are likely to be observed as Blue Stragglers with respect to their parent clusters. We also suggest that ~15% of runaways ejected via this mechanism may be Thorne-Zytkow objects, which may be observed as either M-type Red Giants or WN8 Wolf Rayets. In addition we show how observational effects can impact on the observed frequency of SNB OB runaways.

Further in Chapter 3 we use an N-body code which has the close binary evolution routines used in the population synthesis study incorporated into it. With this, we examine the supernova in a binary ejection scenario within a cluster environment. We show that as the cluster density decreases, the number of runaways via SNB may increase due to gravitational interactions creating more energetic binaries and pairing the more massive stars in the system with each other. We further show, that as the density increases further, collisions occur between the close binaries which should otherwise become SNB runaways, thus reducing the number that are ejected via this mechanism.

Finally in Chapter 3, from statistics of binary runaways created via both mechanism, we compare their characteristics and consider the observational implications of these results.

The nature of runaway binaries, (i.e. whether or not they harbour a compact object and are thus ejected due to the SNB scenario) is of some importance. Many previous studies have failed to find compact objects to the known runaway stars. However, with the upcoming Gaia mission, and its high level of accuracy, compact companions to OB runaways may be detected astrometrically. In Chapter 4 we determine the probability that Gaia could detect compact companions to a representative sample of known runaways.

DE and SNB single runaways are difficult to distinguish observationally. Hence the reason the dominant mechanism which produces OB runaways remains uncertain. Blaauw (1993) suggests that excess rotation in runaway stars may be an indicator of prior close binary evolution and thus implies that the runaways were ejected via the SNB scenario. Following this, we determine rotation rates for 38 OB runaways and add these values to the database of runaways with known rotation velocities. We confirm Blaauw's conclusion that O-type runaways show excess rotation rates suggesting that the majority of O-type runaways are ejected via the SNB scenario. We also show that the B-type runaways show no excess rotation with respect to the rotation velocity of typical B stars. Hence, we expect that the majority of B-type runaways are dynamically ejected.

Acknowledgements

There are many people I wish to thank for their support during this work and I know that the few words here cannot adequately express my gratitude.

To my supervisors Professor Evert Meurs and Dr Laura Norci, my sincere thanks for your patience and guidance over the years. I would also like to thank all the staff I have had the pleasure of meeting at Dunsink Observatory. I feel privileged to have been part of its prestigious academic history and saddened to be now one of the last to research there. I am very grateful to Dr Mark Wilkinson, for all his assistance with my many questions about the N-body codes and cluster dynamics and for the enjoyable experience of working at the Institute of Astronomy in Cambridge. I also appreciate the time Dr Sverre Aarseth spent sitting with me there, trying to discover the source of the many energy errors I seem to so easily generate while using his N-body codes, and in fact for providing the N-body codes themselves which form such an integral part of this work. My thanks are also to: Dr Jarrod Hurley for providing me with the population synthesis routines; Dr Corinne Rossi for getting me started using IRAF and for inviting me to Rome; the staff at Loiano Observatory for the few weeks I spent observing there, or at least trying to, despite the weather.

Words fail me when trying to express my thanks to friends for their support, encouragement and simple friendship. I could not possibly mention everyone here nor do them justice by doing so, but I will highlight a few and the rest I will hug when I see you. To Daniel Kane, Alan Gray, Shane O Connor and Andrew Kinane, my thanks for your longstanding friendship that does not wane with absence, for all the adventures, hikes and sausages over these many years. To Orla McHenry for all the tea and biscuits, without which I would be lost. To Mary Kilgannon for your close friendship that has been there from day one. To Elizabeth Noble for making me smile. To Alan O Sullivan for putting up with me. To Michael Bridges for being inspirational. To Tomo Hayakawa for your enthusiasm. I owe sincere gratitude to both the Trinity Basketball B team and the Brian Boru Handball Club, for all the fun over the years, the victories, the losses and all the friendships.

Lastly I am indebted to my colleagues and close friends Paul Ward and Susanna Vergani, who have been such a central part of my PhD on a daily basis, in particular Paul for your patience and Susanna for your spirit.

"Go confidently in the direction of your dreams. Live the life you have imagined."

Henry David Thoreau

Dedication

I dedicate this thesis to my parents John and Suzanne and my brothers Dáibhid, Ciarán and Diarmuid. I am continually inspired by each of your strengths and talents. To my parents, you have shown me unwaivering support, love and understanding. You have given me a love for life, a curiosity for all things and a thirst for the myriad of experiences that it holds. You have shown me true dignity and fortitude.

Publications

- Ó Maoiléidigh C., Meurs E. J. A., Wilkinson M.
  "Dynamical ejection of OB runaways"
  in preparation

- Ó Maoiléidigh C., Meurs E. J. A., Wilkinson M., Norci L.
  "An investigation into the competitive ejection of OB runaways in dense clusters as a result of close binary evolution and dynamical stellar encounters."
  in preparation

- Ó Maoiléidigh C., Meurs E. J. A., Norci L.
  "Rotation velocities of OB runaways and its implication on the mechanisms which produce them"
  in preparation

- 2006, Meurs E.J.A., O Maoiléidigh C., Norci L.
  "Detecting neutron star induced wiggles in X-ray binaries with SuperGaia resolution"
  ESA SP-588, p. 375-37

- 2005, Ó Maoiléidigh C., Meurs E. J. A., Norci L.
  "Astrometric detection of Neutron Star Companions to High Mass X-ray Binaries"
  Proceedings of I.A.U.S. 230, Dublin *"Populations of High Energy Sources in Galaxies"*

- 2005, Ó Maoiléidigh C., Meurs E. J. A.
  "The production of runaways due to close gravitational encounters in dense clusters"
  Web proceedings, Conference "A Life with Stars", Amsterdam

- 2005, Ó Maoiléidigh C., Meurs E. J. A., Norci L.
  "On the feasibility of detection of neutron star companions to OB runaways using Gaia astrometry"
  New Astronomy, Vol 10, Issue 7, pg 591

Contents

Contents vii

List of Figures xi

List of Tables xv

1 Introduction 1

1.1 Supernova in Binary Scenario 3

1.2 Dynamical Ejection 8

1.3 Observational Evidence 9

1.4 Motivation for this work 12

2 An Introduction to N-body Simulations 14

2.1 Abstract 14

2.2 Simulation Overview 15

2.3 Cluster Conditions 18

2.3.1 Cluster Population, N 18

2.3.2 Distribution of stars 18

2.3.3 Mass Range and The Initial Mass Function (IMF) 19

2.3.4 Initial Size and Density 20

2.3.5 Galactic Field 25

2.3.6 Binary Stars 25

2.3.7 Separation Distribution and Range 26

2.3.8 Mass Ratio's ($q = \frac{M_2}{M_1}$) and Eccentricities (e) 27

2.3.9 Mass Segregation 27

2.4 N-body simulation characteristics 30
2.4.1 A matter of Faith 30
2.4.2 Scaling 32
2.4.3 Escape 33
2.4.4 Multiple Systems and Interactions in Star Clusters 34

3 N-body Simulations & Results **37**
3.1 Runaways and Initial Density 38
3.1.1 Dynamical Ejection 38
3.1.2 Supernova in Binary 45
3.1.3 General Conclusions for Runaways and Initial Density 47
3.1.4 Tidal Tails and Late Stage Escape 49
3.2 Runaways and the Primordial Binary Population 50
3.2.1 Dynamical Ejections 51
3.2.2 Collisions 54
3.2.3 Supernova in Binary Mechanism 55
3.2.4 General Conclusions: Runaways and Primordial Binary Populations 58
3.2.5 Initial Separation - Binary Energy (N_{run} = 20) 60
3.3 Primordial Mass Segregation (N_{run} = 20) 63
3.4 Gas Expulsion (N_{run}= 20) 68
3.4.1 Results and Discussion 70
3.5 Population Size 72
3.5.1 N = 45 (N_{run} = 60) 72
3.5.2 N = 4500 (N_{run} = 20) 75
3.6 The Plummer Model vs Homogeneous Sphere 76
3.6.1 Introduction 76
3.6.2 Results and Discussion 80
3.7 Discussion/Conclusions 86

4 Supernova in a Binary Ejection from Stellar Clusters **91**
4.1 Abstract 91
4.2 Introduction 92
4.3 Population Synthesis 93

4.3.1 Initial Conditions 94
4.3.2 Roche Lobe Overflow (RLOF) and Blue Stragglers 118
4.3.3 Runaways and Thorne-Zytkow Objects(TZO) 120
4.4 N-body simulations with binary stellar evolution 122
4.4.1 nbody6-2 vs Population Synthesis 122
4.4.2 nbody6 SNB vs nbody6-2 SNB 123
4.4.3 nbody6-2: SNB runaways from different cluster environments 124
4.5 Ejected Binary Characteristics 130
4.5.1 Estimating the DE and SNB populations from the observed bound group 137
4.6 Conclusions 141

5 On the Feasibility of Detection of Neutron Star Companions to OB Runaways using Gaia Astrometry 145
5.1 Abstract 145
5.2 Introduction 146
5.3 Program Stars 147
5.4 Range of Theoretical Separations 148
5.5 Range of Detectable Separations 151
5.6 Discussion 152
5.6.1 Probability of Detection by Gaia 152
5.6.2 Number of OB runaways with compact companions that Gaia may detect 156
5.6.3 A Comparison with High Mass X-ray Binaries 157
5.7 Conclusions 160

6 Rotation Velocities of OB Runaways 162
6.1 Abstract 162
6.2 Introduction 163
6.3 Observations 164
6.4 Method - Echelle Spectroscopy 164
6.5 Analysis & Results 167
6.6 Discussion 175

6.7 Conclusions 181

7 Conclusions **183**

8 Future Work **188**

8.1 Cluster Analysis 188

8.2 Radial Velocity Survey 191

8.3 Individual Analysis 191

8.4 Further Simulations 191

A OB runaways **192**

B The Classification of Stars **202**

C Binary Stellar Evolution - Roche Lobe Overflow **205**

D N-body Codes **208**

D.1 Equations of Motion 209

D.2 Force Polynomials and the Hermite Scheme 210

D.3 Nearest Neighbours, Ahmad-Cohen (AC) Scheme 213

D.4 Regularisation 213

D.5 Stellar Evolution 214

D.6 Input Parameters 215

E Errata - Chapter 5 **217**

F Poisson Error **221**

Bibliography **222**

List of Figures

1-1 AE Aurigae and μ Columbae 2

1-2 Illustration of binary evolution 4

1-3 Illustration of O star Velocities 11

2-1 Flow chart for Nbody simulations. A list of input parameters, options & counters is shown in Appendix D.6. 16

2-2 Distribution of the initial semi-major axis of binaries, combined from a number of simulations. 26

2-3 Distribution of the mass ratio of initial binaries, from the output of a number of simulations. 28

2-4 Distribution of the eccentricities of initial binaries from the output of a number of simulations. 28

3-1 Dynamical Ejections: Cumulative Distribution of Ejectees from the Low, High and Medium density clusters: BF05 44

3-2 Time series of cluster evolution 50

3-3 Dynamical Ejections: Comparison of single ejectees from a primordial mass segregated with an unsegregated, medium density cluster. 66

3-4 Dynamical Ejections: Comparison of binary star ejectees from a primordial mass segregated with an unsegregated, medium density cluster. 67

3-5 Density and Potential profiles of the Homogenous and Plummer model . . . 78

3-6 Variation in density and potential for the Homogeneous cluster and the Plummer model cluster 79

3-7 Core radius evolution and half mass radius evolution of a Homogenous and Plummer model cluster 80

3-8 Dynamical Ejections: Medium Density Cluster: Plummer and Homogenous models 81
3-9 Density profiles of medium density clusters with Plummer and Homogenous initial distributions 82
3-10 Density profiles of medium density clusters with Plummer and Homogenous initial distributions. 82
3-11 Density profiles of medium density clusters with Plummer and Homogenous initial distributions. 85
3-12 Summary of Dynamical Ejection percentages. 88

4-1 Sketch showing a binary system and supernova kick geometry 95
4-2 Single star ejections via the supernova in a binary mechanism as a function of ejection velocity, for different Maxwellian kick velocity dispersions. 100
4-3 Binary star ejections via the supernova in a binary mechanism as a function of ejection velocity, for different Maxwellian kick velocity dispersions. 101
4-4 Mass-Velocity plot of single and binary stars ejected via the SNB mechanism 103
4-5 Ejection percentages of single B type stars as a function of initial binary separation range 104
4-6 Ejection percentages of binary B type stars as a function of initial separation range 105
4-7 Final binary velocities with respect to final binary separation Log(A). . . . 106
4-8 Ejection of stars with respect to time from the SNB scenario 108
4-9 Ejection of OB stars with respect to time from the SNB scenario 109
4-10 Mass Velocity plot of runaway SNB single stars 112
4-11 Observed Mass Velocity plot of OB runaways 113
4-12 Root mean square velocities escapees from the SNB scenario as a function of the applied kick velocity dispersion. 116
4-13 Percentage of massive TZO (with respect to the single B star runaway population) as a function of the applied kick velocity. 121
4-14 Velocity Distribution of escaped OB stars. DE and SNB scenarios. 129
4-15 Distribution of ejected binary parameters, semi-major axis, eccentricity, mass ratio 131
4-16 Characteristics of DE and SNB ejected runaway binaries 132

4-17 Eccentricity, semi-major axis and mass ratio versus total binary mass respectively, for DE and SNB ejected binaries 135
4-18 Percentage of dynamically ejected massive B stars with respect to the total ejected via both mechanisms. 144

5-1 Percentage probability of Gaia detecting a neutron star companion for each of our sample stars 154
5-2 Probability of detecting a compact companion to an OB runaway 154
5-3 Percentage of binary systems that survive the supernova explosion of the primary as a function of natal kick velocity 155
5-4 Probability that Gaia could detect an unseen companion to our illustrative sample stars 156
5-5 Percentage probability of Gaia detecting a neutron star companion to each of the HMXRB sample stars 160

6-1 Example of an Echelle spectrum 166
6-2 Flow chart of the reduction and analysis proceedure 169
6-3 Spectral line fitting to two stars 170
6-4 Comparison of the measured vsin(i) values here with published work. 172
6-5 Comparison of measured vsin(i) values measured with the FWHM method and with Spectral Fitting 173
6-6 Cumulative distribution function for OB stars and OB runaways. 177
6-7 Rotation velocities of single stars 179

B-1 Hertzprung-Russell Diagram 204

C-1 Roche Lobe Diagram 206

D-1 Force polynomial fitting 210

E-1 Percentage probability of Gaia detecting a neutron star companion for each of our sample stars 218
E-2 Probability that Gaia could detect an unseen companion to our illustrative sample stars 219

E-3 Percentage probability of Gaia detecting a neutron star companion to each of the HMXRB sample stars 220

List of Tables

2.1 Summary of N-body Simulations: nbody6 23

3.1 Dynamical Ejections (Single Stars): Medium Density Cluster : BF05 41
3.2 Dynamical Ejections (Binary fraction) : Medium Density Cluster : BF05 . 41
3.3 Direct Collision: Medium Density Cluster : BF05 : Statistics I 42
3.4 Direct Collisions: Medium Density Cluster : BF05 : Statistics II 43
3.5 Dynamical Ejections (Single Stars): High Density Cluster: BF05 43
3.6 Dynamical Ejections (Binary Fraction): High Density Cluster : BF05 . . . 43
3.7 Dynamical Ejections (Single Stars): Low Density: BF0 : BF1 52
3.8 Dynamical Ejections : Medium Density : BF0 : BF1 52
3.9 Dynamical Ejections (Single Stars): High Density : BF0 : BF1 54
3.10 Number of collisions per simulation for the three cluster densities 54
3.11 Average number supernova which occur in binary systems for each cluster initial density and binary population 56
3.12 Dynamical Ejections (Single Stars): Medium and High Density Cluster: BF05 61
3.13 Energetic Binaries: Dynamical Ejections (Binary Stars): Medium and High Density Cluster: BF05 62
3.14 Dynamical Ejections (Binary Stars): Medium Cluster: BF05 : Mass Segregation 65
3.15 Dynamical Ejections: High Density Cluster: Gas Expulsion 71
3.16 Dynamical Ejections: Medium Stellar Density Cluster (All OB stars) : N = 45 73
3.17 Dynamical Ejections: Medium Density Cluster: N = 4500 75

4.1 Summary of Population Synthesis Simulations 96
4.2 Summary of the nbody6-2 simulations. 97

4.3 Root mean square velocities of low mass single and binary SNB ejected stars 115
4.4 Root mean square velocities of OB single and binary SNB ejected stars . . 115
4.5 SNB Ejections: Low Density Cluster BF05 : BF1 124
4.6 SNB Ejections: Medium Density Cluster BF05 : BF1 125
4.7 SNB Ejections: High Density Cluster BF05 : BF1 126
4.8 Observed OB runaway binary characteristics 137

5.1 List of observational parameters for our OB runaway sample 148
5.2 Mass and distance estimates for our sample 153
5.3 HMXRBs with high velocities and known orbital periods. 159

6.1 Details of the spectrograph used at Loiano 165
6.2 Observation list. * Indicates binary/multiple systems 165
6.3 Table of estimated vsin(i) values for our runaway sample. 174
6.4 Average rotational velocities (km/s) by spectral type range and class 175
6.5 Statistics of known OB runaways 181

8.1 OB associations 190

A.1 Detailed table of known OB runaways 193

"The best way to escape from a problem is to solve it"

Alan Saporta

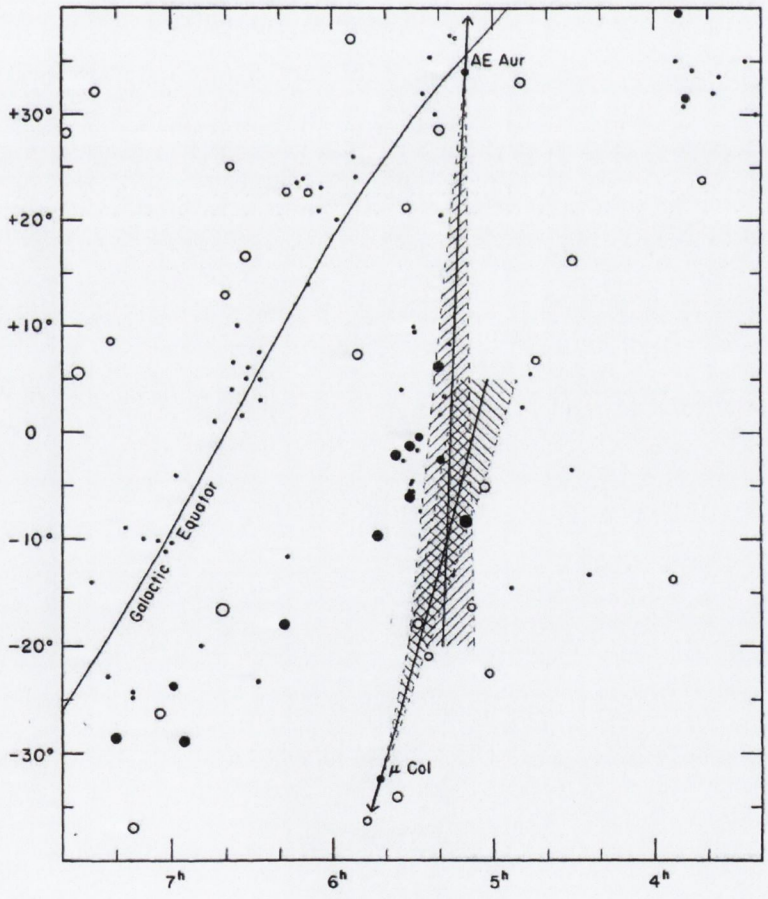
1

Introduction

In 1954 Adriaan Blaauw and William Morgan identified the stars AE Aurigae and μ Columbae as high velocity ejectees from the Orion Nebula moving in opposite directions to each other see Figure 1-1. Typically stars in clusters move with velocities of the order of a few km/s relative to each other, however, AE Aurigae and μ Columbae stars were found to be moving with velocities of the order of a hundred km/s.

This unique observation sparked the beginning of a debate which would last decades, on what mechanism could produce such high velocity massive objects. A number of years later Blaauw (1961), from a compilation of the characteristics of massive stars, namely O and B type which included their velocity distributions, showed that these high velocity objects formed a distinct excess and could be recognised as a separate group of unique objects. The term OB runaway at the time was adopted to identify those high velocity massive stars which had an accurate direction of space motion calculated and for which the distance they had travelled was still small enough to determine their places of origin. The term runaway is now generic and classifies all high velocity stars which have been ejected from their birthplaces, while OB makes the distinction for massive stars. Due to histor-

Figure 1-1: *The Figure below is taken from Blaauw and Morgan's paper and shows their calculated trajectories for the two stars AE Aurigae and μ Columbae as they escape from the Orion Nebula (Blaauw & Morgan, 1954). Original Caption: Fig. 1.- The positions of AE Aurigae and μ Columbae with respect to the Orion association. Arrows show the directions of their proper motions when corrected for the standard solar motion. The paths of the two stars with respect to the stand or rest thus defined are shown by the great circles traced backward from the proper motions. The shaded areas indicate the uncertainty in their directions. The sizes of the arrows correspond to the displacements 4×10^5 years. Stars brighter than apparent magnitude 3.5 are represented by large dots (OB supergiants) and open circles. Small dots represent the fainter OB supergiants.*



ical/observational reasons this includes the spectral type range from O to B5[1]. Blaauw, building on work by Zwicky in 1957, further postulated that the origins of these massive high velocity stars could be due to a supernova occurring in a close binary system. The sudden loss of a large amount of mass from the primary (the initially more massive and exploding star) would cause the orbital velocity (up to a few hundred km/s) of the companion star to be translated into a space velocity as the binary system becomes unbound, thereby ejecting it from the cluster as a whole at a high velocity. This theory satisfied the criteria that (i) the runaways were massive objects since it was expected that massive stars in binaries had massive companions and (ii) that the runaways were predominantly single stars unlike a large proportion of OB stars in OB associations which show high multiplicity. In 1967, Poveda, Ruiz and Allen argued in favour of an alternative scenario. They were unconvinced that the original Blaauw and Morgan runaways, AE Aurigae and μ Columbae and a later discovered ι Orionis, could be well explained by his supernova in a binary scenario. They proposed that gravitational interactions in a system with a configuration such as the Trapezium in the Orion Nebula would be sufficient to produce single, high velocity, massive ejectees. Over the intervening years these two scenarios have suffered set-backs and improvements as their flaws and merits were debated by the community. In the next sections we will illustrate how the two mechanisms have been developed, describe what techniques have been employed, discuss the current thinking, and present the motivation behind this thesis research and a justification for the approaches employed.

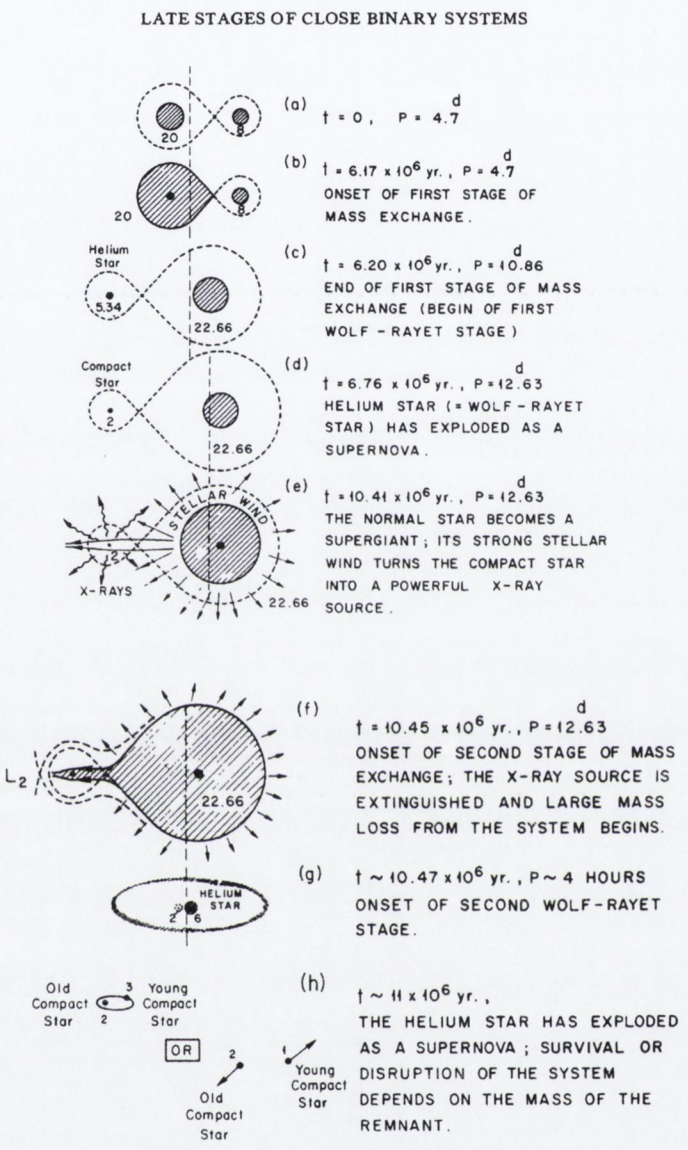
1.1 Supernova in Binary Scenario

Soon after Blaauw was voicing his theory of a supernova in a binary system substantial progress was made on the understanding of close binary stellar evolution. These theories were progressed by many people including van den Heuvel (1976) who produced a series of diagrams elegantly illustrating the process of mass transfer and the possible evolution of a close binary system and creation of an X-ray Binary (XRB), Figure 1-2.

The realisation from the point of view of the supernova in a binary scenario was that in such close systems a large fraction of the mass would be transferred, through Roche Lobe

[1]From here, early B type will signify the spectral range B0 to B5 while late B type will indicate the range from B6 to B9 (see Appendix B for a brief explanation of spectral types and classes)

Figure 1-2: *Illustration of binary evolution from van den Heuvel (1976) pg 41.*



Figs. 2a-b. Subsequent stages in the evolution of the massive close binary of Figure 1. It is assumed that the supernova explosion of the primary leaves a $2\,M_{\odot}$ compact star (neutron star or black hole).

Overflow (RLOF[2], see Appendix C for a detailed explanation), to the companion making it the most massive of the pair. From simple energy relations it can be shown that for a system in a circular orbit more than half the mass of the system need be lost during the

[2]RLOF is the process whereby a star in a binary system may transfer matter to its companion

supernova of the primary in order for the system to become unbound. In general for OB runaways to reach the observed highest velocities the systems would need to be in close configurations making mass transfer inevitable, hence the majority of these systems should remain bound. Knowing that OB runaways were predominantly single stars and that the few that were binaries were double lined spectroscopic binaries[3] (a supernova in a triple system being a relatively rare event) caused a number of concerns as to the validity of this scenario.

If most systems remain bound after the supernova of the primary, then being able to produce massive runaways in sufficient numbers to be comparable to observation presents a difficulty. Amuél et al. (1975) suggested that the number of X-ray binaries was disproportionate to the number of supernova events which should occur in binary systems in the Galaxy. An asymmetric supernova explosion was proposed (Shklovskii, 1970) in which sufficient momentum was transferred from the ejected envelope to the contracting core in order to give it a sizeable velocity adequate to disrupt the system. The possibility of an asymmetric supernova was given more credence as the estimated velocity distributions for pulsars, from the explosions of single massive stars, increased to mean velocities of 200-500km/s (Lyne & Lorimer, 1994; Lorimer et al., 1997; Hansen & Phinney, 1997; Cordes & Chernoff, 1998; Arzoumanian et al., 2002). While it is possible that pulsars with velocities of a few hundred km/s may be produced by a supernova occurring in a close binary system, the highest velocity pulsars, e.g. those with velocities greater than 1000km/s (Harrison & Lyne, 1993), may not be ejected via this mechanism, even from the tightest binaries. Hence a natal 'kick' to the core during the ejection of the envelope of the exploding star is increasingly likely. Pfahl & Rappaport (2002) suggest that the velocity distribution of observed X-ray binaries is indicative of a bimodal distribution of supernova kicks. They contend that the magnitude of the kick may be related to the evolutionary history of the binary system. Specifically, for scenarios which have a rapidly rotating core prior to the supernova explosion a small kick ($\leq$ 50km/s) being given to the formed compact object may result, while a slowly rotating pre-supernova compact object progenitor produce a much larger kick ($\sim$ 300km/s). Kicks have been thought possible from a number of mechanisms, neutrino-magnetic, electromagnetic or hydrodynamically driven, among some other possi-

[3]Double lined spectroscopic binaries are binaries where the spectra from both stars are observed. This implies that the binary consists of two 'normal' stars as opposed to a compact object such as a Neutron Star or Black Hole

bilities (see Lai (2003) for a review) but their true nature is still unknown. A statistical analysis by Arzoumanian et al. (2002) of the pulsar distribution also suggests a bimodal velocity dispersion. Brandt & Podsiadlowski (1995) suggest that kicks of a few hundred km/s will unbind the binary in more than 70% of cases. Further, in order to explain the orbital characteristics of some neutron star binaries and X-ray binaries a natal kick to the compact object is expected in these bound objects. For example, natal kicks are required to explain the spin-orbit misalignment in PSR J0045-7319 (Kaspi et al., 1996; Lai et al., 1995), the high eccentricities of Be/X-ray binaries, the low incidence of double neutron stars in the galaxy (for a review see van den Heuvel & van Paradijs (1997)) and the differences between the runaway velocities of OB-super-giant X-ray binaries and the Be/X-ray binaries (van den Heuvel et al., 2000). If the kick is due to an anisotropy in the ejection of the shell, then this too may explain the aspherical nature of some supernova remnants. We discuss natal kick velocities further, in Chapter 4 and their effect on the ejected and bound portions of runaway stars.

Additional strong evidence has built over the years in favour of the SNB scenario, with it fitting well into a complete binary evolution theory. The fact that high mass X-ray binaries exist with the compact companion thought to be produced by a supernova explosion and that these systems were shown to have the systematically elevated velocities up to those denoted for runaways[4] (van Oijen, 1989; Chevalier & Ilovaisky, 1998; Nelemans et al., 1999) is undeniable evidence for the viability of this scenario to produce high velocity objects. Additionally, bow shocks around systems such as Vela X-1 as the system moves supersonically through the interstellar medium indicates that such systems have elevated velocities (Kaper et al., 1997), lending further support to the theory. Blaauw (1993) shows that there is a tendency for O type runaway stars to have elevated rotational velocities and Helium abundances indicating that they were most likely involved in a stage of mass transfer prior to their ejection (see Chapter 6 for more). However, the high proportion of runaways displaying these properties is suggestive of a stage of mass transfer to the secondary prior to the explosion of the primary. Mass transfer from the primary to the secondary will also rejuvenate the companion possibly making it appear bluer than other stars in the cluster. Hoogerwerf et al. (2001) give evidence for a small number of O type runaways being blue stragglers with respect to the clusters he identifies as their parents, suggesting that they

[4]Observationally OB stars with a velocity above 30km/s and/or high Galactic latitudes (inferring a large velocity ejected them from the plane) are considered to be runaway stars.

had been rejuvenated prior to their ejection. He suggests that ~2/3rds of runaways may be due to the SNB scenario.

On the other hand, many searches over several years by a number of authors have all failed to detect compact companions to the well known OB runaways. Previous searches have tried to detect radial velocity variations from unseen companions (Stone, 1991; Aslanov et al., 1984; Gies & Bolton, 1986), radio pulsar companions (Sayer et al., 1996; Philp et al., 1995) or accretion powered X-ray emission (Kumar et al., 1983; Meurs et al., 2001, 2005). From the point of view of the supernova in a binary scenario and detailed binary evolution characteristics a possible scheme would be that the high mass X-ray binaries and Be/X-ray binaries are the bound group of runaways from this scenario and that the single OB stars are the disrupted group.

Population synthesis models are pursued in order, Chapter 4, to test the predictions made with improved understanding of the evolution of close binary systems, accounting for a kick to the core of the exploding star. These results were then compared with observational characteristics of runaway stars. Population synthesis by previous authors suggest that only a relatively small fraction of O stars (at most 30%) have come about via the supernova in a binary scenario (Portegies Zwart, 2000) but possibly all runaway B stars may be created via this mechanism (assuming the mass ratio in binaries is highly peaked towards unity, stars are rejuvenated to zero age via mass transfer and that the binary fraction among early stars is close to 100%). Furthermore, after the early O and/or B phases in the life of a massive star, many at solar metallicity go on to become Wolf Rayet stars (Chiosi & Maeder, 1986). Roche Lobe Overflow (RLOF) may also cause Wolf Rayets either by increasing the mass of the secondary such that it has a high stellar wind loss, sufficient to eventually strip its Hydrogen envelope or the primary has its own envelope stripped due to it transferring mass to its companion. This leads to the suggestion that the fraction of Wolf Rayet runaways is similar to that of OB stars (Mason et al., 1998; Moffat et al., 1998; Foelmi & Moffat, 2002) at ~10% for WRs to 20% for O stars. Dray et al. (2005) suggest that about 10% of massive stars are ejected dynamically early on, while about 20% may be ejected later on by the supernova in a binary scenario. Thus, the evidence in favour of the SNB scenario is substantial both observationally and theoretically, illustrating that it is a viable scenario which explains the presence of at least some runaways. We will investigate how effective this scenario actually is when coupled with the competing process of dynamical ejections.

1.2 Dynamical Ejection

Escape of stars from star clusters due to gravitational interactions has been well studied in theory, observation and simulation. The theory behind escape is based on quantifying the sum of two body encounters in a cluster which allows a star to gain sufficient energy to escape the system. Henon's 1969 equation shows some qualitative agreement with numerical results so long as the underlying assumptions are met, i.e. that the distribution of velocities is isotropic. However, such a solution cannot account for many real cluster situations such as mass segregation or internal dynamical evolution take effect (as the core contracts the escape rate increases and as the velocity distribution becomes more anisotropic the escape rate becomes enhanced (Giersz & Heggie, 1994)) etc. Monte Carlo and various approximate methods such as Fokker-Planck can do well in simulating large clusters but at low populations where individual interactions become more important such methods have difficulty. While escape may be fuelled by many, relatively weak, interactions sending stars into long orbits before they eventually escape, close encounters (between single stars, a single star and a binary and between two binaries) by contrast, produce the high velocity stars such as runaways. Binary-single interactions were studied in detail by many authors (Hills, 1975; Hills & Fullerton, 1980; Fullerton & Hills, 1982) and are an effective way of ejecting stars with high velocity. Mikkola (1983, 1984) in turn investigated the interactions of binary-binary interactions and determined that the most common outcome of a binary-binary interaction is the creation of two single ejectees and a binary, making it an ideal mechanism to produce high velocity stars. Binary stars, particularly energetic binaries, are known to be the engines of star clusters, halting core collapse and driving cluster expansion, pumping energy into the cluster and ejecting stars (Giannone & Molteni, 1985).

Surprisingly the papers which concentrate specifically on the OB runaway problem using N-body techniques are relatively few (Poveda et al., 1967; Leonard & Duncan, 1988, 1990; Kiseleva et al., 1998; Gualandris et al., 2004; Pflamm-Altenburg & Kroupa, 2006). Poveda and Kiseleva concentrate on small N systems, less than 10 stars and Leonard & Duncan look at more modest populations of N = 45 and up to N = 300. Gualandris at al. and Pflamm-Altenburg & Kroupa each investigate ejections from the Orion Nebula Cluster (ONC) in particular. The justification behind small N systems is that these will disrupt readily producing a cascade of escapees some of which will have high velocities. Such systems are thought to form as independent small groupings in the centres of clusters

which have a contracted denser core and may be treated as an isolated system from the rest of the cluster.

The main difficulties that the dynamical ejection scenario has encountered are that low mass stars are preferentially ejected and that high densities are required in order to produce substantial fractions of high velocity stars. These difficulties can be overcome if one considers current star formation theories. It is possible that extremely dense proto-stellar clusters of 10^6 stars.pc^{-3} exist for a brief time (Bonnell et al., 1998) allowing for a large number of escaping systems. This dense environment results in a large number of multiple systems (accounting for the high multiplicity of massive stars) and interactions leading to mergers between such systems. Scattering experiments by Leonard (1995) show that an appreciable fraction of escaping massive stars may be merger products due to the fact that a binary-binary interaction has a significant probability for stars to collide. This ties well into some aspects of massive star formation theory in that such mergers may be the method by which massive stars form in the first place (Bally & Zinnecker, 2005), BZ05. Alternatively, massive star formation would occur via elevated accretion rates at the centre of dense cluster. One of the side products of such a scenario is that such merged stars may be ejected from the cluster with elevated rotational velocities. BZ05 further suggest that a rare merger between two very massive stars could be the precursor to a rapid supernova and Gamma Ray Burst event. We will investigate under what specific conditions the observed fraction of runaways may be created by dynamical interactions and if these conditions are compatible with observed cluster environments.

1.3 Observational Evidence

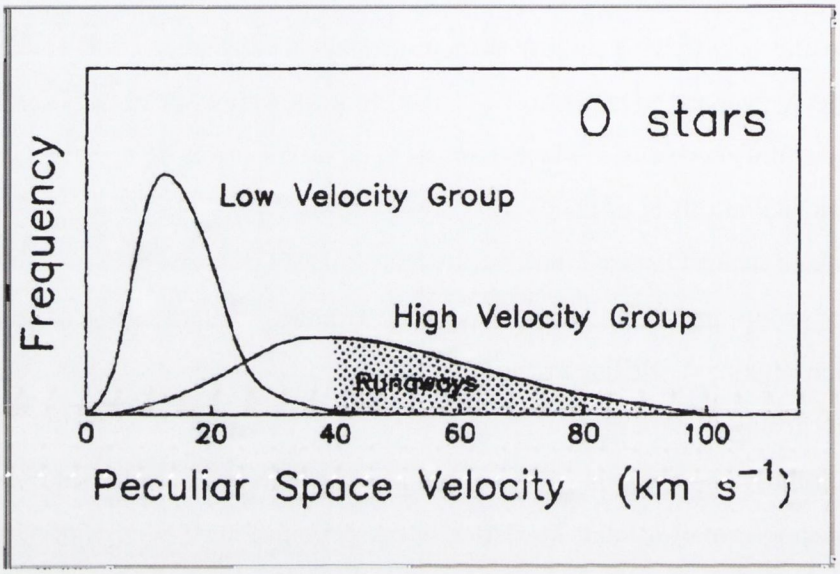
Some of the observational evidence for runaways has been mentioned in the previous sections with relation to the two mechanisms. Here we give a brief summary of observed characteristics of runaways.

- Frequency:

  The frequency of runaway stars has been determined by various authors. A velocity cutoff is often used in order to identify a relatively pure sample of runaways. Gies & Bolton (1986) estimate that about 2% early B-type stars are runaway and between 10-25% of O-type stars are runaways, while Goodwin (1997) suggests that 10-30% of

O stars and 5-10% B stars are runaways. Hoogerwerf et al. (2001) identify 56 OB runaways in the Hipparcos Input Catalogue from a sample of 1118 stars with radial velocity estimates, this gives a B star fraction of ~4.0%. Stone (1991) determines that the true space frequencies for runaways is 46% for O stars, 4% for B stars. Stone assumes that that runaway stars are in fact a subgroup of stars which have their own specific velocity dispersion (i.e. a set of stars whose speeds are specifically influenced by some mechanism which results in a distribution of speeds. In other words no velocity cutoff is applied). Figure 1-3 from Stone (1991) shows the distribution of velocities for O stars identified by Stone. He shows two groups, a high and low velocity group, and highlights the classical runaways (in this case with a velocity greater than 40km/s). He suggests that the known runaways are a subset of this high velocity group. The low velocity group has most stars with velocities less than 25km/s. Similarly the high velocity group has most stars with velocities greater than 25km/s. Such a formalisation is statistically correct since low velocity ejectees may occur from both mechanisms which results in these stars also escaping the cluster. However, it is difficult to disentangle such a grouping from the rest of the stellar population. Hence a velocity cutoff is often adopted in order to isolate a relatively pure sample of runaways. Using the list of frequencies given by Stone and accepting a velocity cutoff of 30km/s gives a frequency of 27% for O stars and 2% for B stars. de Wit et al. (2004, 2005) estimate that an additional 20% of O stars are not associated with any stellar cluster but either have space velocities too small to be considered runaways or have proper motions too small to allow their velocities to be reliably determined. This implies that as many as half of all O stars may have been expelled from their parent clusters. Mason et al. (1998) estimate that ~20% of O stars are field stars and ~8% of O stars are runaways. Moffat et al. (1998) consider both the Wolf Rayet (WR) and O star frequencies and conclude that they may in fact be similar. Specifically the average runaway frequency they calculate is 14% for the O stars. Naturally the difficulty with estimating the specific runaway frequency is incomplete data or biases in searches along with the relatively small numbers involved (in particular for the O stars). From the above we adopt an expected runaway frequency of 2-4% for the runaway B stars and 10-20% for the runaway O stars for comparison with our simulations.

Figure 1-3: *From Stone (1991) the figure illustrates the two distinct velocity groupings which exist for O stars. Stone identifies a high velocity and low velocity group and shows that the classic runaways are simply a subset of the high velocity grouping.*



- Binary Frequency:

  The binary frequency among runaways is a key characteristic relating to the expected mechanism for their production. Most OB runaways are found as single isolated stars in contrast to the cluster and associations where such massive stars have high multiplicity. Gies & Bolton (1986) calculate that ~10% of runaways are binary. Mason et al. (1998) estimate that the observed binary fraction of runaways is ~26%. They estimate that ~5% of runaways are double lined spectroscopic binaries suggesting the dynamical ejection scenario ejected them. The nature of the companion to the remainder of the known runaway binaries is unknown (i.e. 'normal', white dwarf, or compact object (Neutron Star or Black Hole)). Section 4.5 (*Ejected Binary Characteristics*) explores the observed and simulated characteristics of ejected binaries. Recall that some XRBs have characteristically high velocities.

- Rotation Velocity:

  Blaauw (1993) suggests that O star runaways have elevated rotation rates. We develop this observation further in Chapter 6 and consider here the B star population in more detail. Berger & Gies (2001) also find that ~7% of Be stars have elevated space velocities where Be stars are thought to be rapidly rotating B stars with a

circumstellar disk.

- Specific Observations:

  Allen et al. (2006) consider that 4 runaways from 44 observed Trapezia is a likely dynamical occurrence and give considerable weight to the dynamical ejection scenario. Gualandris et al. (2004) show that a four body encounter produced AE Aurigae, μ Columbae and the surviving binary ι Ori (two singles and a binary). Pflamm-Altenburg & Kroupa (2006) determine that the observed number of OB stars in the Orion Nebula Cluster is lower than expected from IMF considerations and infer that since only a small fraction is observed then a large number may have been ejected already by dynamical encounters. Hoogerwerf et al. (2001) traced the orbits of a number of runaways back in time in order to determine their parent clusters and to infer the mechanism that ejected them. They estimate that 2/3 of runaways are ejected via the SNB scenario and 1/3 may be dynamically ejected.

1.4 Motivation for this work

Both theories for the ejection of massive stars have been well evolved over the years resulting in them being established and recognised mechanisms for producing OB runaways. However, determining which of them is the primary mechanism for producing massive high velocity stars is still uncertain. With the current level of computational power and development of N-body codes it is possible to simulate clusters which incorporate both mechanisms in order to investigate the interplay between them. Determining the relative rates at which ejection mechanisms produce runaway stars not only gives insight into the nature of OB runaways but also has significance for the initial conditions for star clusters and for their subsequent evolution.

We divide our investigation into several parts, studying the dynamical interactions of stars, the close binary evolution with supernova in a binary scenario and the observational characteristics of runaway stars.

In Chapter 3 we investigate the dynamical ejection scenario using a variety of parameters in order to see how these parameters affect the production of runaways and to determine which set of parameters may produce the observed runaway characteristics and fraction. This builds on work by previous authors by including stellar evolution, a high binary frac-

tion, physical stellar collisions, a tidal field and by studying the effects of mass segregation, gas expulsion and initial mass distribution on the runaway population.

In Chapter 4 we study the supernova in a binary scenario in the setting of a stellar cluster along with a purely population synthesis analysis. Previous work which concentrated on population synthesis does not account for gravitational interactions between stars, which may alter the initial binary parameter distribution. Binaries may become disrupted or more energetic due to an encounter and initial binary distributions of eccentricities and mass ratio's will be changed and therefore affect the ejection rates of OB runaways via the supernova in a binary scenario.

Chapter 5 considers whether the proposed Gaia satellite will have sufficient resolving power to detect compact companions to OB runaways (previously undetected by many authors with a variety of techniques).

Finally, in Chapter 6 we analyse the observational evidence for elevated rotation velocities of runaways with the aid of new spectroscopic data. We determine rotation velocities for a number of runaways and add these to the database of known rotation velocities for runaways. From this, in conjunction with results from the N-body simulations, we discuss the implications for the ejection scenarios.

2

An Introduction to N-body Simulations

2.1 Abstract

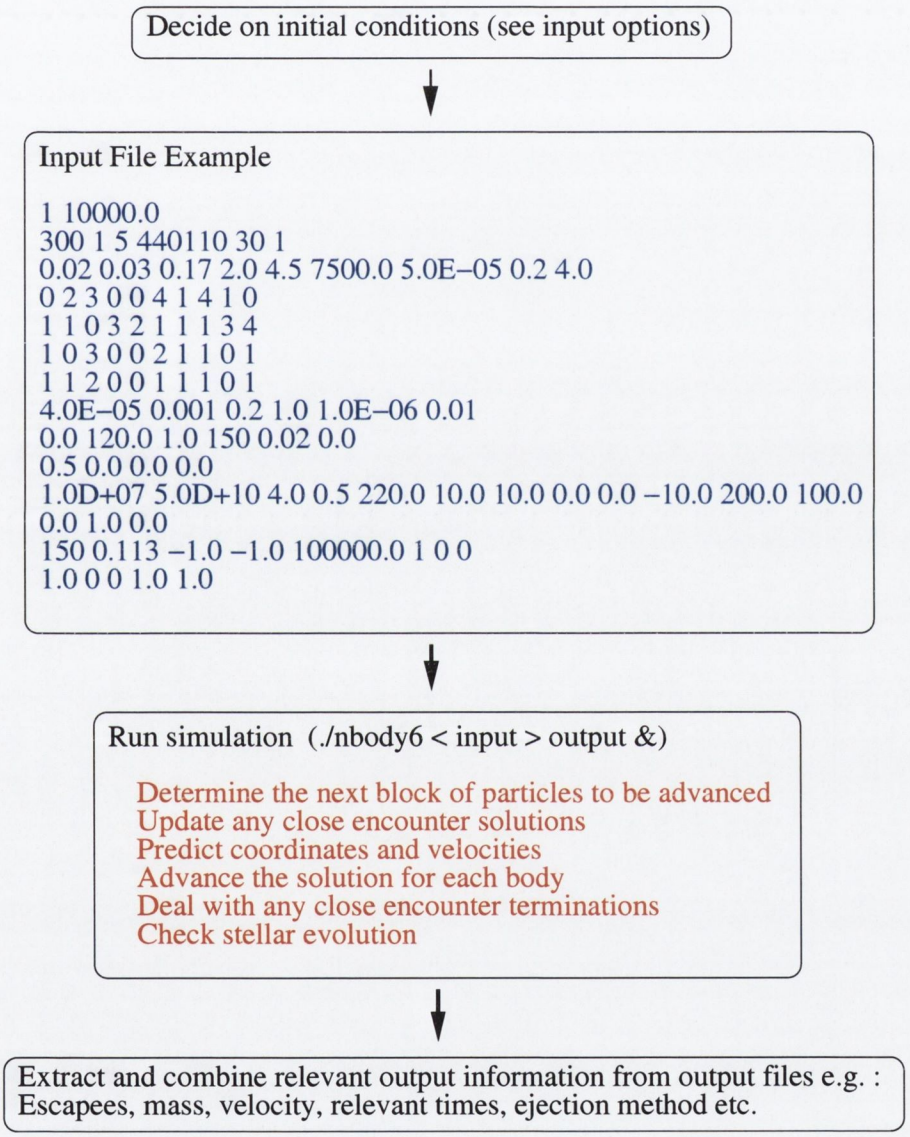
Direct N-body simulations, where the star-star forces are explicitly calculated are an effective means for modelling realistic star clusters and for our purposes, the ejection of high velocity massive stars from such clusters. In the following chapter we will describe simulations of a large number of clusters with different initial parameters in order to consider the effects that such parameters have on the high velocity ejection of massive objects. We consider the concentration of the system in order to determine the initial cluster density which will produce the observed fraction of high velocity massive stars. We show that the initial density must be high, of the order of the Orion Nebula Cluster, in order for the majority of massive runaways to be dynamically ejected. We investigate the binary fraction and initial energy distribution showing that the choice of these can significantly alter the number of dynamically ejected high velocity stars. We estimate the degree to which primordial mass segregation and the expulsion of gas from the system affects the ejection of dynamical runaways. We show that mass segregation can substantially add to the massive

star ejection rate but that a low star formation efficiency where a large fraction of gas is expelled from the system becomes a critical factor in ejection of massive dynamically ejected runaways. We compare models of N = 45, 450 and 4500 stars with a 50% binary fraction and show that small to moderately sized clusters are more effective at producing runaways for a given initial density. Further, we estimate the effect that distribution functions have on the ejection of high velocity stars. We show that a collapsing homogeneous spherical distribution produces more high velocity ejections than a more dynamically stable Plummer model distribution.

2.2 Simulation Overview

Figure 2-1 is simple overview of how a set of N-body simulations proceeds. Considerable time is given to choosing the set of initial conditions appropriate for initialising the simulation one wishes to run. A definition of input parameters, options & counters is included to illustrate the large number of possible options that are available, see Appendix D. It is also important to consider what output is required and in the case of the simulations we ran some of the routines needed to be adjusted and reformatted in order to produce the necessary output for our analysis. Once these choices are made the input file is read by the N-body code and the simulation begins. Depending on the initial conditions and the computational power of the cpu used the simulations may take of the order of minutes to hours to run. Furthermore, simulations may halt if the relative energy difference between time steps exceeds the adopted limit. The code allows one to check the reason for the energy difference and make a correction or simply restart it using a stricter accuracy level, which slows the integration, but may handle the integration which caused the previous excess more effectively. In this way all simulations which run to completion have remained within adopted tolerances and are thus suitable for analysis. The simulation proceeds by updating the position and velocities of each of the stars over a given timestep. Close encounter solutions are treated and any necessary energy checks are made to ensure the simulation runs smoothly. The evolutionary phase of the star is then updated and the next timestep is selected. For more details relating to how the simulation works see Appendix D. A large number of files are created for any given simulation from which the relevant information is extracted, combined with all other runs of similar type for statistical purposes and analysed.

Figure 2-1: *Flow chart for Nbody simulations. A list of input parameters, options & counters is shown in Appendix D.6.*



Definition of input parameters, options & counters.

The input file listed in the flow chart is only one example of the myriad of possible configurations one can chose for an N-body system. The input parameters listed in Appendix D.6 are in the same order as they are required to appear in the input file. For example the first three lines are:

KSTART TCOMP

N NFIX NCRIT NRAND NNBMAX NRUN

ETAI ETAR RSO DTADJ DELTAT TCRIT QE RBAR ZMBAR

KSTART = 1; TCOMP 10000.0 (in units of minutes.)

N = 300 (single stars); NFIX = 1; NCRIT = 5 (Simulation will stop if 5 or few stars are all that remain bound); NRAND = 440110 (arbitrary seed) ; NNBMAX = 30 (Neighbour choice $\sqrt{N} + 10$); NRUN = 1

ETAI = 0.02; ETAR = 0.03 (ETAI and ETAR were chosen after discussion with Sverre Aarseth on appropriate values); RSO = 0.17pc (Initially large since the code will make a more suitable choice); DTADJ = 2.0 (Time interval for a call to the adjust routine for parameter adjustment (N-body units)) ; DELTAT = 4.5 (Time interval for output (N-body units)) ; TCRIT = 7500.0 (Time for simulation to end (N-body units)); QE = 5.0E-05 (Energy tolerance); RBAR = 0.2 (Cluster radius in units of pc); ZMBAR = 4.0 (Average stellar mass in solar mass units. Ignored due to the a later option which chooses a specific mass distribution function)

The fourth line begins a list of 40 options (10 numbers across, 4 lines down) for alternative choices for parameters. Not only may options be switched on or off such as stellar evolution or the galactic tidal field, but there are sometimes several different choices, for example how the stars are to be distributed in space which will depend on the specific problem under investigation. There are also a number of choices relating to the different output options. The point to consider is that it is crucial to take time considering the initial configuration of the system you wish to simulate and all the related parameters. There are clearly many possible choices which makes Dr. Aarseth's code so versatile but also requires a certain degree of familiarity with the code in order to ensure the correct parameters are used for the given simulation under consideration.

2.3 Cluster Conditions

The goal is to focus on combining the mechanism for producing runaways via the dynamical ejection (DE) and supernova in a binary (SNB) scenarios into a full and realistic simulation in order to account intrinsically for many of the effects that are alluded to in theoretical work. The initial conditions for many aspects of a stellar cluster such as initial density, velocity dispersion, population etc. are not well known and vary from cluster to cluster. Investigating within this parameter space we will consider under which conditions massive runaway stars may be generated and best match observations. In reality the observed runaway populations come from numerous and varied clusters, hence investigating a large number of simulations with various initial properties will give insight into the most realistic situation.

2.3.1 Cluster Population, N

The populations of young clusters which are likely birthplaces for OB runaways range from as few as tens (Cep OB4) to thousands of stars (such as the Orion Nebula Cluster). This then represents the population range under consideration. Simulations of the low N models, ~4-45 have been made and are often thought to be useful for representing the inner parts of a larger system (Poveda et al., 1967; Leonard & Duncan, 1988; Kiseleva et al., 1998; Pflamm-Altenburg & Kroupa, 2006) and for gaining valuable insight into the decay of multiple systems. N of a few thousand has been noted as deficient in producing runaways in large numbers and represent a small fraction of young clusters in general (Kiseleva et al., 1998). A moderate number of stars was chosen for the majority of the simulations where N = 450, with N = 45 and N = 4500 also investigated for comparison. Note that Kroupa (1995a,b,c) suggests that most stars in the Galaxy form in binaries in embedded clusters that are dynamically equivalent to a (dominant mode cluster) of 200 binaries with an initial half-mass radius of 0.85pc.

2.3.2 Distribution of stars

We adopt a spherical uniform initial density configuration for out clusters. In section 3.6 we consider the effects a Plummer model distribution would have on the ejection of massive, high velocity stars.

$$\rho_{Ho} = \frac{M(r)}{\frac{4}{3}\pi r^3} = const \tag{2.1}$$

For a density that vanishes for r > a (where a is the size of the system) the potential can be characterised by

$$\phi(r) = \begin{cases} -2\pi G\rho(a^2 - \frac{1}{3}r^2), & r < a \\ -\frac{4\pi G\rho a^3}{3r}, & r > a \end{cases} \tag{2.2}$$

For reference, the escape speed for a particle in a spherical matter distribution is

$$v_e(r) = \sqrt{2|\phi(r)|} \tag{2.3}$$

2.3.3 Mass Range and The Initial Mass Function (IMF)

In order to initialise a somewhat realistic OB association or cluster which has a small population but a significant number of massive stars and still maintains the form of the observed IMF[1] it is necessary to constrain the mass range. Here, following Brown et al. (1997), a lower limit of $1M_\odot$ is taken and an upper limit of $120M_\odot$ (note that $100M_\odot$ is the largest mass for which the stellar evolution code has been calibrated which means that stars above this mass follow the same evolution processes in terms of mass loss rates etc.). There are various IMFs which the code supports and which are well established on observational and theoretical grounds. The multi-part power law of Kroupa, Tout & Gilmore. (1993) was adopted for the IMF, where m is the mass of the star distributed as a function, $\xi(m) \propto m^{-\alpha}$

$$\begin{cases} \alpha = 1.3, & 0.08 \leq m/M_\odot < 0.5 \\ \alpha = 2.2, & 0.5 \leq m/M_\odot < 1 \\ \alpha = 2.7, & 1M_\odot \leq \infty \end{cases} \tag{2.4}$$

We estimate the spectral types via their masses ($\geq$5.9M$_\odot$ < B-type stars < 23M$_\odot$ O stars, Schaller et al. (1992)) which for a cluster population of 450 stars gives ~2 O stars and ~18 B stars initially present in the cluster.

[1]The initial mass function is an empirically determined function that describes the distribution of stellar masses of a population of stars in terms of their theoretical initial mass. The IMF is an important diagnostic tool since the properties and evolution of a star is closely related to its mass.

2.3.4 Initial Size and Density

Many OB stars are found in OB associations. OB associations are loosely bound systems which have stellar densities less than $0.1 M_{\odot} pc^{-3}$ (Ambartsumanian, 1947). Investigations previously by Bok (1934) had already shown that stellar groups are unstable against Galactic tidal forces if their mass densities are lower than $\sim 0.1 - 0.3 M_{\odot} pc^{-3}$, which, due to the short timescale corresponding to OB associations implied that they must be young. Stability against the disruption by interstellar clouds requires the densities to be even larger, greater than $1 M_{\odot} pc^{-3}$ (Spitzer, 1958). However, such a definition does not necessarily include all young clusters where OB stars may be found, for example the Orion Nebula Cluster is a subgroup of the Ori OB1 association. Definitions of clusters and associations have been summarised by Lada & Lada (1991). They define a cluster as a loose grouping of 10 or more physically related stars whose mass density is large enough to render the group stable against tidal disruption by the parent galaxy and passage of interstellar clouds. This, however, does not imply that an association must begin as a loose grouping of stars. It is possible for the initial density to be large and expand to a larger size if the virial ratio (the ratio of the kinetic energy (K) to the gravitational potential energy (W) of the members) is above equilibrium (where virial equilibrium is $Q = \frac{K}{W} = 0.5$) implying an excess in kinetic energy of the constituent stars. An example of how a star cluster may have formed outside of virial equilibrium is one in which the stars forming from a massive interstellar cloud which is in virial equilibrium initially, will collapse and form stars with velocities proportional to the mass of the cloud. Once star formation has occurred the remaining gas will be expelled by stellar winds resulting in an overall loss of mass from the system. This results in the initial system expanding as internal motions are now not gravitationally bound by the remaining stellar mass. The majority of our simulations begin in virial equilibrium. For completeness the effect of gas expulsion on the production rate of OB runaways is investigated in a later subsection (*Gas Expulsion*).

The initial size of OB associations/young open clusters which contribute to the population of OB runaways is hence somewhat ambiguous, since they may form as small as the Trapezium Cluster in Orion with a half mass radius of 0.1-0.3pc consisting of 1000-2000 stars (Kroupa et al. (1999)) or they could have formed as loosely scattered systems as suggested by Blaauw (1991) of the order of tens of parsec in diameter. It has been shown by Leonard & Duncan (1988, 1990) that very dense clusters are not required to produce

at least some runaway stars. However, at what point the rate of their production may be comparable with the observed runaway frequencies is uncertain and is one of the aims of this research. From Leonard & Duncan's discussion on their clusters and their considerations for a runaway to be produced within its main sequence lifetime they adopt a radius of 1pc for their clusters of 45 stars. We define this as the lower limit for the number density of our clusters, $\frac{45}{\frac{4}{3}\pi(1pc)^3}$. At the extreme, the densest cluster known is the Orion Nebula Cluster. McCaughrean et al. (1994); Hillenbrand & Hartmann (1998) estimate this to be $\sim 10^4 stars.pc^{-3}$ which we therefore adopt as a suitable upper limit for the density of the clusters we simulate here. A third cluster size was also chosen as an intermediate size between the two. As a secondary consideration the initial root mean square velocity of the constituent stars in the cluster is checked to see if this also has reasonable values. The virial ratio for the cluster, along with the mass and density of the cluster, defines the root mean squared velocities of the constituent stars. Hence the size of the cluster and the internal velocity dispersions of the stars are intrinsically linked. The observed residual velocities in associations in one coordinate are 1.7-6.5km/s and assuming a Gaussian distribution this corresponds to a three dimensional velocity dispersions of 2.1-8.1km/s. This probably represents an upper limit due to the presence of yet undetected spectroscopic binaries which would have increased the velocity dispersion due to the component velocities of the binary being calculated rather than the system velocity (Brown et al., 1997). Brown et al. choose velocity dispersions for their clusters of 1-4km/s. From Leonard & Duncan (1988)

$$V_{rms} = (\frac{G.M_{Total}}{2.R_{vir}})^{1/2} \tag{2.5}$$

where V_{rms} is the root mean square velocity of the constituent stars in the system, M_{Total} is the total mass of the system, G is the gravitational constant and R_{vir} is the virial radius. Specifically the virial radius may be defined as the inverse of the average inverse distance between all particles in an N-body system, ultimately defining the radius for which a self-gravitating system is in virial equilibrium. Expressed as a formula this is

$$\frac{1}{r_V} =< \frac{1}{|r_i - r_j|} >_{i \neq j} \tag{2.6}$$

which may be more recognisable as the denominator for the potential (W) of an N-body system.

$$W = -G \sum_{i<j} \frac{m_i m_j}{|r_i - r_j|} = -\frac{1}{2} \frac{GM^2}{r_V} \tag{2.7}$$

Equation 2.5 allows one to convert from the initial cluster radius and therefore density to a velocity dispersion. These velocity dispersions are similar to those chosen by Brown et al. and hence are reasonable initial conditions on these two fronts. Table 2.1 summarises a number of important cluster characteristics, including the crossing time and half mass relaxation time of the simulated clusters. The crossing time is the characteristic time changes in the cluster may propagate through the system.

$$T_{cr} = \frac{2.R_{vir}}{V_{rms}} \tag{2.8}$$

The relaxation time is the characteristic time for energy equipartition to occur through gravitational encounters, typically two body interactions. The half-mass relaxation time is usually quoted and is given as

$$T_{0.5,relax} = \frac{0.138.N_{sys}^{\frac{1}{2}}.R_{0.5}^{\frac{3}{2}}}{(G.m)^{\frac{1}{2}}.ln\Lambda} \tag{2.9}$$

where m is the average mass of the stars; $ln\Lambda$ the Coulomb Logarithm $= \gamma.N_{sys}$ where γ is $\sim$0.02, Giersz & Heggie (1996) for systems with a mass spectrum; N_{sys} the number of systems in the cluster; $R_{0.5}$ is the half mass radius (i.e. the radius within which half the mass of the system resides). Note that the half mass relaxation time is an estimate based on the theory of two-body relaxation for equal mass stars. Stars of widely different mass will relax at different rates and in this equation binaries are being treated as single objects.

Table 2.1: Summary of N-body (nbody6) Simulations. N = number of stars; BF indicates initial Binary Fraction. ρ_{Nsys} is the stellar density of objects; ρ_M is the mass density; N_{sys} is the number of stellar systems, a binary being one system (i.e for a cluster with 450 stars with a 0.5 Binary Fraction implies N_{sys} = 300); V_{vrms} is the root mean square velocity as given before Equation 2.5 which for the Plummer model, R_{vir} = b (the characteristic length); R_{vir} is the virial radius; $R_{0.5}$ is the half mass radius.; Q = Virial ratio = $\frac{KineticEnergy}{PotentialEnergy}$; a_{range} is the binary separation range; T_{cr} is the crossing time; $T_{0.5,relax}$ is the half mass, two-body relaxation time; For the Plummer model the relaxation time may be written in terms of the characteristic length, b, as $\frac{0.206.N.b^{\frac{3}{2}}}{(G.M)^{\frac{1}{2}}ln\Lambda}$ (Heggie & Hut, 2003). M_{Tot} is the mass of the cluster; f_{dist} is the distribution function of positions and velocities used; N_{run} is the number of simulations; LD, MD, HD, indicate the Low Density, Medium Density and High Density clusters respectively; PlED are Plummer models with equal central densities to the homogeneous models. The characteristic radius being b = $R_{vir}(Homogeneous)$.; PlEP are the Plummer models with central potential equal to that of the Homogenous models b = $2/3R_{vir}(Homogeneous)$; (Sep) indicates the simulations where the binary separation range was reduced; MD(Large) and MD(Small) indicate the simulations where the number of stars was 10 times more and 10 times fewer than the rest of the simulations; (GasEx) indicates the simulations which considered the effect of Gas Expulsion; (MassSeg) indicates the simulations which were primordially mass segregated.

Name	N	BF	ρ_{Nsys}	ρ_M	V_{rms}	R_{vir}	$R_{0.5}$	Q	a_{Range}	T_{cr}	$T_{0.5,relax}$	M_{Tot}	f_{dist}	N_{run}
			stars.pc^{-3}	$M_\odot.pc^{-3}$	km/s	pc	pc		$R_\odot$	Myrs	Myrs	$M_\odot$		
LD(BF05)	450	0.5	7	26	1.0	2.15	1.70	0.5	10-10^6	4.1	14.3	1065	Homogeneous	40
MD(BF05)	450	0.5	4.10^2	1.6.10^3	2.0	0.55	0.44	0.5	10-10^6	0.5	1.9	1065	Homogeneous	100
HD(BF05)	450	0.5	9.10^3	3.3.10^4	3.4	0.20	0.16	0.5	10-10^6	0.1	0.4	1065	Homogeneous	60
LD(BF1)	450	1.0	5	26	1.0	2.15	1.70	0.5	10-10^6	4.2	20.1	1065	Homogeneous	20
MD(BF1)	450	1.0	3.10^2	1.6.10^3	2.0	0.55	0.44	0.5	10-10^6	0.5	2.6	1065	Homogeneous	20
HD(BF1)	450	1.0	7.10^3	3.3.10^4	3.4	0.20	0.16	0.5	10-10^6	0.1	0.6	1065	Homogeneous	20
LD(BF0)	450	0.0	11	26	1.0	2.15	1.70	0.5	10-10^6	4.2	11.3	1065	Homogeneous	20
MD(BF0)	450	0.0	7.10^2	1.6.10^3	2.0	0.55	0.44	0.5	10-10^6	0.5	1.5	1065	Homogeneous	20
HD(BF0)	450	0.0	1.10^4	3.3.10^4	3.4	0.20	0.16	0.5	10-10^6	0.1	0.3	1065	Homogeneous	20

Continued on Next Page...

Table 2.1 – Continued

Name	N	BF	ρ_{Nsys}	ρ_M	V_{rms}	R_{vir}	$R_{0.5}$	Q	a_{Range}	T_{cr}	$T_{0.5,relax}$	M_{Tot}	f_{dist}	N_{run}
LD(PlED)	450	0.5	7	26	1.0	3.66[a]	2.81	0.5	$10\text{-}10^6$	9.0	32.1	1065	Plummer	20
MD(PlED)	450	0.5	4.10^2	$1.6.10^3$	2.0	0.93[a]	0.72	0.5	$10\text{-}10^6$	1.1	4.2	1065	Plummer	20
HD(PlED)	450	0.5	9.10^3	$3.3.10^4$	3.4	0.34[a]	0.26	0.5	$10\text{-}10^6$	0.3	0.9	1065	Plummer	20
LD(PlEP)	450	0.5	7	26	1.3	2.43[b]	1.87	0.5	$10\text{-}10^6$	5.0	17.7	1065	Plummer	20
MD(PlEP)	450	0.5	4.10^2	$1.6.10^3$	2.5	0.62[b]	0.48	0.5	$10\text{-}10^6$	0.6	2.3	1065	Plummer	20
HD(PlEP)	450	0.5	9.10^3	$3.3.10^4$	4.1	0.23[b]	0.18	0.5	$10\text{-}10^6$	0.1	0.5	1065	Plummer	20
MD(MassSeg)	450	0.5	4.10^2	$3.3.10^4$	2.0	0.55	0.48	0.5	$10\text{-}10^6$	0.5	1.7	1065	Segregated	20
HD(GasEx)	450	0.5	9.10^3	$3.3.10^4$	3.4	0.20	0.16	1.0	$10\text{-}10^6$	0.1	0.24	1065	Homogeneous	20
LD(Sep)	450	0.5	7	26	1.0	2.15	1.70	0.5	$10\text{-}10^4$	4.2	14.3	1065	Homogeneous	20
MD(Sep)	450	0.5	4.10^2	$1.6.10^3$	2.0	0.55	0.44	0.5	$10\text{-}10^4$	0.5	1.9	1065	Homogeneous	20
HD(Sep)	450	0.5	9.10^3	$3.3.10^4$	3.4	0.20	0.16	0.5	$10\text{-}10^4$	0.1	0.4	1065	Homogeneous	20
MD(Small)	45	0.5	4.10^2	$7.9.10^3$	2.2	0.26	0.21	0.5	$10\text{-}10^6$	0.2	0.4	550	Homogeneous	60
MD(Large)	4500	0.5	4.10^2	$1.5.10^3$	4.4	1.19	0.94	0.5	$10\text{-}10^6$	0.5	13.4	10650	Homogeneous	20

2.3.5 Galactic Field

The cluster was initialised with a background Galactic tidal potential as allowed by the nbody6 N-body code as provided by Dr. Sverre Aarseth and described in Section 2.4 and in Appendix D. This includes a central point-mass, a Miyamoto-Nagai density profile describing the disk (Miyamoto & Nagai, 1975) and a logarithmic halo. The central point mass was given a mass of $1.10^7 M_\odot$ and the disk a mass of $1.10^{10} M_\odot$. The Miyamoto potential was given a softening length of 4kpc and vertical softening of 0.5kpc. The Miyamoto-Nagai potential is defined as (from Binney & Tremaine (1987))

$$\Phi(R,z) = -\frac{G.M}{(R^2 + (a + (z^2 + b^2)^{\frac{1}{2}})^2)^{\frac{1}{2}}} \tag{2.10}$$

where R is the radius, b the characteristic length, z the vertical distance from the plane and a the vertical distance from the central point. When a = 0 this reduces to Plummer's spherical potential and when b = 0 this reduces to Kuzmin's very flattened potential. Hence a variety of shapes may be defined in order characterise the potential of a particular galaxy. The cluster is set in a circular orbit in the Galaxy with a velocity of 220km/s at a distance of 10kpc from the centre.

As previously noted the presence of a Galactic tidal field requires an increased density of the cluster in order to withstand complete disruption. The inclusion of the Galactic field also aids in the escape of stars from a bound cluster. It is estimated that the tidal field may be responsible for half of the rate of escape of the stars (Hayli, 1971). Within a tidal field a cluster has two Lagrangian equilibrium points (such points don't exist in an isolated case) through which stars may readily escape. Stars gain energy in the centre of the cluster to travel to regions far from the centre and in many cases preferentially escape through the Lagrange points.

2.3.6 Binary Stars

The majority of stars in the Galaxy are thought to be formed in multiple systems (Binaries, Triples etc.) with the initial fraction tending towards unity in young massive clusters. (see review by Mathieu 1994) and theories of star formation (reviews by Boss 1995 and Clarke 1996). The large primordial fraction of multiple systems may decay rapidly <0.1Myrs, ejecting stars, and diluting the initial fraction. For example, a cluster initially composed entirely of triple systems, a multiplicity fraction of 1, would become a multiplicity fraction

of 0.5 after these systems decay, 1/3 single and 2/3 in binaries, (Goodwin & Kroupa, 2005). A conservative estimate of 50% binary fraction is adopted here and this is used throughout the simulations. An analysis of ejections is also made with 0% binaries and with a 100% binaries for comparison. Note that for a binary fraction of 0.5 and our typical cluster size of 450 stars this results in 150 binaries (300 stars in total) and 150 single stars initially present in the cluster. For a binary fraction of 1.0 then this results in 225 binaries initially. For a binary fraction of 0, then this results in 450 single stars initially.

2.3.7 Separation Distribution and Range

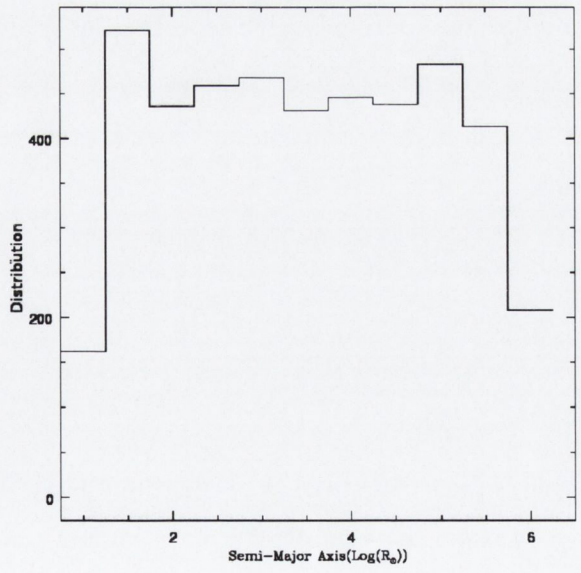
The semi-major axis (a) in binary systems is distributed such that it is flat in the logarithm.

$$\Gamma(a) \propto \frac{1}{a} \tag{2.11}$$

where Γ is the distribution function and (a) is the semi-major axis in units of solar radii.

This distribution is probable for about 80% of binaries and is probably independent of the primary mass (Heacox and Gathright 1994). The range of semi-major axis adopted here draws from the full range of possible/observed separations, from $10R_{\odot}$ to the widest observed of $10^6 R_{\odot}$ (see Figure 2-2).

Figure 2-2: *Distribution of the initial semi-major axis of binaries combined from a number of simulations.*



2.3.8 Mass Ratio's ($q = \frac{M_2}{M_1}$) and Eccentricities (e)

[2] The distribution of mass ratios in binary systems is currently not well known, especially among OB stars. Duquennoy & Mayor (1991) find that the two components have uncorrelated masses for F/G dwarfs like the Sun. However, this may not be an adequate approximation for massive stars, since these are intrinsically rare and yet are frequently paired with a comparably massive star. Garmany et al. (1980) found that the mass ratio's tend towards unity in their study of 67 O star binaries, although they suggested that the deficit of low-mass companions may be due partially to the short lifetimes of O stars. Furthermore, Lucy & Ricco (1979) found that among short-period binaries (P < 25days) there is a much higher proportion of systems with nearly equal masses then can be accounted for by selection effects, strong as they are. They suggest that the degree of correlation between the two mass functions is a function of both orbital period and mass with more correlation at short period and high mass. From a star formation standpoint if massive stars are forming in the cores of massive clouds through accretion or by stellar mergers then it is more likely that such systems will have massive companions. Demirican et al. (1995) give further qualitative evidence that massive stars should form in systems with massive companions. Hence, from these considerations, the binary companion population is drawn from a second IMF and the stars are correlated with each other to create a mass ratio distribution rising towards unity (Figure 2-3).

The expected equilibrium distribution for eccentricities (e) in 3D was both derived (also by other authors) and confirmed by numerical three-body simulations by Monaghan (1976). This is the thermal probability distribution for eccentricities used here (where all energies are equally occupied)

$$f(e) = 2e, \tag{2.12}$$

(shown in Figure 2-4).

2.3.9 Mass Segregation

Mass segregation in clusters arises from the propensity for gravitational encounters to drive the stars in the system towards an equipartition of kinetic energies. Hence, massive stars result in moving more slowly and fall to the cluster centre while low mass stars our found

[2] M_1 denotes the mass of the originally most massive star (the primary) and M_2 then denotes the mass of the companion

Figure 2-3: *Distribution of the mass ratio of initial binaries, from the output of a number of simulations. The distribution is rising towards unity as may be expected for massive stars*

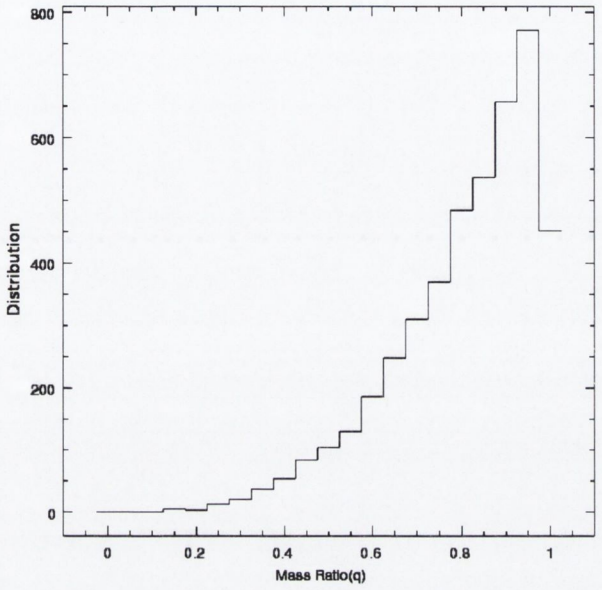
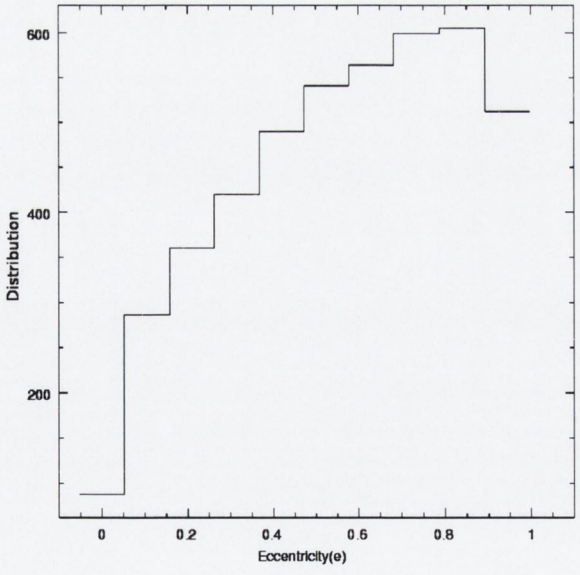


Figure 2-4: *Distribution of the eccentricities of initial binaries from the output of a number of simulations.*



in the outer regions of the cluster with higher velocities and perhaps even having escaped. Mass segregation has been observed in a number of associations and clusters (Hillenbrand,

1997; Carpenter & Sanders, 1998; Clarke et al., 2000; Zinnecker et al., 1993). This tendency for massive stars to segregate to the cluster centre may also be applied to binary systems, particularly closely bound systems, where the combined mass of the binary is considered. While the process of mass segregation can happen on sufficiently small timescales there is evidence that it does not act fast enough to explain the mass segregation evident in some young clusters (Kontizas et al., 1998; Fischer et al., 1998) which would suggest that at some level mass segregation is also primordial. One possible scenario is that the accretion rate in the centre of the cluster is higher due to the deeper potential well (Bonnell et al., 2001) therefore the protostars that are present in the core are able to accrete up to a high mass (Behrend & Maeder, 2001; Klessen, 2001). A second possibility is that the contracting primordial core results in a significant increase in stellar density allowing for collisions between intermediate mass stars to occur in order to form massive stars (Bonnell et al., 1998; Bonnell & Bate, 2002). This also means that as the gas is expelled the cluster may expand due the loss of mass and that a stellar velocity gradient occurs radially from the cluster centre. We will investigate the effect that primordial mass segregation may have on the ejection of high velocity massive stars stars since it would naturally lead to more interactions between the more massive stars in the system and many more encounters between energetic binaries.

2.4 N-body simulation characteristics

2.4.1 A matter of Faith

N-body systems are heavily dependent on initial conditions where two systems with only slightly different initial conditions may result in widely differing final systems. This is true in particular for systems of small N with there being less variation in much larger N systems. Further, numerical simulations constantly introduce small errors to the solution, such that the results diverge exponentially from the true solution with the same initial conditions. In other words, after a relatively short time integrating the orbits of stars in a cluster all the positions and velocities will be wrong with respect to their true unknown values. However, it is expected that many cluster characteristics such as mass segregation, core collapse, relaxation times etc. may be faithfully produced (Heggie, 1996). This is due to the macroscopic statistical nature of a given simulation being thought to be comparable to the real situation. This is evidenced by success of N-body simulations at modelling and giving insight into the observed characteristics of clusters and the processes which occur in them.

In order to then reduce statistical noise for small N systems a large number of runs are performed and averaged, turning the data set into an ensemble model. Each run differs only in its initial seed which creates different realisations of positions, velocities, IMF, binary separations etc. from the same relevant distribution functions. The runs themselves are physically equivalent within a model. The statistical quality of many low N simulations is comparable with that of one single calculation of the full number of stars (Giersz & Heggie, 1994). In general, when comparing models with different parameters (e.g. a mass segregated model with the non-segregated case), the number of runs for simulation runs is twenty. It should be further stressed that the statistical noise is not only a computational effect from the culmination of errors in simulations but is also be a real effect in small N clusters. Some models have a larger number of runs for reasons of practicality and necessity. For example in some cases the quantity of interest is so low by number that more simulations are required. It should also be noted that the main parameters of importance for these simulations are the escape rate and energy/velocity of these escapees. These quantities are in fact the most sensitive values to integration accuracy where lax integration tolerances will lead to greater escape from the cluster with higher energies (Heggie, 1991). This is expected since a close approach which may require detailed

integration can lead to an unrealistic encounter at low accuracy. The energy tolerance used in the code is quite strict and suggested by Dr. Sverre Aarseth as being suitable. However, also note that investigations by Valtonen (1974) show no clear accuracy dependence for the final velocities of stars. This means that even if the accuracy level was insufficient the velocity distribution of escapees is likely to be statistically indicative. The nbody6 code used for these simulations is one of several direct N-body codes developed primarily by Dr. Sverre Aarseth, with contributions from a wide range of collaborators, which are freely available for download on his website *http://www.ast.cam.ac.uk/ sverre/*. Nbody6 is fast and efficient for working on standard PCs where codes such as nbody4 were developed for work on special purpose hardware such as the GRAPE[3] hardware. Nbody6 uses the fourth-order predictor corrector Hermite scheme developed by Makino & Aarseth (1992) which includes the nearest neighbour scheme of Ahmad & Cohen (1973). The concept of regularisation is employed which is a mathematical transformation used for treating the close approach of two point-mass particles in such a manner that the equations of motion are well behaved even as the inter-particle distance tends towards zero. Specifically for binaries and two-body interactions the Stumpff version of the Kustaanheimo & Stiefel (1965) regularisation is employed (Mikkola & Aarseth, 1998). For encounters of compact subsystems chain regularisation is used (Mikkola & Aarseth, 1990, 1993, 1996). For strong interactions in unperturbed triples and quadruples are treated by three-body (Aarseth & Zare, 1974; Heggie, 1974) global regularisation (Mikkola, 1985).

Synthetic stellar evolution is employed, including mass loss, tidal circularisation and collisions. The stellar evolution is advanced using fast fitting functions developed by Eggleton et al. (1989) and advanced by Tout et al. (1997) to included binary evolution and collisions and improved by Hurley et al. (2000). However, nbody6 does not have these binary evolution routines, in particular for implementing Roche Lobe Overflow (RLOF) and spin-orbit coupling. These are included in nbody4 and in the modified version of nbody6, nbody6-2, discussed further in Chapter 4.

The above treatments result in a highly accurate and fast N-body code capable of handling the myriad of process which can occur in a realistic cluster. The code is written in the FORTRAN programming language comprised of ~35,000 lines of code and ~230 routines. For a more detailed look at how the N-body code works and some of the methods

[3]The Grapes(or GRAvity PipEs) are purpose built machines in which the Newtonian force interactions are hard wired into the processor, thereby achieving orders-of-magnitude higher speeds than normal PCs.

alluded to, see Appendix D. A comprehensive summary of nbody6 is available in the nbody6 manual which can be downloaded from Dr. Aarseth's webpage as given above. For a more in-depth look at the development and discussion of N-body codes see the book *Gravitational N-body Simulations* (Aarseth, 2003).

2.4.2 Scaling

Scaling in an N-body system is typically begun by applying what have come to be known as N-body units, coined by Douglas Heggie who suggested their use as appropriate. This yields G = M = R_{vir}, the total energy becomes E = -1/4 and the potential energy W = -1/2, for convenience during the calculation. The values are then scaled to realistic numbers where appropriate. Due to the fact that gravity acts in the same way over all length scales it means that a point-mass N-body system has no characteristic length scale as one might have for say a molecular system where molecules may be weakly attractive at large molecular separations but be strongly repulsive at shorter distances. This then means that the one real parameter which modifies and uniquely characterises an N-body system is N, i.e the actual number of bodies in the system. This is a powerful technique for generalising one's results and allowing the results of a single calculation to be applied to systems of varying physical sizes and densities; it is used by a number of authors when considering OB runaways. However, being able to scale in such a way is true only of systems which use stars as point-masses and where non-dynamical processes such as single and binary star evolution are of little importance. The stars in our simulations have large, finite stellar radii which immediately introduces a scale. This will become significant when these radii are of comparable size to the inter-star separations and can lead to new effects. For example, physical stellar collisions may occur in systems of certain densities where they will not necessarily collide if the cluster size is changed. Further, binary stellar evolution through mass transfer and circularisation will also affect the characteristics of the binary population with an effect on the dynamics of the cluster in general. The relevance of this is that simply scaling may underestimate the number of high velocity massive escapees. By varying parameters such as the virial radius R_{vir} we will be able to determine their influence on the ejection of massive stars.

2.4.3 Escape

Escape from our stellar clusters occurs when the star in question is no longer gravitationally bound to the cluster and is influenced primarily by the Galactic tidal field. Escape may occur due to two-body encounters increasing the kinetic energy of a star through relatively weak interactions until it becomes unbound. Fast escape may occur due to strong interactions between stars which is discussed in detail in the next subsection, or by the binary supernova mechanism as discussed previously or by the internal evolution of the cluster where a reduction of the potential through mass loss may allow already weakly bound stars to escape. From model calculations it has been shown that the bulk of escapees are already weakly bound just prior to the encounter that ejects them. The result is that relaxation of the cluster creates a halo of loosely bound stars which may then be easily unbound by a single interaction (on the relaxation timescale). The escape rate increases as the core contracts and becomes denser which occurs as the system relaxes to some equilibrium state. The escape rate is further influenced by the presence of the tidal field itself as this produces a set of Lagrangian points around the cluster which stars may preferentially seep through when sent into orbits around the cluster. Hence, the escape rate in a cluster is a complex issue, influenced by many factors such as the stellar density, the tidal field, the kinetic and potential energy of the stars and their masses. However, while the escape rate is dominated by two-body relaxation processes, the ejection of high velocity ejectees is dominated by strong interactions between two or more stars typically close to the centre of the system. Escape occurring from relatively weak interactions as stars gain sufficient energy from several encounters in order to just about escape the cluster can have a directional preference through the Lagrangian points. By contrast, for high velocity ejectees, a single energetic encounter occurs which has no directional preference in general and may result in one or more stars escaping the cluster in a relatively short time.

Escape in the simulations is treated by a distance criterion i.e. stars escape when they reach twice the tidal radius (Aarseth 1973). This is adopted even though it has been shown that a population of stars may exist further out of the cluster Terlevich (1987) and that stars which have a velocity above the escape velocity may still exist for long periods on orbits around the cluster (Fukushige & Heggie, 2000) while some of these, in theory, may even return to the cluster (Ross et al., 1997). However, these constitute a small fraction of escapees and typically of low velocity.

2.4.4 Multiple Systems and Interactions in Star Clusters

Two body interactions generally define the relaxation timescale of the system and is a useful quantity in describing the overall evolution of a system. However, close encounters between two or more stars are the way to produce high velocity ejectees and it is useful to describe some details relating to such interactions, (see the Book, 'The million body problem' by Piet Hut and Douglas Heggie for a detailed review). The interactions between a binary and neighbouring single stars, three body-scattering, can be elegantly summarised by Heggie's Law (after Douglas Heggie). Simply stated it is that *Hard binaries get harder, soft binaries become softer. Hard* and *Soft* are relative terms with respect to the typical velocity of stars in the cluster given by the velocity dispersion. Consider a binary-single interaction where η is the binding energy of the binary

$$|\eta| \sim (m_1 + m_2)m_3V^2/(m_1 + m_2 + m_3) \tag{2.13}$$

Heggie & Hut (2003), where m_1, m_2 are the masses of the binary components, m_3 the mass of the third star and V is the speed of m_3 relative to the barycentre of the binary. This, as the authors say, is an approximate watershed binding energy, above which binaries tend to become more bound and below which they tend to become less bound from an interaction. As can be seen from the equation, if the relative velocity of the third, interacting star, relative to the barycentre of the binary is high, then this energy is likely to be above the binding energy of the binary and will unbind it, i.e. the binary is *Soft.* By contrast, if the interacting star is relatively slow moving then its interaction will result in tightening the binary, i.e. the binary is *Hard.* For soft binaries interacting with a single star there are three possible results: ionisation (by analogy with atomic scattering) whereby the binary unbinds, a 'fly-by' where the binary interacts and survives, or exchange, whereby one of the components (usually the least massive) is replaced by the interacting star (usually more massive). Considering the hard binaries, then the energy that is donated to the third body from the interaction comes from the binding energy of the binary and the third body escapes with a much higher velocity then it started with. However, it may be that insufficient energy is imparted to it on this first encounter and so it recedes only to return and interact once more, where it again may escape or not. This may occur many times making a temporarily bound triple system (also known as 'resonance'), after which the system eventually disrupts with the result of a hardened binary and an ejected star.

In section 2.3.6 we discussed that the existence of binary and multiple systems in large

fractions in stellar clusters is well established and most likely primordial. The importance of such systems should not be underestimated, since even in systems without any primordial binaries the few that do form from interactions become the central engine of the cluster, bringing core collapse to a halt and driving further evolution by systematically ejecting in-falling stars from the dense centre. In fact, a typical binary in an open cluster may have an orbital velocity many times that of the velocity dispersion of the cluster and with a large fraction of binary systems in a given cluster most of the energy of the cluster (the kinetic and potential energy of the single and binary stars with respect to the centre of the cluster) may be locked in their binding energies. Hence binaries are extremely important from the point of view of cluster evolution and we'll see that they are additionally crucial to the production of runaway stars. Considers the fact that if there is a large initial fraction of binaries in a cluster binary-binary interactions may become as common as binary-single interactions. For binary-binary and binary-single encounters, it turns out that there is a considerable probability of the formation of a hierarchical triple system which may be long-lived forgoing further interactions with passing stars. A hierarchical triple system may form as the binary temporarily captures a passing single star. It may also be formed by analogy with the binary-single exchange process as described previously. In a binary-binary interaction, where one binary is very hard and one binary soft, the interaction may be similar to a binary-'single' interaction which has an appreciable chance of an exchange occurring, where one component of the softer binary becomes exchanged with the hard binary, which is typically more massive since it is composed of two stars. This hierarchical triple system then becomes an ideal mechanism for ejecting stars much later in the evolution of the cluster since a relatively small interaction may make it unstable resulting in the ejection of the single star. Further, stellar evolution (but most likely binary stellar evolution) of any of the components may result in disrupting the system. A binary-binary interaction is in itself the more efficient way of producing runaways stars since for a given interaction one may have all four stars being ejected as singles (ionisation), two singles ejected and one binary remaining (most common) or some combination thereof, a hierarchical triple (which is likely to eventually disrupt) and a single. In addition a binary-binary interaction is much more likely to produce a binary ejectee than a binary-single interaction. Giannone & Molteni (1985) show that the interactions between hard binaries produce the high-velocity escapees and that moderate interactions result in the general cluster expansion. It was shown by

Hoffer (1983) that physical collisions may occur during binary-binary interactions and they do so with a relatively high probability in dense systems. Binary-single interactions may also produce a merger by either elongating the orbit of the binary such that the stellar radii at periastron touch and/or by tightening the system. A fly-by may perturb the system once but if a star is temporarily captured by a binary in a hierarchical triple then the probability of the stars in the binary colliding is greatly enhanced. Hut & Inagaki (1985) estimated such a merger rate. Collisions between stars are of particular interest since they are indicative of dense systems, they may produce massive ejectees and are candidates for becoming blue stragglers.

3

N-body Simulations & Results

As mentioned in the introduction the observed percentages of runaway B and O type stars lie at 2-4% and 10-20% respectively. In the following section and subsections we present the results of the N-body simulations to see under what conditions these percentages may be produced via the dynamical ejection scenario. The spectral types of the stars are estimated via their mass (e.g $\geq 5.9 M_{\odot}$ B-type stars $< 23 M_{\odot}$ O stars (Schaller et al., 1992)). We then determine the runaway fractions as the total number of runaways of a given spectral type divided by the initial total of stars of that spectral type. In order to then consider differences between results from various simulations we apply the student t-test. This is a statistical hypothesis test in which the test statistic has a Student's t distribution if the null hypothesis is true. This test uses the standard errors of the two statistics that are being compared along with the difference between the two statistics. This allows one to determine if the two statistics are in fact different considering the size of their errors.

As noted in section 2.4.1 stellar evolution is employed in all stars, including mass loss, circularisation and collisions. However, close binary evolution is not implemented in this version of the code which means processes such as Roche Lobe Overflow (RLOF) are not

treated. Nevertheless, the SNB ejection rate may be estimated by considering those stars which are ejected via this mechanism. We may also determine if the dynamical interactions have an affect on the SNB runaway ejection rate. Subsequently, in Chapter 3, binary stellar evolution will be included allowing for a more robust analysis of the supernova in a binary scenario. We simulate the clusters for ~300Myrs. This corresponds to 75, 600 and 3000 crossing times T_{cr} for the low, medium and high density clusters respectively.

3.1 Runaways and Initial Density

3.1.1 Dynamical Ejection

As the cluster density rises the rate of interactions increase and the cluster relaxation time is reduced resulting in the cluster evolving more rapidly. This results in dynamical ejections of massive stars with high velocities within a few million years. This is a crucial aspect of the dynamical ejection scenario since the more massive O-type stars are relatively short lived, typically less than approximately 10 Myrs, requiring them to be ejected as runaways within this timeframe in order for this scenario to be effective. It is also expected that the number of ejected high velocity massive stars will be larger in high density clusters then in low density clusters.

3.1.1.1 The Low Density Simulations (N_{run} = 40; Dynamical Ejections)

We do not show a table of results here since, at this density, no dynamically ejected OB runaways are produced after 40 simulations. A small fraction of low mass stars is ejected and escape the cluster by 300Myrs, 2.6% of the total. Approximately 1% of these are ejected with high velocities, >30km/s. This indicates that OB runaways are unlikely to be dynamically ejected in any appreciable fraction from clusters of such low density. The field star percentage is defined here as those stars which escape and have velocities less than the runaway velocity. The field star percentage for dynamically ejected O and B stars is zero at this density. Field OB stars were, in the past, regarded as stars which have formed far from HII regions, (Massey et al., 1995). However, since most stars are thought to have been formed in clusters then the field star population is likely comprised of stars which have been ejected from their parent clusters (de Wit et al., 2004, 2005). The relaxation time of the cluster is a few million years which means that the cluster in general changes slowly

resulting in the more massive stars evolving before they have time to interact strongly and be ejected.

3.1.1.2 The Medium Density Simulations (N_{run} = 100; Dynamical Ejections)

Table 3.1 shows relative percentages of escaping single stars which were ejected from the cluster as a result of a dynamical interaction. Recall that stars are deemed to have escaped from the cluster when the have reached a distance of twice the tidal radius from the cluster centre. In general a star will no longer be bound to its birth cluster but will become part of the field star population. The first column indicates the velocity with which the single star left the cluster. The ranges 0-10km/s etc. indicates the percentage of stars which left the cluster with velocities between these limits. **% Total** (Column 2) is the percentage of all single stars which escaped the cluster. **% of early B stars** (Column 3) is the percentage of single early B-type stars to have escaped the cluster. This is the number of B-type stars which have escaped divided by the total number of B stars initially, multiplied by 100. **% of early B stars** $= \frac{Escaped\ \ early\ \ B\ \ Stars}{Initial\ \ Total\ \ of\ \ early\ \ B\ \ stars} * 100$. Similarly, **% of O stars** (Column 4) is the percentage of O stars to have escaped the cluster. The runaways are then, the escaped O and B stars with velocities greater than 30km/s. In this case 0.6% indicates that of the 1750 B stars (from 100 cluster simulations with approximately 17.5 B stars per cluster on average) only 11 B stars escape the cluster with a velocity greater than 30km/s. As indicated previously the error is governed in general by poissonian statistics. For the percentage of O stars ejected then only 1 O star became a runaway, hence the error is equal in size to the frequency. However, recall that the standard error is somewhat smaller as it accounts for the fact that this result is from many simulations.

Table 3.2 shows the percentage of stars that escape that are binary systems. In this instance only the **Total** and **B star** percentages are shown since no binary with an O star component is dynamically ejected during any simulation. Once more the first column indicates the ejection velocity range. The second column is then the percentage of all stars which escaped which are binaries, thus

$$\%EB = \frac{Total(EB)}{Total(E)} \tag{3.1}$$

where EB, is Escaped Binaries and E, is Escapees (Single + Binary Stars). Rearranging the previous equation then allows one to determine the total percentage of binaries with

respect to the initial total of stars using the values from the previous table.

$$\%EB_T = \frac{(\%ES_T) * (\%EB)/100}{(1 - \%EB/100)} \tag{3.2}$$

where % EB_T indicates the percentage of escaped binaries with respect to the initial total of stars (450000), % ES_T indicates the percentage of escaped single stars with respect to the initial total. For example, 0-10km/s 26.6% of all escaped stars are binaries with velocities between 0-10km/s and 7.12% of the **initial total** are single stars (from Table 3.1). For 100 simulations there are 45000 stars. Hence, ES_T = 7.12, EB = 26.6 and % EB_T = $\frac{Escaped Binaries}{Initial\ \ Total\ \ of\ \ early\ \ B\ \ stars} * 100 = 2.58\%$

The 0.6% B star runaway frequency as shown in Table 3.1, falls short of the observed percentage. However, it shows that even in a moderately dense cluster 15-30% of runaway B stars may be ejected via dynamical ejections. The field star percentage is 4.6% for B stars and 1.3% for the O stars. Table 3.2 shows the corresponding binary percentages for the ejected stars. What is important to note is that no high velocity massive binaries are ejected. Of the order of 10-20% of runaways are binaries, with several of these to be known double lined spectroscopic systems and none confirmed to have a hidden neutron star companion. Hence, while this density produces a fraction of high velocity massive escapees, it is insufficient to produce the expected fraction of high velocity massive binaries.

Table 3.1 also shows the fraction of dynamically ejected O stars. This fraction is extremely low by comparison to what is observed and may indicate that few runaway O stars are in fact dynamically ejected. However, what is interesting to note is that the O star that is ejected is as a result of a collision between two lower mass stars. From scattering experiments Leonard (1995) suggests that a sizeable portion (>50%) of massive runaways may be products of lower mass merged stars that are ejected as a result of the dynamical interaction and collision process. The simulations here show that not only may collisions occur but they may be the most effective way of producing O star runaways. Furthermore, it is important to note that while the overall fraction of O star runaways is small with respect to the initial O star population it is large with respect to the fraction of runaways present at the time. O star lifetimes are of the order of 8Myrs for a $23M_{\odot}$ star but the O star runaway here was created at 9Myrs. This means that all the cluster O stars may have reached the end of their lives by 9Myrs and the only O star left is then a runaway formed from a collision. Obviously this is an important effect for the formation of a high fraction of observed O star runaways. The increase in B star runaways due to collisions is

less dramatic and lower than suggested by Leonard (1995) due to the comparatively long lifetimes of B stars and a larger number ejected stars without collisions. However, from the total number of runaways which experienced a collision before being ejected in Table 3.4 (23%), and the distribution of collisions Table 3.3 (38.1% (Two low mass stars) + 25.1% (B star and a low mass star) + 4.0% (Two B stars) for B stars only) results in 12 ± 7% of ejected B star runaways being formed from the collision of two lower mass stars and subsequent ejection of the merged product.

Table 3.1: *Dynamical Ejections of Single Stars: N = 450 : Medium Density : N_{run} = 100 where N_{run} = 100 is the number of simulations run : All errors throughout this thesis are, 1 σ unless otherwise stated. The standard error of the mean may be determined by SE = $\frac{\sigma}{\sqrt{N_{run}}}$. (E.g. 0-10km/s B stars (2.5% and σ = 0.3%; => SE = 0.03)*

Escape Velocity	% of Total	% of early B stars	% of O stars
0-10km/s	7.12 ± 0.14	2.5 ± 0.3	0.65 ± 0.65
10-30km/s	0.51 ± 0.04	2.1 ± 0.3	0.65 ± 0.65
>30km/s	0.81 ± 0.09	0.6 ± 0.2	0.65 ± 0.65

Table 3.2: *Binary percentage of dynamical ejections: Medium Density*

Escape Velocity	% of Total Escapees	% of B Escapees
0-10km/s	26.6 ± 0.8	12.6 ± 4.8
10-30km/s	17.2 ± 3.4	5.3 ± 2.8
>30km/s	7.0 ± 3.8	0

3.1.1.3 Collisions

Since collisions may play a significant part in the runaway process we show a number of statistics relating to collisions in the medium density cluster simulation. On average 2.2 stars merge due to a direct collision from a dynamical interaction per cluster. Tables 3.3 and Tables 3.4 show a list of collision statistics. This gives an idea of the importance of stellar collisions of massive stars at higher densities. It is to be expected that the more massive stars are more likely to collide more often than the low mass stars due to their larger radii, gravitational enhancement of the cross-section and tendency to segregate to denser regions in the cluster. The only difficulty with creating OB stars in this way is

that when the collision is between two massive stars then the number of massive stars is obviously diminished rather than enhanced. Therefore the rate at which additional OB stars are created is less than 1/4 per cluster. The majority of massive collided stars has relatively low velocities and result in a supernova before escaping the cluster. While a merged object has a shorter lifetime than its original components it may be a runaway for its entire subsequent lifetime which makes this scenario so effective. The observational significance of these collision runaways will be discussed further in chapter 5 (Rotation Velocities of OB Runaways) since the collision of two stars results in significant mixing and an enhanced rotation velocity of the merged product.

Table 3.3: *Medium Density Cluster. Direct Collisions - Statistics I. Supernova mass (SNM) stars indicate stars greater than $9M_{\odot}$ which may erupt in a supernova, LMSN indicates a star with a mass lower than the supernova mass adopted here. LMO indicates stars lower than an O star mass $23.3M_{\odot}$. LMB indicates stars lower than an early B star mass, $5.9M_{\odot}$.*

Collision Type	Percentage of Total Collisions
Two O stars -> O star	2.4 ± 1.2
One O star + LMO -> O star	11.3 ± 2.6
Two LMO -> O star	5.4 ± 1.8
Two B stars -> B star	4.0 ± 1.7
One B star + LMB -> B star	25.1 ± 2.9
Two LMB stars -> B star	38.1 ± 4.8
Two LMB stars -> LMB star	13.7 ± 2.9
Two SNM stars -> SNM star	16.1 ± 3.1
One SNM star + LMSN -> SNM star	16.7 ± 3.1
Two LMSN -> SNM star	26.8 ± 4.0
Two LMSN -> LMSN star	40.4 ± 4.9

3.1.1.4 High Density Simulations (N_{run} = 60; Dynamical Ejections)

Table 3.5 and 3.6 show the DE percentage of ejections for single and binary stars respectively from the cluster. At this density the fraction of B star runaways that occur as a result of dynamical interactions is (From the table, 1.4 + 2.6 = 4.0%), which could account for the entire fraction of observed B-type runaways. The percentage of high velocity O stars is approximately 4.4% which represents 20-40% of the observed fraction of O star runways.

Table 3.4: *Direct Collisions - Statistics -II. The percentage of B star runaways which experienced a collision before being ejected.*

Ejected Velocity	% of Escapees (Early B stars)
0-10km/s	0 ± 0
10-30km/s	7 ± 5
>30km/s	23 ± 15

The field star percentage is ~12% for B stars and that bit lower for O stars, 2.2%. The binary percentage of B star runaways is (calculated from the table for the runaway velocity >30km/s) is 23%. Note that the binary fraction is the number of binary stars divided by the total number of binary and single stars ($\frac{Binary}{Binary+Single}$) which is comparable to the observed fraction. The O star runaway binary fraction is uncertain due to the low numbers output from the simulations, however it appears to be comparable to the B star fraction, $20 \pm 20\%$.

Once more a high fraction, $50 \pm 35\%$, of O star runaways come from the collision of two stars. The fraction of DE B star runaways which experienced a collision is similar to the medium density cluster at $20 \pm 8\%$. In general there is a ~50% increase in the number of collisions from the medium density cluster to the high density cluster but with the collision statistics similar to that of the medium density cluster.

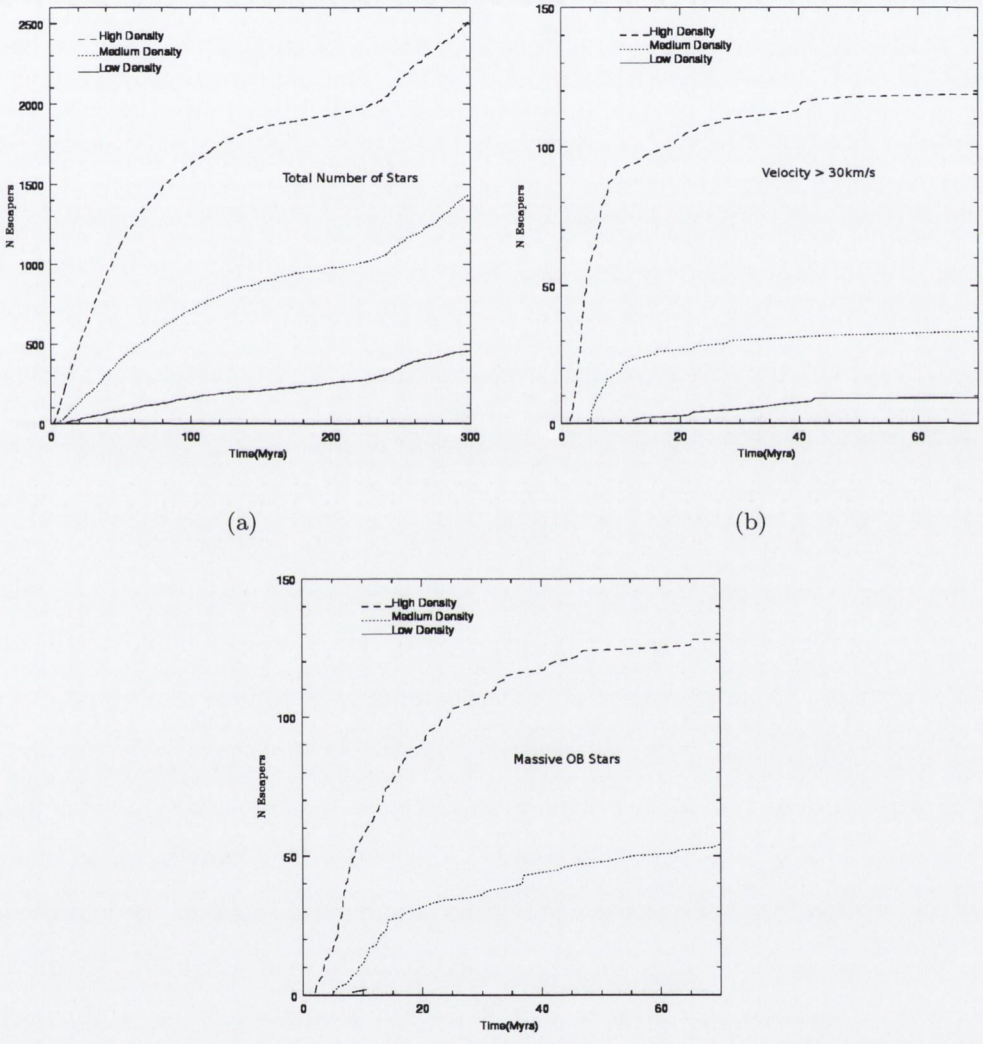
Table 3.5: *Dynamical Ejections: High Density Simulations: Singles*

Escape Velocity	% of Total	% Early B stars	% O stars
0-10km/s	12.3 ± 0.24	7.5 ± 0.60	0
10-30km/s	1.3 ± 0.065	5.0 ± 0.70	2.2 ± 1.5
>30km/s	0.63 ± 0.05	4.0 ± 0.94	4.4 ± 2.2

Table 3.6: *Dynamical Ejections: High Density Simulations: Binaries. Values in the Square brackets indicate the expected binary fraction above the velocity limit rather than between the limits.*

Escape Velocity	% of Total Escapees	% of B Escapees	% of O Escapees
0-10km/s	26 ± 0.78	35 ± 4.55	100 ± 50 [40%]
10-30km/s	26 ± 2.86	40 ± 8.8	0
>30km/s	12.5 ± 4.0	23 ± 11	20 ± 20

Figure 3-1: *Dynamical Ejections: Figure a) Shows the cumulative distribution for escapees from the High, Medium and Low density simulations as labelled. Figure b) Shows the cumulative distribution for ejectees with velocities greater than 30km/s. Figure c) Shows the cumulative distribution for massive OB star escapees. Note that each population is different, ~2,500 escapees of all masses, 120 escapees of all masses with velocities greater than 30km/s and 132 escapees with OB masses. The OB runaway escapees are not plotted due to the small numbers involved.*



(a) (b)

(c)

The Figures 3-1a,b,c) show the ejections for the high, medium and low density cases discussed. The ejections can be seen to begin much sooner for both high velocity high mass ejectees the greater the initial density. While this is a natural expectation it is worth noting

since it means that massive ejectees from a dense cluster will have a larger portion of their main sequence lifetime left and will live it outside of their parent clusters.

3.1.2 Supernova in Binary

As noted, routines to handle complex binary stellar evolution are not in place in this version of the code. Hence, in the current code when a star in a close binary evolves and its radius increases it may come into contact with its companion where they are then merged into one single object. This may occur in particular for massive stars where their evolved radii may be 100's of solar radii in size. This is much different from the real situation where a number of different effects may occur, altering the parameters of the binary such as separation and masses of the individual components. Hence we will only make a rough estimate of the contribution the supernova in a binary mechanism will make in this instance. This is done by considering the total population of stars which are ejected via the SNB mechanism and estimating the number these which may contribute to the massive high velocity runaway population by considering the component masses and their separations.

3.1.2.1 The Low Density Simulations (N_{run} = 40; SNB Ejections)

There are 150 binaries per cluster, hence from 40 simulations there are 6.10^3 initial binaries. Over the total time we simulate the cluster, 300Myrs, the total number of binaries divided by the number of binaries where one of the components explode in a supernova (156) shows that only 2.6% ($156/6.10^3$) of the primaries erupt in a supernova. We consider the ejection velocities of the disrupted binaries and from the initial separations determine whether or not a phase of mass transfer is likely to have occurred. The most common binary evolution scenario is Case B mass transfer where the companions is still on the main sequence when RLOF begins which we adopt for all cases. We calculate the maximum separation for which the primary star would still be able to fill its Roche lobe (Eggleton et al., 1983).

$$a_{max} = R_{max}(\frac{0.6 + q^{\frac{2}{3}} ln(1 + 0.q^{-\frac{1}{3}})}{0.49}) \tag{3.3}$$

where a is the semi-major axis, q is the mass ratio $\frac{MassSecondary}{MassPrimary}$ and R_{max} is the maximum radius the primary is likely to expand to. The amount of mass transferred to the companion may then be taken as proportional to the square of the mass ratio (Vrancken et al., 1991; Bethe & Brown, 1998).

$$M^{AMT}_{Companion} = M^{BMT}_{Primary}(q + 0.7q^2) \tag{3.4}$$

where BMT and AMT refer to Before Mass Transfer and After Mass Transfer. This then allows us to consider if an ejected companion star is likely to have mass transferred to it or not before ejection and if this additional mass would change its spectral type. However, it must be stressed here that this is a simplified approach which does not account for the large number of binary evolution processes which may occur or any consideration for changes in orbital separation as a result. Chapter 3 will deal with the supernova in binary scenario in more robust detail and the approach here still allows us to view how changing the initial cluster density may affect the SNB massive runaway population.

In order to determine the number of OB runaways we identify all the stars which are ejected from the cluster via the SNB mechanism at runaway velocity. Using the equations above we estimate the effect a phase of mass transfer might have had on the mass of the ejected star and from this determine the number of massive O and B-type stars likely to be ejected with a high velocity. From these determinations we found that at most 11% of SNB systems are likely to produce B-type runaways. This 11% then corresponds to a B star runaway frequency of $2.4 \pm 0.1\%$. While this in itself is encouraging, as this is close to the observed value for B star runaways, it is likely to be an upper limit.

3.1.2.2 The Medium Density Simulations (N_{run} = 100; SNB Ejections)

With a greater number of dynamical interactions resulting in disrupted binaries in a system of higher density then these simulations show that only 1.8% of primaries erupt while in a binary. The weakly bound, wide orbit systems are more easily disrupted. However, the binaries which survive gravitational interaction may be hardened, resulting in a closer, more energetic system (further details of this effect are discussed in Chapter 3). The estimated frequency is then $3.38 \pm 0.01\%$ of B star runaways (close to 40% higher than the low density situation). No O star runaways seem likely to be ejected but this may be due to the simple approach used to estimate mass transfer.

Note that only a small number of binaries contribute to the runaway fraction from the supernova in a binary scenario, $\sim$0.6 per cluster. This means that while dynamical interactions disrupt a large number of binaries the strongly bound systems are hardened, resulting in a greater likelihood that they will subsequently contribute to the runaway population via the supernova in a binary scenario. The increase in the number of SNB runaway massive stars from the low density simulations to these higher density simulations

is due to a small number of systems being hardened. Furthermore, binaries which escape the cluster due to dynamical interactions are no longer evolved by the code and may also contribute to the runaway population if the primary erupts in a supernova.

3.1.2.3 The High Density Simulations (N_{run} = 60; SNB Ejections)

At this density only 1.2% of binaries now survive long enough for their primaries to erupt in a supernova. Nonetheless, $2.4 \pm 0.03\%$ of B stars attain runaway velocities. The number of dynamically ejected binaries is much greater at this density, hence the increase of runaways which may be subsequently produced via the SNB scenario after the binary has been ejected from the system is much larger. In this case the rate of runaway production would be higher than that of the medium density cluster. This implies that for densities greater than the medium density cluster as defined here the rate of runaway production may be significantly underestimated by estimates made by purely population synthesis methods. This is essentially due to the adopted separation distribution and range. In population synthesis codes this is often the simple flat logarithmic distribution suggested by observation. However, the distribution relevant for the ejection of OB runaways changes in a dynamical environment resulting in a higher probability of a SNB runaway being produced.

3.1.3 General Conclusions for Runaways and Initial Density

From the runaway fractions estimated in the previous section we may then compare both mechanisms and determine the ratio at which they produce the total number of runaways. The ratios of DE:SNB in terms of runaway B stars from our Low, Medium and High density systems may be determined from the results of our simulations using the percentage frequency of B star runaways ejected via both mechanism. Since no B star runaways are dynamically ejected from the low density cluster then the ratio of DE:SNB is (0:100). The medium density cluster has runaway frequencies given as: From Table 3.1 the DE B star runaway frequency is 0.6%; From section 3.1.2.2 the SNB B star runaway frequency is 3.38%. Hence the ratio of DE:SNB is (15:85). Similarly the high density cluster has runaway frequencies given as: From Table 3.5 the DE B star runaway frequency is 4.0%; From section 3.1.2.3 the SNB runaway frequency is estimated to be 2.4%. This gives a ratio DE:SNB of (65:35). These fractions indicate that between the medium and high density clusters the dominant mechanism for runaway production changes from being the SNB

scenario to the DE mechanism.

From observation it is estimated that the field O star fraction is ~20%. While it is difficult to estimate the O star fraction for the SNB scenario, since mass transfer is not robustly treated by us or in the code and will have a large effect on these systems, we consider the field star fraction from the DE point of view. Only the high density cluster ejects O stars in appreciable numbers with ~7% of O stars escaping the cluster. This suggests that unless the initial density is significantly higher then the SNB scenario could account for a large number of field O stars.

The binary fraction also allows some indication as to which density is the more likely initial condition. The fraction of double lined spectroscopic binaries among O stars is approximately 5% indicating that both components are 'normal' stellar objects and not compact companions (Mason et al. (1998) estimate that 5% of O star runaways are double lined spectroscopic binaries but that the total binary fraction is 26%). This means that dynamical interactions must at least account for this 5% fraction, since the supernova in a binary scenario has significant difficulty in ejecting such a binary.[1] Further, no compact companions to the known OB runaways have been found after extensive searches by many authors (see Chapter 1) which suggests that the rest of the binaries in the runaway population are also dynamically ejected (meaning that the total observed binary fraction of ~26% are dynamical ejectees). The medium density cluster produces no high velocity binaries which means that a higher density cluster may be the more likely case for runaway ejection. The high density cluster does produce a significant binary fraction ~23%, which indicates that clusters of this initial density are likely to occur in appreciable fractions. If this is the case then the dynamical ejection scenario may account for the majority of the both single and binary B star runaways. If the high density cluster is close to the realistic case then ~ 5% of O stars are dynamically ejected, 25-50% of the observed percentage. The fraction of O star binary runaways is harder to assess since the SNB O star fraction is difficult to determine accurately from these simulations due to small numbers. However, population synthesis models suggest that the SNB scenario may only be able to account for ~30% (Portegies Zwart, 2000), of the observed O star runaways which means that the DE could also dominate the ejection of O star runaways.

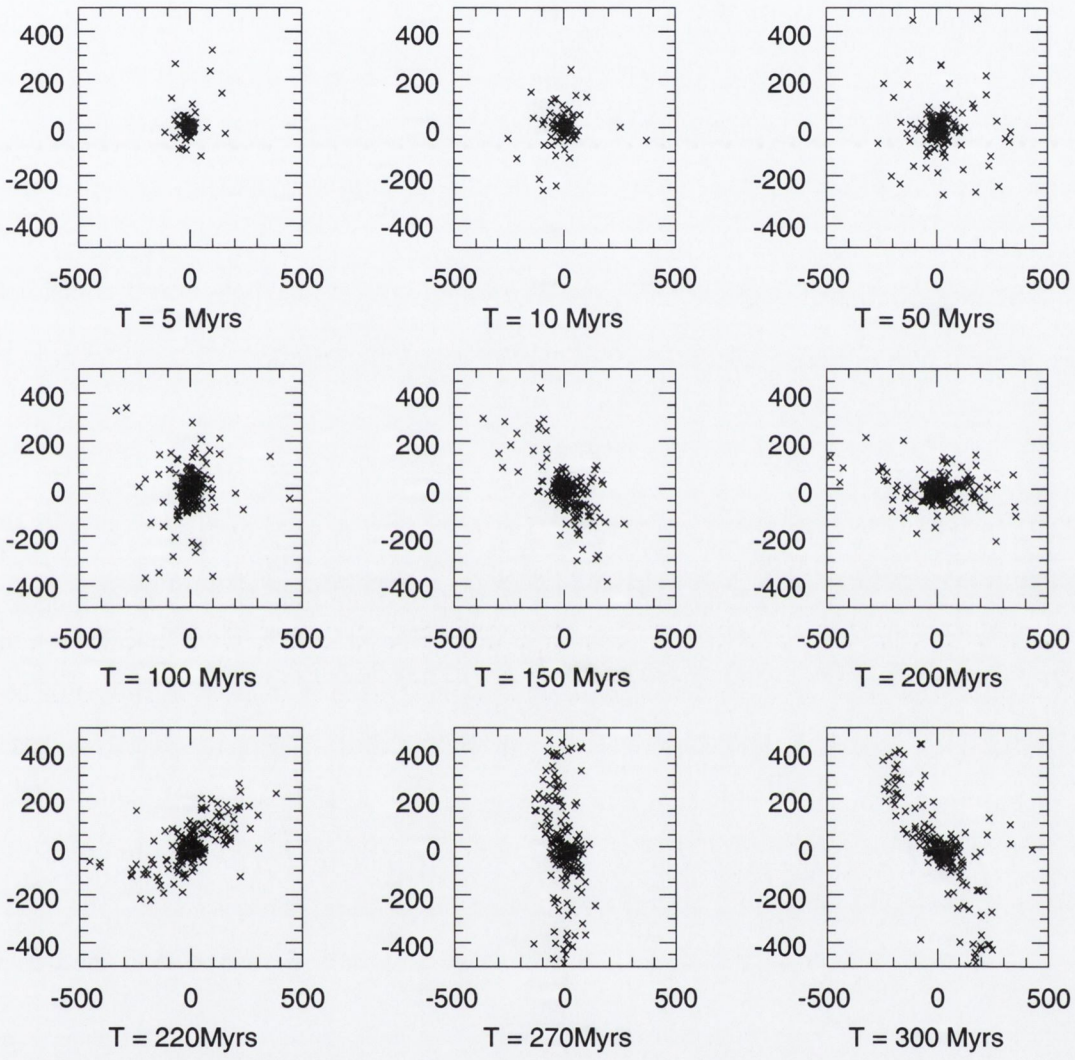
[1] A supernova in a triple system could produce a spectroscopic binary ejectee (van den Heuvel, 1985) however such an event is likely to be relatively rare

3.1.4 Tidal Tails and Late Stage Escape

The rate of escape in the N = 450 simulations for all the simulations increases after approximately 220Myrs. In Figure 3-1 a) of escape versus time there is a significant rise in the number of escaping systems around this time. This is due to the combination of slow escapees and the tidal field. Figure 3-2 shows a time series of plots from one of the simulations (unscaled units). The view is as seen where the Galaxy is face on. Due to the presence of the Galactic tidal field there is a preference for ejectees to escape through the Lagrangian points at opposite edges of the cluster. This elongates the cluster as seen in the figures.[2] As is seen from the figures after approximately 200Myrs the outer edges of the cluster begin moving in larger numbers beyond twice the tidal radius (in this case 500 units) and are therefore removed as escapees in the code, hence the escape rate increases around this time.

[2]Note that the change in orientation in the cluster over time is only due to its orbit in the Galaxy making it appear to be changing when in fact the orientation relative to the Galactic centre is the same throughout (i.e. the cluster is not itself rotating).

Figure 3-2: *Time series of cluster evolution projected onto the 2-D plane of the galaxy. The axes are unscaled N-body units.*



3.2 Runaways and the Primordial Binary Population

It is well known from observation that many stars are members of binary or multiple systems, particularly among young massive stars. Such binaries are thought to have been formed primordially, before the forming stars have evolved beyond their proto stellar age and the unaccreted gas has been ejected from the cluster. Binaries have been shown to

be key elements in the production of runaways via both mechanism so it is important to consider the effect that a different primordial binary population will have on the results. We investigate two additional initial binary fractions, each at the three initial cluster densities as before and include in the analysis the results from the previous section. The binary fractions are zero (henceforth BF0, no initial binaries), a half (BF05, the value adopted in the previous section), and one (BF1, all stars begin as a member of a binary system). The important dynamical mechanisms that are to be considered in the following discussion are: binary formation through multiple single star encounters resulting in capture (note that tidal interaction may also result in the formation of a binary); binary-binary interactions resulting in the dissociation and ejection of binaries and single stars, collisions and the formation of hierarchies. How large a role these mechanisms play depend on the initial binary fraction and the initial density of the cluster.

3.2.1 Dynamical Ejections

3.2.1.1 Low Density (N_{run} = 20; Dynamical Ejection)

Table 3.7 shows the DE results for BF0 and BF1. At these low densities the interaction rate is similarly very low. The escape rate of single stars is greatest in the BF05 see 3.1.1.1. There are 50% more single star escapees at BF05 than the BF0 case (very few binaries form throughout the cluster lifetime). It is greater than the BF1 case simply due to the fact that there are more stars in binaries in the BF1 case which are more likely to escape as binaries rather than being disrupted and escaping as single stars. This is indeed the case since the binary escape rate is largest for BF1 (twice as many binaries escape as in the BF05 cluster).

3.2.1.2 Medium Density (N_{run} = 20; Dynamical Ejection)

Table 3.8 shows the results for BF0 and BF1 initial binary fractions. The single star escape rate of BF0 is now similar to that of the BF05 cluster (Table 3.1 in the previous section), with the BF1 cluster showing a notable decrease in single ejectees. This means that at this density the BF0 cluster is forming a system which has a small number of similarly hard binaries to the BF05 cluster. However, the few binaries that do form at this density eject single stars with a low velocity and the BF05 cluster has many more massive and high velocity ejectees than the BF0 cluster. As noted previously the BF1 cluster ejects a much

Table 3.7: *Dynamical ejections from the low density cluster for two initial binary fractions. (Single Escapees): (BF1) 100% Initial Binaries(Top): (BF0) 0% Initial Binaries(Bottom). BF = Binary Fraction*

Escape Velocity	% Total	% Early B stars	% Binaries: Total	% Binaries: Early B
BF1				
0-10km/s	1.1 ± 0.1	0.6 ± 0.4	60 ± 6	50 ± 50
10-30km/s	0.09 ± 0.03	0	0	0
>30km/s	0	0	0	0
BF0				
0-10km/s	1.6 ± 0.1	0	0	0
10-30km/s	0	0	0	0
>30km/s	0	0	0	0

larger number of binary systems as opposed to single stars which accounts for the decrease in single star escapees with respect to the BF05 cluster. At higher velocities this has less of an effect as both the BF05 and BF1 eject a similar fraction of high velocity massive stars. This implies that the exact initial binary population is not overly significant when considering the ejection of runaway massive single stars from clusters. While the binary fraction of ejectees at low velocities is much higher (nearly double) from BF1 to BF05, it is comparable at higher velocities.

Table 3.8: *Medium Density(Single Escapees)DE: (BF1) 100% Initial Binaries(Top): (BF0) 0% Initial Binaries(Bottom). 3.6 ± 3.6% of O stars are runaways in the BF1 simulations. No O stars were ejected in the BF0 simulations.*

Escape Velocity	% Total	% Early B stars	% Binaries: Total	% Binaries: Early B
BF1				
0-10km/s	4.5 ± 0.2	2.9 ± 0.9	50 ± 3	33 ± 17
10-30km/s	0.6 ± 0.08	1.4 ± 0.6	26 ± 7	44 ± 26
>30km/s	0.26 ± 0.05	0.6 ± 0.4	8 ± 5	0
BF0				
0-10km/s	8.2 ± 0.3	2.2 ± 0.7	0.6 ± 0.2	10 ± 10
10-30km/s	0.1 ± 0.04	0	4 ± 4	100 [0.4 ± 0.3]
>30km/s	0.02 ± 0.01	0	50 ± 35	100 [0.2 ± 0.2]

3.2.1.3 High Density (N_{run} = 20; Dynamical Ejections)

Table 3.9 shows the results for BF0 and BF1 initial binary fractions. At this higher density the BF0 case now produces a much larger fraction of single low velocity escapees than either BF05 (Table 3.5 in the previous section) or BF1, between 1.5-2 times as many. No O stars were ejected from BF0 but, 3.6 ± 3.6% of O star runaways were ejected from BF1. The larger number of escaping single stars in BF0 is due to a higher number of stars in BF05 and BF1 which remain in their original binaries. By the same token a much larger number of binaries are ejected from BF05 and BF1 than in BF0. At higher runaway velocities BF0 produces fewer massive ejectees, however, the number that it does produce, 2.6 ± 0.8% is larger than the number produced via the BF05 at medium densities. This is a key point in considering that the initial binary population may matter little on the DE single massive runaway population. As noted previously, the primordial formation of binaries may in fact be heavily influenced by dynamical interactions in a dense environment. As such it is unsurprising that a binary population is formed which will eject massive stars. Interestingly, the BF05 case not only produce more massive low velocity single star escapees but also produces a similar **number** of single low velocity massive B star binary escapees to the BF1 cluster. From Tables 3.5 and 3.6, 0-10km/s massive B stars has a frequency of 7.5% for single stars and a binary fraction of escapees of 35%. Table 3.9 0-10km/s massive B stars has a frequency of 2.9% for single stars and a binary fraction of escapees of 59%. Recall that to convert the binary fraction of escapees to a binary fraction of the initial total use Eqn 3.2. This gives a B star binary frequency with respect to the initial total number of B stars for BF05 and BF1 as 4.0% and 3.8% respectively. The consequence for massive runaways is that the BF05 cluster produces ∼1.3 times as many massive single runaways as BF1 which has (3.1 ± 0.9 B single runaways). The binary fraction of B type runaways is non-existent for BF0 but for both BF05 and BF1 is ∼25% which implies the exact initial binary fraction may not be important in terms of ejecting a significant fraction of massive high velocity binaries. They both also produce similar fractions of O star single runaways at ∼4% with a poorly sampled binary fraction of ∼20%.

Table 3.9: *Dynamical Ejections. High Density(Single Escapees) : BF1, 100% Initial Binaries(Top): BF0, 0% Initial Binaries(Bottom). BF1(3.6 ± 3.6% single O star runaways.)*

Escape Velocity	% Total	% Early B stars	% Binaries: Total	% Binaries: Early B
BF1				
0-10km/s	8.3 ± 0.3	2.6 ± 0.9	51 ± 2	59 ± 19
10-30km/s	1.6 ± 0.1	3.7 ± 1.0	26 ± 4	55 ± 17
>30km/s	0.62 ± 0.08	3.1 ± 0.9	12 ± 4	27 ± 13
BF0				
0-10km/s	19 ± 0.4	11.9 ± 1.7	0	0
10-30km/s	1.0 ± 0.1	5.5 ± 1.1	2 ± 1	11 ± 7
>30km/s	0.15 ± 0.04	2.6 ± 0.8	0	0

3.2.2 Collisions

It is of general interest to consider how the collision rate changes with binary fraction, for the creation of blue stragglers and the formation of massive runaways.

Table 3.10: *Number of collisions per run with respect to initial density [LD;MD;HD] and initial binary fraction[BF]. The errors are as usual 1σ*

BF	[LD]Collisions/Run	[MD]Collisions/Run	[HD]Collisions/Run
0	0.04 ± 0.04	1.14 ± 0.21	1.41 ± 0.24
0.5	0.75 ± 0.14	2.15 ± 0.17	2.87 ± 0.21
1.0	0.80 ± 0.20	3.45 ± 0.41	3.05 ± 0.42

3.2.2.1 Low Density (Collisions)

Table 3.10 shows the average number of collisions per run for each of the simulations. At low density there are a low number of collisions with the BF0 cluster being lower than the BF05 and BF1 clusters which have a comparable number of collisions. This is reasonable since as noted by Leonard (1995) a binary-binary interaction has a significant probability of resulting in a stellar collision and at low density close encounters between stars are less common. As can be seen from table as either the binary fraction or the density increase

then the number of collisions increase significantly.

3.2.2.2 Medium Density (Collisions)

At this density several collisions occur even in the BF0 cluster. As may be expected with having more binary-binary interactions more collisions occur in the BF05 and BF1 clusters (a 90% increase in collisions from BF0 to BF05 and a further 60% increase from BF05 to BF1).

3.2.2.3 High Density (Collisions)

The number of collisions is once more lowest for BF0, with only a small increase in collisions by comparison to the medium density cluster. The interesting thing to note is that the BF1 medium density cluster now has a greater number of collisions than that of the BF1 high density cluster. The most plausible explanation as to why this occurs in a high density cluster is that collisions may occur due to binary-binary interactions or binary-single interactions, with a higher probability for the former. Collisions are moderated by the formation of hierarchies where a number of bodies interact with each other over a prolonged period, for example in a hierarchical triple. In such a system the single body orbiting the close binary dissipates energy from the binary as it interacts on longer and longer orbits until it is ejected. However, these subsequent interactions increase the probability of a collision occurring. What occurs in the BF05 case is that between the high density and medium density clusters the ratio of hierarchies is similar to the ratio of collisions that occur for both clusters. The BF1 cluster at high density has few long-lived hierarchies than the medium density cluster resulting in the number of collisions being lower. What is likely to have occurred is that with a BF1 cluster and a medium density a limit in number of hierarchies that can form is reached due to a combination of the interaction rate and the binary population.

3.2.3 Supernova in Binary Mechanism

3.2.3.1 Low Density (N_{run} = 20; SNB Ejections)

The estimate for the number of ejected SNB ejected stars is made in the same fashion as described in section 3.1.2.1. Table 3.11 shows the average number of supernova which occur in binaries per cluster for each of the different initial binary populations and cluster

densities. At this density the ejection rate of single secondaries due to a supernova in a binary is determined solely by the initial primordial population. Binaries do not form readily via interactions and this results in a virtually non-existent ejection rate for BF0 cluster. As expected, 1.5 times as many supernova occur in a binary system in BF1 than in BF05 since the actual number of binaries has increased from 150 per cluster to 225 (i.e. 225/150). Similar to the BF05 cluster the BF1 cluster 2.6% of the initial binaries experience a supernova. The percentage of possible ejected high velocity massive stars is then about 1.5 times greater from BF05 to BF1, giving an upper limit of 4.0±0.3%. Again we caution that the real fraction in such systems is likely to be smaller once mass transfer is considered in greater detail.

Table 3.11: *Average number of supernovae occurring in binary systems per simulation. LD - Low Density, MD - Medium Density, HD - High Density.(Error less than 10%)*

Binary Fraction	Total:LD	Total:MD	Total:HD
0	0.0	2.20	1.92
0.5	3.95	2.72	1.82
1.0	5.95	3.15	1.85

3.2.3.2 Medium Density (N_{run} = 20; SNB Ejections)

From Table 3.11 the notable result is that a population of supernovae now occur in binary systems from the BF0 case as capture events result in the formation of binary systems. The BF0 escape rate is about half that of the BF05 case but the ejection rate at moderate velocities ($\sim$ 10km/s) is very similar to the BF05 rate. At higher, runaway velocities, there are no ejected stars from BF0. However, what is important is that at this density a number of binaries may form from single star interactions and begin to eject stars via the supernova in a binary mechanism. The total number of stars now erupting as a supernova in binary system is only $\sim$1.2 times greater in the BF1 (1.5%) case over the BF05 (1.8%) case. This is once more due to the disruptive nature of binary-binary interactions. The estimated B star runaway ejection percentages increase from 3.38±0.01% (BF05; Section 3.1.2.2) to 4.0 ±0.2% (BF1).

3.2.3.3 High Density (N_{run} = 20; SNB Ejections)

It is noticeable that at this density is that the total number of supernova in binary occurrences is the same regardless of initial binary population, see Table 3.11. This is a striking result and suggests that at this density the cluster relaxes in such a way as to form similar populations of massive close binaries which have a component that explodes as a supernova. While the BF05 and BF1 clusters eject more binaries in general it is still notable how similar the number of supernovae in binaries actually occurring are in each of the cases. However, BF05 and BF1 do produce a substantially greater number of single star higher velocity escapees than BF0 due to their initial separation distribution. This is much closer than the separation distribution for the dynamically formed massive binaries in BF0. This is reasonable since it is difficult to form close binaries via capture. The BF0 cluster may then produce up to 1.4% B star runaways, BF05 as before 2.4% and BF1 2.8%. The conclusion here is that an initial binary fraction and separation distribution may define the B star runaway ejection rate in disperse clusters but it has a weaker dependence once the density of the cluster is high. This means that at high density dynamical encounters can substantially modify the initial binary fraction and change the parameters which are relevant for OB runaway ejection, such as binary separation.

3.2.4 General Conclusions: Runaways and Primordial Binary Populations

- One can generate a significant population of massive high velocity stars without a primordial binary population. At sufficiently high densities energetic binaries form and dynamically eject stars with high velocities. These massive close binaries then may produce further ejectees due the supernova eruption of one of its components resulting in a significant population of runaway stars from the supernova in a binary mechanism as well.

- The fraction of escaped binaries increases as the initial binary population increases since more binaries are available to be ejected. However, the fraction that escape at runaway velocities is very similar regardless of whether the initial binary population is 50% or 100%.

- At the high density suitable for producing a substantial number of runaway stars the initial primordial population has only a small bearing on the rate of collisions that occur. At lower densities the rate of collisions is higher when the initial binary population is higher.

We have shown here that the initial binary population affects the rate of single and binary star ejections and collisions for both mechanisms. At low and medium density this effect is large with more binary and single star escapees occurring in general with a larger binary population via both mechanisms. At high density it seems that the initial binary population is of small consequence in terms of collision and ejection rate of massive stars. It is likely that at this density the system evolves rapidly to its own equilibrium state and disrupts, hardens and collides single stars and binaries in such a way that the initial population of binaries becomes somewhat unimportant. However, it is important to note that with a more energetic binary population where all the binaries are hard in a high density cluster, the primordial population and initial distribution of binary parameters will be more difficult to alter by gravitational interactions. If one assumes that the high density initial system is the likely initial state of the cluster in order to produce a substantial portion of massive runaway stars then the conclusion is that the exact initial population of binaries is not of large consequence unless they are very closely bound primordially. What is important in order to fit the observations is that there are at least some primordial

binaries since the BF0 case ejects no high velocity binaries. At lower densities the initial primordial binary population becomes much more significant in terms of ejection rates and collision rates. However, even with 100% initial binaries the medium density cluster does not produce any high velocity massive binaries. This is of some significance since high velocity massive double lined spectroscopic binaries are observed among the runaway stars which would indicate that they are likely to be produced in the denser environments.

3.2.5 Initial Separation - Binary Energy ($N_{run} = 20$)

By assuming a closer distribution of separations for the primordial binaries one may expect that both scenarios produce a higher number of runaways due to the fact that the ejection velocities depend on the energy of the binary. Both mechanism derive their runaway velocity from the orbital velocity of the stars in the binary. The dynamical ejection scenario will now have a harder population of binaries which will interact strongly. In competition to these harder interactions is the rate of interaction which may decrease due to the fact that harder binaries will have a smaller cross-section for interaction. By contrast the SNB scenario will have more closely bound massive stars whose companions may be ejected as runaways once the primary erupts in a supernova.

Considering the medium density and high density simulations, a set of simulations were run at these densities with an initial separation range of $10 - 10^4 R_\odot$ where the initial separation range in the previous simulations was $10 - 10^6 R_\odot$.

Table 3.12 shows the single star ejections for the medium density and high density clusters and Table 3.13 shows the binary star ejections for both clusters. For the medium density cluster a larger population of DE escaping low velocity low mass single stars escape from the standard simulations then the cluster simulated here. By contrast, a larger binary population escapes from the closely bound simulations. At larger velocities the DE single stars become more numerous in the closely bound simulations as the increase in orbital energy results in higher velocity escapees. The increase in B star runaways from the standard simulation is 3 times. Equally significant, ~10% of low velocity O stars are dynamically ejected which is encouraging since DE O stars seem under-produced in the previous simulations by comparison the observed fraction of field stars.

At high density there are 1.5 times fewer single dynamically ejected escapees. This, however, is offset by the fact that there are equally 1.5 times more binary escapees. In general the escape rates are comparable between the standard simulations and these simulations. This is qualitatively similar to the results found by Leonard & Duncan (1988). However, at runaway velocities and high masses the percentage of dynamically ejected stars is now higher by a factor of 1.2. The most significant result is that there is a substantial and significant increase in the population of O star ejectees. Approximately 10% O stars are being ejected with runaway velocities and ~2/3 of these produced as a result of collisional mergers. Further, a ~25% binary fraction of O star runaways is also produced.

At medium density only 1.3% of initial binaries have a companion which erupts in a supernova. This reduction in supernovae occurring in binaries is as a direct result of many more binaries merging before the primary explodes. However, the more energetic, tighter binaries still produce more massive B star runaways, 4.5 ± 1.1%. This is 1.3 times the number of massive B star runaways as in the standard simulation.

Similarly in the high density cluster 1.3% of initial binaries have a companion which erupts in a supernova. However, the number of massive SNB B star runaways is still smaller than the medium density cluster here as with the previous simulations, 3.6 ± 1.0%. The reason for this decrease is discussed in detail in Chapter 3, section 3.4.2.3 and is deferred till then. Nonetheless, this is a 1.5 times increase from the standard simulations with a high density cluster.

Table 3.12: *Dynamical Ejections (Single Stars) for an initial distribution range for binary stars of* $10 - 10^4 R_\odot$. *Medium Density Simulations (Top) : High Density Simulations (Bottom).*

Escape Velocity	**% of Total**	**% Early B stars**	**% O stars**
Medium Density			
0-10km/s	5.2 ± 0.2	1.5 ± 0.7	0
10-30km/s	0.41 ± 0.07	1.5 ± 0.7	10.0 ± 5.7
>30km/s	0.22 ± 0.03	1.8 ± 0.6	0
High Density			
0-10km/s	7.7 ± 0.3	4.5 ± 1.2	0
10-30km/s	1.0 ± 0.1	4.5 ± 1.2	6.7 ± 4.7
>30km/s	0.73 ± 0.07	4.8 ± 0.9	10.0 ± 5.7

In summary, the effect of a smaller initial range in separations has a significant affect on both mechanisms. Increasing the runaway B star population by broadly 1.3-1.5 times for the SNB B star runaways and ~1.2 times by dynamical ejections. The effect on the ratio of DE:SNB ejected runaway B stars is then that the SNB fraction of runaways increases. The compelling result for the DE scenario is that the O star population becomes close to what is observed along with an appreciable binary fraction of runaways. This lends further support to the high density cluster with a closely bound initial binary population as a possible initial condition for young OB star clusters.

Table 3.13: *Dynamical Ejections (Binary Stars) for an initial distribution range for binary stars of* $10 - 10^4 R_\odot$. *Medium Density Simulations (Top) : High Density Simulations (Bottom).*

Escape Velocity	**% Binaries: Total**	**% Binaries: Early B**	**% Binaries: O stars**
Medium Density			
0-10km/s	39 ± 3	55 ± 28	0
10-30km/s	27 ± 8	0	0
>30km/s	0	0	0
High Density			
0-10km/s	41 ± 2	58 ± 16	0
10-30km/s	34 ± 6	46 ± 15	0
>30km/s	11 ± 5	21 ± 14	25 ± 25

3.3 Primordial Mass Segregation (N_{run} = 20)

Mass segregation was discussed in the section on Initial Conditions at the beginning of this chapter. As noted, mass segregation may occur rapidly through dynamical processes and it is also important to investigate the possibility and ramifications of primordial mass segregation. This may have occurred due to the mass of the innermost stars becoming much larger due to the accretion of gas and the general in-fall of matter (Bonnell et al., 2001) or through collisions between intermediate mass stars resulting in massive star formation (Bonnell et al., 1998; Bonnell & Bate, 2002). These massive stars may then halt subsequent star formation in the cluster as they 'switch on' becoming main sequence objects and their strong stellar winds eject the gas on a short timescale (of the order of a cluster crossing time). They then leave a central region of the cluster containing the more massive stars surrounded by the lower mass stars.

Typically the initial positions of the stars are chosen in the code according to a specific distribution. In the simulations here stars were distributed uniformly within a spherical volume. A Plummer model (Plummer, 1911) or King models (King, 1966) with various parameters are other examples of frequently used distributions to model star clusters (see section 3.6 for more on the Plummer model). Velocities for the stars are then randomly selected in magnitude and direction so long as the star is initially bound to the cluster, which is based on its position, mass and velocity within the cluster. In order to simulate primordial mass segregation with the code the massive stars need to be placed in the centre of the cluster with low velocities. The intention is, through a self consistent manner, to create an approximate form of mass segregation in our clusters, which is in a state of approximate equilibrium and which retains the massive stars in the centre of the cluster. This is done by allowing the system to segregate dynamically as has been done by other authors (Vine & Bonnell, 2003) and suggested in Mackey et al. (2007). The dynamical segregation configuration is then considered to be similar to primordial segregation and these values of velocities, masses and positions can then be used as the initial conditions for a new, primordially mass segregated, cluster. It should be stressed that this is not how we expect primordial mass segregation to have occurred, it is simply a sufficient means for artificially creating a mass segregated system. Hence, for a dedicated simulation, the system was set up as in the original model but for reasons relating to the input and the code all the stars were initially single. This is due to the original setup of the code which

allows for the masses, velocities and positions of stars to be read in from a file as the initial conditions for the cluster. It is more difficult to consistently change the code in order for binaries and their related parameters such as eccentricity and periods to be also included in the input and since the goal is simply to produce a form of mass segregation a single star cluster is expected to suffice for these purposes. The system was allowed to evolve dynamically (stellar evolution was switched off (see Appendix 2.2 for more on alternative options in the nbody6 code)) for a short time and the ratio of the average distance from the cluster centre of the massive stars (arbitrarily greater than $3M_{\odot}$) to that of the less massive stars was calculated for each time output. We assume a sufficient degree of mass segregation to have occurred when this ratio has reached a minimum, i.e. the massive stars are, on average, at a smaller distance to the cluster centre then the low mass stars. The mass, velocities and positions of the stars are now used as the initial conditions for a new unscaled system which has 50% binaries (where the binaries are generated from splitting the masses of the massive stars). A small adjustment was made for consistency by scaling the total mass of the system by a constant, due to the fact that the binaries were created from the massive single stars in order to give the same number of massive stars as in the other simulations.

Table 3.14 shows the dynamical ejection results. Figures 3-3 and 3-4 show a comparison of the results for single and binary ejectees with the unsegregated medium density cluster. Figures 3-3 shows that there is a significant increase in the number of escapees at all velocities and mass cutoffs. The increase in dynamical ejections is of the order of 20% more than that of the unsegregated case for all stars and of the order of 30% more for high velocity massive runaways.

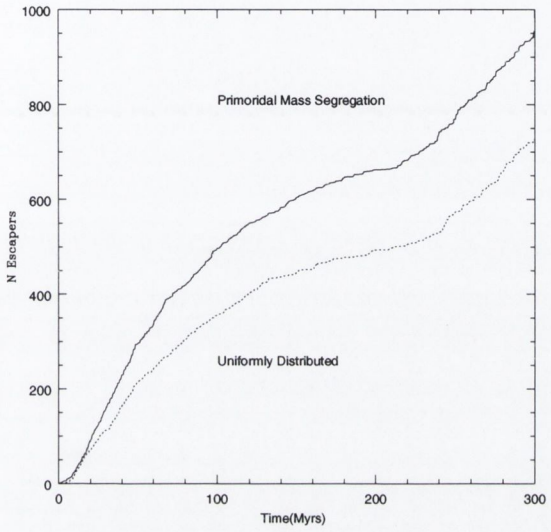
Figures 3-4 shows that there is a significant increase in the number of dynamically ejected massive binaries, up to three times as many, as that of the unsegregated cluster. Further, ~50% of massive B star runaways are binaries where in the medium density unsegregated cluster no B star runaway binaries were ejected. What is interesting to note is that while the number of escapees from the initially mass segregated clusters are higher than the unsegregated counterpart, the ejection rates do not appear to be all that dissimilar. The higher number of ejectees coming from the mass segregated models appear to be due to an extension of the ejection rate over a longer period. This may be due to the fact that the ejections from the mass segregated model are produced almost immediately while

there is a lapse of a few million years in the homogeneous cluster as the system relaxes before higher velocity and massive star ejections occur. This time is probably due to the contraction of the cluster, mass segregation and the formation of a dense core in which such energetic encounters may occur. The first ejected high velocity massive stars typically occur around 4 Myrs in the unsegregated cluster, which is reasonable since mass segregation is expected to occur of the order of the relaxation time $t_{seg} \sim \frac{<m>}{m_{massive}}.t_{rh}$ (which is in such a cluster of the order of 2Myrs), where t_{seg} is the mass segregation time, $< m >$ the average cluster mass, $m_{massive}$ mass of a population of massive stars, t_{rh} the half-mass relaxation time (Binney & Tremaine, 1987). Such a configuration is naturally already present in a primordially mass segregated model hence the ejection of stars occurs more readily. The time for mass segregation to be complete is of the same order of time for the first hard interactions between massive stars to occur in the core and to eject stars, this may also be the criterion for maximum mass segregation in a given cluster (Mackey et al., 2007). The conclusion is that a mass segregated system is likely to have a marked increase in the number of ejected massive stars and multiple systems. It is also important to note that the ejections in the mass segregated cluster occur at early times. If gas removal is fast and driven by the massive stars having formed in the centre of the cluster, then this will cause the central region to expand suppressing the interaction rate. The crossing time of the cluster is less than half a million years which is then the same order of time which one might expect gas ejection to occur (Boily & Kroupa, 2003a). However, also note that according to Vine & Bonnell (2003) the mass segregated core is likely to survive gas expulsion even at low star formation rates, which would lead to a central core of massive stars. The massive stars survive the ejection of gas due to the fact that they have low velocity dispersions and it is likely that star formation efficiency will have been higher in the core than the rest of the cluster due to greater accretion rates.

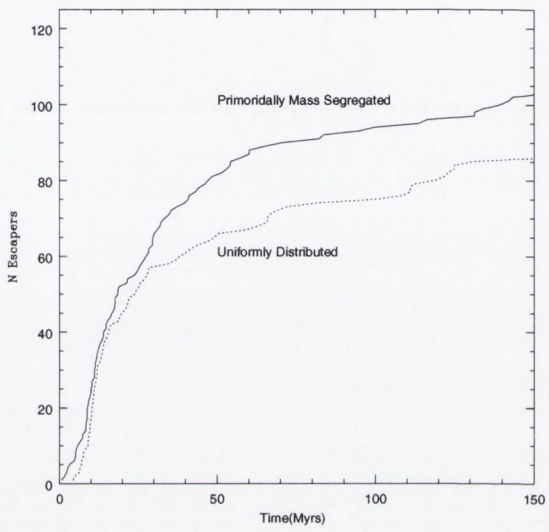
Table 3.14: *Dynamical Ejections: Single and Binary star ejectees. Primordial mass segregated medium density cluster.*

Escape Velocity	**% Total**	**% Early B stars**	**% Binaries: Total**	**% Binaries: Early B**
0-10km/s	9.1 ± 0.3	2.9 ± 0.9	28 ± 2	36 ± 14
10-30km/s	0.7 ± 0.1	2.9 ± 0.9	23 ± 5	62 ± 29
>30km/s	0.23 ± 0.6	0.9 ± 0.7	23 ± 15	56 ± 41

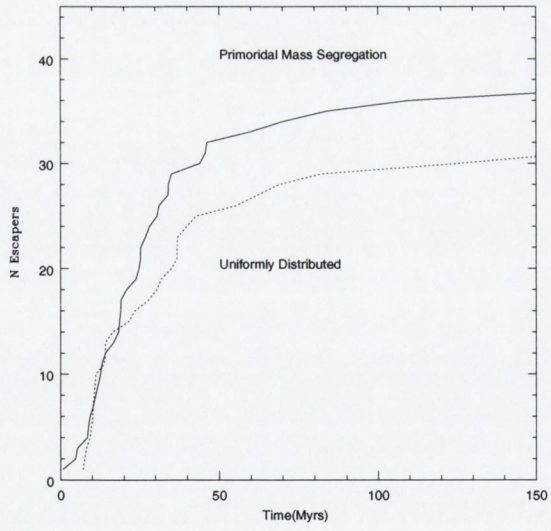
Figure 3-3: *Escaping stars for the primordially mass segregated case and the initially uniformly distributed case. Figure a) (Left) Shows the single escapees. Figure b) (Right) shows the single escapees with velocities greater than 10km/s. Figure c) Middle shows the single OB escapees. OB runaways are not shown due to the small numbers involved*



(a) All Single Escapees

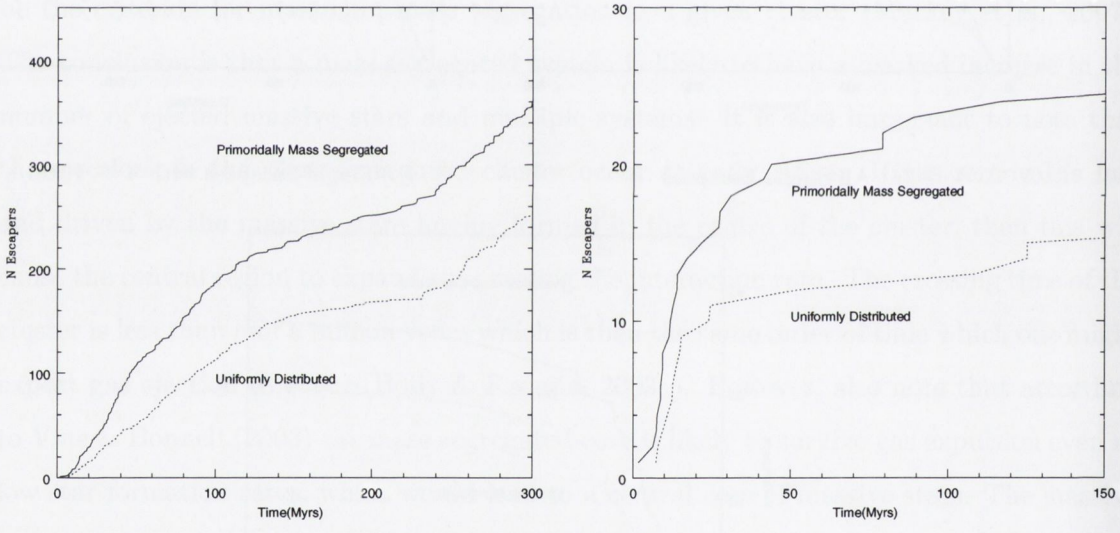


(b) Single Escapees with V > 10km/s



(c) Single OB Escapees

Figure 3-4: *Escaping stars for the primordially mass segregated case and the initially uniformly distributed case. Figure a) (Left) Shows the binary escapees. Figure b) (Right) shows the binary escapees with velocities above 10km/s.*



(a) All Binary Escapees

(b) Binary Escapees with V > 10km/s

3.4 Gas Expulsion (N_{run}= 20)

Lada & Lada (2003) show from observations of star formation regions that the fraction of gas used up by stars when created is relatively small, and may not exceed 10-30% of the original total. This would suggest that young stars in young clusters should be embedded in gas. However, many young clusters such as the ONC, R136 and 30 Doradus have had their gas content already removed implying that gas expulsion must occur rapidly. Hills (1980); Lada et al. (1984); Goodwin (1997); Melioli et al. (2006) among others suggest that this expulsion may occur in less than a crossing time even for dense systems. Fellhauer & Kroupa (2005) suggest that star formation efficiency (SFE) may be related to the concentration or size of the cluster, with low density systems having higher star formation efficiencies. A low star formation efficiency can result in the cluster becoming completely unbound after the gas is blown out which could explain the disperse nature of OB associations and their expansion. With a cluster becoming unbound and expanding this is expected to have a significant effect on the ejection of high velocity stars. The fraction of stars that is retained by the cluster also depends on the radial density profile of the pre-expulsion cluster (Boily & Kroupa, 2003a,b),BK03, and on the relative distributions of stars and gas (Adams, 2000). BK03 also show, both analytically and through simulations, that star clusters must develop massive cores of high binding energy if they are to remain bound at low star formation efficiency. The expulsion of residual gas from star clusters has been modelled by several authors (Lada et al., 1984; Goodwin, 1997; Geyer & Burkert, 2001; Kroupa & Burkert, 2001; Boily & Kroupa, 2003a). The typical method is to represent the gas as an additional external potential which is removed on a certain time-scale. Gas removal from a cluster may be expected to be effectively instantaneous, i.e. to occur in less than a crossing time. Thus, we can approximate gas removal by modelling the cluster as a system that is initially out of virial equilibrium (equivalent to starting the simulations at the end of the gas expulsion phase).

In the following we show how the virial ratio is chosen for the initial set up of these simulations.

The scalar virial theorem is

$$2K + W = 0 \tag{3.5}$$

where K is the kinetic energy $= \frac{1}{2}M < v^2 >$ and $|W|$ may be defined as $\frac{GM^2}{R_g}$ from Binney & Tremaine,where R_g is the gravitational radius defining the size of the system. Rearranging

then gives the root mean square speed of the cluster's stars v_i, where M_{init} is the total initial mass of the cloud

$$< v_i^2 >= \frac{GM_{init}}{R_g} \tag{3.6}$$

Note that Spitzer (1969) showed that the gravitational radius is a fraction of the half mass radius $r_h \sim 0.4r_g$ and knowing the half mass radius one can determine what the virial radius is for a given distribution (cf. the above with Eqn 2.5).

Gas expulsion is considered instantaneous here, therefore the velocity dispersion which is coupled with the original mass of the system (i.e. the mass of the gas cloud) is the velocity dispersion expected for the stars which actually form. The fraction of stars which form from the initial gas cloud is related via the star formation efficiency parameter, defined as

$$\epsilon = \frac{M_*}{M_{gas} + M_*} = \frac{M_*}{M_{init}} \tag{3.7}$$

where M_* is the mass of the formed stars, M_{gas} is the mass of the expelled gas and M_{init} is the original total mass. The ratio of the kinetic energy to the potential energy of the cluster is called the virial ratio, Q, and the system is said to be in virial equilibrium when Q = 0.5. We are now interested in the virial ratio after the gas has been expelled. We may write this using the equations above and considering the potential and kinetic energy remaining in the cluster. The gravitational potential comes from the remaining mass, contained within the mass of the constituent stars in the cluster M_*. The kinetic energy is now in the velocity of these stars of mass M_*.

$$Q = \frac{K}{W} \tag{3.8}$$

$$Q = \frac{R_{vir.} < v_i^2 > .M_*}{G.M_*^2} \tag{3.9}$$

using equation 3.6 for the root mean square velocity and equation 3.7, which then gives the virial ratio after gas expulsion in terms of the star formation efficiency.

$$Q = \frac{1}{2\epsilon} \tag{3.10}$$

hence for a star formation efficiency of $\epsilon = 1$, where all the material is converted into gas Q = 0.5 (virial equilibrium).

For systems with a star formation efficiency as low as 0.2 a centrally bound core may still survive (Baumgardt & Kroupa, 2007). The reason for this is that the stars form from a virialised system (though this may not be strictly true);then, assuming a Maxwellian

dispersion of velocities, it is likely that some stars will have very low initial velocities which will still be lower than the escape velocity for the cluster once the gas is expelled. Therefore a small bound core may survive depending on the subsequent dynamics of the system. Unbound stars are however, not lost instantaneously since they escape with a velocity of the order of the root mean square velocity. This means that stars may be associated with the cluster for a long time, until ~40Myrs after the gas has been expelled. These stars then produce a tail in the surface brightness profile and produce observed excess light at large radii. Models with 40-50% star formation efficiency produce the best matches to observation (Bastian & Goodwin, 2006). We conservatively chose a star formation efficiency of 0.5 corresponding to a virial ratio of 1.0 for our high density configuration. Note for comparison that Scally et al. (2005) estimate that the ONC has a virial ratio of about 1.5.

3.4.1 Results and Discussion

The results for the dynamical ejections from the high density simulations with Q = 1 initially are shown in Table 3.15. The simulations are then compared with the standard high density simulations from subsection 2.4.1.4 where Q = 0.5. As expected the rate of escape with an expanding systems after gas expulsion is higher than the escape fraction from the standard high density cluster. This is due to the high mean velocity of stars within the system which thus escape easily, requiring little interaction to do so. However, the rate of ejection of higher velocity stars is curtailed due to the lack of close interactions. This also results in over twice as few massive stars escaping and of the order of 1/100th of the number of massive runaways being produced. Clearly this has serious consequences for the viability of the dynamical ejection scenario for producing massive runaways. As mentioned, previous investigators have shown that a bound cluster may survive even at relatively low star formation efficiencies. However, they also note that the cluster core is significantly expanded and here this becomes the debilitating factor for DE runaways as it results in fewer strong interactions.

The average core radius is typically twice that of the standard high density cluster which is consistent with results from Baumgardt & Kroupa (2007) who present a broad suite of simulations covering SFE, gas expulsion timescales and cluster size. They further show that the more concentrated the system is initially, the greater the effect gas expulsion has. This is easily understood since the more concentrated the initial system is, the higher

the average velocity of the components. Once the gas is expelled the system is free to expand comparable to that rate. Naturally, primordial mass segregation will make the system more resilient to the disruptive effects of gas expulsion which in fact gives further evidence that mass segregation should be primordial since a rapidly expanding system can not dynamically segregate quickly. Thus, since the high density cluster has been shown to able to produce statistics similar to the observed values particularly in terms of high velocity massive binary ejectees then it is likely to be a viable mechanism. However, gas expulsion reduces the rate significantly and the relative increase in dynamical ejections as a result of primordial mass segregation is unlikely to compensate adequately for this. This implies that a larger initial density may be required in order to produce a significant number of both single and binary star massive runaways which may be consistent with observation. This density may have to be of the order of 10^5 stars per pc or higher. Large primordial densities are not unrealistic, as has also been suggested by Bonnell & Bate (2002) in order to generate massive stars through collisional processes in star clusters. DE runaways must then be produced by clusters which are extremely dense initially. Stellar collisions and mass accretion occur in the cores, producing massive stars and resulting in a primordially mass segregated cluster. Once the massive stars blow out the residual gas, star formation halts and the cluster rapidly expands, perhaps leaving a dense core of massive stars of high multiplicity. These massive stars dynamically interact on short timescales resulting in massive high velocity stars being ejected through an expanding halo of lower mass stars. Note that ejections of pre-main sequence stars may occur in such a scenario (Sterzik & Durisen, 1995; Sterzik et al., 2001), perhaps before the gas has been expelled from the system.

Table 3.15: *Dynamical Ejections: High Density Cluster: Gas Expulsion*

Escape Velocity	**% of Total**	**% of early B stars**	**% Binaries: Total**	**% Binaries Early B**
0-10km/s	14.6 ± 0.4	6.3 ± 1.3	40 ± 2	42 ± 7
10-30km/s	0.14 ± 0.03	0	17 ± 8	100 [0.09]
>30km/s	0.08 ± 0.03	0.02 ± 0.02	0	0

3.5 Population Size

It is of interest to know if the frequency of high velocity escapees will scale with the population of the cluster. To what degree this changes the number of ejected runaways is of importance since the initial populations of young clusters vary from 10's to 1000's of stars. As noted in the previous section it may be the case that stars form in initially large systems but which become mass segregated and fragmented in such a way as to leave small N clusters in the core. On the other hand if the system is initially much larger this may result in a higher number and fraction of ejections.

3.5.1 N = 45 (N_{run} = 60)

Following Leonard & Duncan (1988) we adopt a system with the same population size, N = 45, and binary fraction of 50%. We also constrain the mass range in order to have a system which has a significant population of massive stars. If we used a typical IMF and the mass range as before, 1-120$_\odot$, then only a few massive stars would be likely to be generated in an N = 45 cluster. Hence, we constrain the mass range and create a cluster comprised entirely of massive stars, 5.9-120M$_\odot$ (i.e. all stars are OB). Changing the mass range in this way will alter the dynamics of the system making it difficult to compare our results directly with any of the previous simulations. The number density is equivalent to the medium density cluster but the central potential is now much larger and has a shorter relaxation time. It should also be noted that the ratio of B stars to O stars is also slightly different to the previous N = 450 simulations since we've constrained the mass range. Recall that in our 450 star clusters there were ~2 O stars and ~18 B stars initially. In this case there are ~41 B stars and ~4 O stars initially. However, what is important here is to see the fraction of OB runaways which may result from such a system and try and add it to our overall framework. The cluster may also be thought of as super-segregated system. Considering the analysis of the previous section a primordially segregated system may leave a core of massive stars which may then become isolated due to rapid gas expulsion and the outer stars escape from the system. Thus our N = 45 cluster is an extreme case of such a cluster, but may in part be indicative of the real situation. The simulations here differ from Leonard & Duncan (1988, 1990) simulations since mass loss, circularisation and physical collisions are now included in the code and we integrate our system for a much longer time.

The dynamical ejections for single and binary OB stars are shown in Table 3.16. We

compare our results with the medium density cluster simulations discussed at the beginning of this chapter since the number densities are equivalent although it is expected that the dynamics be different (see Table 3.1). For ease of reference we refer to that medium density simulation as MD450. The MD450 cluster dynamically ejects on average (over 100 runs) only 0.11 B star runaways. By contrast, since the cluster discussed here is made entirely of OB stars it dynamically ejects on average (over 20 runs) 0.18 runaway B stars per cluster, 1.6 times more than the MD450 cluster. However, this leads to an ejected percentage of B star runaways of only 0.4 ± 0.1% since we have defined the ejection percentage as $\frac{\Sigma RunawayBstars}{\Sigma Bstars}$. This is 40% smaller than MD450 B star runaway fraction. The O star percentage is relatively higher at 2.5% since no O stars were ejected from MD450. While this is an idealised version of the real situation it does highlight two factors. One, that such a cluster composed entirely of massive stars does not result in an increase in the dynamically ejected OB runaway percentage. Two, dynamical ejections in a low N system can produce a reasonable percentage of OB runaways which would naturally become larger at higher densities.

Table 3.16: *Dynamical Ejections: Medium Stellar Density Cluster (All OB stars) : N = 45*

Escape Velocity	% early B stars	%O stars	% Binaries: B stars	% Binaries: O stars
0-10km/s	4.5 ± 0.43	0.5 ± 0.5	22 ± 5	0 ± 0
10-30km/s	1.2 ± 0.22	1.3 ± 0.8	12 ± 6	67 ± 42
>30km/s	0.43 ± 0.14	1.3 ± 0.8	20 ± 7	0

The frequency of SNB ejected massive runaways is estimated in the usual fashion. The rate of ejection of SNB massive stars per cluster is 4 times that of the MD450 due to the fact that every binary supernova has a massive companion B star. This, however, once more results in a lower relative fraction of ejected B stars with the SNB scenario producing potentially only 1.8 ± 0.4% of the B stars as runaways, nearly half the expected percentage of MD450. The O star percentage is potentially 1.7% ± 1.2.

Overall such a low N system is viable for producing the entire observed fraction of OB runaways. With 0.4% from DE and 1.8% from SNB then we have 2.2% ejected B star runaways. The total O star percentage is low at (2.5% + 1.7%) 3.2% but more detailed analysis of mass transfer is likely to produce companion systems of much larger mass before

the eruption of the primary in a supernova. Further, the occurrence of massive binary runaways at this stellar density lends greater weight to such a configuration. Hence, a low N massive system of medium to high density as defined here is a strong contender for being the type of system from which OB runaways are produced. The key is to whether or not such a system consists of the vast majority of all OB stars and is what is produced from star formation scenarios. The former point is a crucial issue. As we have seen, even though both mechanisms produce many OB runaways the relative fractions are reduced due to the larger number of OB stars present in the first place. If a significant population of OB stars exist outside of the cluster centre then this would reduce the OB runaway frequency even further, particularly for DE runaways. The latter point of producing such a massive centrally segregated system may fit well into a star formation framework as noted in the previous section, where massive stars can only be produced in the centre of a dense cluster either due to increased accretion rates or collisions that occur there. Even those stars which are produced further from the centre will be drawn to the centre due to energy equipartition. Once the gas is expelled then a central isolated system may be the natural result composed of the majority of OB stars. Many clusters have central massive Trapezia such as the trapezium in the ONC which dynamically eject massive stars (also see Allen et al. (2006). Our previous objection to the medium density cluster as being a viable candidate for the initial density for a cluster was the fact that no massive runaway binaries were dynamically ejected. However, we now find a ~17% high velocity massive binary ejection rate from such a massive cluster. This is encouraging since, as noted, the core of a cluster with an initially larger population will also expand once gas is expelled. Hence, even were the system to have a high density initially the surviving central region will have a core density typically lower. Hence, we conclude that a medium to high density low N system is a credible neighbourhood for producing massive runaway DE stars. Note that Clarke & Pringle (1992) suggest that the IMF may be skewed at high masses in order to explain the observed fractions of O stars and suggest that massive stars form in small groupings of N = 20-30 and they too require that such groupings be highly concentrated. The DE:SNB runaway B star ratio is 18:72 for N = 45 which is quite similar to the ratio for the medium density cluster of N = 450 but with the total runaway percentage now only 2.2% instead of 4.0%. Hence, for a high density low N cluster the ratio may be similar to the high density N = 450 cluster and have a total runaway ejection percentage, ~3.2%

that is between the expected 2-4% instead of the 6.4% found for the high density N = 450 cluster and gives a DE:SNB ratio of 50:50 for ejected B star runaways.

3.5.2 N = 4500 (N_{run} = 20)

We finally consider a cluster of much larger size with a population of 4500 stars, a binary fraction of 0.5 and a number density equivalent to the aforementioned MD450 cluster (this corresponds to a cluster initial radius of 1.185pc and due to the densities being equivalent, a higher velocity dispersion of 4.4km/s). The relaxation time is however much longer at 13.4Myrs.

The results are shown in Tables 3.17. The percentage of massive escapees due to dynamical interactions is severely curtailed despite a larger population of stars. The central escape velocity for MD450 is $\sim$ 5km/s while here it is $\sim$10km/s. This may explain in part the reduction of high velocity massive escapees. In general 3 times as few stars escape the cluster and $\sim$6 times fewer massive runaways occur by comparison to the MD450 cluster.

The escape rate for massive SNB stars is significantly smaller, $\sim$1.6 times, than the MD450 case and is estimated to be $\sim$1.0%. The larger escape velocity in this system can account for this difference as stars are slowed considerable before being able to escape resulting in fewer stars escaping in general and fewer high velocity escapees.

These results indicate that as the system becomes more massive the potential can become a dominating factor restricting the ejection of a large fraction of high velocity stars by comparison to a smaller system. The ratio of DE:SNB for B star runaways in this instance is 10:90, with the total fraction from both scenarios being 1.11%. If clusters were predominantly formed with this population size and density then the SNB scenario will account for the vast majority of OB star runaways. On the other hand, if such populous cluster were to predominantly produce OB runaways then their initial densities much be much larger and their binary separation distribution range smaller.

Table 3.17: *Dynamical Ejections: Medium Density Cluster: N = 4500*

Escape Velocity	% of Total	% of early B stars	% B star Binaries
0-10km/s	1.13 ± 0.020	0.07 ± 0.03	20 ± 10
10-30km/s	0.164 ± 0.009	0.09 ± 0.04	0
>30km/s	0.062 ± 0.013	0.11 ± 0.06	0

3.6 The Plummer Model vs Homogeneous Sphere

3.6.1 Introduction

Many authors adopt a Plummer model configuration for the initial state of their clusters. The Plummer model was first used to fit globular clusters and galaxies and has since been used in simulations for general clusters due to its simplicity. However it is not well established that this is indeed the state of a young cluster immediately after star formation has ceased. Mackey et al. (2007) show that Plummer models are not ideal when applied to the simulations of young clusters.

Nevertheless, it is important to characterise the effect on the runaway ejection rate of beginning with a system with a different initial matter distribution. Considering two different distributions it is necessary to determine in what way the two distributions may be similarly matched. On the one hand the gravitational potential of the system is what governs the overall dynamics of the cluster while on the other hand the stellar number density is a key factor behind the rate of interactions, where this may be loosely considered as being proportional to ρ^2. This results in two distinct configurations which need to be explored. We may ask the questions a) "For a given number of stars arranged in one of two ways with a given central number density (and hence interaction rate), how does the number of runaways/type of runaways vary with potential well depth?" and b) "For a given number of stars, arranged in one of two ways within a potential well of given central depth, how does the number of runaways/type of runaways vary?"

In the previous simulations we adopted a simple uniform initial density configuration for the positions of stars within the cluster, see section 2.3.2.
The Plummer model has a density distribution given as

$$\rho_{Pl}(r) = (\frac{3M}{4\pi b^3})(1 + \frac{r^2}{b^2})^{-\frac{5}{2}} \tag{3.11}$$

with a potential given by

$$\phi = -\frac{GM}{\sqrt{r^2 + b^2}} \tag{3.12}$$

where M is the total mass and b the scale parameter which sets the concentration of the cluster. The half mass relaxation time is

$$t_{rh} = \frac{0.206.N.a^{\frac{3}{2}}}{(G.M)^{\frac{1}{2}} ln\Lambda} \tag{3.13}$$

Figure 3-5a) shows that the Plummer model has a fairly uniform central density at small radii which then rapidly falls off rapidly at larger radii.

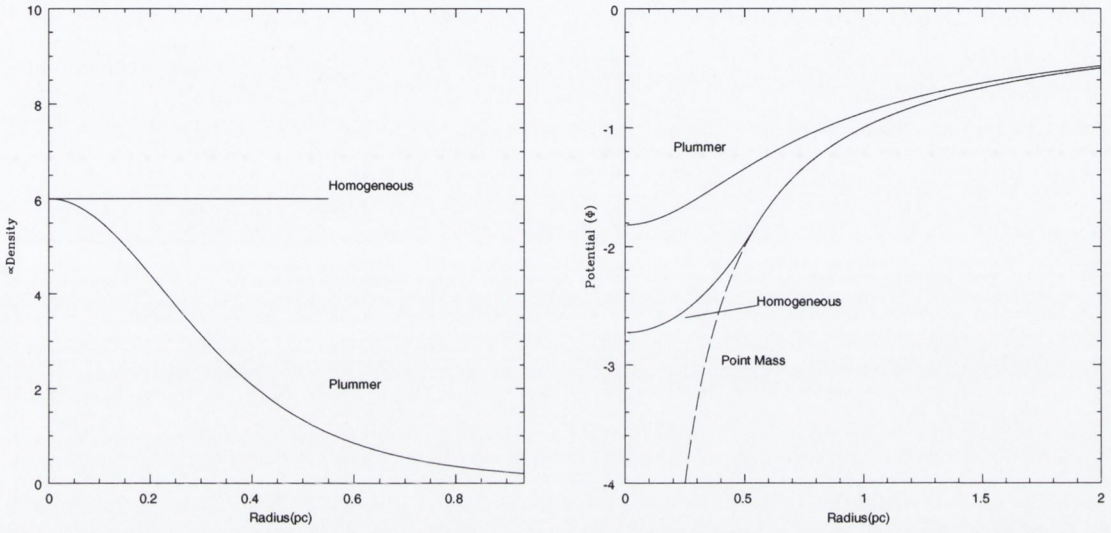
For case a where the central densities are equal (i.e. at r = 0) we have

$$\rho_{Pl}(0) = \rho_{Ho} \tag{3.14}$$

which from equations 3.11 and 2.1 implies $b = a$ (Hereafter, PLED model). This, however, is still not an ideal situation since in the Plummer model the density drops rapidly. One could alternatively consider an increased central density for the Plummer model to that of the homogeneous sphere such that the densities averaged for the whole cluster are similar. This in itself offers hazards since it would now be the case where the interaction rate in the core may be increased for the case of the Plummer model since it is in the core where the majority of energetic encounters occur. Furthermore, both systems will collapse creating a denser central region, at least for a time, than they initially began with, which will complicate matters even more. Therefore setting the central densities equivalent is a suitable starting point bearing in mind the previous comments when it comes to considering the results. It should also be noted that setting the central densities equal results in a half-mass relaxation time for the Plummer model a little over twice that of the homogenous sphere. Hence, one will expect the Plummer model to evolve more slowly than the homogenous sphere. The corresponding potential profiles for this case are also shown in Figure 3-5b).

Again some consideration is required as to how exactly the potentials of the two distributions are to be compared. While it may be preferable in a sense to have the average potentials equivalent such that in some way the majority of objects in either system experience the same potential, this causes a similar issue as mentioned for the central density situation above. Namely that it would require a deeper central potential for the Plummer distribution which then would become a shallower potential as one moves from the centre of the cluster (see Figure 3-6c), which means that the potentials in some parts of the cluster would be higher in one distribution then the other and in other parts be lower. It is reasonable to consider the effect on the results if the entire cluster is consistently higher or lower for a given distribution, hence the central potentials are set to be equal (see Figure 3-6b). The corresponding density distribution is shown in Figure 3-6a) where the initial central density is higher for the Plummer model. From equations 2.2 and 3.12 above, equal central potentials are obtained when $b = \frac{2}{3}a$ (Hereafter, PlEP model). With these parameters the half mass relaxation time is now less than 1.2 times greater for the Plummer model than

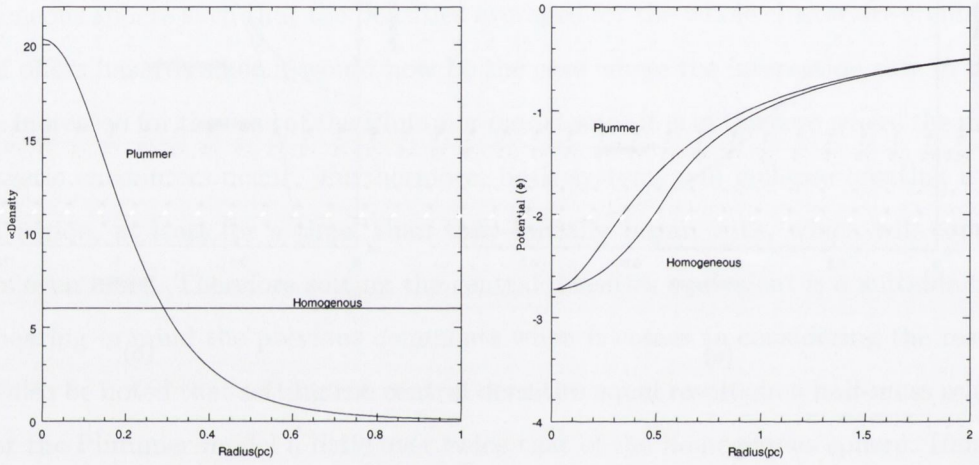
Figure 3-5: *Figure a(left) shows the variation in density for the uniform density case and the Plummer model case where the scaling factor b = a. Figure b(right) shows the corresponding potentials for the Plummer model, homogeneous sphere and the dashed line shows a point mass potential for comparison.*



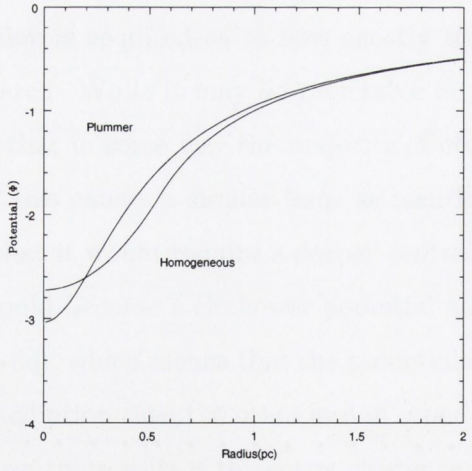
(a) (b)

the homogenous distribution. Hence one would expect the evolution of both clusters to be comparable.

Figure 3-6: *Figure a(left) shows the variation in density for the Homogeneous cluster and the Plummer model case where the central potentials are initially the same. Figure b(right) shows the potentials corresponding to equal central potentials. Figure c(middle) shows an arbitrary situation where the potentials are sought to be matched on average.*



(a) (b)



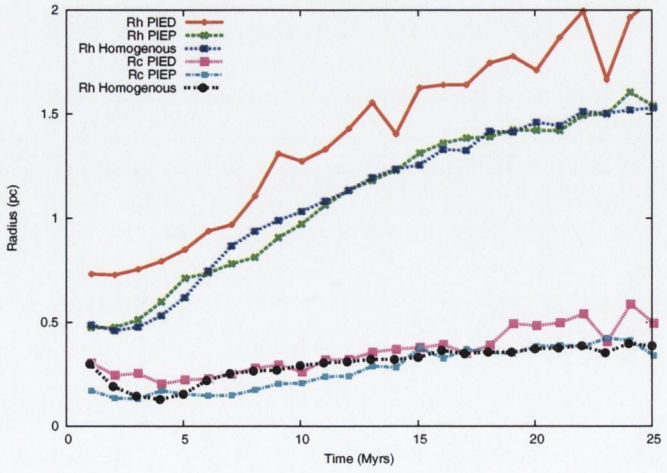
(c)

3.6.2 Results and Discussion

The PlED model where the central density of the Plummer cluster and the homogenous cluster are equal, results in larger virial radius, a shallower central potential and smaller overall velocity dispersion. Naturally then the half mass relaxation time is longer, over twice that of the homogenous cluster, which means that the PlED model evolves on a longer timescale. By contrast the PlEP model where the central potential of the Plummer cluster and the homogenous cluster are equal results in a much more comparable set of parameters in terms of virial radius and half mass relaxation time. In the following discussion we concentrate on the medium density cluster since its dynamical evolution occurs over a reasonable time-frame with relaxation time of ~1.9Myrs where by contrast the relaxation times of the high and low density clusters are ~0.4Myrs and ~14.3Myrs respectively.

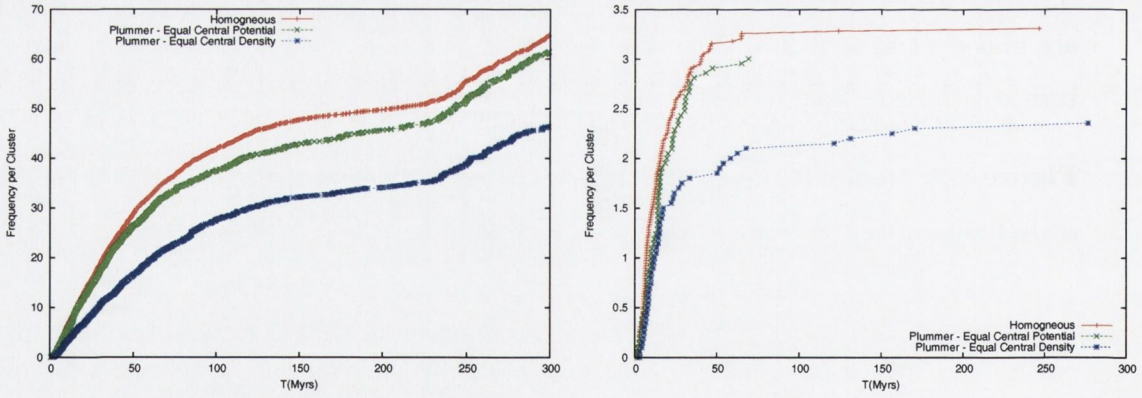
Figure 3-7 shows the evolution of the core radius defined by Casertano & Hut (1985) and half mass radii of the three systems (averaged over a number of runs). The homogeneous cluster core contracts readily as the system collapses until a rebound occurs and the system expands and begins to eject stars. By contrast neither of the Plummer models undergo the same change in terms of contracting half mass radius or core radius. Judging by how well each of the radius profiles match, then the PlEP model appears to follow the homogenous evolution more closely with the PlED model being slightly larger in general. While these are imperfect measures to the extent of similarities in the evolution of such systems they turn out to be indicative.

Figure 3-7: *Medium Density clusters. Figure shows the half mass radii (Rh) and core radii (Rc) evolution of the Homogenous, PlEP and PlED distributions.*



Figures 3-8 show the cumulative distributions of escape for the three systems. The PlED model produces 1.4 times fewer escapees and approximately 1.5 times fewer B star escapees and ~**five** times fewer massive runaway B stars. This large difference in ejected runaways is mainly due to the energetics of the PlED system. The smaller central potential than the homogenous system and smaller velocity dispersion results in interactions which are generally less energetic. Furthermore, a larger core in PlED throughout the evolution of the system indicates that the central region doesn't become as compact as the homogenous model, resulting in weaker encounters which becomes fewer high velocity massive stars. By contrast the half mass and core radii evolution of the PlEP model is relatively consistent with the homogenous system. However, the PlEP model still produces 10% fewer escapees and up to ~50% fewer massive runaways. The collision rate is also lower with approximately 10% fewer collisions occurring. It would seem that the central potential is linked more closely to the ejection rate more so than the central density and that the general initial contraction of the homogeneous system is more effective at ejecting the massive stars.

Figure 3-8: *Medium Density clusters. Figure a)(Left) Total escapees from both Plummer models and the homogeneous model per cluster with respect to time. Figure b) (Right) Total massive B star escapees from both Plummer models and the homogeneous model with respect to time.*



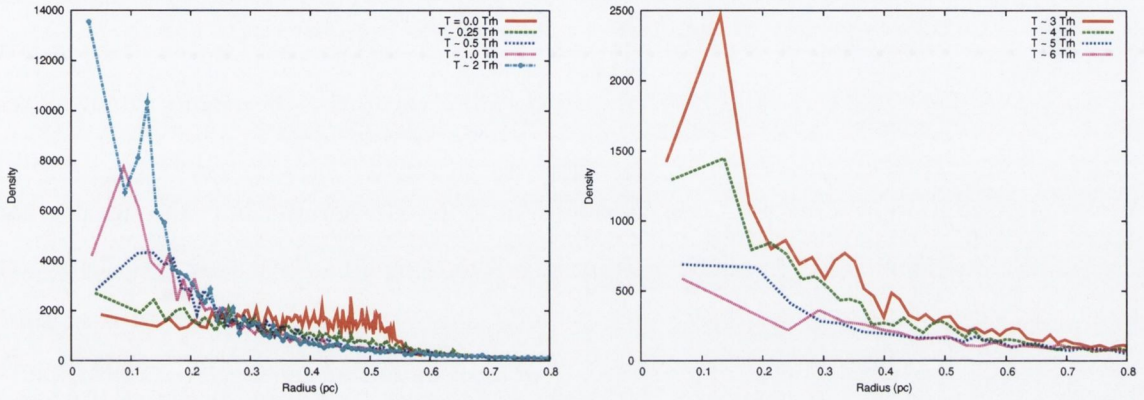
(a) All Escapees

(b) B Star Escapees

Figures 3-9 show the time evolution of the cluster mass density profiles for the Homogeneous cluster. Similarly Figures 3-10 show the evolution of the Plummer model density profiles. The densities are determined by combining the outputs from several runs resulting in an average value. The profiles are noisy due to the low number of stars comprising the clusters and since each cluster evolves differently. Nevertheless, global trends are evi-

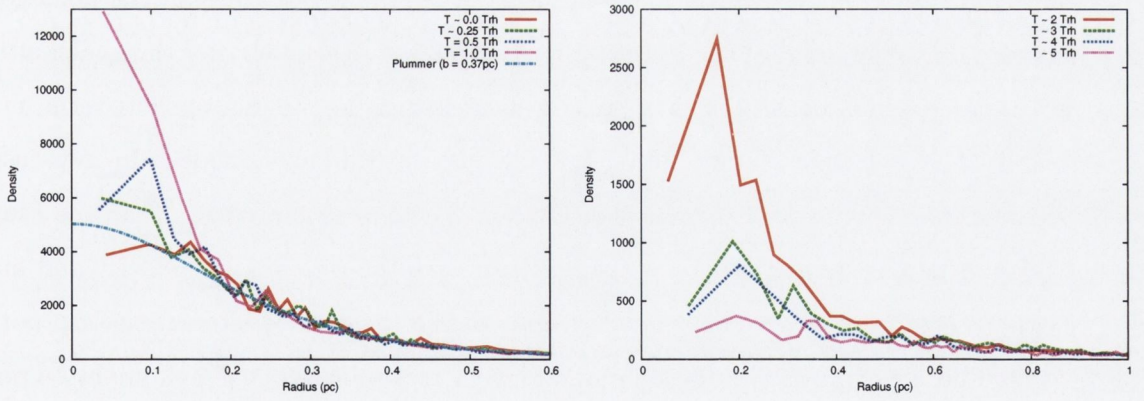
dent and are indicative of the general situation for a given cluster. Figure 3-9a) shows the evolution of the cluster up to twice the initial relaxation time Trh.

Figure 3-9: *Medium Density clusters. Homogeneous cluster mass density profile averaged over a number of simulations. Several relaxation times (Trh) are shown. Figure a(left) shows profiles up to 2 Trh. Figure b(right) shows the profiles up to 6 Trh. Trh ~ 1.9Myrs initially.*



(a) (b)

Figure 3-10: *Medium Density clusters. Plummer model cluster mass density profile averaged over a number of simulations. Several relaxation times (Trh) are shown. Figure a(left) shows profiles up to 2 Trh. Figure b(right) shows the profiles up to 6 Trh. Trh ~ 1.9Myrs initially.*



(a) (b)

The red line is the initial density distribution which is reasonably constant as expected for a uniform initial density. As the system evolves, the green and dark blue lines, the outer regions become more disperse and the central region increases in density as the massive stars

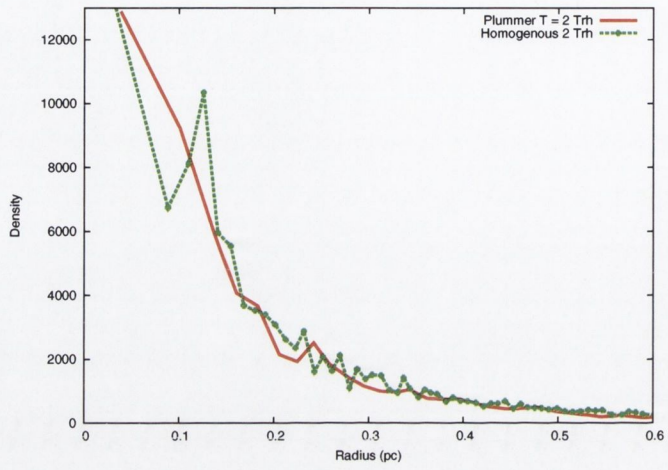
begin to sink towards the centre of the cluster. This leads to a significantly increased central density, pink line, by the order of a relaxation time. Note that the relaxation time changes as the cluster evolves, hence we use the initial estimate of the relaxation time and consider that this estimate may be less reliable at later times. In a relatively short time (twice the relaxation time) the system has reached a maximum density and begins to eject massive stars from the central region, this is evidenced by the peak on the blue line at ~0.1pc. Furthermore, looking in detail at the statistics from the simulations, the first massive star is ejected at ~2.6Myrs (1.4 Trh). By ~4Myrs a stream of high velocity runaway massive stars are ejected. This time also coincides with a minimum core radius value Figure 3-7. Figure 3-9b) shows the subsequent evolution of the system and how the density has now decreased significantly from the maximum as the central massive stars are ejected and the system expands globally. The density profile consistently becomes flatter over time. By 10Myrs (5 Trh) the central density is lower than the initial density ($\sim 1,500 M_{\odot} pc^{-3}$). By contrast Figures 3-10a) shows the evolution of the Plummer model density profile up to 1 Trh ($\sim$ 2.3Myrs). For comparison the initial function profile is shown, light blue line, which corresponds well to the density determined from the clusters, red line. Once more the central region increases in density, however the outer regions appear to retain the original profile. Note that the initial density was $\sim 5,000 M_{\odot} pc^{-3}$ but that the maximum density is comparable to that of the Homogenous cluster at 1 Trh. What is significant is that the high density in the Plummer model appears to decreases more rapidly than the homogeneous cluster. This suggests that the Plummer model ejects stars on a shorter timescale, although the prolonged high density in the homogeneous cluster may be due to short-term multiple systems forming which didn't form as readily in the Plummer model. In any case this results in more high velocity massive ejectees in the homogenous cluster than the Plummer model. It is reasonable that the potential dominates the rate of high velocity and massive ejections even though the concentration may define the rate of interactions the potential may define the energetics of these interactions. A more consistent match might be possible with a slightly more compact Plummer model, perhaps by matching the half mass radii which would result in a characteristic Plummer radius of 0.34 instead of 0.37 and an equal relaxation time to that of the homogenous cluster. It's also worth noting that both profiles are comparable in their outer regions Figures 3-11.

Considering the high and low density clusters adds little more to what has been discussed

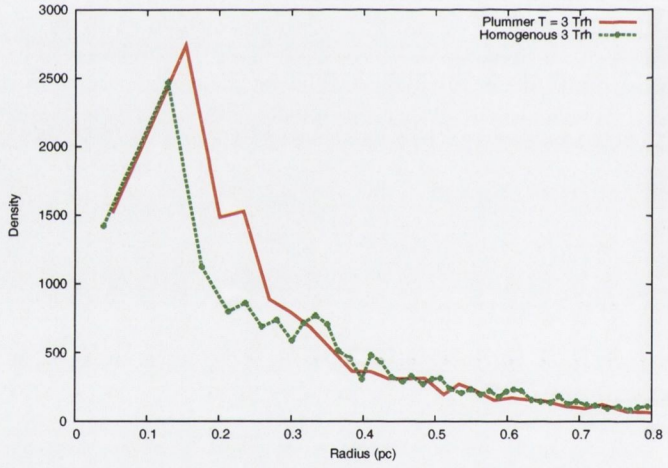
above. The low density cluster has little dynamical evolution which ejects stars making the effect of the Plummer distribution negligible. A point of note is that the escape of low mass low velocity stars is greater in the Plummer model due to stars being more weakly bound in the outer regions than that of the homogenous cluster, thus allowing them to escape more easily. The evolution of the high density clusters is similar to that of the medium density cluster but on shorter timescales and greater energetics of ejections. The same differences in ejections occur when comparing the PlEP, PlED and homogenous models as for the medium density cluster discussed.

Hence we may conclude that a Plummer model distribution of velocities and positions of stars in clusters of low N may evolve in a comparable way to the homogenous model in terms of the rate of ejections of massive runaway stars if the central potential is larger in the Plummer model than that of the homogenous cluster. The models may be more equivalent if their half mass radii are equal. The initial density evolution, as massive stars fall to the cluster centre, of the homogenous system appears to differ from that of the Plummer model with equal central potentials which results in a greater number of ejected massive stars. After approximately 1-2 relaxation times then the density profiles of the Plummer and homogenous clusters appear to be similar.

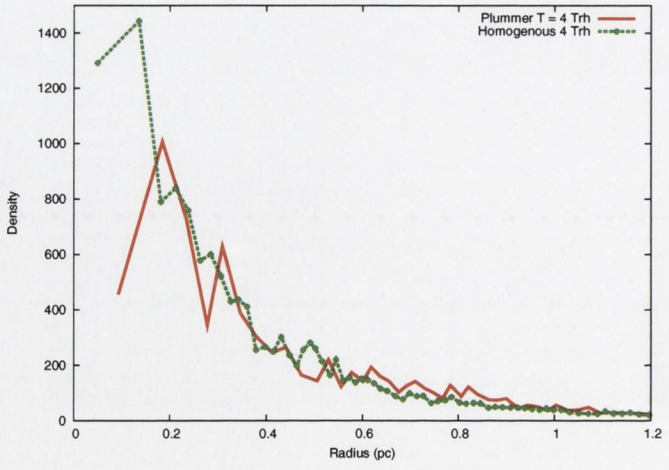
Figure 3-11: *Medium Density clusters. Density profiles at different times for both the Plummer and homogenous cluster*



(a)



(b)



(c)

3.7 Discussion/Conclusions

The dynamical ejection of massive stars is clearly not a simple problem and may be affected by a number of different factors. The dominant factor is the cluster concentration or more strictly the cluster potential, as this generally determines the fraction of massive high velocity escapees from a given cluster. We have also shown how these fractions have changed as we have examined the primordial binary population and energy, mass segregation, gas expulsion, initial cluster population and mass distribution. The difficulty then remains in determining which parameters correspond to a general cluster configuration from which massive runaways are ejected. The population of a cluster generally characterises the dynamics of that system and since there exist a wide variety of clusters where runaways are produced then runaways may be produced, from a number of systems that are dynamically different. If we assume for the moment that the majority of runaways must be dynamically ejected, we may then estimate the conditions that would require this to be the case. A highly concentrated (higher than the high density cluster we simulated), primordially mass segregated, intermediate sized initial cluster with a large binary fraction is likely to be a sufficient starting point. The core must survive the ejection of gas as this will result in a rapid expansion hampering the further ejection of massive stars. Such a highly concentrated, mass segregated, high multiplicity core for star clusters is not unlikely if one considers current theories relating to the formation of massive stars. Massive stars have a higher mass ratio than their lower mass counterparts in general, they have a greater multiplicity fraction and they are found in the cores of young clusters with low velocities. From a star formation point of view it may even be a necessary condition that they occur in such a way, since in the core of a gas cloud mass accretion rates and collision rates are significantly higher. Such an environment may be the only way to produce the most massive stars. When the gas is ejected, the cluster expands and is likely to become unbound but the timescale for this is so rapid that early ejection of massive high velocity stars may already have occurred at the most dense and turbulent time in the cluster's history. Pflamm-Altenburg & Kroupa (2006) suggest that the ONC may have had many more massive OB stars than are currently observed and these may have been ejected already. A binary and two single star runaways have already been identified as dynamical ejectees. However, the ONC is a particularly dense cluster and many OB associations are large in extent. Nevertheless, with a large velocity dispersion initially dense clusters could expand

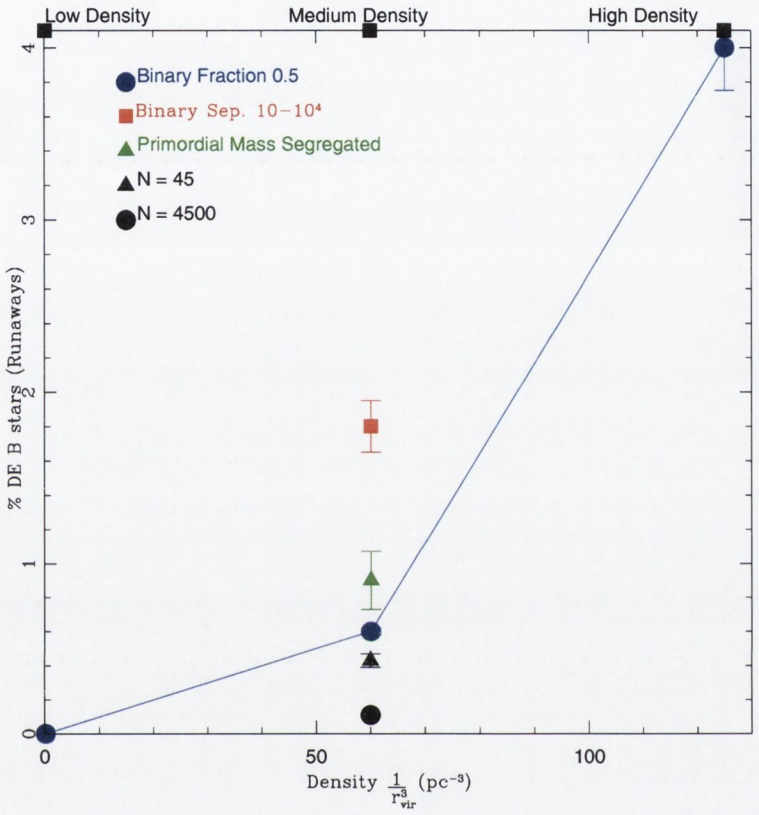
to current sizes within a short time and a large velocity dispersion would be indicative of high initial density as implied. Accurate velocities to within a few km/s are required in order to determine the velocity dispersions and expansion velocities of such associations which are currently unavailable with Hipparcos. The upcoming Gaia mission is likely to make a significant improvement in being able to determine size, age, membership, velocity dispersion and expansion velocities of clusters that contribute to the runaway population. It is also likely to offer a more complete database of runaways which will allow for a more accurate determination of the DE:SNB ratio of ejection for OB runaways.

Figure 3-12 shows a plot of the percentage of dynamically ejected B stars which become runaways as a function of density $\frac{1}{r_{vir}^3}$, where r_{vir} is the initial virial radius, and for: An initial binary fraction 0.5; Decreased initial binary separation to 10-10^4; A primordially mass segregated cluster; A population of N = 45; A population of N = 4500. The results are only shown for the medium density cluster for clarity. The binary fractions of 0 and 1, and the gas expulsion results are also omitted. As can be seen from the plot, the increase in stellar density results in a large increase in the frequency of ejected B star runaways. The initial binary binding energy also has a strong effect. By contrast, primordial mass segregation offers only a modest increase while a population of small N clusters comprised entirely of OB stars shows a moderate decrease in B star runaway frequency. The large N = 4500 cluster ejects only a small fraction of its B stars at high velocity, however, at medium density its relaxation time is long making it difficult to eject massive stars.

We summarise the key elements of the previous chapter in the following

- A moderate population size for young clusters to eject OB runaways may be indicative for the ejection of OB runaways due to two contributing factors. Firstly, primordial mass segregation and gas expulsion may result in a dense central region comprised of massive stars, surrounded by a large population of low mass stars. From this, dynamical ejections may readily result in the ejection of OB runaways from the dense massive core. For example, the ONC is comprised of several thousand stars and has ejected at least a massive binary and two massive single stars at high velocities via dynamical interactions. This allows for the massive stars to interact and eject each other in large fractions. In our N = 4,500 cluster, the massive stars were randomly dispersed and with a long relaxation time the massive stars had insufficient time to segregate to the cluster centre dynamically and interact. Secondly, the escape velocity

Figure 3-12: *This plot shows a summary of ejection percentages of B star runaways for a number of the initial conditions described in the previous chapter. The results are only shown for the medium density cluster for clarity. The binary fractions of 0 and 1, and the gas expulsion results are also omitted.*



in our 4,500 cluster is ~10km/s by comparison to the ~5km/s in the 450 star cluster which means that some of the lower velocity stars will be slowed below the adopted velocity for OB runaways. However this is likely to only cause a small decrease in the number of observed OB runaways. Hence, the ejection rates of OB runaways from our moderately populated clusters should still be indicative of the ejection rates of OB associations which are been shown to have a large population of low mass stars.

- The initial density of the cluster is the dominant factor for producing high velocity massive runaways via dynamical interactions. An initially high density is required in order to produce dynamically ejected massive binary runaways and this may be an indicative factor since massive binary DE runaways exist in possibly large fractions, perhaps up to ~26%. The ratio of DE:SNB OB runaways then depends on the initial density since at high densities the DE scenario may dominate OB runaway production,

in particular the B star runaways. Furthermore, the initial stellar densities simulated here do not even go as high as has been claimed for primoridal clusters. At higher densities in primordial systems where protostars embedded in gas are interacting the effect of collisions plays a much greater role and is possibly the mechanism by which massive stars are formed in the first place. If stars are so closely separated that their collision probability is high then the likelihood of a strong interaction leading to the ejection of a fast escpee is similarly high. Hence, a larger primordial density is likely to contribute to a greater number of O type runaways being produced via the DE mechanism due to enhanced collision rates and strong interactions. However, it is important to note that we have already shown that the density in our high density simulations is sufficient to account for the entire observed runaway B star population, a frequency of ~4%, from dynamical ejections.

- An initial binary population is required in order to eject a significant fraction of DE OB runaways. However, with no binaries initially and at sufficiently high densities, a closely bound binary population may form which can lead to a substantial number of massive OB runaways being ejected from the SNB scenario. Overall, the actual fraction of binaries initially present in the cluster appears to have little significance on the final number of DE OB runaways. Although this assumes that the adopted range of initial binary separations is correct. If the initial binary separations are closer then the initial binary fraction is likely to be more significant.

- The binary binding energy has a modest increase on the ejection rates of both dynamically and SNB ejected OB runaways. Overall the SNB mechanism benefits most from the increase in binary binding energy and this results in a slightly greater increase in its OB ejection rate by comparison to the DE scenario. Hence, the DE:SNB ratio increases in favour of the SNB scenario with increasing binary binding energy. However, the DE mechanism is now more likely to eject massive binaries with high velocity and the more massive O stars. Thus, a large initial binary binding energy for massive stars in a binary may be indicated due to the ejection of massive stars with high velocity.

- Primordial mass segregation results in a dense core of massive stars with high multiplicity. This increases the ejection rate OB runaways due to dynamical interactions

occurring readily between the more massive stars.

- Gas expulsion may be a limiting factor for a significant fraction of OB runaways to be dynamically ejected. If gas expulsion is rapid and in the absence of primordial mass segregation the entire system expands significantly leaving little opportunity for massive stars to dynamically interact and be ejected at high velocity. Hence the SNB scenario would largely dominant the production of massive OB runaways.

- We have explored a number of realisations of cluster types where OB runaways may come from. In reality there exist a wide variety of clusters which will have begun with varying initial conditions such as population size, initial density etc. The ratio of DE to SNB OB runaways for a given cluster is then likely to vary significantly, especially considering the stochastic nature of the processes involved in the first place. However, the simulations presented here should be sufficient in order to provide some constraint on the expected ejection rate for OB runaways for a given cluster if the initial conditions of the cluster could be inferred to some degree of accuracy. The basic requirement for the production of a substantial number of OB runaways via the DE scenario is that the majority of massive stars should exist in a close configuration at some stage of their evolution. This is likely to occur at an early stage of cluster evolution since as clusters age they expand in general. Many young clusters are disperse, loosely bound systems but they may have expanded quickly to these sizes from an initially high density phase. Dynamical ejection of OB runaways from a given cluster would be indicative of an initially dense configuration. However, it is difficult to trace the vast majority of OB runaways to their clusters of origin, which limits any statistical analysis of the properties of clusters which have ejected OB runaways.

4

Supernova in a Binary Ejection from Stellar Clusters

4.1 Abstract

The following Chapter explores the supernova in a binary scenario within, and outside of a cluster environment. We explore the effects that different natal kick velocities and ranges of initial binary separations have on the massive, single and binary star runaway populations. We consider the velocity dispersion of single and binary massive runaways and show that, while a kick is required to produce the observed characteristics of Be/XRBs it is likely to be systematically smaller than kicks given to OB-supergiant systems. This may be interpreted as additional evidence for a bimodal natal kick velocity distribution. We consider the observational properties of runaways, their rotation rates and the number expected to be found as Blue Stragglers. It is expected that 80-100% of SNB OB runaways have enhanced rotation rates and that 20-30% may be observed as Blue Stragglers with respect to their parent clusters. SNB binaries are expected progenitors for Thorne-Zytkow objects (TZOs)

and from these simulations it is expected that 35-60% of massive SNB ejected binaries become TZOs. These high velocity massive objects may be observed as WN8 stars. Using a modified version of nbody6 (viz. nbody6-2), we explore the SNB ejection of OB runaways from stellar systems taking into account dynamical interactions and the evolution of such systems. We show that the SNB runaway population may be increased in a dynamical environment as stellar interactions may harden the SNB runaway progenitors. However, it may be expected that at larger densities stellar collisions and disruptions play a more significant role reducing the SNB runaway rate. Finally, we compare the rate of ejection for both scenarios (SNB and DE) and show that at low and medium densities the SNB runaway mechanism is dominant but produce an insufficient number of runaways to match observations. At high densities the DE mechanism is dominant but too many runaways are produced by comparison to observation. The most likely scenario is that the initial density is between the medium and high density configurations if we exclude consideration for gas expulsion. The role of gas expulsion was discussed in the previous Chapter and is a likely necessity in cluster formation. This means that the SNB scenario may dominate the production of OB runaways due to the cluster expanding rapidly and few dynamical interactions resulting. However, DE runaway binaries are observed which necessitates a dense configuration in at least some instances in order to eject them. Finally we discuss the characteristics of ejected runaway binaries ejected via both mechanisms and compare with observations. We make a tentative estimate as to the number of single runaways we might expect from both mechanisms based on the observed fraction of runaway binaries. From this we estimate that between 15-60% of O star runaways and 30-70% of B star runaways are dynamically ejected with the rest being ejected via the SNB scenario.

4.2 Introduction

N-body studies of open clusters that incorporate realistic treatments of binary stellar evolution have shown that stellar evolution affects the binaries significantly and that, even in low density environments, the complex interplay between binary stellar evolution and dynamical gravitational interactions can play an important role in the overall cluster evolution and in determining the properties of the final binaries (Hurley & Shara, 2003). The nbody6 code does not have a full set of routines for dealing with complex close binary evolution but it does allow for a good analysis of the ejection of stars and the competition between

the two ejection mechanisms. The precursor nbody4 however, includes a sophisticated set of fast look-up functions for synthetic stellar evolution, originally formulated by Eggleton et al. (1989) and subsequently refined into a comprehensive network that includes binaries (Tout et al., 1997). The work of Hurley et al. (2000) extended and improved this fitting scheme (see section D.5 for more). The scheme for rapid binary evolution is being updated on an ongoing basis to comprise more and more complicated systems and the synchronising effects of tides with stellar rotation (Hurley et al., 2002). The nbody4 version of Dr. Aarseth's suite of N-body codes is used on Grape machines and some of the present work was carried out in the Institute of Astronomy (IoA) in Cambridge, on their Grape-6 and MicroGrape machines with the grateful assistance of Dr Mark Wilkinson and Dr Sverre Aarseth. At the same time Dr Aarseth had been working on and finished a new version of nbody6 (denoted here as nbody6-2) which includes the aforementioned algorithms to treat binary stellar evolution from nbody4 with the purpose that it could be run without the Grape hardware, i.e. on a standard PC. This updated code was then used to complete the set of simulations begun in Cambridge. Having a full set of both single and binary stellar evolution algorithms, alongside a complete dynamical integrator, is the ideal setting for considering the realistic situation where both mechanisms for producing runaway stars work in competition with each other.

4.3 Population Synthesis

In the following sections we will explore the supernova in a binary mechanism without dynamical interactions, in order to gain a better understanding of the various evolutionary parameters involved. In the later sections we will show how these purely evolutionary results change when considered in the framework of a real cluster where dynamical interactions may alter the result, i.e. nbody4/nbody6-2 results.

Previous studies into the supernova in a binary system mechanism have used detailed sets of algorithms for binary stellar evolution (Leonard & Dewey (1993); Dray et al. (2005); de Donder et al. (1997); Tauris & Takens (1998)) or used the same fitting algorithms from an alternative N-body code, viz **SeBa** Portegies Zwart (2000), hereafter PZ00. The intention here is to produce a set of population synthesis results in order to consider the details of changing kick velocities and initial binary separations on the final runaway fraction. These results will be compared with previous population synthesis studies where applicable and

used for comparison with the results from the full N-body simulations of nbody6-2. For consistency the most suitable set of algorithms to use are those from the nbody4/nbody6-2 code itself which were provided by Dr Jarrod Hurley as a separate code and required minimal adjustment.

4.3.1 Initial Conditions

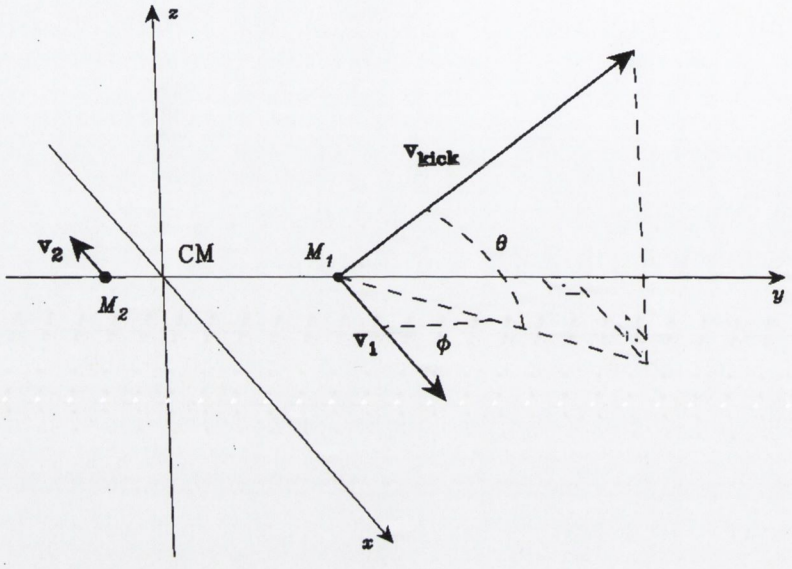
10^6 binaries were simulated with the set of parameters for eccentricities and mass ratios as for the nbody6 simulations, previously discussed in the section *Initial Conditions* in Chapter 2. Five simulations were made varying the initial binary separation range for each simulation: $10-10^2 R_\odot; 10-10^3 R_\odot; 10-10^4 R_\odot; 10-10^5 R_\odot; 10-10^6 R_\odot$. Several simulations with different mean natal kick velocities applied to the compact companion were made, each time for an initial binary separation range of $10 - 10^4 R_\odot$, in order to consider in detail the effect of choosing different kick velocities on the surviving binary runaway population. A simulation with a restricted kick, where no kick was given to a forming Black Hole, was also made in order to consider the effects of such a scenario. Stars in this setup gain a space velocity only through a rapid mass loss event such as a supernova. In general, if the system becomes disrupted, the velocity of the companion star is its orbital velocity at that instant (excluding the small effect the impacting supernova shell has on the companion), while for that of the primary (exploding) star it is taken as its orbital velocity at the instant of eruption, plus any applied kick to the remaining core. If the system remains bound (these binaries would be candidate X-ray binary systems) then it gains a space velocity due to the loss of mass from the primary and a contribution from the kick velocity given to the compact object. The following equations indicate the change in orbital speed of the primary (subscript (1)), the secondary (subscript (2)) and the system if it remains bound (subscript (sys)), where V_{sys} is the post-supernova centre of mass speed of the bound binary relative to the initial centre of mass speed. Figure 4-1 illustrates the binary configuration; Equations and Figure are from Brandt & Podsiadlowski (1995), BP95.

$$v_1^{'} = v_1 + v_k \tag{4.1}$$

$$v_2^{'} = v_2 \tag{4.2}$$

$$V_{sys} = \frac{V_{orb}}{M_1^{'} + M_2}[(\frac{\mu \Delta M_1}{M_1})^2 - 2\frac{\mu \Delta M_1 M_1^{'}}{M_1}\frac{v_k}{V_{orb}}Cos\theta Cos\phi + (M_1^{'}\frac{v_k}{V_{orb}})^2]^{\frac{1}{2}} \tag{4.3}$$

Figure 4-1: *Caption and Figure from BP95, page 464. **F**igure 1. Sketch showing a binary system and supernova kick geometry. The angle θ specifies the angle between the direction of the kick velocity vector and the initial orbital plane, and ϕ is the angle between the initial direction of motion of star 1 and the projection of the kick velocity vector on to the orbital plane.*



v_k = randomly orientated kick speed; $v_1^{'}$ and $v_2^{'}$ are the post-supernova speeds of the primary and secondary respectively; V_{orb} is the initial relative orbital speed $\sqrt{\frac{G(M_1+M_2)}{a}}$, where a is the semi-major axis of the binary; $\mu = \frac{M_1 M_2}{M_1+M_2}$; $\Delta M = M_1 - M_1^{'}$; $M_1^{'}$ = mass of supernova remnant (i.e. Neutron Star or Black Hole). The speed imparted to the system by the supernova mass loss of the primary is calculated from the loss of momentum from the system, $v_1 \times \Delta M$, and the addition of the effect of applied kick speed shared over the whole system.

Tables 4.1 and 4.2 summarise the population synthesis and nbody6-2 simulations made in this Chapter.

Table 4.1: *Summary of population synthesis simulations. The* a_{Range} *indicates the range in which the initial binary separation is distributed;* σ *is the 1-D rms velocity dispersion for a Maxwellian distribution used for selecting the supernova natal kick velocity.* **nbody6-2** *is the set of simulations where the distribution of parameters was input from the initial conditions (mass, velocity, positions) of a set of nbody6-2 runs in order to compare directly the results from the nbody code with those of the population synthesis.* **BH** *is the model which does not apply a natal kick to a Black Hole upon formation but does apply natal kicks to forming Neutron Stars.*

a_{Range} ($R_\odot$)	σ km/s	Number of Simulated Binaries
$10 - 10^2$	190	10^6
$10 - 10^3$	190	10^6
$10 - 10^4$	190	10^6
$10 - 10^5$	190	10^6
$10 - 10^6$	190	10^6
$10 - 10^4$	0	10^6
$10 - 10^4$	48	10^6
$10 - 10^4$	380	10^6
$10 - 10^4$	570	10^6
$10 - 10^6$ **nbody6-2**	190	7.5×10^3
$10 - 10^4$ **BH**	190/0	10^6

Table 4.2: *Summary of the nbody6-2 simulations. N = number of stars; ; ρ_{Nsys} is the stellar density where N_{sys} is equal to the number of systems, a binary being one system (i.e 0.5 Binary Fraction implies $N_{sys} = 300$); ρ_M is the mass density; V_{vrms} is the root mean square velocity as given in Equation 2.5; R_{vir} is the virial radius; $R_{0.5}$ is the half mass radius; Q = Virial ratio = $\frac{KineticEnergy}{PotentialEnergy}$; a_{range} is the binary separation range; T_{cr} is the crossing time = $\frac{2.R_{vir}}{V_{rms}}$; $T_{0.5,relax}$ is the half mass, two-body relaxation time = $\frac{0.138.N_{sys}^{\frac{1}{2}}.R_{0.5}^{\frac{3}{2}}}{(G.m)^{\frac{1}{2}}.ln\Lambda}$ where m is the average mass of the stars, G the gravitational constant, $ln\Lambda$ the Coulomb Logarithm = $\gamma.N_{sys}$ where γ is ~0.02 (Giersz & Heggie, 1996) for systems with a mass spectrum, Stars of widely different mass will relax at different rates and binaries are being treated as single objects.; M_{Tot} is the cluster mass; f_{dist} is the distribution function of positions and velocities used; N_{run} is the number of simulations for a given set of parameters. LD, MD, HD, indicate clusters of Low Density, Medium Density and High Density respectively. BF indicates Binary Fraction.*

Name	N	BF	ρ_{Nsys}	ρ_M	V_{rms}	R_{vir}	$R_{0.5}$	Q	a_{Range}	T_{cr}	$T_{0.5,relax}$	M_{Tot}	f_{dist}	N_{run}
			stars.pc^{-3}	$M_\odot.pc^{-3}$	km/s	pc	pc		$R_\odot$	Myrs	Myrs	$M_\odot$		
LD(BF05)	450	0.5	7	26	1.0	2.15	1.70	0.5	10-10^6	4.1	14.3	1065	Homogeneous	60
MD(BF05)	450	0.5	4.10^2	$1.6.10^3$	2.0	0.55	0.44	0.5	10-10^6	0.5	1.9	1065	Homogeneous	40
HD(BF05)	450	0.5	9.10^3	$3.3.10^4$	3.4	0.20	0.16	0.5	10-10^6	0.1	0.4	1065	Homogeneous	40
LD(BF1)	450	1.0	5	26	1.0	2.15	1.70	0.5	10-10^6	4.2	20.1	1065	Homogeneous	40
MD(BF1)	450	1.0	3.10^2	$1.6.10^3$	2.0	0.55	0.44	0.5	10-10^6	0.5	2.6	1065	Homogeneous	30
HD(BF1)	450	1.0	7.10^3	$3.3.10^4$	3.4	0.20	0.16	0.5	10-10^6	0.1	0.6	1065	Homogeneous	30

4.3.1.1 Kick Velocities

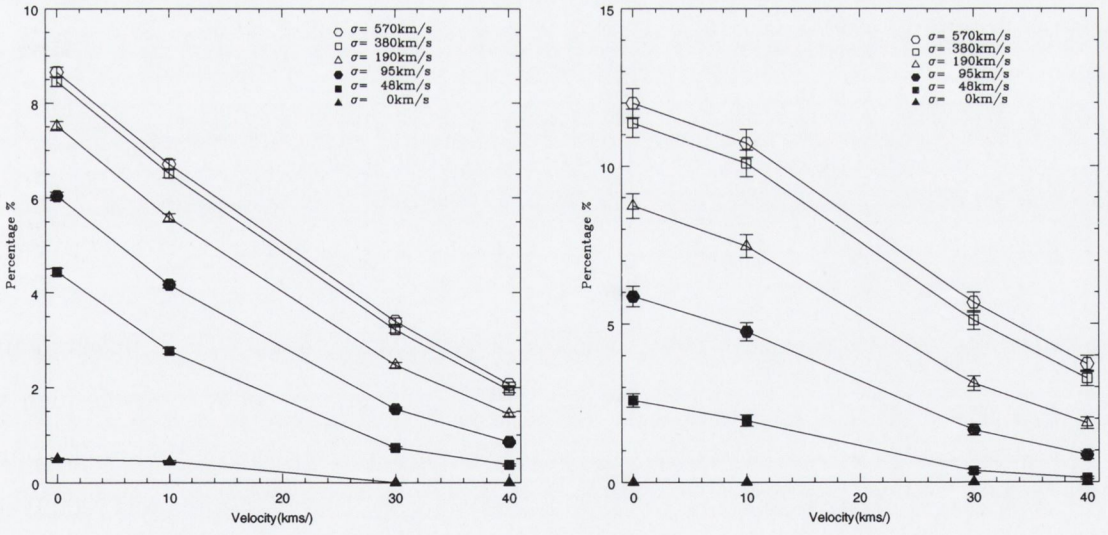
In the following we will expand upon the discussion of the kick velocities, which were described in the introduction to the SNB scenario in Chapter 1, and consider how the details relate to the production of massive runaways. The same kick velocity distribution, as is employed in the nbody codes, is applied in the population synthesis models, i.e. that of Hansen & Phinney (1997). A kick is applied to remaining compact object whether it is a Neutron Star or a Black Hole. Recall that the kick velocity distribution is determined primarily from observations of pulsar velocity distributions. There is some debate as to whether or not Black Holes gain a kick velocity or if kicks to Black Holes are significantly smaller than the corresponding Neutron Star kicks (Jonker & Nelemans, 2004; Nelemans et al., 1999). Considering anisotropic mass loss, a smaller kick for Black Holes is reasonable, since the amount of mass ejected during the formation of a Neutron Star is likely to be greater than that ejected when a Black Hole is formed. Dray et al. (2005) conclude that a significant decrease occurs in the number of O and WR runaway stars produced when kicks are restricted to Neutron Stars only and are not imparted to Black Holes. Our population synthesis simulations with a natal kick applied to a forming Black Hole and those without a natal kick being applied to a forming Black Hole result in ~3-7% more B type runaway stars and ~30-40% more O type runaway stars **both** in binaries and in singles, when a kick is applied to the forming Black Hole (consistent with Dray's results). The reason fewer single high velocity massive stars are created when a kick is not given to the forming Black Hole is that they become 'trapped' in the original binary. If no kick is given to the Black Hole that remains after the star explodes it is very likely that the system will remain bound, particularly if the pre-supernova system is closely bound and undergoes a phase of mass transfer. To explain why there are more binary runaways when a kick is applied is less straight forward. There are 1.5-2 times as many bound binaries when no kick is given to the Black Hole upon formation then when a kick is applied. However, in order to produce a high velocity binary it must be closely bound before the explosion of the primary. Such a closely bound system is able to remain bound even when a substantial natal kick is applied and this kick contributes to the overall system velocity (see Equation 4.3). The magnitude of this additional system velocity due to the supernova kick is comparatively small to the kick velocity itself but it is sufficient to promote a binary which would gain a moderate system velocity from the loss of the supernova shell alone to runaway velocities. Hence, the

number of bound binaries that achieve runaway velocities when a kick is applied becomes greater than when no kick is applied.

The magnitude and origin of this natal kick velocity in general remains unclear, leading to various choices being made by investigators over the years when using population synthesis models guided by observational velocity distributions of pulsars. Dray et al. (2005) used a kick velocity dispersion as found by Lyne & Lorimer (1994) $Vmean_{3D}$ = 450km/s; PZ00 chose a distribution as determined by Hartman (1997) with $Vmean_{3D}$ = 370km/s, using Paczynski (1990)'s distribution with σ = 600km/s. In the codes used for this investigation, the kick is drawn from a Maxwellian velocity distribution with $\sigma = 190km/s$ and $Vmean_{3D}$ ≈300km/s. Hobbs et al. (2005) also adopt a Maxwellian velocity distribution for pulsars, this time with σ = 265km/s and $Vmean_{3D}$ ≈400km/s. In order to see the possible ramifications of different kick velocities on the runaway population in detail, several simulations with significantly varying mean velocity dispersions drawn from a Maxwellian distribution are considered here. The results are plotted in Figures 4-2 a) and b). Figure 4-2a) shows that in order to have a percentage of single B star runaways (v > 30km/s) at the level observed (2-4%) a minimum kick velocity dispersion of approximately 95km/s is required. These simulations illustrate that there is a maximum of about 4% runaway B stars when the kick velocity dispersion is above 570km/s, where all the supernovae which occur in binaries disrupt. The O stars in Figure 4-2b) have a larger percentage of runaways which becomes a maximum around 6%. Figures 4-3 a) and b) depict the percentage of runaway binaries. As noted previously when no kick was applied to a forming Black Hole there was a decrease in the number of ejected binaries at high velocity. This trend is more evident in these plots where the number of ejections show a similar decrease as the single stars at low ejection velocities, but the number of binaries at high runaway velocities is *greater* as soon as a small kick is applied, notwithstanding the fact that a lower kick velocity results in more binaries remaining bound. The number of binaries that survive does decrease in a systematic way with a higher kick velocity but the distribution over different ejection velocities changes due to the applied kick, also increasing the system velocity when the binary survives. However, overall the binary fraction appears to changes only moderately with respect to the ejection velocity. Naturally the quantity of surviving binaries varies with different kick velocities as more binaries are disrupted. The fraction of runaway binaries with respect to the total number of runaways (both single and binary) are then derived by determining the percent-

age from Figures 4-3a) and 4-2a). Figure 4-2a) shows that for σ = 190km/s the frequency of single stars ranges from 1.75-7.5%. The corresponding binary frequency ranges from 0.5-1.25%. Hence the Binary Fraction for σ = 190km/s is: $\frac{1.25}{1.25+7.5}$ = 14%; $\frac{0.5}{0.5+1.25}$ = 25%; 14-25%. Therefore: 1-2% when σ is 570km/s; 14-25% when σ is 190km/s; 70-80% when σ is 48km/s and with zero kick velocity 90-100%. The binary fraction is an important tracer to the ejection mechanism for runaways and the kick velocity if it could be correlated to the observed number of runaway binaries with a compact companion. This will be discussed in more detail in section 4.5 *Ejected Binary Characteristics* later in this chapter.

Figure 4-2: *Figure a) (Left) shows the percentage of single B-type stars that are ejected via the supernova in a binary mechanism with respect to the initial total of B stars as a function of ejection velocity, for different Maxwellian kick velocity dispersions. Figure b) (Right) shows the percentage of ejected single O-type stars with respect to the initial total of O stars as a function of ejection velocity, for different Maxwellian kick velocity dispersions.* **Note:** *The order of legend follows the order of the curves from top to bottom (i.e. the top curve corresponds to σ = 570km/s and the bottom curve corresponds to σ = 0km/s.). The x-axis values indicate ejections greater than the velocity shown. (e.g. 0km/s is the % of all stars which are ejected with a velocity greater than zero).*

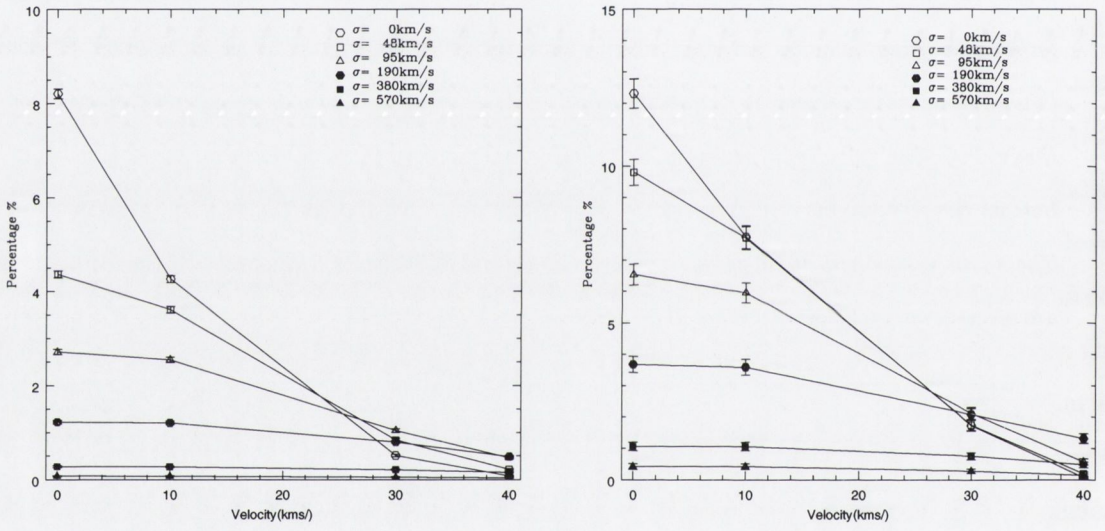


(a) Single B stars

(b) Single O stars

It should also be noted that there is growing evidence for a bimodal kick velocity distribution (Fryer et al., 1998; Arzoumanian et al., 2002; Pfahl & Rappaport, 2002; van den Heuvel et al., 2007). Arzoumanian et al. (2002) suggests a bimodal kick velocity

Figure 4-3: *Figure a) (Left) shows the percentage of B type stars in Binaries that are ejected via the supernova in a binary mechanism with respect to the initial total of B stars as a function of ejection velocity, for different Maxwellian kick velocity dispersions. Figure b) (Right) shows the percentage of O type stars in Binaries that are ejected via the supernova in a binary mechanism with respect to the initial total of O stars as a function of ejection velocity, for different Maxwellian kick velocity dispersions.* **Note:** *the order of legend follows the order of the curves from top to bottom but this time reversed from the previous figures (i.e. the top curve corresponds to σ = 0km/s and the bottom curve corresponds to σ = 570km/s. The x-axis values indicate ejections greater than the velocity shown. (e.g. 0km/s is the % of all stars which are ejected with a velocity greater than zero)*



(a) Binary B stars

(b) Binary O stars

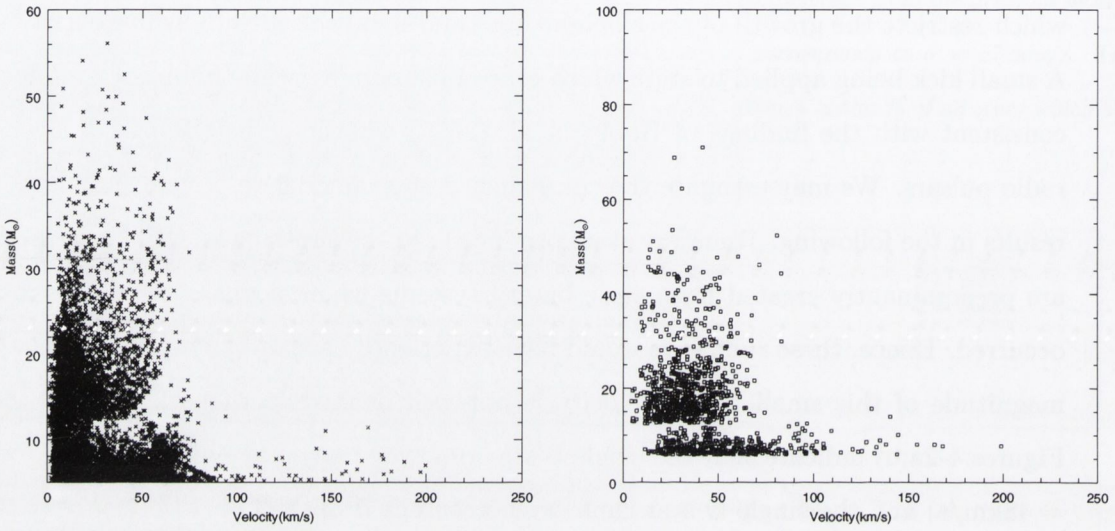
distribution with means = 90km/s and = 500km/s such that ~40% of pulsars gain small kicks from the low velocity distribution and 60% experience kicks from the high velocity distribution. This is consistent with Fryer et al. (1998) who estimate that ~30% of neutron stars are born with essentially a negligible kick velocity. Pfahl & Rappaport (2002) estimate that the class of HMXRBs with long orbital periods (>30days) and low eccentricities (<0.2) must have formed with the newborn neutron star gaining a kick of < 50km/s. Van den Heuvel et al. (2007) suggest that the low mass, low kick velocity neutron stars in double neutron star binaries are the result of electron-capture collapse of the degenerate O-Ne-Mg cores of helium stars less massive than about $3.5M_{\odot}$ (where this is the second born neutron star). By contrast the higher-mass, higher velocity neutron stars are formed by the collapse

of the iron cores of higher initial mass stars. This suggestion is drawn from Podsiadlowski et al. (2004) who argue that O-Ne-Mg degenerate electron-capture core collapse can only occur in binary systems, due to the fact that an interacting binary star with an initial mass range of about 8-11$M_{\odot}$ cannot reach the AGB (Asymptotic Giant Branch) phase and will lose its hydrogen envelope by RLOF leaving a helium core of sufficient mass to become a neutron star. Single stars, by contrast, within the 8-11$M_{\odot}$ range reach the AGB phase which restricts the growth of their helium core and finally result in a white dwarf forming. A small kick being applied to stars which erupt in supernova while in binary systems is also consistent with the findings of Hobbs et al. (2005) who note the absence of low velocity radio pulsars. We may estimate the consequence of a bimodal velocity distribution on our results in the following. Runaway stars produced via the supernova in a binary mechanism are predominantly created from close binary systems where a phase of mass transfer has occurred. Hence, these runaways would have experienced a small kick velocity. The typical magnitude of this smaller kick velocity is not well defined, perhaps less than ~50km/s. Figures 4-2a,b) indicate that the single B star runaway percentage drops below 0.5% (for σ = 48km/s) and the single O star runaway percentage drops below ~1% (for σ = 48km/s) which has a significant impact on the feasibility of this scenario.

Figure 4-4a) shows a mass-velocity plot for single stars from the model results with a separation range $10 - 10^6 R_{\odot}$. As can be seen from this plot, high velocity stars may be produced with velocities up to 200km/s and high mass stars up to $60M_{\odot}$ may be produced with velocity around 80km/s. Figure 4-4b) shows a mass-velocity plot for binary systems. This plot again shows the tendency for a lower mass system to reach higher velocities; notice that even the bound systems may have velocities up to 200km/s and have masses up to $60M_{\odot}$. Note that, correspondingly, the single B stars gain velocities up to 200km/s and that the single O stars have a maximum velocity typically less than half this, i.e. $\sim 75 - 100 km/s$.

Figure 4-5a) and Figure 4-5b) show how the ejection velocities of disrupted binaries change for B stars and O stars respectively, with regard to the range in the initial binary separation distribution as a percentage of the initial total number of B and O stars. The peaks in both figures indicate the initial separation range where escaping O and B stars are more likely. As can be seen, O stars are ejected more effectively with a close distribution up to $10^3 R_{\odot}$ while the B stars are ejected preferably from a distribution with a wider

Figure 4-4: *Figure a)(Left) Mass-Velocity plot of single OB stars via the supernova in a binary mechanism. Figure b) (Right) Mass-Velocity plot of binary OB systems where the masses are the current masses of the original secondaries. The poorly populated regions in both figures are due to the history of the binary and is related to the adopted routines describing its evolution, resulting in certain masses being less likely to gain a velocity as a result of a supernova event.*

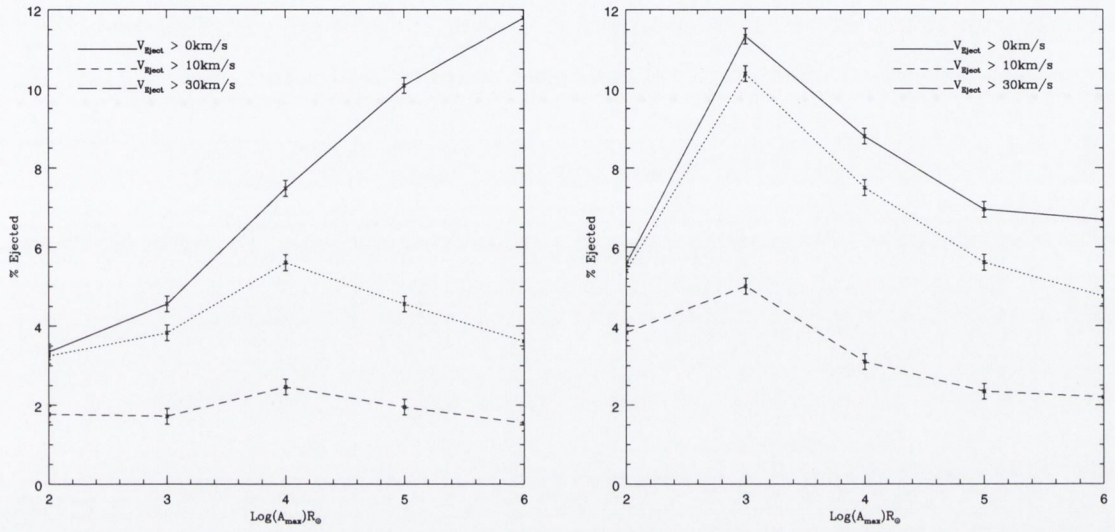


(a) Single OB stars

(b) Binary OB stars

range. The peaks (in all but one of the curves) occur due to a combination of both more stars experiencing mass transfer and being more energetic at that separation. As the separation decreases further, the likelihood of the binary surviving increases, which becomes a dominant effect for runaway B stars with initial separations less than $10^4 R_\odot$ and for O stars (which are systematically harder to disrupt than B star binaries of the same initial separation due to them being more massive, recall that the B stars are between 5.9-23$M_\odot$ and the O stars are >23$M_\odot$) with initial separations less than $10^3 R_\odot$. The difference, in ejection percentage of stars with runaway velocities, from the highest values (a peak) to the lowest value, a factor of 2.3 for O stars and 1.6 for B stars. The percentage of escaping B stars is comparable with the observed values and consistent with those found by other authors; e.g. PZ00 shows that using only the SNB scenario under certain conditions (such as all massive stars are found in binaries) all B star runaways may be produced via the supernova in a binary mechanism and suggests that only 30% of O star runaways may occur due to this mechanism. Our results show that even with a large population of very tight

Figure 4-5: *Figure a)(Left) Ejection percentages of single B type stars as a function of initial binary separation range. Figure b) (Right) Ejection percentages of O type stars as a function of initial separation range. The x range values are the maximum in the separation range used, A_{max}, with a constant minimum of $10R_{\odot}$ (i.e. $Log(A_{max}) = 2$ corresponds to the range $10 - 10^2 R_{\odot}$)*



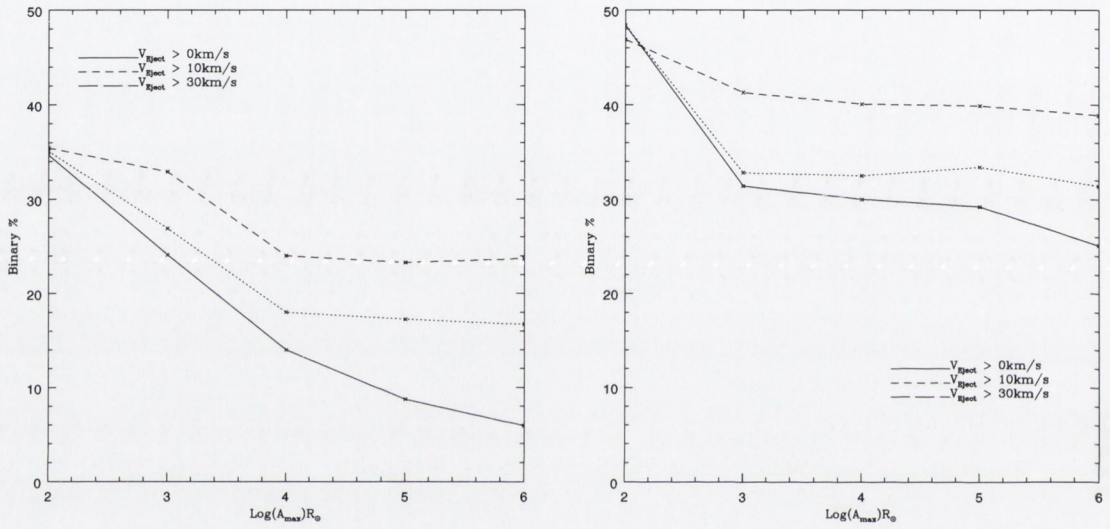
(a) Single B Stars

(b) Single O stars

binaries between $10 - 10^3 R_{\odot}$ the percentage of O stars that are ejected is still 2-4 times lower than the observed values (Recall frequency: 2-4% of B stars are runaways;10-20% of O stars are runaways). Figures 4-6a) and 4-6b) illustrate that the binary fraction among the O and B stars falls as the initial separation range is increased, as might be expected due to wider systems being easier to disrupt. Notice that at greater masses (B to O) and higher velocities the binary fraction increases. A more massive system is more energetic resulting in a larger ejection velocity. In the next section we show that the root mean square velocity of ejected binaries exceeds that of ejected single stars which results in the binary fraction increase with respect to ejection velocity. Note that this will only continue up to a point where the highest velocity stars will be single. Hence, one would expect a sizeable fraction of O star runaways to have compact companions and considering the kick velocity arguments of the previous section this would be in excess of 40%. The runaway binary fraction is over twice that predicted by de Donder et al. (1997) which is likely to be due to differences in the evolutionary processes applied in the codes and the initial conditions adopted here. The higher predicted fraction is consistent with PZ00 who

estimate the binary fraction among runaways to be 20% for B stars increasing to 40% for earlier B and O-type stars.

Figure 4-6: *Figure a)(Left) Ejection percentage of binary B stars as a function of initial binary separation range. Figure b) (Right) Ejection percentage of binary O type stars as a function of initial separation range. The x range values are the maximum in the separation range used, A_{max}, with a constant minimum of $10R_{\odot}$ (i.e. $Log(A_{max}) = 2$ corresponds to the range $10 - 10^2 R_{\odot}$*

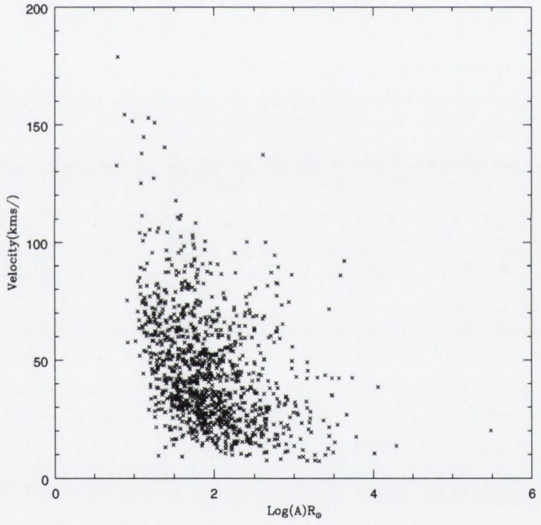


(a) Binary B Stars

(b) Binary O Stars

Figure 4-7 is a scatter plot indicating the relationship between final binary separation and ejection velocity of binary systems. The vast majority of high velocity systems have separations less than $10^3 R_{\odot}$. As can be seen from the distribution of points the higher the velocity of the binary the more tightly bound the system is likely to be. For example, only one ejectee with a velocity greater than 100km/s has a separation greater than $10^2 R_{\odot}$. This is an important observational constraint and suggests that since the radii of massive stars may increase to large values towards the end of their lifetimes, a large portion of these are likely to have an X-ray phase, as the expanding stellar shell fills its Roche lobe, allowing accretion to occur on the compact object. One may compare this with Table 5.3 in Chapter 4 where 13 known high velocity XRBs have periods less than 600 days with 50% having periods less than 10 days. The higher the velocity the shorter the period. In section 4.5 we will discuss the characteristics of runaway binaries ejected via both mechanisms in detail.

Figure 4-7: *Final binary velocities with respect to final binary separation Log(A).*

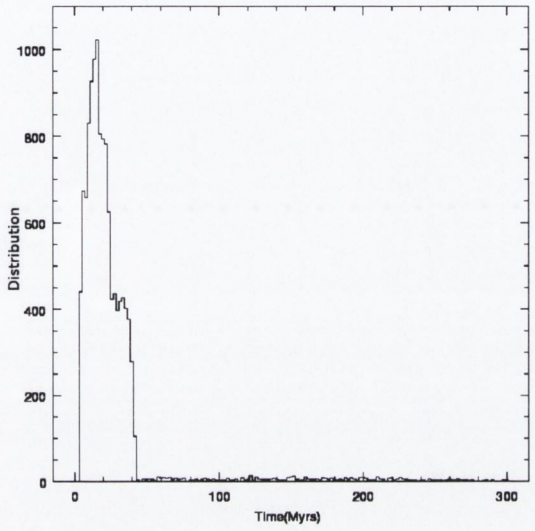


4.3.1.2 Runaway Timescales and Observations

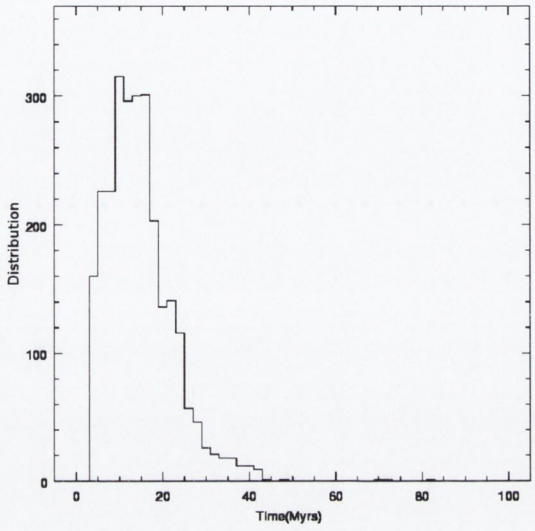
The timescale for ejection is of particular interest since it is important to consider the lifetime that stars remain as runaways. Using the simulations of $10-10^4 R_\odot$, a kick velocity dispersion of $\sigma = 190 km/s$ and 10^6 binaries we present the distribution of ejected stars with respect to time in Figures 4-8 and 4-9. Looking at Figure 4-8a) by far the majority of ejections occur within 40Myrs. However, considering only B and O type ejections Figure 4-8b) and Figure 4-8c), the vast majority of O stars are ejected within 10Myrs and the vast majority of B stars within 20Myrs, peaking a bit later. Comparing these results to those of the timescale of ejection for dynamical ejections it is likely that dynamical ejections will be favoured initially since stars are ejected by this mechanism typically a few million years prior to that of the first SNB ejections. Hence, if there is a substantial number of massive stars ejected dynamically, this may have a significant effect on the ejection rates for a supernova in a binary ejection.

Figure 4-9a) shows that the production of B star runaways continues at a reasonably constant rate up to about 25Myrs, where there is a sudden and dramatic drop off in runaway ejections. 25Myrs corresponds to the lifetime of about a 9-10$M_\odot$ star. This therefore explains why the drop off is so abrupt. The last of the stars which may erupt as a supernova in a binary system occur around this time. By contrast Figure 4-9b) shows that the production of O star runaways peaks around 7Myrs and declines relatively rapidly to zero about 11Myrs. 7Myrs is around the maximum lifetime of the least massive O stars (M $\sim$23.3$M_\odot$) but O star runaways may have had mass transferred to them late in their lives, rejuvenating them, allowing them to live for a few million years longer as O stars. This leads to two distinct peaks in the actual fractions of runaway O and B stars. Previously the O and B star fractions represented the total number of O and B stars with runaway velocities divided by the total number of O and B stars originally in the cluster. This was done for convenience and allows for easy comparison between models with different parameters. Furthermore, the observed runaway fractions are much more complicated values since they come from clusters at varying epochs and are taken from a global total of runaway stars also at different epochs (i.e. they represent a general average over these parameters). Portegies Zwart (2000) (Hereinafter PZ00) addresses this issue by making a correction to his estimates by considering the time a star remains as a runaway with respect to the lifetimes of the initial population of stars. Further, he considers the (e.g. O and B)

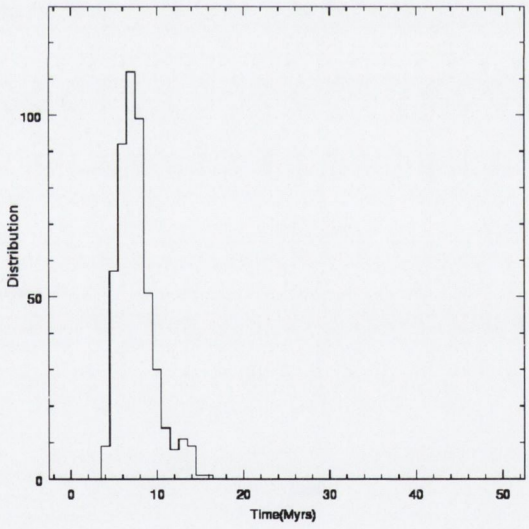
Figure 4-8: *Figure a)(Left) shows the distribution of all ejected stars over time. Figure b) (Right) shows the distribution for B stars only. Figure c) (Below) shows the distribution for O stars only.*



(a) All Stars Ejected



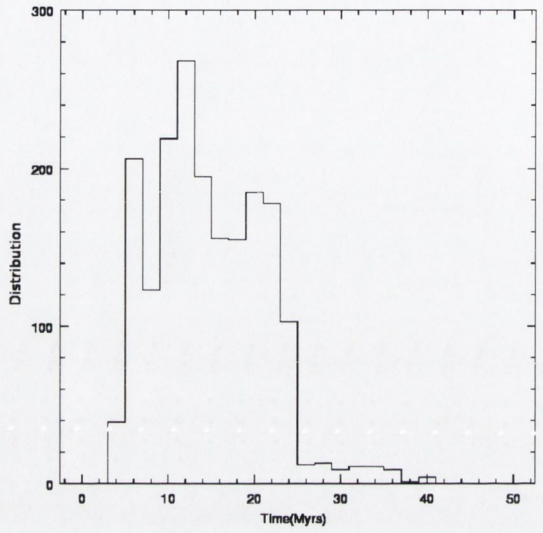
(b) B Stars Ejected



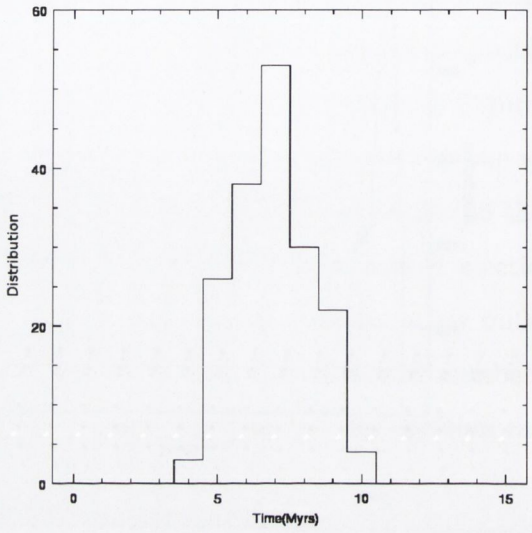
(c) O Stars Ejected

population total as the initial total number of primaries from the binaries of O and B type, rather than the actual total number of O and B stars. For our analysis, we count all O and B stars, both primary and secondaries, to give the total. The fraction of ejections is then the number of O or B-type runaways divided by the number of O or B-type stars present at that time. Figure 4-9c) shows how the O and B runaway percentages change over time. As

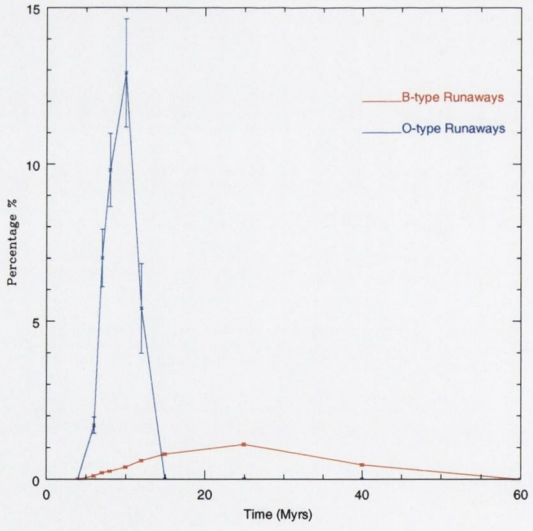
Figure 4-9: *Figure a)(Left) shows the number of runaway B stars produced over time. Figure b) (Right) shows the number of runaway O stars produced over time. c) (Below) shows the runaway percentage of O and B stars over time.*



(a) B Star Runaways



(b) O Star Runaways



(c) O and B Star Runaways

the runaway O star production rate peaks around 7Myrs an observed runaway frequency of ~12% results and (as the massive primaries begin to erupt in supernova) so too does the total fraction of runaways. This observed frequency decreases rapidly towards zero by ~11Myrs as the O star rejuvenated runaways reach the end of their lives. The percentage

of observed runaway B stars maximises around the same time as the rate of B star runaway production ceases, i.e. around 25Myrs. These peaks occur not only due to the total number of runaways reaching a maximum, but also due to the large numbers or runaways that have mass transferred to them prior to ejection, rejuvenating them, which allows them to live longer as massive runaways, than cluster stars, with whom they had the same initial mass (see section 4.3.2 *RLOF and Blue Stragglers* for more details on mass transfer and runaway stars). This results in the runaways living longer than the cluster OB stars in general, hence there is an increase in the observed runaway fraction since the denominator (Total = Cluster stars + Runaway Stars) of the ejection fraction = $\frac{Number\ of\ Runaway\ OB\ stars}{Total\ Number\ of\ OB\ stars}$ becomes smaller relative to the numerator. As the cluster stars come to the end of their lives a few OB runaways may still remain, though this is likely to be for a relatively short duration and note that cluster OB stars will also have undergone mass transfer in other binaries. This maximum percentage (1.1%) is slightly lower than PZ00's corrected estimate for observed runaways. The average percentage is significantly lower, in the region of ~0.3%. The difference between the number of observed runaways between O and B types is then self evident as far as the SNB mechanism is concerned.

If the fraction of runaway O stars is 10-20% the SNB mechanism may offer a large fraction of these if observed fractions are drawn from a majority of clusters with ages ~7Myrs. If this is the case, then the B star fraction at this epoch is severely deficient at producing runaways, and remains so, even up to its maximum possible threshold. This indicates, by contrast to PZ00, that the O star fraction of runaways may be higher than the 30% he suggests, and is likely to be greater than 50%. It also suggests that the B star runaways from this mechanism are at best 50% of the runaway B star population and at worst less than 10%. From a substantial fraction of known open cluster, 160 (30 O, 130 B0-B5) listed in the WEBDA[1] database with age and spectral type determinations, we estimate an average cluster age of ~9Myrs for the O-type clusters and ~36Myrs for the B-type clusters. This implies that the O and B star runaway percentage from the SNB scenario is observed with percentages of ~12% and ~0.5% respectively. It should be pointed out again that the chosen masses we assume are representative of O and B5-type stars but they may be overestimates. Alternative values of OB stars being of a minimum

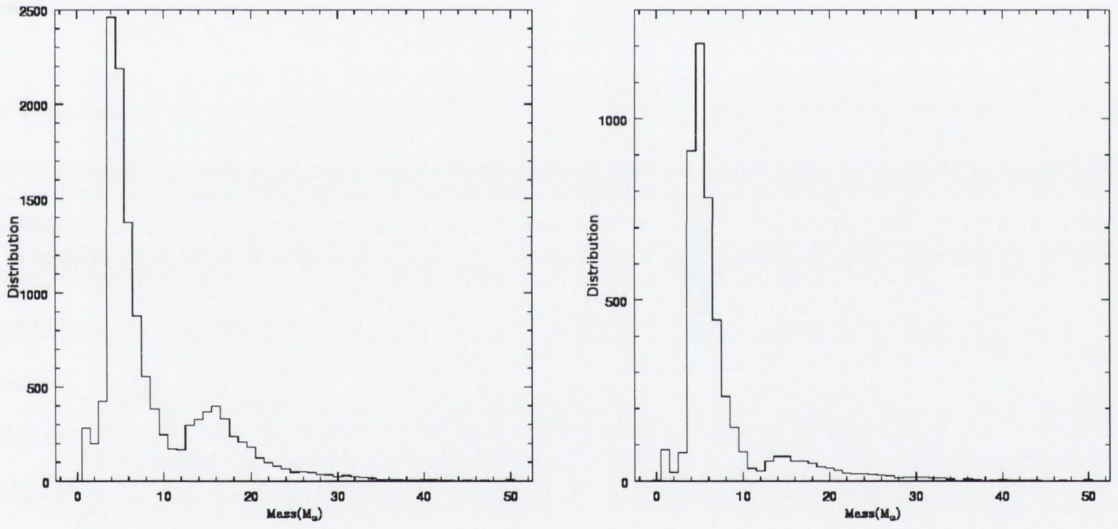
[1]WEBDA is a site devoted to open star clusters and is the Web version of the database known as BDA. It is mainly intended for professional and amateur astronomers. It is operated at the Institute for Astronomy of the University of Vienna at the web address http://www.univie.ac.at/webda/webda.html

mass for our range of O stars $>17M_{\odot}$ and early B stars 4-$17M_{\odot}$ respectively. In this case the fraction of runaways is lower and the time where such a fraction reaches a maximum naturally increases.

From the dynamical ejection point of view from the previous chapter, the observational constraint in terms of time of ejection is related to the initial density of the cluster. The more concentrated the cluster, the faster it evolves dynamically and produces ejected stars. At high densities this occurs earlier than the lifetime of O and B. This means that the fraction of dynamically ejected O and B stars changes little after it reaches a maximum, since dynamically ejected OB runaways have the same lifetimes as the cluster OB stars, except for those runaways that are collision products .

Figure 4-10a) is a histogram of ejected masses which shows two distinct peaks. The larger peak, which corresponds to spectral types of about B5, is due to the fact that stars of mass $\sim 8M_{\odot}$ (which will experience a supernova explosion) are more common then stars of greater mass. Since these binaries are likely to have a high mass ratio, companions of similar mass will be ejected. Figure 4-11 shows these peaks remains when considering only the runaway stars. The second peak, around B1/B2, is of interest. It should be stressed that such a peak arises due to the routines which calculate binary stellar evolution and the choices made for parameters (e.g. conservative versus non-conservative mass transfer, mass loss rates etc). Hence, alternative choices may very well effect this outcome. Nonetheless, from a histogram of spectral types of known OB runaways listed in Appendix A, Figure 4-11, there does appear to be a peak at this early type. This is then a tentative suggestion that the supernova in a binary is a contender for a primary mechanism to produce runaways. Although, one should also note that it is very possible that the observed peak may be an observational selection effect since more massive stars may evolve much more rapidly and hence be unobserved as runaways and less massive stars are dimmer and would be missed to a much higher degree by observations (recall also, that the earlier OB runaway surveys specifically concentrated on O-B5 spectral types) which may lead to the entire first peak in Figure 4-10b) being unobserved.

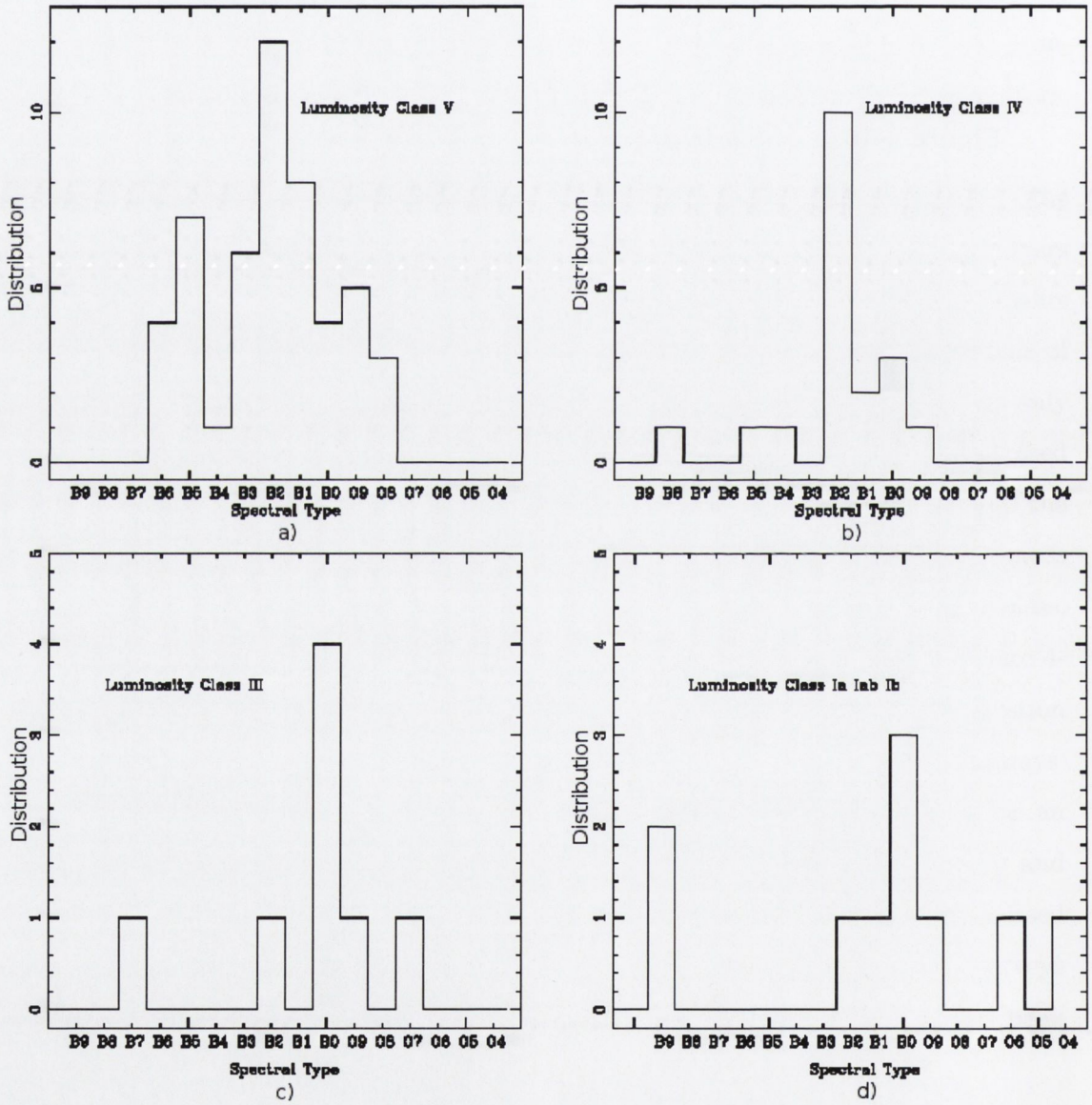
Figure 4-10: *Figure a)(Left) shows the mass distribution for all ejected stars. Figure b)(Right) shows the mass distribution for stars with a velocity greater than 30km/s*



(a) All Stars

(b) Stars with V > 30km/s

Figure 4-11: *88 OB runaway stars which had a spectral type and luminosity class identified (various sources)*



4.3.1.3 SNB ejected binaries with compact companions and large ejection velocities

Tables 4.3 and 4.4 show the root mean square velocity, V_{rms}, for high and low mass populations of single and binary stars ejected via the SNB mechanism with velocities greater than 10km/s. As can be seen from the tables the (V_{rms}) for ejected binary B stars is systematically higher than the (V_{rms}) for ejected single B stars by a few km/s, typically ~46km/s and ~37km/s respectively. The difference between these two populations decreases as one considers higher velocity cutoffs. The reason that the (V_{rms}) is so high for binaries with a compact companion is that the probability of the surviving binary is proportional to how closely bound it is. Hence, close binaries are preferentially selected to survive. Recalling equations 4.1, 4.2, 4.3, if the binary system becomes disrupted due to the supernova explosion of the primary the remnant compact object has a velocity proportional to its pre-supernova orbital velocity and a contribution from the kick velocity, while the secondary has a velocity proportional to its pre-supernova orbital velocity. If the system remains bound, then the system velocity is proportional to the pre-supernova relative orbital velocity, the amount of mass lost and the magnitude and direction of the natal kick velocity. This of course implies that single stars have greater velocities than the corresponding binaries, but recall that the probability that the system survives is greatly enhanced if the system is closely bound which means that the relative velocity of the components is high. Therefore, the majority of bound binaries with compact companions will have high velocities and a high (V_{rms}), whereas there is also a large population of single stars (the original companion) ejected with low velocities from wide binaries. This also explains why the binary fraction becomes greater as the velocity cutoff is increased. However, this increase has its limits and as one considers higher velocity cutoffs then the binary fraction begins to decrease (as more single stars are found at greater velocities) which begins to be apparent at a cutoff of 42km/s.

If the majority of massive high velocity bound systems which are produced via the supernova in a binary mechanism are the observed HXRBs then the binary fraction of runaways may be well accounted for. The large (V_{rms}) for ejected binaries is consistent with the fact that OB-supergiant XRBs have observed mean tangential velocities around 42km/s (Chevalier & Ilovaisky, 1998),CI98. However, CI98 also observe that the Be/XRBs have systematically lower tangential velocities (~15km/s) than the OB-supergiants. Van

Table 4.3: *Root mean square velocities of low mass single and binary SNB ejected stars with velocities greater than 10km/s. Low mass systems, later than B5-type stars ejected by the supernova in a binary mechanism. Binaries are stars with a compact companion. The V_{rms} for the low mass population (i.e. less than $6M_{\odot}$) excludes the presence of very high velocity low mass evolved stars. Massive binaries which survive a common envelope phase (i.e. do not result in coalescence/collision as they spiral-in) become very tightly bound low mass systems whose component stars have had their outer envelopes stripped leaving a pair of naked helium stars. The primary may still erupt as a supernova which results in the secondary being ejected at high velocities due to their close separation. These which have a V_{rms} of 214km/s ± 42km/s for binaries and a V_{rms} of 333km/s ± 47km/s for single stars. However these systems are very rare.*

Model	Single Stars (V_{rms})	Binary Stars (V_{rms})
$10 - 10^2$	0.0	0.0
$10 - 10^3$	59.5	59.4
$10 - 10^4$	42.7	62.5
$10 - 10^5$	39.5	64.0
$10 - 10^6$	40.6	64.5

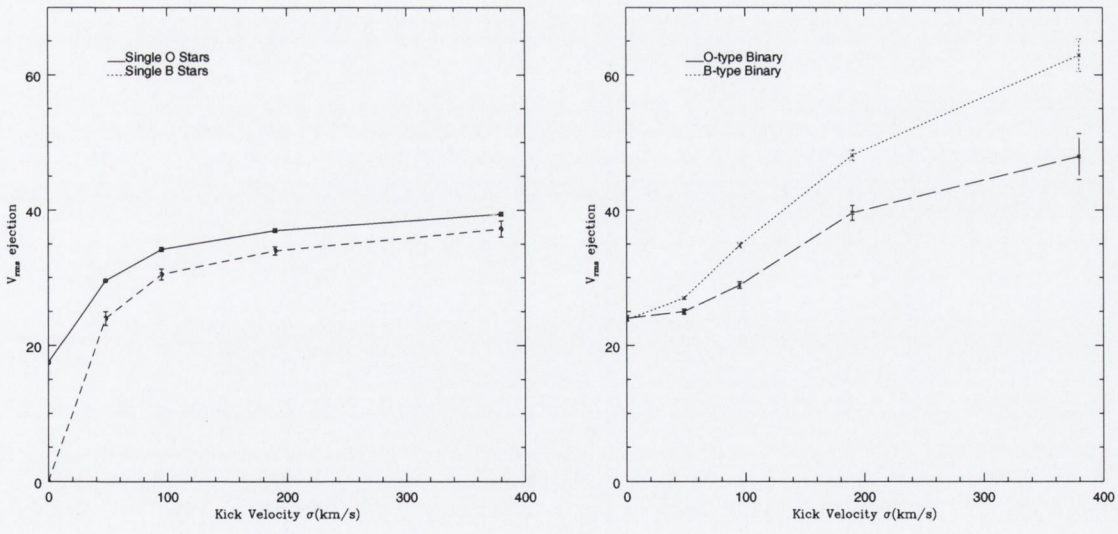
Table 4.4: *Root mean square velocities of OB single and binary SNB ejected star with velocities greater than 10km/s. B stars and B star primary masses. Stars ejected by the supernova in a binary mechanism. Binaries are stars with a compact companion.*

Model	Single Stars (V_{rms})	Binary Stars (V_{rms})
$10 - 10^2$	36.2	36.0
$10 - 10^3$	37.1	42.0
$10 - 10^4$	36.8	46.7
$10 - 10^5$	36.1	45.0
$10 - 10^6$	36.4	45.1

den Heuvel et al. (2000), (VDH00), show that this conforms well with current theories of binary evolution, where differences in the fractional helium core as a function of stellar mass and conservation of orbital angular momentum during mass transfer results in narrower pre-supernova orbits for OB-supergiant systems and larger fractional amount of mass ejected. Such a trend is not seen easily in the bound population of runaways from the V_{rms} values in Table 4.4. The reason for this is that Be/XRB and OB-supergiant XRB systems are not simply O and B bound systems. They are instead subgroups of the bound population of

binaries whose primaries have exploded in a supernova and hence have specific observational characteristics. Following VDH00, we assume that our bound systems with eccentricities above 0.3 and masses between 12-18$M_{\odot}$ are likely to be Be/XRBs. Isolating the ejected binaries, from our (σ = 0kms/) simulations, with these characteristics results in a V_{rms} of 9.4km/s which is consistent with VDH00's results where no kick velocity is applied to the forming compact object. However, the V_{rms}, velocity for massive O star binaries, which may be the supergiant XRB progenitors, is only 34.0km/s, lower than the value determined by VDH00, though still substantially larger then that of the Be/XRBs. It is important to note that they chose a constrained specific set of parameters to produce the observed values whereas here we have a more complete scenario with a combination of various distributions in terms of mass ratio, eccentricity, IMF etc. Applying a kick velocity however does make a significant difference as Figures 4-12a,b) show.

Figure 4-12: *Figure a) (left) shows the change in root mean squared velocity of single star escapees as a function of the applied kick velocity dispersion, σ, from a Maxwellian distribution. Figure b) (right) shows the corresponding plot for binary stars. Note that no single O stars are ejected when a kick velocity of zero is applied. These stars all remain trapped in the original binaries hence the V_{rms} is zero.*



(a) Single Stars

(b) Binary Stars

This places restrictions on the mean kick velocity which is likely to be imparted to the surviving system. From simulations with a mean kick velocity to the Be/XRB systems of 160km/s (σ = 95km/s) results in an average V_{rms} of 22km/s which is very consistent with

the space velocity of 19 ± 8km/s quoted by VDH00 for the Be/XRBs (a factor $\frac{4}{\pi}$ times the tangential velocity, to estimate the space velocity). Also a kick is required for Be/XRBs in order to produce the observed eccentricities. We therefore suggest that Be/XRBs are produced via a lower kick velocity distribution than occurs when producing single star pulsars. Simulations with a larger kick with (mean > 300km/s, σ 190km/s) are required in order to result in the HMXRBs having a space velocity value of ($42 \times \frac{4}{\pi} = 53$km/s). This may be realistic if the kick velocity is related to the amount of mass lost during the supernova resulting in significant differences between the two populations. This is a further suggestion that the kick velocity distribution is bimodal and that the kicks are dependent on the evolution of the system which may vary significantly in binaries over single stars. Therefore, the pulsar kick velocity distribution which is likely to be predominantly from single stars may not be indicative of kicks occurring in stars in binary systems.

4.3.2 Roche Lobe Overflow (RLOF) and Blue Stragglers

From the population synthesis models it is possible to determine what fraction of runaway stars underwent Roche Lobe Overflow before being ejected by the SNB mechanism. This is important since RLOF drastically changes the secondary. As large amounts of the primary's outer layers are accreted by the companion this will increase its mass, thus becoming rejuvenated and will become a Blue Straggler with respect to other stars in the birth cluster. The companion's rate of rotation also increases, as angular momentum from the accreted material is deposited on the stellar surface. The percentage of runaways which undergo mass transfer and hence spun-up or seen as Blue Stragglers with respect to their parent cluster is relevant for observational studies. Elevated rotation velocities and the Blue Straggler nature of the runaway may be used as a way of inferring the mechanism for runaway production and may aid in identifying the parent cluster (Hoogerwerf et al., 2001).(also see Chapter 5 *Rotation Velocities of OB Runaways*)

From an analysis of our simulations, 100% of O star runaways and 80% of B star runaways are found to undergo RLOF prior to being ejected. While this implies that all of the O stars will appear as Blue Stragglers only 58% of the B stars become Blue Stragglers. This is due to the fact that 75% of the runaway B stars experience a common envelope, CE, phase (and by contrast none of the O stars go through a CE phase). RLOF may begin in a binary system but be halted abruptly by the formation of a CE and instead of mass being transferred to the secondary the CE is ejected from the system. A CE phase does not happen in all cases but it occurs sufficiently often to reduce the B star runaway Blue Straggler percentage from a possible 80% to 58%. It is also important to consider how long a runaway may be observed as a Blue Straggler. 98% of the Blue Straggler O star runaways become Blue Stragglers prior to being ejected, this means that most O star runaways spend their entire runaway lifetime as Blue Stragglers. Massive O star runaways being Blue Stragglers for their entire lifetimes may be expected since the primary in such a massive O-type binary is likely to be one of the most massive stars in the cluster. If it transfers mass to its companion, the companion is then likely to be more massive than the initial primary, but less evolved, and hence appear as a Blue Straggler while still in the original binary. The primary will subsequently erupt in a supernova and eject the Blue Straggler. By contrast only 42% of Blue Straggler B star runaways become Blue Stragglers prior to being ejected. The average ratio of lifetimes for runaways which become Blue

Straggler after they are ejected can also be determined from the simulation data: Blue Straggler lifetime (T_{BS}) to runaway lifetime (T_{run}), $\frac{T_{BS}}{T_{run}} = 0.23$, for B star runaways. This still implies that B star runaways should be seen as Blue Stragglers ~30% of the time since 42% are already Blue Stragglers before being ejected and some of those that become Blue Stragglers after they are ejected will become so relatively quickly. These results are however inconsistent to those by PZ00. PZ00 applies a weighting to his results to determine the fraction of Blue Stragglers among runaways at any given time. He determines that 40% O star runaways and 10% B star runaways are likely to be observed as Blue Stragglers. The difference between the results is likely due to the analytic formula he uses which estimates the time a runaway spends as a blue straggler by considering the current age of the star and how much it has been rejuvenated, which overestimates the turn-off mass of the cluster resulting in stars being more often ejected as runaways before becoming Blue Stragglers. By contrast, in this code the time which a star appears as a Blue Straggler with respect to cluster is calculated during the simulation, which means the lifetimes of the stars as runaways and as Blue Stragglers may be determined directly. For runaway binaries with a compact companion, all of the O star runaway binaries are Blue Stragglers and all become Blue Stragglers before their ejection. 59% of runaway B binaries are Blue Stragglers but 63% of them become Blue Straggler prior to ejection. Of the remaining 37%, the Blue Straggler lifetime to runaway lifetime ratio is $\frac{T_{BS}}{T_{run}} = 0.21$, similar to that for single B stars.

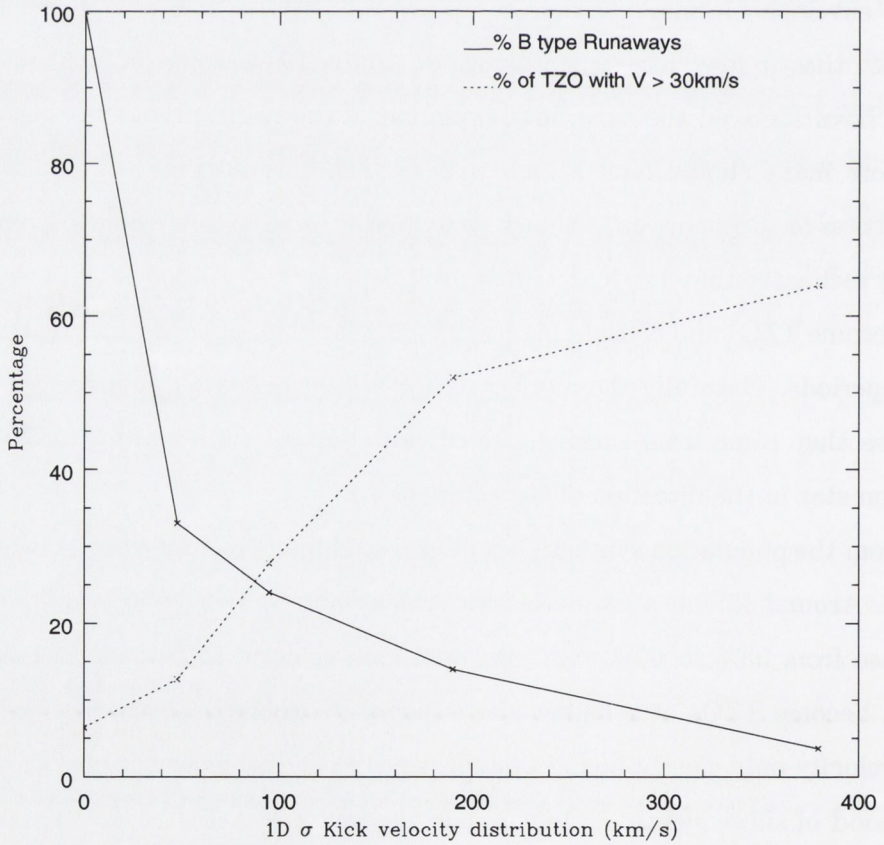
4.3.3 Runaways and Thorne-Zytkow Objects(TZO)

Thorne-Zytkow objects are 'normal' stars with a degenerate neutron star in its core. They were proposed for the first time by Thorne & Zytkow (1975) from whom the name derives. One possible scenario for the formation of a TZO is as follows. In binary systems which survive the supernova eruption of the primary, the secondary will continue to evolve, and if the separation is close enough (which in many cases it will be) a common envelope will form as the secondary expands and moves off of the main sequence to become a red giant (RG). Orbital energy is dissipated as the neutron star moves through the surrounding envelope reducing its orbital separation by several orders of magnitude and in some cases merging with the core of the giant, resulting in a TZO. A significant fraction of the envelope is likely to be lost by the secondary during this process due to friction and accretion caused by the spiral-in, estimated from simulations to be ~20% (Terman et al., 1995). How a TZO may appear observationally depends on various factors including the amount of mass in the envelope. It may continue to appear as a RG or it may appear as a WR due to the fact that it may have a strong wind. Since TZOs come from close binary systems which have survived the supernova explosion of the primary and the kick to the neutron star core many should have a high velocity. This would then suggest that a significant proportion of supernova in a binary generated runaway stars would become TZOs. Taam (1996) estimates that Be/XRBs with orbital periods < 100 days will eventually spiral in and become TZOs and considering Figure 4-7 a large number of runaway binaries have such short periods. Naturally the number of TZOs that is created is a function of the applied kick, as they come from surviving binaries in general (unless a fortuitous kick sends the neutron star in the direction of the companion).

From the population synthesis results here, a high percentage of ejected binaries become TZOs. Around 35% at a low natal kick velocity and up to 60% at high kick velocities. The increase from 35% to 60% with increased kick velocity in fraction of coalescing binaries which become TZOs at a higher kick velocity is expected due to the fact that at a high kick velocity only closely bound systems survive. These close systems then have a greater likelihood of subsequently coalescing and becoming TZOs. For O star masses, the binary fraction that become TZOs is consistently lower at around 25% irrespective of the applied kick. As seen from Figure 4-13, the percentage of high velocity TZOs increases with an increasing natal kick velocity. Even though the number of TZOs decrease with increasing

kick velocity, the fraction that will have a high velocity increases. Figure 4-13 also shows the percentage of TZOs among B type runaway systems. This percentage decreases with kick velocity since fewer systems survive the supernova explosion of the binary. However, even with a mean kick distribution as high as 300km/s (σ = 190km/s), close to 15% of runaways could be a TZO. TZOs may be WN8 stars as suggested by Foelmi & Moffat (2002), who selected them as candidates based, in part, because of the fact that they have high velocities (Moffat, 1989) or have large distances from the Galactic plane (van der Hucht, 2001). De Donder et al. (1997) from their model calculations, predict that 20-30% of WR+OB binaries produce TZOs.

Figure 4-13: *Figure shows the percentage of massive TZOs (with respect to the single B star runaway population) as a function of the applied kick velocity (solid line). It also shows the percentage of TZOs with high velocities with respect to the total TZO popuiation (dashed iine).*



4.4 N-body simulations with binary stellar evolution

4.4.1 nbody6-2 vs Population Synthesis

A set of 7.5×10^3 initial binaries (which corresponds to 50 simulations with 450 stars and a 0.5 Binary Fraction) from the low density nbody6-2 simulations were evolved using the population synthesis routines in order to compare the results from both procedures directly. While the routines governing the details of binary evolution are essentially the same, there are some differences when adding stellar evolution routines to a full N-body code. This can result in the final binary systems being discrepant when comparing results from each code. The main difference which is of interest here is related to RLOF in nbody6-2. RLOF may only begin in nbody6-2 when the binaries have been circularised by tidal forces, while in the population synthesis routines circularisation is not a requirement for RLOF to begin. The consequence of this difference is that greater mass is lost from the primary before mass transfer can occur (due to the time delay for circularisation to be complete) and in many cases can result in mass transfer not occurring at all. This means that the stars ejected from binaries via the eruption of the primary when using nbody6-2 are generally less massive than those evolved with the population synthesis algorithms alone. The knock-on effects are that coalescence and a common envelope phase also occur more often with the nbody6-2 code. This has positive and negative influences on the number of ejected of stars from binaries as a result of the eruption of the primary. For very close binaries coalescence will obviously now convert a binary into a single star and no runaway may result. The common envelope phase may produce a reduced mass primary and secondary resulting in fewer massive runaways. However, it may also reduce the orbital separation and if only a small fraction of mass is lost to the envelope then a massive runaway can still result. On the other hand, mass transfer occurring less often in nbody6-2 results in fewer massive B and O star runaways. Recall that in the population synthesis routines all O stars had mass transferred to them before they became runaways and in many cases it was because of this additional mass that they became massive enough to be O stars. The larger significance of these details are that nbody6-2 generally produce more ejectees when the masses of the stars are ignored. At higher masses, nbody6-2 produces fewer massive ejectees than the population synthesis method. This is important for higher mass O runaways but less significant for the lower mass B type runaways. The reason for the difference is that, as we have seen in the previous chapter, mass transfer occurs in the majority of cases when producing both O

and B type runaways. However, for B star runaways, the vast majority are already B-type before mass transfer occurs. Thus, the O type runaway fraction is reduced in nbody6-2 due to mass transfer being less common. The B type runaway fraction is then only ~15% lower in nbody6-2 than the Population synthesis results but with most of these being of lower mass B type stars ~6-10$M_{\odot}$. We can consider these ramifications when analysing the results from nbody6-2.

4.4.2 nbody6 SNB vs nbody6-2 SNB

With a full set of binary stellar evolution routines incorporated into the gravitational stellar dynamics code, the following set of simulations using nbody6-2 (see section 3.4.2) and analysis should offer a good understanding of the interplay between the two runaway mechanisms and provide more reliable statistics in terms of binary fractions, masses, velocity dispersions and ejection rates, particularly for the supernova in a binary scenario.

It is important to know to what degree the SNB scenario ejection rate is affected by the inclusion of binary evolution routines. Recall that in nbody6 when a star in a binary moves off the main sequence and expands it may touch its companion. When it does the stars are merged into a more massive star equal in mass to the sum of the two. This is not the physical case and is essentially what the algorithms in nbody6-2 treat more appropriately. When a star moves off of the main sequence and expands, it most commonly fills its Roche lobe at which point matter may stream to the secondary and be accreted. In this way the secondary gains mass and the primary loses it. The consequences in terms of runaways produced via the supernova in binary mechanism are two-fold. In the first place, the merging of stars in nbody6 instead of complex binary interactions obviously reduces the number of runaways produced via the supernova in a binary mechanism, since the binary has essentially been removed, especially considering that this is more likely to happen for more massive stars and in closer systems. Comparing the low density simulations of nbody6-2 and nbody6, the number of supernovae occurring in binary systems is increased by 60% from nbody6 to nbody6-2. This is evidenced further by the large number of merged stars which occur in nbody6 (over 10 per simulation) whereas nbody6-2 has only a fraction ($\sim$ 0.6) which coalesce after a previous and complex binary evolution process. In the second place, mass transfer in nbody6-2 produces secondaries of higher mass which may become high mass runaways. However, this alters the separation of the binary and can result in a lower

velocity ejected companion stars. Overall, this then results in a reduction in the number of SNB ejected stars from nbody6-2 to nbody6. The estimated fraction of massive runaways ejected via SNB is overestimated by over 50% in nbody6 by contrast to nbody6-2.

4.4.3 nbody6-2: SNB runaways from different cluster environments

4.4.3.1 Low Density (SNB Ejections)

Table 4.5 shows the results for SNB ejectees for 1.0 and 0.5 initial binary fraction, as before indicated by BF1 and BF05 respectively. From the 100% initial binary simulations, BF1, the percentage of B-type stars that are runaways is 1.76±0.51%. This agrees well with the population synthesis value from simulations with a binary range of $10 - 10^6 R_\odot$ which produce 1.55 ± 0.02% B stars as runaways. The O star runaway population is more difficult to compare due to low numbers as it is 1.9 ± 1.9% (only 1 O star was ejected) in nbody6-2 while it is 2.2 ± 0.2% from the population synthesis. The percentage of B star runaways, from the 50% initial binary fraction simulations, BF05, is 1.1 ± 0.4%. This is consistent with the BF1 simulations where 1.5 times the initial number of binaries increase the runaway ejection rate by the same fraction of 1.5.

Table 4.5: *Low Density: Percentage of escaping single B stars as a result of the SNB scenario. Errors are 1σ. BF1: 1.9 ± 1.9% single O star runaways (only 1 O star was ejected as runaway).*

Escape Velocity	% Total	% of early B stars	BF Total	BF early B stars
BF05; N_{run} = 60				
0-10km/s	0.34 ± 0.04	1.02 ± 0.25	0	0 0
10-30km/s	0.34 ± 0.04	1.81 ± 0.39	2 ± 1	5 ± 5
>30km/s	0.11 ± 0.02	1.10 ± 0.31	14± 6	20 ± 14
BF1; N_{run} = 40				
0-10km/s	0.51 ± 0.05	0.80 ± 0.32	0	0
10-30km/s	0.52 ± 0.05	3.82 ± 0.74	1 ± 1	4 ± 2
>30km/s	0.18 ± 0.03	1.76 ± 0.51	17± 8	27 ± 12

Accordingly, the ratio of DE:SNB mechanism may be determined using the results from Table 4.5 and the calculated DE values which are not shown since they are similar to the results from section 3.1.1 : for BF05 [8:92 (B-type runaways); 0:100 (O-type runaways)], BF1 [0:100 (B-type runaways) , 0:100 (O-type runaways)]. In conclusion, the SNB population from a low density cluster is, as expected, unaffected by being in a cluster and is well

approximated by a population synthesis analysis. There is a 1.5 times decrease in B star runaways from BF1 to BF05 simulations.

4.4.3.2 Medium Density (SNB Ejections)

Table 4.6 shows the ejection results for the SNB for BF05 and BF1 binary fractions. There is a ~20-40% increase in SNB B star runaways at this density by comparison to the low density cluster. The ejected percentage of B star runaways is : BF1, 2.46 ± 0.6%; BF05, 1.3 ± 0.4%. While this is not of the same order of the increase as the nbody6 simulations, it shows that the trend for the SNB scenario to be enhanced in a denser environment continues with close binary evolution included. The increase in SNB runaways is due to the hardening of the energetic binaries in the cluster.

Table 4.6: *Medium Density: Escape percentages for the SNB scenario single stars and binary fraction. BF05: 1.6% ± 1.6% O single runaways; BF1, 1.6% ± 1.6% single O runaways (only 1 O runaway was ejected in both cases)*

Escape Velocity	% Total	% of early B stars	BF Total	BF B stars
BF05; N_{run} = 40				
0-10km/s	0.22 ± 0.03	0.57 ± 0.29	0	0
10-30km/s	0.19 ± 0.03	2.02 ± 0.42	0	0
>30km/s	0.14 ± 0.03	1.29 ± 0.41	19± 8	40 ± 22
BF1; N_{run} = 30				
0-10km/s	0.32 ± 0.06	0.63 ± 0.21	0	0
10-30km/s	0.23 ± 0.04	2.41 ± 0.58	0	0
>30km/s	0.26 ± 0.04	2.46 ± 0.62	7± 4	18 ± 9

As noted previously, an appreciable number of dynamically ejected massive binaries escape from the system. We now investigate this possibility using the population synthesis code to evolve these ejected binaries. The population synthesis results show that few in fact later become SNB runaways despite their short periods. Heavy mass transfer in such close eccentric systems often results in a white dwarf primary together with a more massive main sequence companion. Common envelope evolution is also a typical occurrence which results in decreasing the mass of both components. Hence, the ejected massive binary fraction does little to increase the SNB runaway population.

Once more we calculate the relative fractions of DE:SNB runaways and for reference the

DE values may be related to section 3.1.1: [BF05, 39:61 (B-type runaways)]; [BF1, 32:68 (B-type runaways)]; No single O stars were ejected via the SNB scenario]

4.4.3.3 High Density (SNB Ejections)

Table 4.7 shows the SNB results for both BF05 and BF1. In a similar fashion to nbody6 the number of SNB ejected runaways in nbody6-2 is now lower than the medium density cluster: BF1, 2.0 ± 0.8%; BF05, 1.2 ± 0.4%.

Table 4.7: *High Density: Escape percentages for the SNB scenario single stars and binary fraction. BF1: 22 ± 2.2% single runaway O stars. (only 1 O star runaway was ejected)*

Escape Velocity	% Total	% of early B stars	BF Total	BF B stars
BF05; N_{run} = 40				
0-10km/s	0.16 ± 0.03	0.74 ± 0.44	0	0
10-30km/s	0.20 ± 0.03	1.41 ± 0.42	25 ± 25	5 ± 5
>30km/s	0.084 ± 0.02	1.18 ± 0.42	8± 8	13 ± 13
BF 1; N_{run} = 30				
0-10km/s	0.23 ± 0.05	0.81 ± 0.51	0	0
10-30km/s	0.17 ± 0.04	1.36 ± 0.64	16 ± 9	7 ± 7
>30km/s	0.0014± 0.003	1.98 ± 0.80	7± 7	0

At this point we will look in more detail at precisely the mechanisms which are changing the SNB fractions. The SNB runaways typically come from the most massive binaries in each of the clusters. Being the most massive they sink to the core where they can undergo interactions. In the low density simulations the time to sink to the cluster centre is long and little interaction occurs between the stars in general. Hence, the number of SNB runaways is determined from the initial distribution of binary parameters. At higher densities dynamical interactions may occur more readily, perturbing the binaries. In the high density simulations ~25% of the binaries which produce SNB runaways have an exchanged companion, while over 50% of SNB reactions which produce lower velocity ejectees occur in systems which have exchanged a component. The exchanged companions are more massive stars than the original secondary, making it an effective way to closely pair massive stars. ~30% of SNB runaways already have an elevated velocity and are found far from the cluster centre before the supernova occurs and ~40% of SNB reactions in general occur far from the cluster centre.

Why the medium density cluster appears to have the highest ejection rate of SNB runaways is more difficult to assess. About 30% of binaries which become SNB runaways suffer significant interactions which elevate their velocities and eject them from the core. However, no exchange interactions are seen to have occurred for the subsequent runaway systems, although for SNB in general, ~40% have exchanged companions before the supernova of the primary. This leads to the following conclusion, that the increase in SNB is primarily due to the hardening of binaries as a result of close encounters, which is evidenced by the ejection of the binaries from the core with relatively low velocities prior to supernova. Higher velocity binaries which escape are more closely bound, which they need to be in order to survive a strong interaction. This results in a SNB runaway being unlikely to occur as discussed in the previous section. At high density exchange interactions are likely to occur, increasing the mass of the ejected star, however, this does not appear to have an effect on the B star runaway population in general (although it may be more significant for producing the most massive runaway O stars).

Two possibilities remain that subsequently reduce the SNB runaway population as the cluster density is changed initially from medium density to high density. These are disruptive interactions and collisions. It is more likely that the increase in collisions in the high density simulations is the cause for the decrease since such closely bound massive systems are difficult to disrupt while a collision as discussed in the previous Chapter may occur with significant probability in a binary-binary interaction. In fact, from evolving the original binaries of the massive runaway stars, (using the population synthesis routines) which instead collided and were dynamically ejected in the high density simulations, we find that of the order of 10% of the original binaries could have become SNB runaways had they not suffered a collision in the cluster and were ejected. This 10% accounts well for the decrease in massive runaway rates from the medium density to high density cluster. At even higher densities, it might then be expected that collisions play a larger role in decreasing the SNB massive runaway rate.

The relative fractions of DES:SNB runaways are, again using section 3.1.1 as a reference for the DE values are: BF05 [77:23(B-type runaways), 100:0 (O-type runaways)] and BF1 [59:41 (B-type runaways) 50:50 (O-type runaways)]

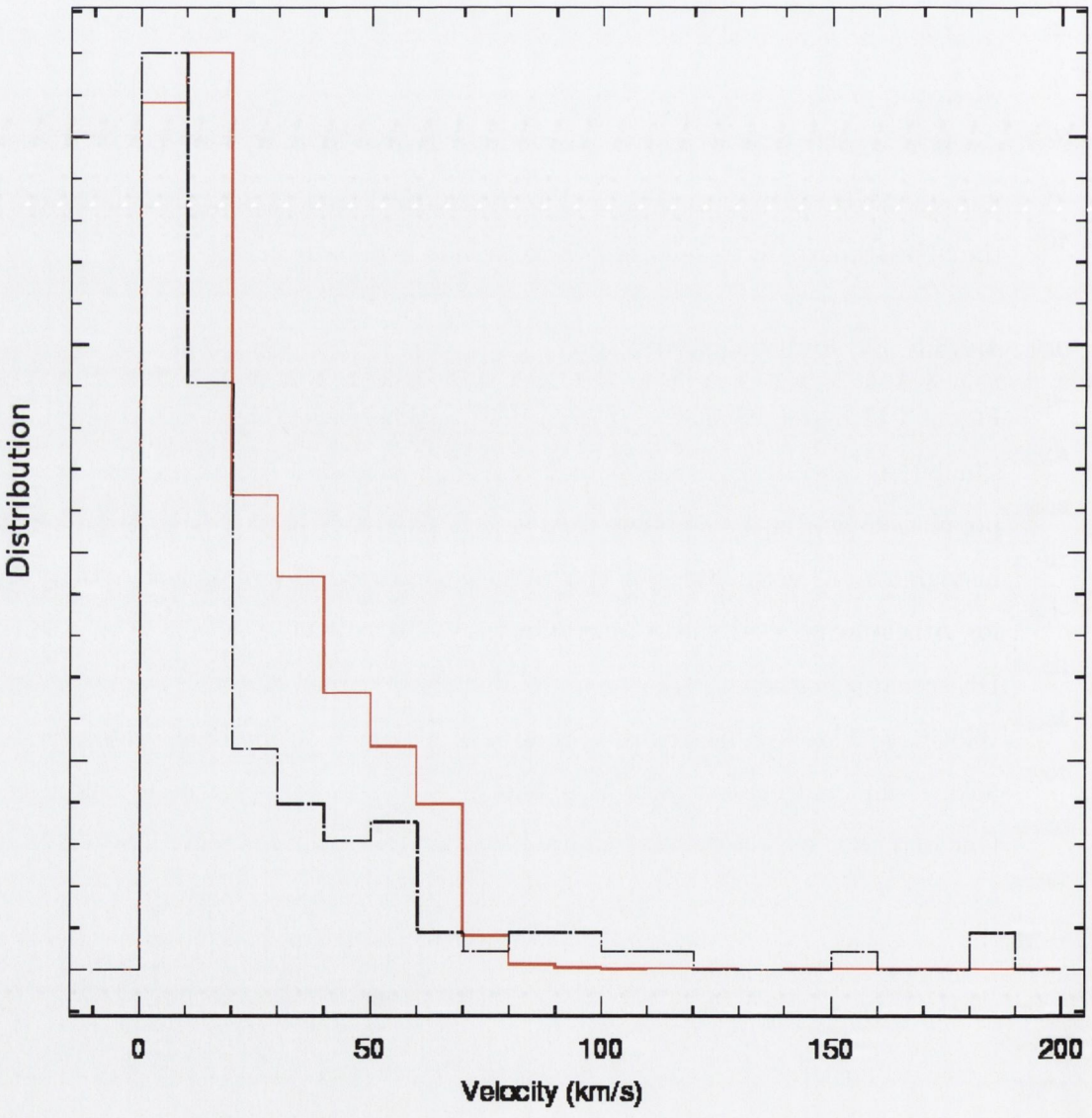
4.4.3.4 A note on O star SNB ejections

The percentage of O stars ejected from these nbody6-2 simulations is in general lower than the population synthesis values. There are two reasons why this occurs in this case. The first is due to the aforementioned differences in the binary evolution routines which result in mass transfer occurring more often in the population synthesis simulations than in nbody6-2. This has the largest effect on the production of O star runaways via the SNB mechanism, since only on rare occasions are two O stars paired with each other even when the mass ratio is peaked towards unity. This means that mass transfer is a necessary condition in many cases in order to produce an O star companion which will be ejected when the primary erupts in a supernova. Secondly, the population synthesis simulations produce ~2.2% single O star runaways, this means that even with 40 simulations less than 2 O star SNB runaways are likely to be produced. Hence, the lack of O star runaways from the SNB scenario in some of the above results is not surprising.

4.4.3.5 Velocity Distributions

Figure 4-14 shows the relative velocity distributions of the DE scenario from the high density simulations and the SNB ejections from the population synthesis results $10 - 10^4 R_\odot$. The population synthesis results are used since they constitute a larger statistical sample. The histograms are normalised for comparison purposes. Disentangling velocity distributions for either mechanism with observations is clearly difficult. What is apparent is that the DE scenario produces a steeper initial distribution than the SNB and then tails to higher velocities. The SNB mechanism produces a higher fraction of lower velocity stars, around 50km/s and much fewer very high velocity stars, a sharp decline occurs around 70km/s. One may then expect that extreme velocity massive stars are more likely to be dynamically ejected.

Figure 4-14: *For populations of DE and SNB escaped B stars the distribution of velocities are compared. The distributions are normalised for comparison with the DE population comprised of 200 stars and the SNB population 6000 stars. The red full line is the SNB distribution and the black dashed line is the DE distribution.*



4.5 Ejected Binary Characteristics

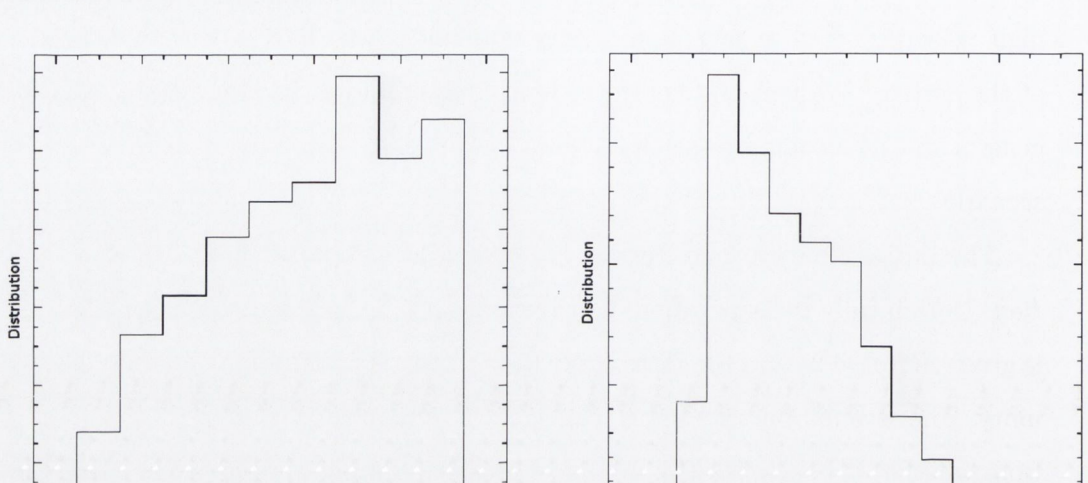
The characteristics of ejected binaries are important, not only for the observational determination of the type of ejection mechanism that may have given the binary system a high velocity, but also in making some estimate of the likely further phase of evolution of the system. We will first consider the characteristics of dynamically ejected binaries in general and then compare the characteristics of massive runaway binaries ejected via either scenario.

The initial binary parameters are discussed in Chapter 2 in the section *Initial conditions*. Specifically the separation distribution is flat in the logarithm $\Gamma \propto \frac{1}{a}$, the eccentricity is given as f(e) = 2e and the mass ratio distribution is correlated, leading to a peak towards unity. The escaped binaries are typically those who have experienced some level of interaction, whether it be a weak (fly-by) encounter or a strong complex encounter. Figures 4-15 a,b and c) show the eccentricity, separation and mass ratio distributions for all of the escaped binaries in the high density simulations. The eccentricity and mass ratio change little from the initial distribution since the majority of the interactions do not involve exchange processes and are relatively weak. However, the final separation distribution is different. This may be understood from the fact that in the high density simulations the mean velocity of the stars is relatively high. Recall that the definition of whether a binary is soft or hard relies on the mean velocity of the interacting objects in the system. Hence, there are fewer hard binaries in the high density simulation and the softer binaries are rapidly ionised. This leads to a reduction in the number of systems with large separations. Naturally the escaped binaries have survived interactions which otherwise would have disrupted them. This results in a distribution of more closely bound systems, which have higher binding energies, to be ejected.

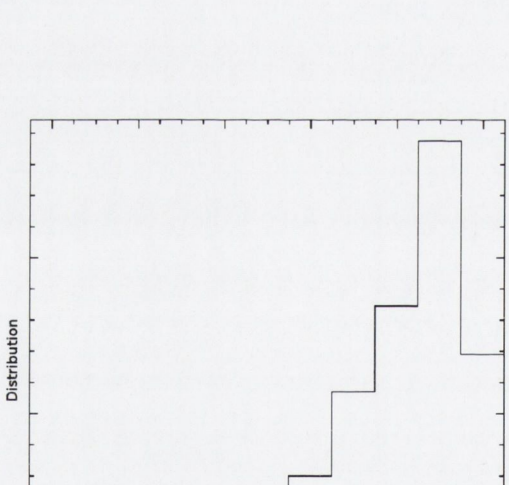
As noted in the previous sections the high density cluster produces binaries with a high velocity but the number produced is less than 0.4 per cluster, making the production of a statistic difficult. However, even with these small numbers, the changes in distributions are evident. Figures 4-16 a,c,e) show the distributions of massive DE runaway binaries immediately after the interaction which accelerated them has occurred.

Figure 4-16 a) shows the distribution of DE binary eccentricities. There is a large peak at zero eccentricity indicating that many high velocity ejected binaries are expected to be in circular orbits. This is due to tidal interactions readily circularising massive close binaries

Figure 4-15: *Figure a(left) Eccentricity distribution of escaped binaries. Figure b(right):Semi-major axis distribution of escaped binaries. Figure c (bottom): Mass ratio distribution Q of escaped binaries. Figures represent a total of 800 binaries.*



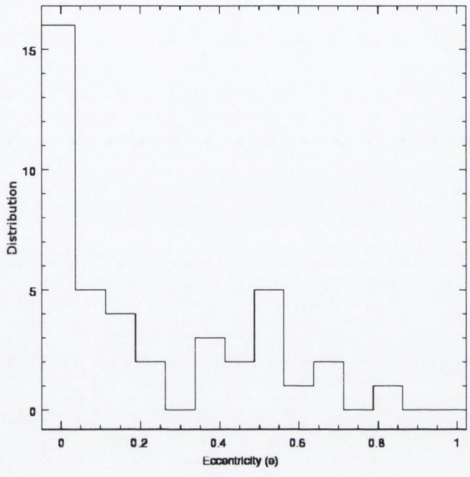
(a) (b)



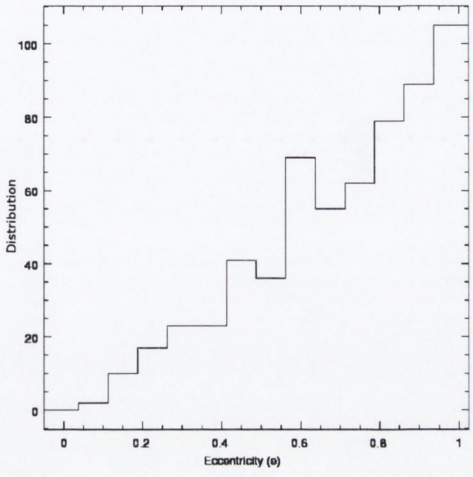
(c)

before they have been ejected. Some of these are also contact systems. Around 50% of the binaries have eccentricities less than 0.1. The remainder of DE massive high velocity binaries have eccentricities less than 0.6. Figure 4-16 b) shows the distribution of SNB ejected binary eccentricities. Over 80% of these systems have eccentricities greater than

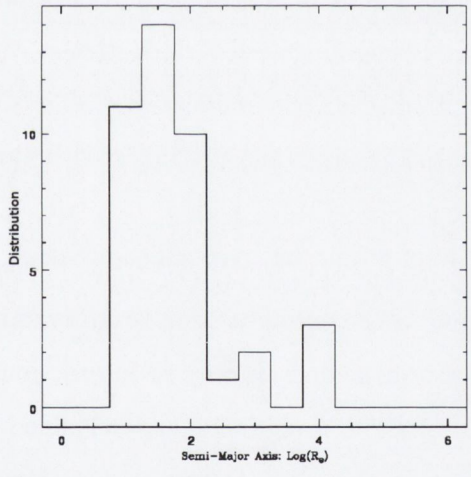
Figure 4-16: *Figures a,c,e are the distributions of eccentricity, semi-major axis and mass ratio for the* **DE** *binaries. Figures b,d,f are the distributions of eccentricity, semi-major axis and mass ratio for* **SNB** *ejected binaries with compact companions.*



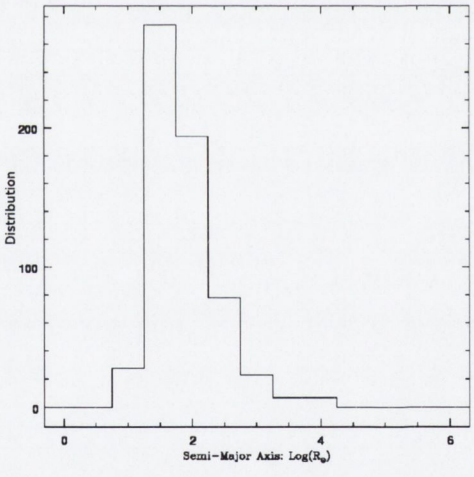
(a) DE Mechanism



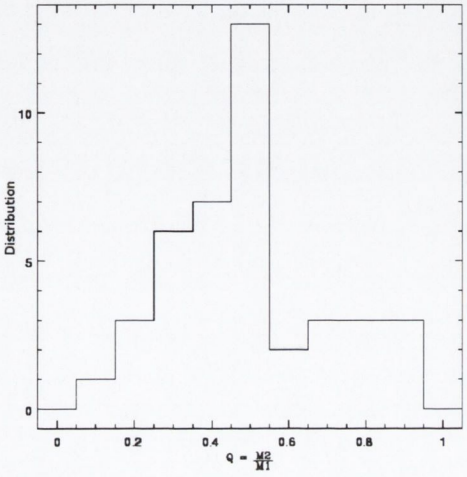
(b) SNB Ejection



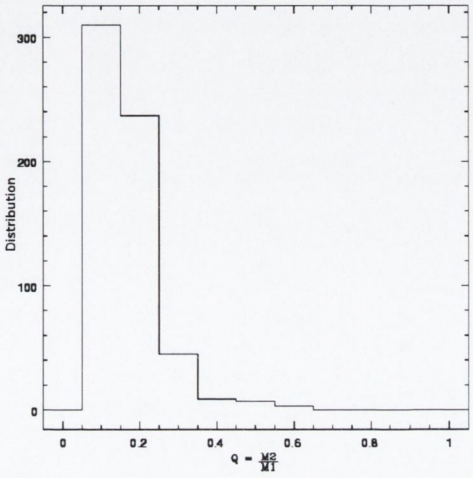
(c) DE Mechanism



(d) SNB Ejection



(e) DE Mechanism



(f) SNB Ejection

0.5 which is expected, since >75% of HMXRBs are Be/XRB systems. These systems have large eccentricities and X-ray emission occurs when the compact companion moves through the Be-star disk at periastron (van den Heuvel et al., 2000). Hence, we may say that DE binary runaways typically have low eccentricities and that SNB binary runaways have high eccentricities in general. However, circularisation, which may occur on short timescales, will also further alter these distributions over time. For binaries with a main sequence companion, circularisation is dependent on the binary period and radius $t_{cirt} \propto \frac{M^2}{R^5}$ where M is the mass and R the radius of the primary (Tassoul & Tassoul, 1992), which means that short period massive binaries will circularise within the main sequence lifetime.

Figure 4-16 c) shows the distribution of binary separations for the DE binaries. 70% of DE binaries have separations less than $100R_{\odot}$ (60% periods less than 10 days) and 90% having separations less than $1000R_{\odot}$ (90% periods less than 100 days). Comparing to SNB binaries, Figure 4-16 d), 68% have separations less than $100R_{\odot}$ (42% periods less than 10days) and 96% have separations less than $1000R_{\odot}$ (84% have periods less than 100days). VDH00 suggest that binaries with a compact companion with periods less than 10 days will circularise. Be/XRBs for example, that generally have periods greater than 16 days are those whose eccentricities are relatively unaffected by circularisation. Thus DE binaries will be typically close systems with low eccentricities, while SNB ejected binaries are also short period systems but most of which are expected to be highly eccentric.

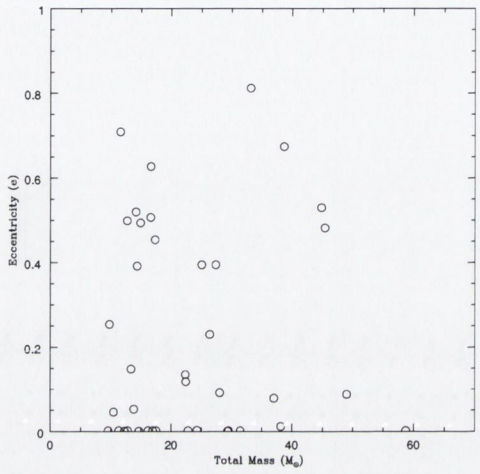
Figure 4-16 e) shows the distribution of mass ratios for DE binaries. It has often been stated that the ejected runaway binary mass ratio may be peaked towards unity since the stars involved in encounters would experience exchange during an interaction. The peak at high mass ratio is indeed largely due to binaries which have an exchanged companion: ~30% of high velocity massive binaries have an exchanged companion. However, as can be seen the majority of mass ratios peak towards 0.5. Lower mass ratio binaries are thus preferentially ejected with high velocities, which is consistent with the analysis of Leonard & Duncan (1990). Their Figure 6 shows the results of scattering experiments between binaries of equal total mass but a distribution of component masses (i.e. no total mass dependency). Binaries with a larger primary mass are more likely to be ejected, in other words binaries of lower mass ratios. Hence, at runaway velocities binaries with mass ratios towards unity are not dominant. From the exchange process and our results here the distribution of mass ratios for runaways is possibly bimodal. Kroupa et al. (1999) gives

evidence for binary mass ratio distributions due to interactions but concentrates on the distributions above a relatively small ejection velocity of 2km/s. While the numbers in his plots are low above the cutoff limit of 20km/s, they are generally consistent with values here. By comparison Figure 4-16 f) shows the mass ratios for SNB ejected binaries. As expected the majority of mass ratios is less than 0.2, since we are considering OB mass stars where the minimum B star mass is $5.9M_{\odot}$ and with a neutron star mass (which is the most common type of companion) of $\sim 1.4M_{\odot}$ (although neutron stars up to $3M_{\odot}$ are used in these simulations which puts the mass ratio upper limit at ~ 0.5) then mass ratios less than ~ 0.2 are typical. The higher mass ratio systems are typically from binaries with massive black hole companions.

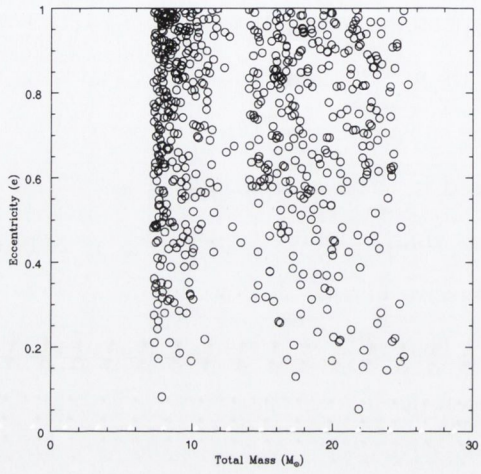
Extensive scattering experiments of binary-single and binary-binary encounters have been made over the years (Mikkola, 1983, 1984; Hut & Bahcall, 1983; Leonard & Duncan, 1990; Leonard, 1995; Sigurdsson & Phinney, 1993; Bacon et al., 1996). However, only a few of these studies focussed their attention on high velocity massive runaways or on runaway binaries. Leonard & Duncan (1990) do discuss the binary parameters in their simulations but their statistics are low. They show that most of their simulated binaries have a high mass ratio Q $\geq$0.5 and have eccentric orbits $0.4 < e < 0.7$. Figures 4-17 a-f) show scatter plots of the eccentricity, mass ratio and separation of DE and SNB ejected massive runaway binaries with respect to the total mass of the binary. Little dependence on the total mass of the system with respect to the eccentricity is seen, even though circularisation will have a larger effect for higher mass systems later on, as already as mentioned. For dynamically ejected binaries, the more massive the binary the smaller the separation seems to be. For DE binaries, the mass ratio distribution appears to shows a small dependence on mass as the more massive the primary, the more massive the companion is likely to be and the more difficult it is to dynamically eject such a massive system. Hence lower mass, low mass ratio systems are favoured. The SNB ejected binaries show an obvious mass ratio trend in ejected binaries, since the companion in general has a narrow range of possible masses. In cases where the companion is a black hole the total mass of the system is higher for larger mass ratios.

Observationally it is of interest as to how these dynamically ejected binary characteristics compare with the general characteristics for SNB ejected binaries. We give a point-wise summary of the details discussed previously.

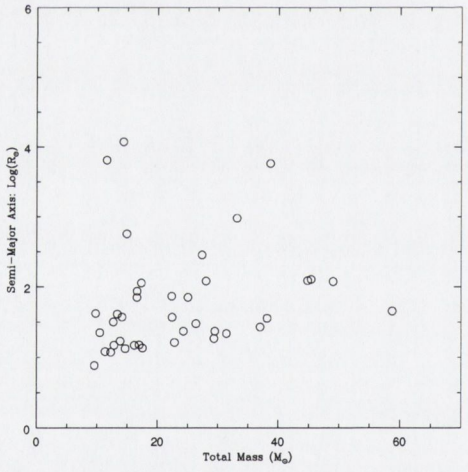
Figure 4-17: *Figures a,c,e are the distributions of eccentricity, semi-major axis and mass ratio versus total binary mass for* **DE** *binaries. Figures b,d,f are the distributions of eccentricity, semi-major axis and mass ratio versus total binary mass for* **SNB** *ejected binaries with compact companions.*



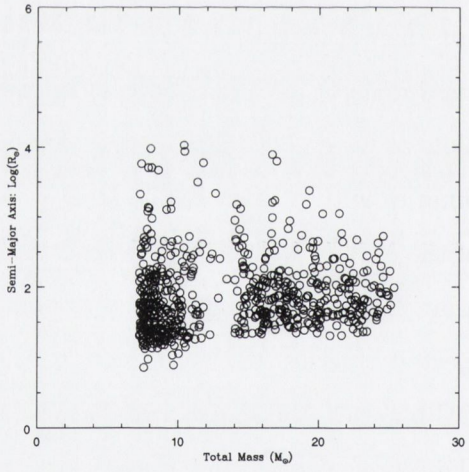
(a) DE Mechanism



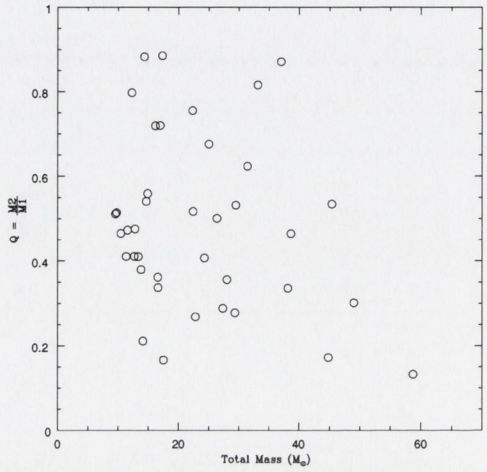
(b) SNB Ejection



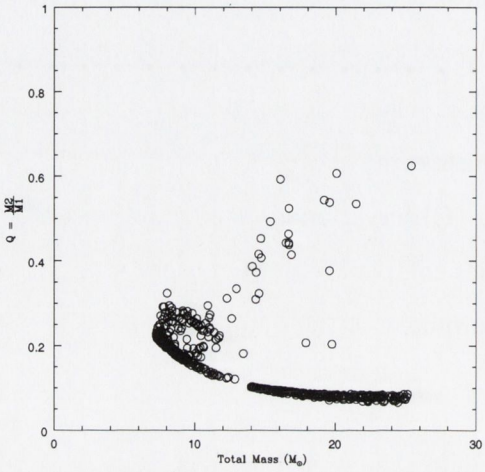
(c) DE Mechanism



(d) SNB Ejection



(e) DE Mechanism



(f) SNB Ejection

- **Mass Ratio:** Naturally the mass ratio in SNB systems is low since the most common type of companion to the O or B star is a neutron star. This results in a mass ratio typically lower then 0.2. However, note that the more massive the primary the more likely it is that it may host a massive black hole. The actual percentage of SNB runaway binaries with black hole companions is nonetheless small, ~4%, from the population synthesis results. By contrast the mass ratio for DE runaway binaries is likely to be between 0.2-0.6 with ~30% of systems experiencing an exchange interaction resulting in a higher mass ratio towards unity for those systems.

- **Total Mass:** DE massive runaway binaries typically have greater masses than their SNB ejected counterparts with ~50% of them having masses greater than $20M_{\odot}$ where only ~20% of the SNB binaries have such large masses.

- **Period:** SNB ejected, massive, high velocity binaries have on average greater periods than DE runaway binaries (see semi-major axis).

- **Eccentricity:** SNB ejected massive runaways are expected to have large eccentricities with >80% of them having an eccentricity larger than 0.5. The eccentricity range for DE massive runaway binaries is between 0.0-0.5 and are likely to circularise rapidly due to the small separations (~30% of systems are contact systems).

Table 4.8 shows the binary parameters for the known binary runaway stars listed in Appendix A. Clearly the binary parameters of these runaways are in general poorly known. It would be of interest to improve this where possible, by future observational studies. Without a more complete sample of both dynamically ejected high velocity simulated binaries and a better sample of observed parameters little can be conclusively said about how the properties of runaway binaries are related to those that are dynamically ejected or ejected via a SNB in general. A case by case analysis would be required at this juncture. For example, McSwain et al. (2007) suggest that the binaries HD 14633 and HD 15137 runaways are 'quiet' XRBs, making them likely SNB ejected binaries. The observed binary fraction among runaways is discussed in Chapter 5 and it is noted here that the DE scenario is thought to produce the double lined spectroscopic binary runaways as the SNB scenario would be expected to produce a runaway binary with a compact companion (eg. Neutron Star/Black Hole) rather than a binary with two 'normal' stars. From the above results, it is then unsurprising that few runaway binaries have well identified companions since many

are likely to be low mass ratio, short period, close systems where the dimmer companion (particularly NS) may be obscured by the much brighter massive O or B star.

Table 4.8: *Runaway Binary Parameters: The first six listed are double lined spectroscopic binaries and are separated since they are good candidates as DE runaways. Values are taken from the VizieR catalogue query database and some papers (Gies & Bolton, 1986; Leonard & Duncan, 1990; Boyajian et al., 2005; Pourbaix et al., 2005; McSwain et al., 2007).*

HD	HIP	Period	Mass Ratio (q)	e
3950	3346	5.5412	0.45	0.0
4727	3881	4.2827	0.7	0.03
37043	26241	29.1338	0.57	0.764
191567	99283	1.81837	0.6	0.0
198846	102999	2.99963	0.96	0.1458
220057		4.41508	0.96	0.55
	5391			
	9498			
14633	11099	15.4083	0.06	0.68
15137		30.35	0.06	0.48
37737	26889	7.84		0.43
41161	28881			
41534	28756			
52533	33836	22.1861		0.30
59215	36246			
69080	40341			
110879	62322			
124195	69491	1.4901	0.52	0.030
175876	93118	1.32	0.98	0.0
180183	94899			
227877				
235807	110362	5.4150		0.24

4.5.1 Estimating the DE and SNB populations from the observed bound group

It is evident that the observed runaway binary population can offer insight into the mechanism that produces the majority of OB runaways. We present in the following an exploratory estimate as to the number of single runaways via each mechanism from the

observed runaway binary population.

The XRB population is part of the bound group from the SNB mechanism which produces massive runaways. From the previous sections the simulations give us the relative numbers from the high velocity bound binary stars to the corresponding number of high velocity unbound single stars. Hence, we may determine a lower limit to the expected fraction of runaways that are likely to have been produced via the SNB mechanism using the known XRB population. The known number of XRBs with velocities greater than 30km/s is approximately 14, as listed in Table 5.3, Chapter 4. Of the 14 cases 6 are O-types and 8 are B-types (B0-B1). As a tentative measure we estimate the fraction of O and B type runaways that we may expect from the supernova in a binary scenario. From the population synthesis results we show that the bound fraction of runaways produced by SNB is of the order of ~40% for O stars and ~25% for B stars. If the 6 O runaway XRBs correspond to 40% of the SNB runaways then 9 O stars are expected to be single runaways. However, McSwain et al. (2007) suggest that HD 14633 and HD15137 may be quiet XRBs. Hence, for an adopted 40% binary population the 8 binary O stars should have 12 corresponding single O stars. From Appendix A (which is a composite listing of known O and B runaways), there are 19 single O stars known. This implies that if 12 single O stars are produced via the SNB scenario then the SNB mechanism may account for $\sim 12/19 = 63\%$ of the total O star percentage. Similarly, 8 B-type XRBs implies 24 single B stars from the SNB scenario. There are 69 classic single B stars listed in Appendix A. This means that if 24 single B stars are SNB ejected then this implies that $24/69 = 35\%$ of known runaways are produced via the SNB mechanism. While these numbers are rough they do suggest that the single star fraction of both O and B star runaways generated from the SNB scenario may be substantial. However, there are a number of effects which will play a role. The known XRB population is a selective bias since dedicated searches for strong X-ray emissions sources were employed. The OB runaway searches are likely to cover a smaller volume in the Galaxy then the XRBs and thus not be comparable to the number of runaways estimated on the basis of the number of high velocity XRBs observed.

Similarly we may expect that runaway double lined spectroscopic binaries are most likely ejected due to dynamical interactions. From the runaways listed in Appendix A there are 1 O-type and 5 B-type double lined spectroscopic binaries. From the simulations only the high density cluster produced any high velocity massive binaries. The percentage

of B-type binaries from these results is ~20% and while the O-type percentage is more ambiguous due to the low numbers involved it appears to be higher ≥25%. This implies that over 15 single B stars and over 3 O stars are dynamically ejected. This gives a B star binary percentage of 20/69 = 39% and an O star binary percentage of 3/19 = 16%.

The O star percentages even with these rough estimates appear to match reasonably well. SNB and DES 63% and 16% respectively. However, from Appendix A, four O star runaway binaries remain with an unknown companion. Thus, the mechanism that ejected them is uncertain and was not included in these estimates. If we now consider these stars we may do so in a number of ways, i.e. all four are DE binaries, two are DE and two are SNB ejected, all four are SNB ejected binaries. Including the previous result we have 12, 15 or 18 single SNB stars with 8, 10, or 12 corresponding binaries respectively. Similarly, 3 , 9 or 15 DE single runaway corresponding to 1, 3 or 5 DE binaries respectively. If all the additional binaries are DE then the single star ratio DE:SNB is 15:12, if two DE and two SNB then the ratio is 9:15 and if both are SNB then the ratio is 3:18. This gives 56%, 38% or 14% single DE O star runaways. Considering the B stars then 8 B star binaries have unknown ejection mechanisms. If we consider three possibilities only, they are all DE binaries, they are evenly 4 DE and 4 SNB binaries, they are all SNB binaries. We obtain then 24, 36 and 48 SNB binaries respectively and 20, 36 and 52 DE binaries respectively. This gives the ratio in the cast that both binaries are DE binaries 52:24, they are evenly distributed 4 DE binaries and 4 SNB binaries 36:36, they are all SNB binaries 20:48. This gives 68%, 50% and 29% DE B star single stars runaways. Overall this suggests that the O star DE percentage is 15-60% and the B star DE percentage is 30-70%. This illustrates how important it is through further observation to identify the binary nature of massive runaways and identify both components.

It is important to note that the above analysis is only an initial suggestion in order to link observational numbers to simulation results. It requires many further considerations such as for example,

- The observed number OB binaries is small which leads to large errors in the estimated number of single stars and the general fractions.

- We have assumed that the observed numbers of OB runaways, single and binary, and OB stars in general are indicative. This may not be true. For example, young O stars are sometimes difficult to detect as they can be hidden within their parental clouds

- We have assumed that the observed runaways are all coming from the same type of cluster density. We have assumed that DE binary runaways have come from dense clusters of a particular population and that all DE runaways come from similarly sized and dense systems. This is not necessarily true since there exist a large number of clusters with different properties in terms of number of constituent stars, ages and probable initial densities.

4.6 Conclusions

Figure 4-18 shows the percentage of dynamically ejected stars with respect to different ejection velocities. As has been noted before the low density simulations barely produce any escapees via the dynamical ejection mechanism. Once a moderately sized density is applied then a sizeable portion of massive stars are dynamically ejected, and many with high runaway velocities, resulting in an increased ratio of DE to SNB runaways. The percentage of dynamically ejected runaway B stars is then between ~20-35% depending on the initial binary fraction. At the highest density the dynamical ejections are dominant and produce between ~60-80% of the total B star runaway fraction. Clearly the density has a dramatic effect on the ratio of ejection mechanisms and one needs to consider the constraints that may specify the most likely density a cluster might have. Once a typical initial cluster density is assumed based observed and theoretical estimates then the ratio of DE:SNB runaway ejections may be established. The natural constraint is of course the fraction of ejected massive stars as seen observationally. If we maintain that this lies in the region of 2-4% then we may consider what the likely initial condition is. While previous population studies have shown that the supernova in a binary mechanism may produce the observed percentage, they do so by assuming that the initial binary separation population is of the order of $10-10^4 R_\odot$. We have shown in the previous sections how the escape rate varies with initial binary separation and that with a larger range the escape rate of massive runaways is below what is observed. In the section *Initial Separation - Binary Energy* in Chapter 2, we have shown that while the dynamical ejection of high velocity stars is increased by having a more tightly bound initial population the overall result is that there is an overall increase in the fraction of SNB B star runaways ejected by comparison to DE B star runaways (i.e. the supernova in binary scenario has a larger increase in ejectees than does the dynamical ejection mechanism due to a more closely bound population). Furthermore, it was shown that with an increase in density the massive runaway ejection rate from the supernova in binary scenario actually increases due to the fact that dynamical interactions produce a more tightly bound massive set of binaries than the original distribution. Assuming a 50% binary frequency, the high density simulations give a B star runaway percentage too high overall (4% DE, 1.2% SNB) and the medium density simulations give a runaway ejection percentage at the lower end of the observed percentage (0.64% DE, 1.3% SNB). This points to a density between these two ranges being suitable to reproduce the observed fractions.

While the decrease in separation range did enhance the B star dynamical ejection rate moderately, it had a more pronounced effect on the O star runaway population. It is a probable scenario that the reason that so few O stars were produced in other simulations is that they rarely were situated in sufficiently close binaries. Considering that less than two O stars on average are generated for any given simulation and that the distribution of separations is random over the entire separation range, it is unlikely to have O star systems tight enough to be ejected. Naturally dynamical evolution may create such systems through exchange processes and hardening of binaries, however it seems apparent that even at the highest densities this is insufficient, evidenced by the relatively low fraction of high velocity ejected O stars. An O star population that begins its life with very close separations fits well into star formation theories, since if these were created in the dense environment at the centre of a contracting molecular cloud than the likelihood of them pairing at close distances is greatly enhanced (Moeckel & Bally, 2007). The scenario would then be an initially moderate density system between the high and medium densities that were adopted and simulated here, and a narrow binary separation range for the massive stars at the very least. However, recall that the expulsion of gas from the system has a severe effect on the subsequent evolution and dynamics of the cluster. While a dense core may survive there will without doubt be a large effect on the dynamical ejection rates. If DE were to still produce massive runaways this would require a much denser system than the high density system considered here. However, as noted previously such an extremely dense initial state of a cluster is not unreasonable.

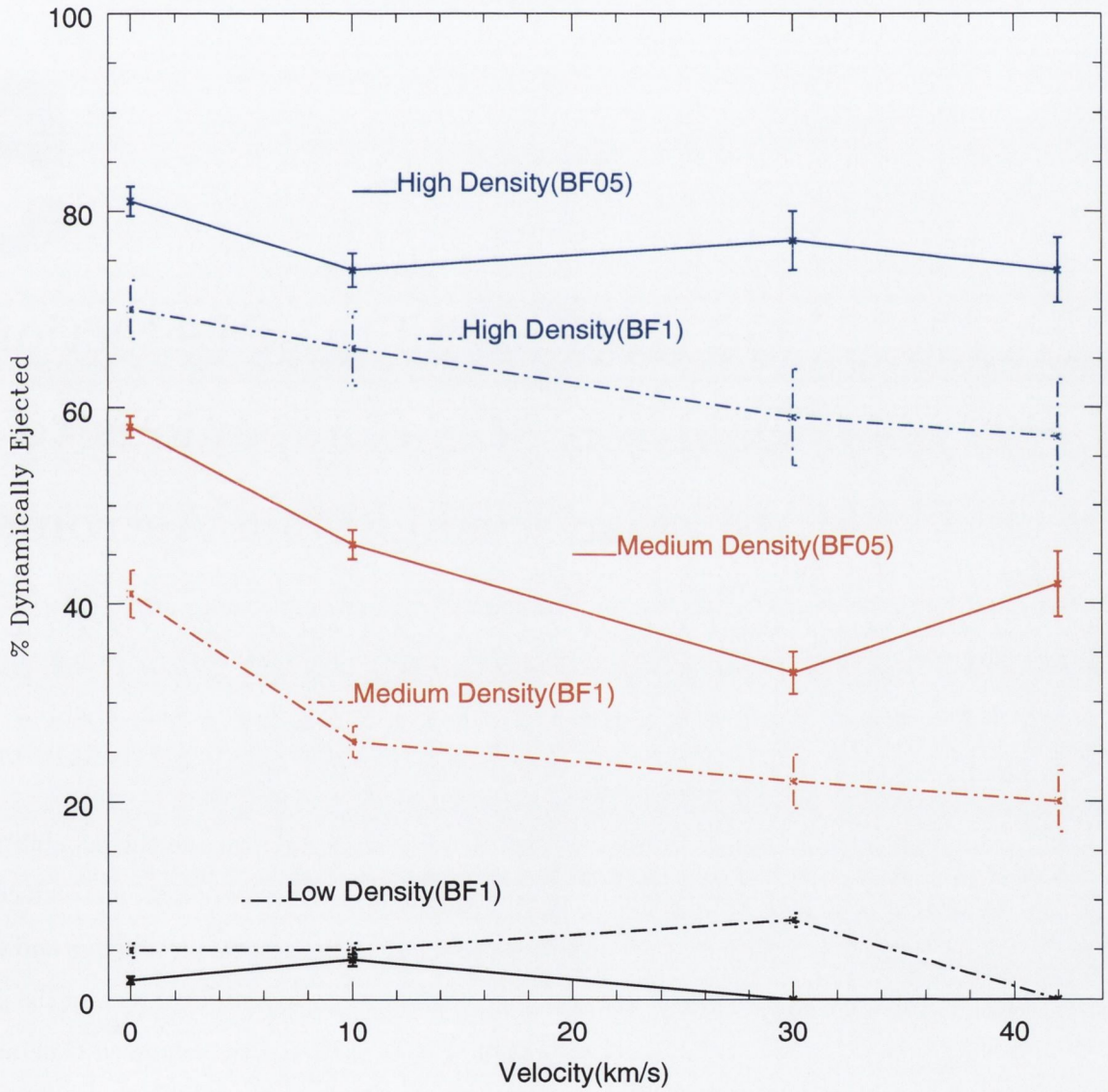
From an analysis of the characteristics of ejected binaries ejected via both mechanisms we have shown that DE runaway binaries are typically more massive and have a higher mass ratio than their SNB ejected counterparts. We show that DE binary runaways have typically shorter periods than SNB binary runaways and that DE binaries have lower eccentricities in general. Finally we have made a first estimate of the number of runaway single stars via both mechanisms based on the number of observed binaries. This estimate is 15-60% of O stars and 30-70% of B stars are DE runaways.

With the population synthesis simulations we have investigated how the frequency of SNB ejected runaways change with different sized kick distributions. We also show how the frequency is changed depending on the initial binary separation. Utilising the velocity distributions of ejected binaries via the SNB scenario we show under what conditions the

velocity distributions may compare with those observed for Be/XRBs and OB-supergiant XRBs. From this we suggest that the kick velocity distribution is bimodal with a lower kick velocity occurring in Be/XRBs (mean ~160km/s) while kicks occurring in OB-supergiant systems are systematically larger (mean ~300km/s). We have determined that nearly all SNB ejected O and ~30% of B star runaways will be observed as Blue Stragglers with respect to their parent clusters. It is further likely that ejected high velocity, high mass binaries, will coalesce and drag the compact companion to the core of the 'normal' star. Thus, ~15% of single star runaways may be Thorne-Zytkow objects. However, these may be observed as M-type red giant stars or WN8 Wolf Rayets.

The observational influence of when runaways are seen is also discussed. We show that this, due to mass transfer, particularly in O star runaways, can result in an observed O star runaway frequency of ~12% and an observed B star runaway frequency of 0.5%. Thus, observed runaway O stars may be predominantly ejected via the SNB scenario and runaway B star be ejected in the majority by dynamical interactions.

Figure 4-18: *Percentage of dynamically ejected massive B stars with respect to the total ejected via both mechanisms, $N = 450$. BF indicates initial binary fraction of the cluster, BF05 = 0.5, BF1 = 1.0. The error bars are standard errors of the mean $SE = \frac{\sigma}{\sqrt{N}}$. The solid black line unmarked at the bottom of the plot is the Low Density cluster with BF05.*



5

On the Feasibility of Detection of Neutron Star Companions to OB Runaways using Gaia Astrometry

5.1 Abstract

For an illustrative sample of classical OB runaway stars, we examine the capability of the upcoming Gaia satellite to detect compact companions by the use of astrometric techniques. For the OB runaway stars in our sample we estimate initial system parameters and consider the modifying evolutionary effects of mass transfer and supernova explosion of the primary. The possible system configurations that follow from this, and the expected Gaia accuracy, determine the likelihood of detecting a movement of the photocentre due to an unseen companion. As the size of the natal kick imparted to the core of the exploding star is increased, the overall probability of detecting a neutron star companion decreases as more systems become disrupted. The overall detection probabilities for our illustrative sample

range from 2% to 27%, which imply that within a distance of approximately 5kpc from the Sun around 48 detections of compact companions to runaway stars can be expected. For comparison, around 15% of High Mass X-ray Binaries would exhibit wobbles detectable with Gaia.

5.2 Introduction

Over the years a number of theoretical and observational characteristics have been estimated, specific to each scenario, in order to determine which mechanism is at work in the production of OB runaways. However, the observational evidence offered no definitive answer until recent years due to insufficient data sets, small number statistics or biases in the early searches. Finally, Hoogerwerf et al. (2001) showed that both mechanisms are at work. By tracing the paths of several runaways and pulsars back to their parent clusters they were able to infer which of the two mechanisms produced them. For the case of the supernova in a binary scenario this raises an interesting question, since it is expected that in many cases the two components remain together after the explosion (the relative fractions having been discussed in the previous section dependent on the applied kick velocity and initial separation range): where are the compact companions to the OB runaways? As noted previously, many searches for compact companions to OB runaways have been conducted, since that would be a strong indicator that the supernova in a binary scenario is the mechanism at work. However, these searches failed to find a compact companion to OB runaways despite the fact that the presence of High Mass X-ray Binaries (HMXRBs), Be and Wolf Rayet (WR) stars with neutron star companions and binary pulsars shows that binary systems can and do survive the supernova explosion of one or both its members. These types of systems are indeed established phases of close binary evolution. Determining whether or not classical OB runaways have compact companions will give insight into a number of factors pertaining to close binary evolution and also into any additional kick velocity imparted to the compact object due to asymmetries in the explosion, that might disrupt the system.

What we seek to do is to use the very high positional accuracies which the Gaia satellite will achieve for a large number of stars including OB runaways, to infer the presence of an unseen compact companion from the non-linear motion of the OB runaway. In the Section 5.3 (*Program Stars*) we take a few representative classical OB runaways and

determine their masses and distances. In the Section 5.4 (Range of Theoretical Separations) we estimate their initial masses and a corresponding theoretically expected range of orbital separations. In the Section 5.5 (*Range of Detectable Separations*) we determine the range of orbital separation within which Gaia's positional accuracy would be sufficient to infer the presence of a hidden companion for these specific cases. Finally we illustrate and discuss the results, and further estimate the overall number of runaways with compact companions Gaia is likely to detect; we also consider the Gaia detectability of neutron star companions to HMXRBs.

We want to stress here that these few runaway stars are selected as illustrative cases; it is not intended to engage in detailed and comprehensive close binary evolution calculations. Therefore, we want to achieve reasonable estimates of original masses and possible separations, with which a comparison with expected Gaia capabilities can be made.

5.3 Program Stars

Among all runaway stars, we are interested in systems which are likely to have survived the supernova explosion of the primary (the initially most massive star). Such systems probably have been closely bound in order to survive the eruption and as such are expected to have experienced a phase of mass transfer. Mass transfer may be evidenced by the secondary (the mass accreting star) exhibiting a high helium abundance, Y, and/or a high rotational velocity, vsin(i)[1]), (Blaauw, 1993). In order to demonstrate the feasibility of the proposed use of Gaia we chose the sample of well known O-type runaways in Blaauw (1993) for which rotation velocities and helium abundance measurements are listed. These values indicate 5 suitable stars that will have experienced mass transfer, suggesting that their high space velocities are due to the supernova in a binary scenario (Table 5.1). One star also fulfilling these criteria, HD 149757, has been left out from consideration, since Hoogerwerf et al. (2000) recognised this to be a disrupted system after associating it with pulsar PSR J1932+1059 that was ejected in a different direction.

In Table 5.1, the apparent V magnitudes, spectral types and colour indices for the stars were obtained from the SIMBAD database. From the tables of Schmidt-Kaler (1982), the absolute visual magnitude and intrinsic colour indices were estimated on the basis of the

[1]vsin(i) is the projected equatorial rotation velocity where i is the angle of the rotation axis to the line of site. Typically the angle i is unknown.

spectral types, interpolating where necessary. The visual extinction was determined from the colour excess, $A_V = R.E_{(B-V)}$, where the expression used for R is as given by Schmidt-Kaler, viz. $R = 3.3 + 0.28(B-V)_o + 0.04(B-V)^2$; hence the distance to each object was estimated using its apparent and absolute V magnitudes. The helium abundances and rotation velocities are as listed by Blaauw (1993).

The luminosity and effective temperature for a given spectral type are also taken from the tables of Schmidt-Kaler and were used to find the current normal stellar component masses utilising the stellar tracks with solar metalicity of Schaller et al. (1992). The estimated values for the mass in solar masses and distance to each of the objects in parsecs are listed in Table 5.2.

Table 5.1: *List of observational parameters for our OB runaway sample*

HD	Sp Type	V	M_V	$(B-V)$	$(B-V)_o$	A_V	Y	vsin(i)
24912	O7.5III	4.042	-5.85	-0.020	-0.31	0.94	0.18	200
30614	O9.5Ia	4.301	-6.85	-0.012	-0.25	0.77	0.18	85
66811	O4I	2.210	-6.80	-0.197	-0.31	0.36	0.20	536
203064	O7.5III	5.043	-5.80	-0.061	-0.31	0.80	0.12	274
210839	O6I	5.090	-6.50	0.171	-0.31	1.56	0.17	214

5.4 Range of Theoretical Separations

From the estimated masses of the OB runaway stars in Table 5.2 we determine what the likely initial system parameters were and how these were changed due to mass transfer as well as a supernova explosion of the primary. According to Belczyński & Bulik (1999), when the initial mass ratio $q = (\frac{M_2}{M_1}) < 0.8897$, the secondary is still on the main sequence when the primary erupts in a supernova. If $q > 0.8897$ then it is likely that the secondary will lose its hydrogen envelope due to mass transfer or a common envelope phase before the subsequent eruption of the primary. If this system survives the explosion of the primary, then it would result in a bound runaway system, with a Wolf Rayet-like star plus a compact companion as its components. Our sample stars are O-stars that have already evolved off the main sequence. Hence, choosing q = 0.8897 reflects this intermediate evolutionary stage

[2] $(B-V)_o$ is the intrinsic colour magnitude and (B-V) is the apparent colour magnitude, where B is the Blue spectral band and V the Visual spectral band

of our sample stars, while ensuring that the final system is not a Wolf Rayet plus compact object binary. This q value further conforms to the idea that OB binaries generally have mass ratios close to one (Garmany et al., 1980).

The present illustrative calculations are simplified by neglecting the effects of stellar wind on the evolution of binaries, as per Belczyński & Bulik (1999). We assume further that mass transfer continues until the primary is stripped of its hydrogen envelope leaving a helium core. The final mass of the primary after mass transfer is approximated (Bethe & Brown, 1998) as

$$M_1^{AMT} = 0.3 M_1^{BMT} \tag{5.1}$$

The subscript 1 refers to the primary (the initially most massive star). The superscripts BMT and AMT refer to the initial parameters Before Mass Transfer and the final parameters After Mass Transfer, respectively. Of the $0.7 M_1^{BMT}$ lost from the primary as it evolves off the main sequence and fills its Roche Lobe, some is transferred to the companion and some is lost from the system. The amount of mass transferred to the companion may be taken as proportional to the square of the mass ratio (Vrancken et al., 1991; Bethe & Brown, 1998). Hence we estimate the initial mass of the primary from the final mass of the secondary (i.e. the observed OB runaway) as

$$M_1^{BMT} = \frac{M_2^{AMT}}{(q + 0.7q^2)} \tag{5.2}$$

The subscript 2 refers to the secondary (the initially least massive star). The initial mass of the secondary is then determined from the adopted mass ratio

$$M_2^{BMT} = M_1^{BMT} q \tag{5.3}$$

Having obtained an estimate of the typical initial masses for a system, we now consider at which distances these two masses could be from each other. We conservatively take the minimum value of the initial semi-major axis a, which is taken to be a circular radius, to be the sum of radii of the two zero age main sequence stars in the binary, each of which follows from the initial masses in (5.2) and (5.3).

$$a_{min,theor} = R_1 + R_2 \tag{5.4}$$

The maximum separation is that for which Roche lobe overflow of the primary will still ensue and will transfer mass to the companion. The maximum radius that the primary reaches is that which is foreseen by the stellar track models of Schaller et al. (1992). By rearranging

Eggleton et al. (1983) Roche lobe radius equation we find the maximum separation for each of our sample stars from the maximum radius. Thus,

$$a_{max,theor} = R_{max}\left(\frac{0.6 + 0.8897^{\frac{2}{3}} ln(1 + 0.8897^{-\frac{1}{3}})}{0.49}\right) \tag{5.5}$$

where R_{max} is the maximum expected radius for the star. Within this range of $(a_{min,theor}, a_{max,theor})$ we distribute the semi-major axis a, flat in the logarithm

$$\Gamma(a) \propto \frac{1}{a} \tag{5.6}$$

This is consistent with observation and used in population synthesis codes.

In order to estimate how this distribution changes in the subsequent evolution of the system we determine what effect mass transfer and the supernova explosion of the primary have on the original $\frac{1}{a}$ distribution. Pols & Marinus (1994) give the change in semi-major axis due to mass transfer,

$$a^{AMT} = a^{BMT}\left(\frac{M_1^{AMT} \times M_2^{AMT}}{M_1^{BMT} \times M_2^{BMT}}\right)^{-2}\left(\frac{M_0^{AMT}}{M_0^{BMT}}\right)^{2\beta+1} \tag{5.7}$$

where M_0 is the total mass of the system. The parameter β gives an estimate of the amount of specific angular momentum of material leaving the binary (see Pols & Marinus (1994) for a discussion) and following Belczyński & Bulik (1999) we let $\beta = 6$. The change in semi-major axis due to a supernova explosion is given by Brandt & Podsiadlowski (1995), which includes references to earlier versions of Equation 5.8. We refer the reader back to Chapter 3, Figure 4-1 which shows the configuration and coordinate system for the binary system. Equating the energies in terms of the semi-major axis before and after the supernova explosion for initially circular orbits and rearranging gives

$$a^{ASN} = a^{AMT}\left[\frac{1 - \frac{\Delta M}{M_0^{AMT}}}{1 - (\frac{2\Delta M}{M_0}) - (\frac{V_k}{V_{orb}})^2 - 2(\frac{V_k}{V_{orb}})cos(\theta)cos(\phi)}\right] \tag{5.8}$$

where the superscript ASN is the value of the semi-major axis After the SuperNova, ΔM is the amount of mass ejected from the primary due to the supernova explosion, V_{orb} is the orbital velocity of the supernova precursor relative to its companion just before the explosion, V_k is the natal kick velocity imparted to the core of the primary, θ is the angle between the direction of the kick velocity vector and the initial orbital plane and ϕ is the angle between the initial direction of motion of the supernova progenitor and the projection of the kick velocity vector on the orbital plane. The values for the above

parameters are chosen as follows. The amount of mass lost from the primary is the amount necessary to leave behind a $1.4M_{\odot}$ neutron star or $\Delta M = M_1^{AMT} - 1.4$. The value for V_k (the kick velocity imparted to the core of the primary as it erupts) is uncertain and its direction (described by θ and ϕ) is random since its nature is unknown. As mentioned in the previous chapter and the introduction the kick velocities have been determined from studies of radio pulsar proper motions which indicate mean birth speeds between 100-500km/s (Lyne & Lorimer, 1994; Hansen & Phinney, 1997; Cordes & Chernoff, 1998) implying that they receive a kick of this size at birth due to asymmetries in the supernova that produced them. However a recent statistical analysis favours a bimodal pulsar velocity distribution with peaks at around 100km/s and 500km/s (Arzoumanian et al., 2002). Pfahl & Rappaport (2002) also find evidence for a bimodal kick velocity distribution on the basis of the orbital eccentricities of Be/X-ray binaries. Still other authors expect a significant fraction of pulsars to be born with a zero or small (from a few tens of km/s to 200km/s) kick velocity (Madau & Blaes, 1994; Fryer et al., 1998; Blaauw & Ramachandran, 1998). De Cuyper et al. (1976), Stone (1982) and Leonard & Dewey (1993) expect that an asymmetric kick of the order of 100-200km/s will not be sufficient to disrupt the majority of closely bound binary systems. For our illustrative purposes, we chose a range of kick velocities from 0km/s to 200km/s as this allows for most of our systems to remain bound and have observable compact companions. We examine directions over the full range of θ within $\pm\pi$, and ϕ from 0 to 2π to produce a final separation distribution for a given kick velocity by placing the resultant systems into sample bins according to their separations.

5.5 Range of Detectable Separations

Following in the footsteps of the Hipparcos satellite, the main goal of Gaia is to collect high-precision astrometric data for a complete sample of stars down to a magnitude of V$\sim$20, which corresponds to about 10^9 stars. This is some 10^4 times more stars than Hipparcos, out to a thousand times greater distance and ranging from 3 to 200 times more accurate in determining positions and proper motions. The nominal accuracy of Gaia is reasonably constant with only a small variation across a range of spectral types: $< 4\mu$arcsec down to around V = 12, after which detector saturation is reached and the accuracy decreases to tens of μarcsec at V = 15, down to hundreds of μarcsec at V = 20. The drop in accuracy increases as the magnitude of the star increases. However, for our illustrative sample the

maximum magnitude hardly exceeds V = 5 so we adopt 4μarcsec as our accuracy limit across the board [3].

The presence of a compact companion to an OB runaway can be inferred due to its non-linear motion, resulting from its orbit about the centre of mass of the system as it travels through space. This means that the semi-major axis must be greater than some threshold value in order for the perturbation to normal straight line motion to be detectable. This value can be written in terms of the angular positional accuracy of the detecting instrument $\Delta\alpha$, the distance to the binary d, the total mass of the system M_0 and the mass of the unobserved object. As to the latter, we assume that a neutron star of $1.4M_\odot$ is formed during the supernova explosion. Hence we have the minimum semi-major axis above which Gaia will be accurate enough to determine the non-linear motion of the OB runaway

$$a_{min,det} = \frac{\Delta\alpha d M_0}{1.4} \tag{5.9}$$

There is also a maximum semi-major axis, above which Gaia will be unable to determine whether the motion is non-linear or not. This is due to an insufficient amount of the orbit being sampled within Gaia's mission lifetime of 5 years. Quist (2001) estimates that Gaia would still be able to recognise astrometric binaries with sub-stellar companions with periods up to 25 years and we conservatively adopt this as our maximum period, giving

$$a_{max,det} = \{\frac{T^2 G M_0}{4\pi^2}\}^{\frac{1}{3}} \tag{5.10}$$

where T is the period (=25yr) and G is the gravitational constant. The estimated values for the minimum and maximum detectable semi-major axis in Astronomical Units are listed in Table 5.2.

5.6 Discussion

5.6.1 Probability of Detection by Gaia

From the analysis in the previous section we can determine the final theoretical distributions of possible semi-major axes[4], for each of the five illustrative runaway stars we are interested

[3] see Table 8.5, Gaia, Concept and Technology Study Report,2000

[4] This is the altered $\frac{1}{a}$ distribution due to mass transfer of matter to the companion from the primary and the eruption of the primary resulting in a sudden mass loss from the system

Table 5.2: *Mass and distance estimates for our sample, together with the estimated minimum and maximum detectability limits for Gaia*

HD	Mass($M_\odot$)	Distance(pc)	$a_{min,det}$(AU)	$a_{max,det}$(AU)
24912	39	618	0.07	29.4
30614	36	1191	0.13	28.7
66811	40	536	0.06	29.7
203064	39	1019	0.12	29.4
210839	60	1016	0.18	33.9

in. Equation 5.8, that describes the effects of the supernova explosion (of the primary) on the semi-major axes, includes the natal kick velocity imparted to the core of the primary and informs whether the systems become disrupted or not. The final theoretical distributions refer obviously to those systems that remain bound after the supernova explosion. Then, using the semi-major axis range for which Gaia is able to detect a non-linear motion due to a compact companion, as described previously and listed in Table 5.2, we estimate the fraction of these surviving systems that is within this range. For this fraction of the surviving systems Gaia would be able to detect a 'wobble' in the OB runaways straight line motion due to a hidden companion. This yields the probability of detecting a compact companion, which for our sample stars is shown in Figure 5-1 as a function of natal kick velocity, the precise value of which is uncertain. The resulting probabilities display a large spread, from as low as 2% up to 27%. Apart from the natal kick velocity, distance is an obvious factor affecting the calculations and for our sample this ranges from around 500pc up to 1.2kpc.

Recalculating the probabilities for the set of stars for a fixed kick velocity of 100km/s and allowing a variation of their distances gives Figure 5-2. The probability of identifying a companion is almost inversely proportional to the distance to the system, which is consistent since the angular separation α is equal to $\frac{a}{d}$ where a is the physical separation of the OB star and its companion and d the distance to the system. A secondary effect in Figure 5-2 is due to the system mass which is integral to the evolution of the system separation because the amount of mass transferred and lost depends on the initial mass and this subsequently determines the amount of mass ejected during the supernova explosion which alters the final system parameters. Furthermore the final mass of the system affects the probability

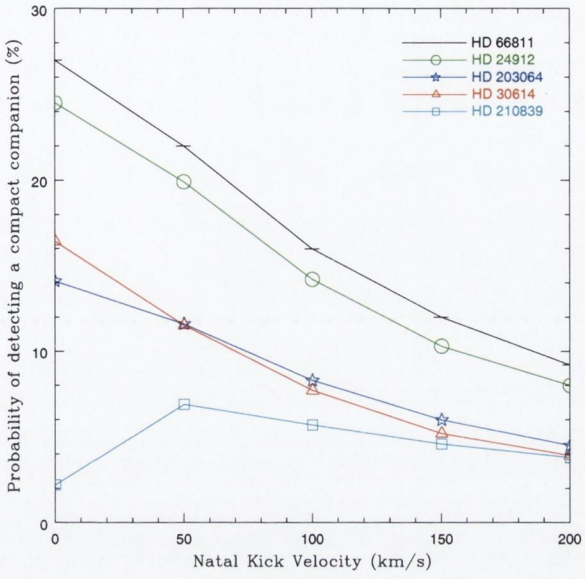


Figure 5-1: *Percentage probability of Gaia detecting a neutron star companion for each of our sample stars, considering all theoretically possible system configurations that survive the supernova of the primary*

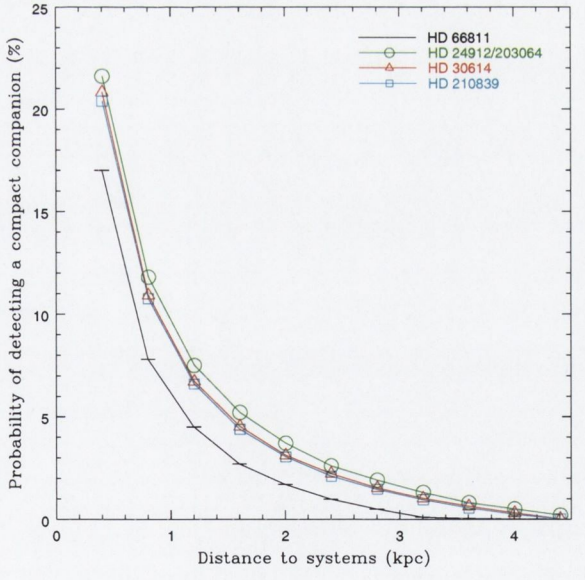


Figure 5-2: *Detection probability as in Figure 5-1, adopting a kick velocity of 100km/s and varying the distance, illustrates the effect of different system masses*

of detection since it defines the minimum and maximum semi-major axes allowing that Gaia detects a variation in straight line motion. Hence we see that HD 66811 has the highest probability of detection in Figure 5-1 since it is the closest and close to being the least massive of our sample resulting in a small minimum detection separation limit for Gaia, thus extending the useful parameter range. Similarly HD 210839 has the least probability of detection; even though it is not the furthest away it's close to being so and it is by far the most massive of our sample.

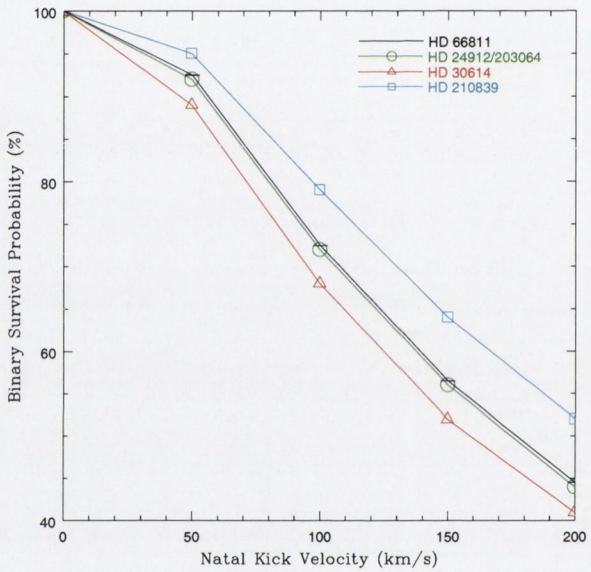


Figure 5-3: *Percentage of binary systems that survive the supernova explosion of the primary as a function of natal kick velocity*

It is clear from Figure 5-1 that the adopted kick velocity has a significant effect on the probability of companion detection. In essence the effect of the kick is to elongate the orbits and to dissociate more and more systems as its value increases. This latter point is illustrated in Figure 5-3, that presents the probability of supernova survival as a function of natal kick velocity for the five cases considered here. None of these systems become disrupted for a zero natal kick velocity, but an increasing number do for larger values of the natal kick. In any observational sample of runaway stars it is a priori not known which systems remained together and which ones have been disrupted. Comparing the fraction of surviving systems that is within reach of Gaia with the initial set of systems (that is, the initial semi-major axis distributions $\propto \frac{1}{a}$ between $a_{min,theor}$ and $a_{max,theor}$) gives then

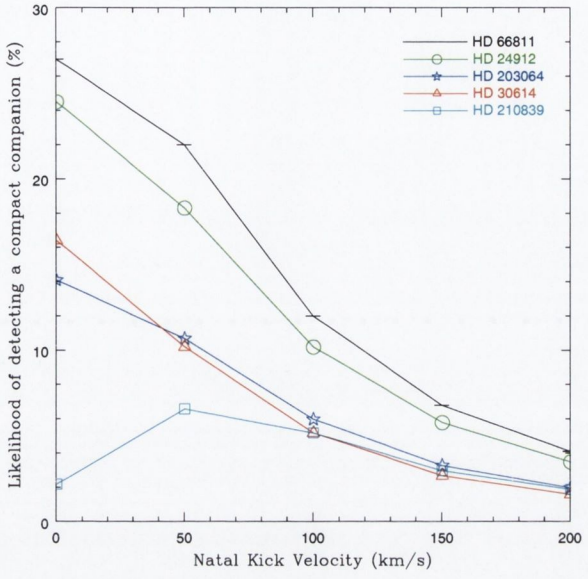


Figure 5-4: *Probability that Gaia could detect an unseen companion to our illustrative sample stars, with respect to all possible initial system configurations*

a better estimate of detection probability among an observational sample of runaway stars. Such a comparison is presented in Figure 5-4, which indicates for the five illustrative systems selected as examples that for natal kicks around 200km/s the probabilities are suppressed with respect to Figure 5-1 by a factor of about 2, while remaining relatively unchanged for natal kicks < 100km/s.

5.6.2 Number of OB runaways with compact companions that Gaia may detect

Hoogerwerf et al. (2001) list 56 runaways which have significant parallaxes ($\pi - 2\sigma_\pi \geq 0mas$) and proper motions $\sigma_\mu/\mu \leq 0.1$, with space velocities greater than 30km/s with respect to the local standard of rest. They derive that approximately two-thirds of these runaways are the result of a supernova explosion in a binary system. Conservatively adopting this estimate leaves 37 runaways which are a result from a supernova in a binary within, approximately, a 700pc radius of the sun. Assuming that this is indicative of the supernova produced runaway density in the Galaxy, we hence estimate the number of runaways that are likely to have a compact companion detectable by Gaia.

The distance for which Gaia's accuracy limit of 4μarcsec remains valid is dependent on

the limiting apparent magnitude this criterion holds for, which is V = 12. We determine the corresponding distance using

$$d = 10^{\frac{V - M_V + 5 - A_V}{5}} \tag{5.11}$$

Hoogerwerf et al. (2001) list masses and likely ejection mechanisms for the runaways for which they determine a parent group. Those ejected by a supernova in a binary system have a median mass of $10.4 M_{\odot}$ which corresponds to approximately a B1.5V spectral type, giving an absolute magnitude of $M_V \approx$ -3 (Schmidt-Kaler, 1982). Adopting an average extinction rate of 0.3 magnitudes per kpc allows a distance of 5kpc. This yields ~1890 OB runaways, produced by the supernova in a binary mechanism, which are within reach of Gaia. We have shown that the probability of detection is dependent on distance, and following the analysis in Section 5.5 we expect Gaia to detect compact companions to 48 of these, adopting a kick velocity of 100km/s. This drops to 16 for a 200km/s kick and increases to 106 for a 50km/s kick. It is easy to see why no compact companions to runaways have been identified to date with astrometry since these values range from a little under 1% to 6% of the total number, if using the high accuracies expected for Gaia. However, it is encouraging to note that Gaia will be sufficiently accurate to detect the presence of compact companions to at least several of the runaways.

5.6.3 A Comparison with High Mass X-ray Binaries

As mentioned in the introduction in Chapter 1, some HMXRBs have been shown to have runaway characteristics, such as high velocities and large scale heights from the galactic plane (van Oijen, 1989; Van Rensbergen et al., 1996; Chevalier & Ilovaisky, 1998). For example, Van Oijen (1989) considers HMXRBs and runaway stars as different subgroups of OB stars with high velocities. Therefore HMXRBs are normally not included in samples of runaway stars such as in Blaauw (1993), however, as a test of the ideas pursued by the present article we seek to investigate the ability of Gaia to detect the known neutron star companions to these objects astrometrically. Van Oijen (1989) lists 24 HMXRBs, most with a radial velocity. We have used the SIMBAD database to update Van Oijen's radial velocities and also to complement his radial velocities with proper motion measurements where possible. We consider here those cases with space velocities $\geq$ 30km/s (which in a few instances is reached while only a radial velocity or proper motion is known), so as to conform to the criterion of Blaauw for runaway velocities as before. Notice that γ Cas is

nominally just below 30km/s, but this value for its velocity is possible when error ranges on radial velocity and proper motion are taken into account. In order to obtain specific test cases we require also known orbital periods, for which we have used the HMXRB Catalogue of Liu et al. (2000). The resulting objects, with known orbital periods and large space velocities, are listed in Table 5.3. There are, inevitably, a few exceptions to this procedure. Three of Van Oijen's objects are not included in Table 5.3 even though they meet our criteria: Cyg X-1, which is a black hole binary, for the reason that the ideas developed in the previous Sections apply specifically to neutron star companions; Cir X-1 is a Low Mass X-ray Binary (LMXRB) and is listed in the LMXRB Catalogue of Liu et al. (2001); SS433 is not listed as a HMXRB by Liu et al. (2000) and also has a very peculiar spectrum that does not allow a straightforward interpretation of its radial velocity. Then, one of Van Oijen's objects, γ Cas, does have an orbital period (Harmanec et al., 2000) which is not [yet] included in the HMXRB Catalogue of Liu et al; given its period we have included γ Cas in Table 5.3. Finally the microquasar LS 5039 was suggested as a high velocity binary by the referee and is also included in Table 5.3; its orbital period is given by McSwain et al. (2004).

We calculate the probability of detection for this sample of HMXRBs as described in the previous sections and show the results in Figure 5-5 which may be compared to Figure 5-1 for the case of Blaauw's O-type runaway sample. Two systems not included in Figure 5-5 are Cen X-3 and V441 Pup due to the fact that they have a near zero probability of detection. This is mainly as a result of their very large distances, of 9 and 7.2 kpc respectively. It is instructive now to see which systems from Table 5.3 would actually be detected based solely on their observed periods and Gaia's expected accuracy. Two systems sit within the range of Gaia detectability, X-Per and γ Cas, and these two are the most probable ones to be detected as is evident from Figure 5-5. X-Per's orbital period corresponds to a separation of approximately 4AU while Gaia's range of detectable separations for this system is 3 to 24 AU. γ Cas' period translates into a separation of approximately 2AU while Gaia's range of detectable separations for this system is approximately 1 to 24 AU. It has been suggested by a number of authors that γ Cas' companion is in fact a white dwarf (Murakami et al., 1986; Haberl, 1995; Kubo et al., 1998; Apparao, 2002), in which case its evolutionary history would differ from the description in the previous sections. We note that a white dwarf companion instead of a neutron star would involve a fairly comparable companion

Table 5.3: *HMXRBs with high velocities and known orbital periods. In the case where a radial velocity was given by Van Oijen (1989) and listed in the SIMBAD database the SIMBAD value was preferred if the values differed.* [1] *Combined radial velocity and proper motion from the SIMBAD database.* [2] *Combined proper motion with the estimated radial velocities listed in Van Oijen (1989).* [3] *Estimated radial velocity only, as listed in Van Oijen (1989).* [4] *Proper motion only, from the SIMBAD database.* [a] *Orbital period from Harmanec et al. (2000).* [b] *Values taken from McSwain et al. (2004).*

NAME	HD	V(km/s)	Distance(kpc)	P_{orb}(days)
QV Nor		172[3]	5.6	3.73
Vela X-1	77581	91[2]	1.9	8.96
LS 5039		> 90[b]	2.9	4.43[b]
V725 Tau	245770	87[1]	2.7	111
V441 Pup		82[3]	7.2	34.5
V884 Sco	153919	80[1]	2.0	3.41
V615 Cas		57[2]	1.7	26.45
V801 Cen	102567	46[1]	1.4	187.5
Cen X-3		38[3]	9.0	2.1
BP Cru		37[3]	1.7	41.6
X Per	24534	32[2]	0.7	580
V662 Cas		30[4]	2.9	11.6
γ Cas	5394	28[1]	0.2	204[a]

mass and that if the companion is greater than $0.5M_{\odot}$ the wobble will be detectable by Gaia. Harmanec et al. (2000) estimate the mass of the companion to be in the range $0.7M_{\odot}$ to $1.9M_{\odot}$, thus it is likely that γ Cas will be detected as an astrometric binary. Notably, a third system, HD 102567 lies just outside the range of detectability with a separation of approximately 2AU and a Gaia range of detection between 3 and 20AU.

Two detections of compact companions out of thirteen cases in Table 5-5 implies that around 15% of high velocity HMXRB systems can be detected by Gaia through astrometric techniques, assuming that the orbital periods and distances in Table 5.3 are indicative of HMXRBs generally. Naturally this result must be treated with care since it is based on small numbers, however it is a favourable basis for expecting detections of compact companions to high velocity HMXRBs using Gaia.

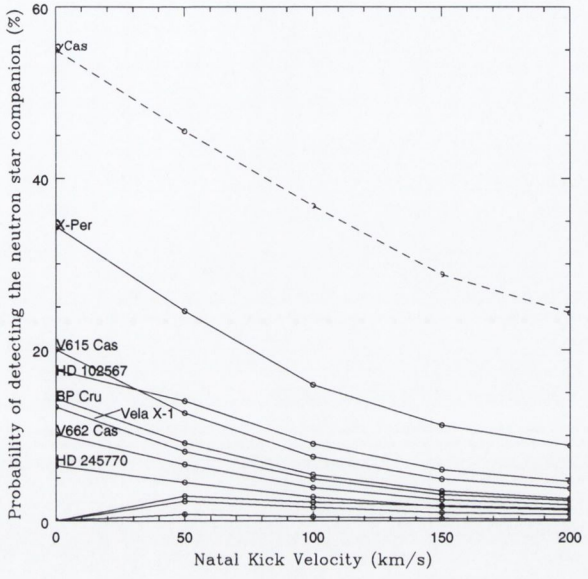


Figure 5-5: *Percentage probability of Gaia detecting a neutron star companion to each of the HMXRB sample stars, considering all theoretically possible system configurations that survive the supernova of the primary. Three systems with a small probability of detection and without a label are HD 153919, QV Nor, LS 55039, in decreasing order of probability of detection as shown in the figure. The result for γ Cas is dashed since the neutron star nature of its companion is not totally established (see text).*

5.7 Conclusions

The goal of this study is to determine the feasibility of detecting neutron star companions to a sample of five illustrative classical OB runaways using Gaia astrometry. We determined a theoretical distribution of separations for these OB runaways with compact companions and estimated the range of separations for which Gaia would be accurate enough to determine the non-linear motion of the OB runaway due to its invisible compact companion. Hence we calculated the probability that a compact companion would be detected by Gaia. We find a range of probabilities dependent on distance, mass and kick velocity of the system in question, from a few percent to around twenty five percent. We also generalise our results to show that Gaia should indeed detect a small percentage of all OB runaways with compact companions through astrometric techniques within several kpc, yielding a number of detections of the order of 48 for a moderate kick velocity of a 100km/s within 5kpc of the Sun. The eventual number of detections will reflect the size of the kick velocities imparted to the core of the exploding primary. As a test of the ideas proposed in this paper we make

an analysis of HMXRBs with high velocities and known orbital periods and determine that Gaia will detect as much as 15% of these systems confirming that this is an effective method for detecting compact companions to massive high velocity objects.

6

Rotation Velocities of OB Runaways

6.1 Abstract

Rapid rotation may be used as an observational tool for indicating the probable mechanism by which a runaway was ejected, either via dynamical ejections or as a result of a supernova occurring in a close binary system. With such a goal in mind we increase the number of known runaways with estimated projected rotation velocities, vsin(i), by 33%. We observe 38 runaways with the echelle spectrograph at Loiano Observatory, Bologna, Italy. We determine the rotation rates of these observed stars by both: measuring the Full Width at Half Maximum of the observed line profiles and calibrating with known standards; fitting the observed profiles with synthetically generated profiles.

With a more complete database of runaways with estimated rotation velocities we compare the distribution of vsin(i) values for both O and B runaways with those of O and B stars in general. We confirm the conclusions of both Blaauw (1993) and Hoogerwerf et al. (2001) that O star runaways are typically rapidly rotating objects and show that at least 40% of them have rotation rates larger than 250km/s. Since fast rotation in O stars may be

indicative of both mechanisms either through mass transfer (SNB) or ejection of collided stars (DE)we suggest that ~40% of O star runaways are ejected due to the SNB scenario. Conversely we show that B star runaways do not appear to be excessively rotating objects by comparison to B stars in general. However, there is evidence that at least some runaways are excess rotators due to the fact that B star runaways have 2-3 times more emission type stars then their cluster counterparts. With this in mind we conclude that less than 40% of runaway B stars are ejected via the SNB mechanism.

6.2 Introduction

The rotation rate of OB runaways offers a possible avenue by which their previous history may be inferred and as such the most likely mechanism by which they are ejected. As noted previously, if the ejection mechanism is a supernova in a binary system then a stage of mass transfer from the primary to the companion is likely to have occurred. This may increase the mass of the companion, alter the chemical composition of the star and also results in increasing the stellar rotation rate as a consequence of the angular momentum carried by the accreting material. It may then be expected that OB runaways which have been produced via the supernova in a binary scenario are spun up with respect to normal cluster stars and have elevated helium abundances. Blaauw (1993) showed that a number of O star runaways do have increased rotation rates and helium abundances. However, it was shown that a high helium abundance or rotation rate is not an unambiguous sign of mass transfer as intrinsically rapidly rotating stars have altered chemical abundances due to their fast rotation (Fliegner et al., 1996; Huang & Gies, 2006). Nevertheless there are examples where mass transfer has produced a rapidly rotating mass gainer in a close binary system (Simon, 1999; Barai et al., 2004) and even a relatively small amount of mass transfer may result in a substantial spin-up of the companion (Packet, 1981; Langer et al., 2003). Hence, if OB runaways are found to have elevated rotation velocities then it may still be indicative of a previous phase of mass transfer.

With a sufficiently large sample of runaways with rotation velocities determined it may be possible to estimate if both O and B runaway stars are indeed spun up objects or more importantly to calculate the fraction that exhibit enhanced rotation. This can then be used to identify what fraction of OB runaways are likely to have been ejected as a result of the supernova in a binary scenario. In order to increase the sample of runaways with known

rotation velocities (prior to now ~60%) a series of spectroscopic observations was made. A description of these observations, the reduction procedure and analysis follow in the next section. 38 stars were observed, 26 new rotation velocity estimates were determined, and 11 were added to previously determined values, increasing the total number of well known runaways with measured rotation velocities to 110, which is ~80% of the well known runaway population. Table A in the Appendix shows a list of known runaways and their parameters. Note that here we exclude from the calculations Mdzinarishvili & Chargeishvili (2005)'s list of candidate runaways due to the fact that they are not well established.

6.3 Observations

A series of observations was made over a number of observing runs at the 1.52m telescope of the Bologna Astronomical Observatory, Loiano, Italy. Observations were made using the moderate dispersion echelle spectrograph on BFOSC (Bologna Faint Object Spectrograph & Camera). Details of the spectrograph are presented in Table 6.1. Runaways which were observable from the position of Loiano Observatory (Lat. 44° 15' 30" N Long. 11° 20' 12" E 785m a.s.l.) and predominantly those without previously determined rotational velocities were selected. Table 6.2 gives the names of the stars observed, their full details being in Appendix A. The main objective was to observe absorption line profiles of He I $\lambda\lambda$4026, 4471 and Mg II λ 4481 which are strong throughout O and B-types, are typically free of strong pressure broadening and are those most commonly used by other authors for rotation velocity determination. Where possible, more than one observation of the same star was made in order to improve the quality of the results.

6.4 Method - Echelle Spectroscopy

An echelle grating essentially consists of a series of high angled ruled slits which have widths close to the wavelength of the diffracted light. The incident light is diffracted over successive orders at specific angles with the angular spacing between orders decreasing monotonically resulting in the higher orders being very close to each other. Echelle gratings are designed to

Table 6.1: *Details of the spectrograph used at Loiano*

Parameter	
UT Dates	1-6th/25th May 2006
	9-10th Oct 2006
	24/26th July 2006
Detector	EEV CCD 1300X1340 pixels
Orders	13
CCD pixel size (μ m)	20
Maximum Spectral Resolution	4200
Wavelength Range	3300 - 11000 Å
FWHM at 4471	2.4 Å
Dispersion	26 Å/mm

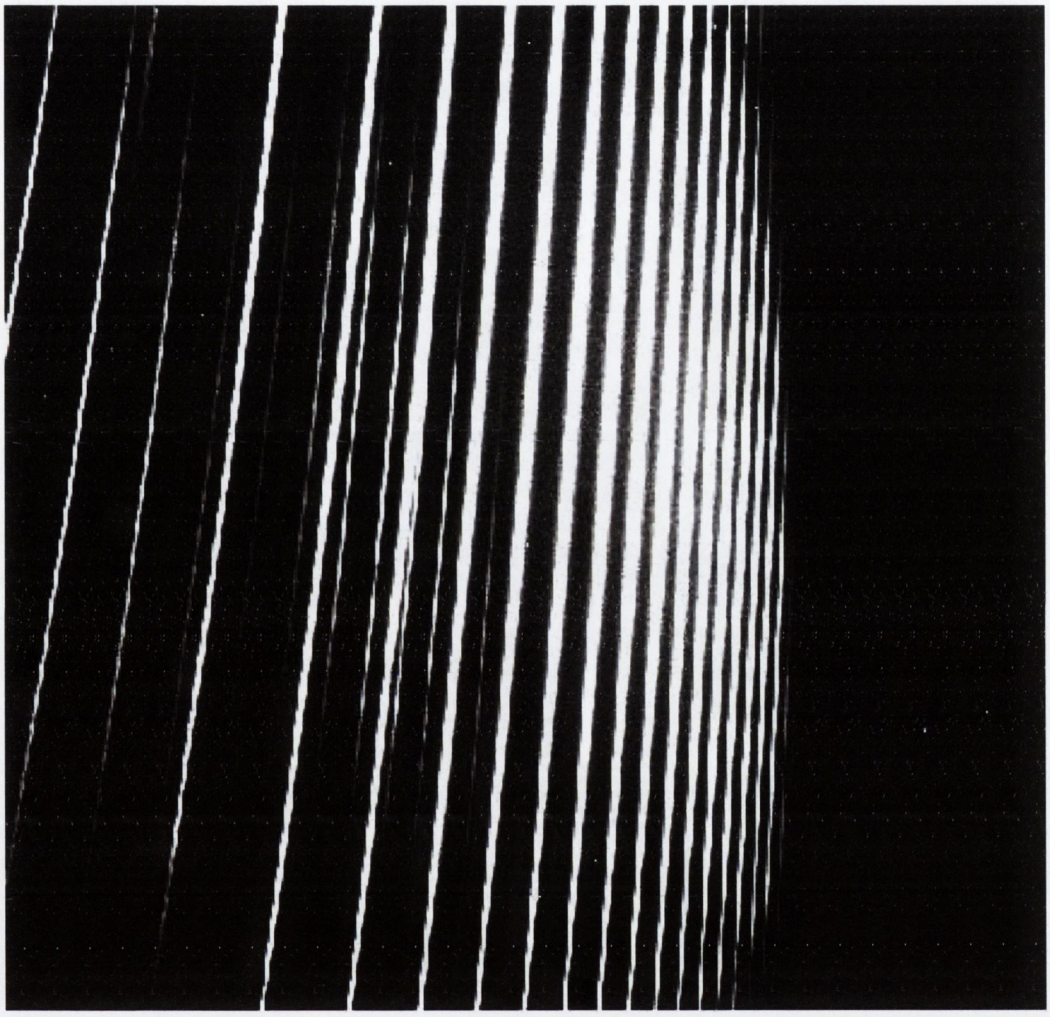
Table 6.2: *Observation list. * Indicates binary/multiple systems*

HIP 5316	HD 26684	HD 97991	HD 192281	HD 235807*
HIP 5391*	HD 30112	HD 125924	HD 192575	
HIP 9498	HD 30650	HD 149363	HD 195965	
HIP 115566	HD 39478	HD 149757	HD 197911	
HIP 102449	HD 44172	HD 157857	HD 220057	
HD 11606	HD 51477	HD 187567	HD 201910	
HD 14220	HD 78584	HD 188001	HD 206327	
HD 17114	HD 91316	HD 181409	HD 220172	
HD 24834	HD 93521	HD 191567*	HD 227877*	

concentrate the majority of the incident intensity on to a particular order. This is done by cutting the groves of a grating so that the reflecting surfaces are at a certain angle, known as the 'blaze angle' and the process itself is called blazing. This allows for the majority of the incident light to be scattered into a particular diffraction order of interest. Since the orders may be overlapping a cross-disperser is placed in the beam path which acts as an order separator. This results in a series of parallel spectral strips each with a specific wavelength range (which may overlap with the wavelength range of adjacent strips) and of relatively high resolution. An example is shown in Figure 6-1. The spectra are dispersed along the horizontal axis with each vertical bright strip being a particular spectral order over a particular wavelength range.

The reduction was carried out with the program IRAF (Image Reduction Analysis Facil-

Figure 6-1: *Example of an Echelle spectrum. Orders/Apertures are the vertical bright strips corresponding to a particular wavelength range (E.g. Aperture 1 ∼ 8750-10250 Å, Aperture 12 ∼ 3550-4200 Å. Spurious lines which arise from periodic errors in the positions of the rulings are generated by imperfections in the gratings.*



ity). The documents used as a guide to reduction were freely available on the web (Massey, 1997; Willmarth & Barnes, 1994). I also received grateful assistance from Dr Corinne Rossi, University of Rome "La Sapienza". Each image was bias-subtracted, flat fielded (thereby removing some of the blaze profile in each order) and extracted with the various IRAF routines. The Helium-Argon lamp taken with each image provided the necessary wavelength calibration. A high-order (typically 8-9) polynomial fit to the line-free continuum regions allowed the spectrum to be normalised to unity at which point it could be used for analysis.

6.5 Analysis & Results

Projected stellar rotation vsin(i) may be estimated by comparing a star's line profile to computed rotation profiles. The lines chosen are meant to be free of strong pressure broadening and yet be strong enough so that the rotation profile can be measured. Helium I λ 4026, λ 4471 are commonly used in hot OB type stars even though the λ 4471 line has a substantial blend. For cooler stars, late B type, the Mg II λ 4481 line is strong and ideal so long as the rotational broadening is large compared to the splitting of the doublet. Early studies of stellar rotation compared line profiles to computed rotation profiles which was a comparatively time consuming endeavour (particularly prior to computational data management). Many studies also made use of a standard star observed during the same observing run which had previously determined low rotation and used this as a calibration to determine the rotation of the rest of the stars in the sample. Slettebak et al. (1975),SL75, showed that a careful calibration of the FWHM (Full Width at Half Maximum) is sufficient to determine the projected rotational velocity. This led to a system of standards being compiled for massive stars (Slettebak et al., 1954, 1955, 1956, 1975). This has allowed for a simple and effective way of estimating the vsin(i) of a non standard star by comparing the calculated FWHM with the published standard giving the corresponding rotation velocity. These standard stars cover a wide range of spectral types, classes and from low ($\sim$10km/s) to high ($\sim$350km/s) rotation velocities. This streamlined the process of estimating rotation velocities, allowing for a great number of stars to have their rotation velocities estimated and became the dominant method in the field as a result. However, these standards are particularly affected at high rotation velocities because the profile depends on the angle of inclination. Errors of 10-20% may be expected from simple line-width estimates where by contrast errors can be greatly reduced by detailed fitting of the entire line profile. In the following analysis we adopt primarily a fitting of the line profile to synthetic lines while including the FWHM estimate for comparison.

There are a number of effects which cause spectral lines to be broadened. Doppler shifts of the light coming from different parts of the stellar disk as the star spins results in a wider line profile. The degree of Doppler broadening is then dependent on the orientation of the rotation axis with the line of sight. Since this orientation in most cases is unknown the rotation velocity is estimated as vsin(i) where i is the angle of orientation (e.g. $i = 90^o$ indicates the line of sight is along the equatorial plane). The average of sin(i) over the

hemisphere along the line of sight which gives a range for i from 0 to $\frac{\pi}{2}$ is $\frac{\pi}{4}$. The average rotation velocity for a given set of stars is then $< v > = < vsin(i) > 4/\pi$, which means that vsin(i) values are on average lower than the actual rotation velocity. Turbulence due to the thermal motions of the gases on the photosphere also cause broadening of spectral lines. This may be microturbulence, which is due to the velocity distribution of individual elements or macroturbulence which is due to large scale motions of gases. For hot stars, such as O and B-type, rotation typically dominates the broadening of lines.

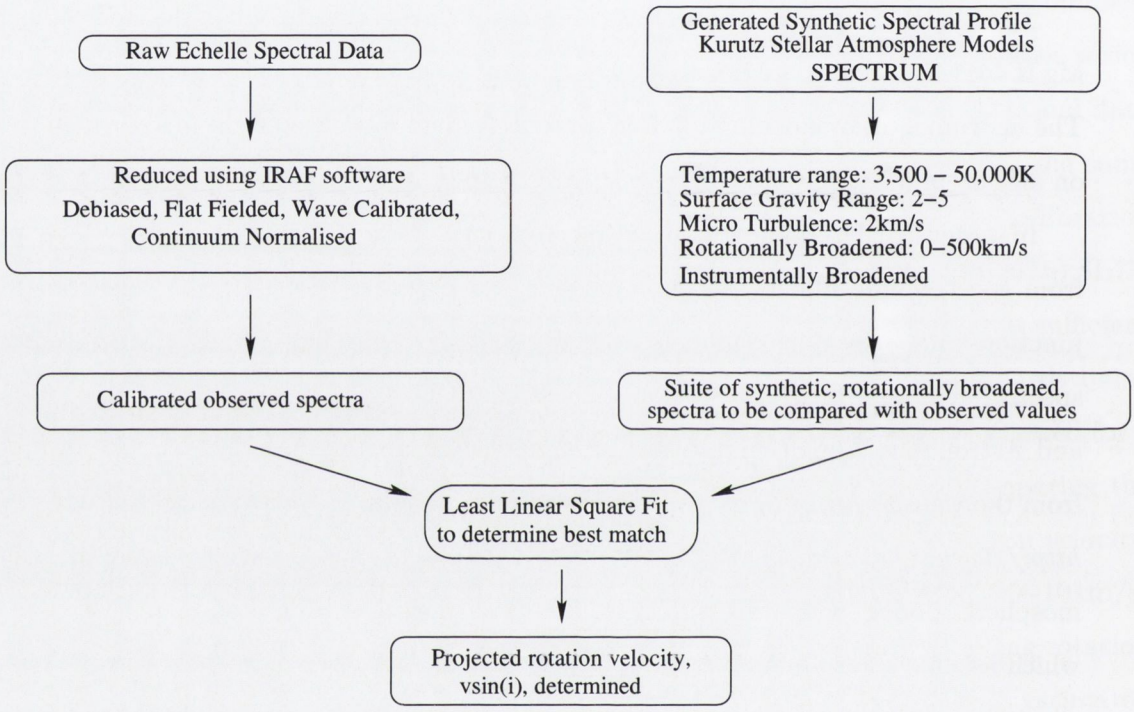
The FWHM was estimated from a Gaussian or Lorentzian line fit to the He I 4471 and/or Mg II 4481 lines which are those listed in the most recent set of Slettebak's Standards, SL75. The instrumental broadening FWHM was determined from the bright unsaturated arc lines on and around λ 4471 and is listed in Table 6.1.

In order to determine the rotation velocities from matching synthetic line profiles from spectral line fits to the observed line the program SPECTRUM was used in conjunction with atmosphere models from the Kurucz [1] database. SPECTRUM is a stellar spectral synthesis program developed by Richard O. Gray at the Department of Physics and Astronomy, Appalachian State University, North Carolina which can be downloaded from the website *http://www.phys.appstate.edu/spectrum/spectrum.html.* Kurucz's website *http://kurucz.harvard.edu/grids.html* offers a large list of previously computed stellar atmosphere models which are sufficient for these purposes. The models chosen are those which assume solar abundances and a constant micro-turbulent velocity (2km/s) which is consistent with a similar procedure by Huang & Gies (2006). The range of available model effective temperatures (Teff) is from 3500K up to 50,000K chosen at intervals of 2000°. The surface gravity ranges from 2-5 in intervals of 0.5 dex and as Teff increased the lower limit increased (i.e. at 50,000K the surface gravity choices were 4.5 and 5 only). With these models a synthetic spectrum was generated using SPECTRUM in the wavelength range 4000-5000Å. Note that these models are local thermodynamic equilibrium (LTE) models and as such are not necessarily ideal for O stars where non-LTE effects may become important. Once a synthetic profile had been generated it was convolved with an instrumental profile using the program SMOOTH2 provided by Gray (which assumes the instrumental profile is a Gaussian). This profile was then rotationally broadened with the program AVSINI, again provided by Gray, in order to produce a suite of profiles with vsin(i) of 5-

[1] Kurucz R.L. Harvard-Smithsonian Centre for Astrophysics

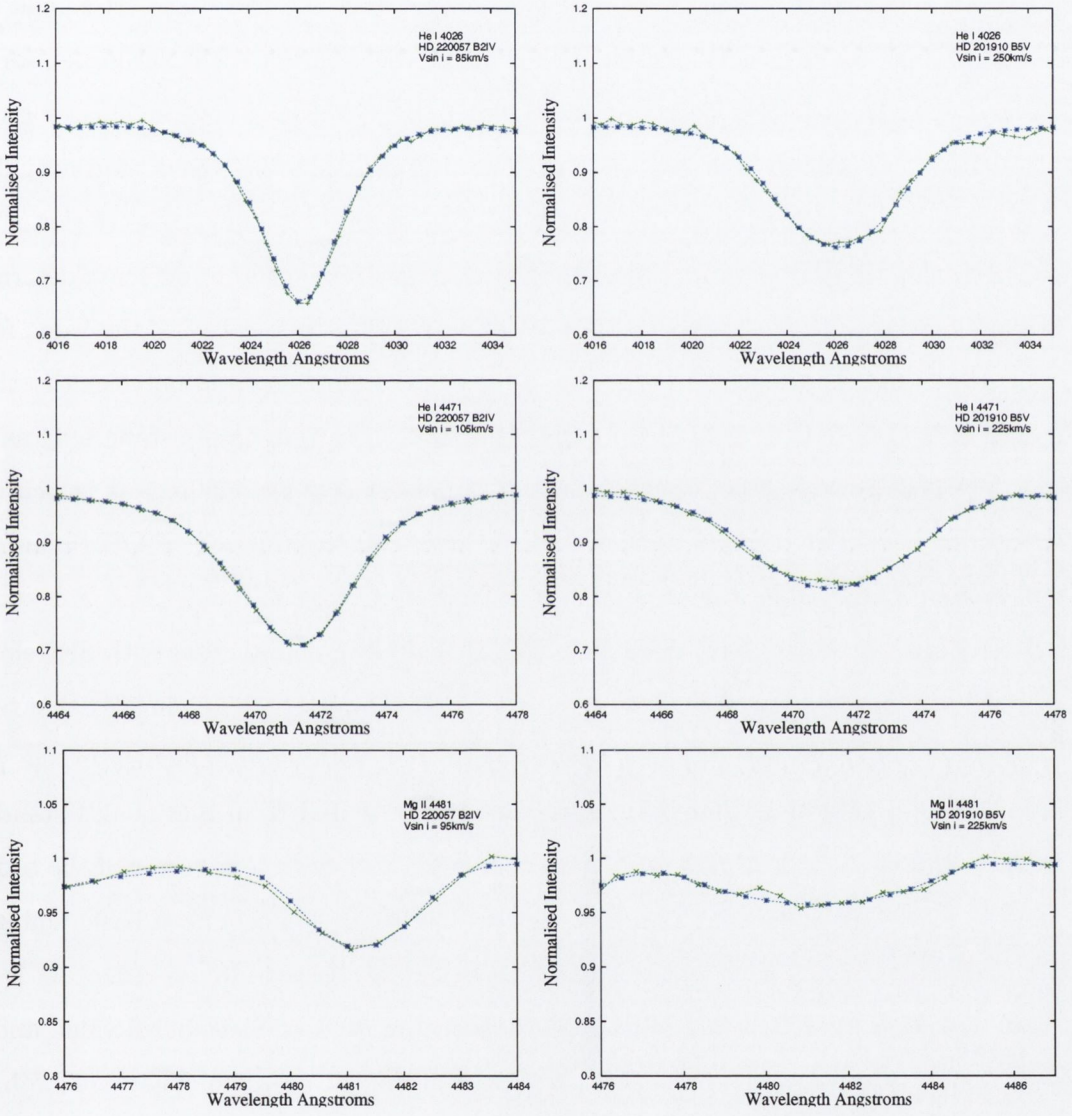
400km/s in 5km/s intervals. The full set of profiles was then compared with the He I lines λ 4026, λ 4471 and the Mg II line λ4481 where possible. The fitting is initially made with a linear least squares algorithm and then checked by eye since noisy spectra are difficult to fit in such a manner. An overview of the analysis proceedure is given in Figure 6-2. Examples of the line fits are shown in Figure 6-3.

Figure 6-2: *Flow chart of the reduction and spectral fitting proceedure*



11 stars from the sample have previously determined rotational velocities listed in the catalogues, (Glebock et al., 2001; Abt et al., 2002) and from the online SIMBAD database. In order to check the consistency of our results a comparison of previously published vsin(i) values and the values calculated here is shown in Figure 6-4. Several stars have multiple measurements and instead of the average a comparison with each measurement is shown. The linear relations for the vsin(i) values are shown below. Eqn 6.1 is a least-linear square fit of vsin(i) using the measured FWHM with Slettebak's standards as a calibration compared with previously published data. Eqn 6.2 is a least-linear square fit of the calculated vsin(i) estimated from fitting the observed line profiles with synthetic spectral profiles compared

Figure 6-3: *Spectral line fitting to two stars, one of moderate rotational velocity ~100km/s (left) and one higher ~ 225km/s (right) are shown. Plots for the same stars are vertically distributed (i.e. HD220057 is the left column and HD201910 is the right column). Note that the intensity scale is changed with respect to the other plots for the Mg II λ 4481 line since it is relatively weak in these stars. The dotted blue line is the generated synthetic spectral line and the green line is the observed spectral profile.*



with previously published data.

$$vsin(i)[Published] = (1.18 \pm 0.05)vsin(i)(FWHM) - 7 \pm 10kms^{-1} \quad (6.1)$$

$$vsin(i)[Published] = (0.93 \pm 0.03)vsin(i)(Synthesis) + 17 \pm 8kms^{-1} \quad (6.2)$$

Figure 6-4 shows that the results where the line profiles are fit to synthetic line spectra

are in generally good agreement. The large scatter is to be expected since the comparison is made with various values of vsin(i) extracted from a number of data sources, using distinct measurement techniques, calibrated against different standards and includes only a small number of comparisons here (i.e with 11 previously determined values). Considering the most recent determinations, which are typically made via a similar synthetic line fitting procedure as here, results in an even closer agreement in most cases. It should be noted that the effects of gravity darkening and shape distortion are not accounted for in these estimates. According to Brown & Verschueren (1997) this will have an effect for stars with rotation near critical break-up velocity. They suggest that the effects of gravity darkening will result in the line profiles of rapidly rotating stars resembling those of slower rotators. They compare vsin(i) values determined from a template spectra and those determined via model spectra. They determine that for early B type stars, e.g. B3, the value for vsin(i) up to ~200km/s using HeI λ4026 may be trusted. At higher rotation velocities the vsin(i) value may be underestimated for early type stars in certain circumstances by as much as 15%. However, this possible increase in rotation velocity for our highest velocity rotators will not have a significant effect on our estimate for the fraction of OB runaways which may have large vsin(i) values.

Figure 6-4 shows that where the FWHM is used in conjunction with Slettebak's published standards don't appear to agree very well. However, this is in part due to the low numbers employed here. The hot stars with high rotational velocities in the plot (HD 149575 and HD 93521) are both spectral type O9V and from Slettebak's standards the comparative FWHM of HD 149757 is commented to have a large error of the order of 15-20%. Slettebak notes that vsin(i) values greater than 200km/s have basic ambiguities in the problem of assigning rotational velocities on the basis of line widths. As it happens our estimate for HD149757 with FWHM is within 10% of Slettebak's value and for HD 93521 is within 15% of the previously observed overall average. They are both however lower values by comparison to those published which is likely due to the the difficulty in assigning a Gaussian or Lorentzian profile to such rapidly rotating stars and matching broad wing profiles accurately (Abt & Morell, 1995). These two stars are the main cause for the discrepant line fit to observed values and excluding them results in a much more consistent line fit. However, their divergence illustrates the point that basing the estimate of vsin(i) solely on the FWHM can lead to inaccurate results particularly for rapidly rotating stars.

Considering a comparison of FWHM values and spectral synthesis measurements using all the results gives the relation which shows a reasonably good correlation. (see Figure 6-5). Once more at high velocities the FWHM method appears to underestimate the rotational velocity.

Figure 6-4: *Comparison of the measured vsin(i) values here with published work. The solid line represents the ideal one-to-one relation. The x's are the measured FWHM using Slettebak's standards compared with published values. The squares are the measured vsin(i) values determined by fitting the line profile with synthetic lines compared with published values . The dotted lines represent a linear least square fit. The equations for this fit are given in equations 6.1 and 6.2.*

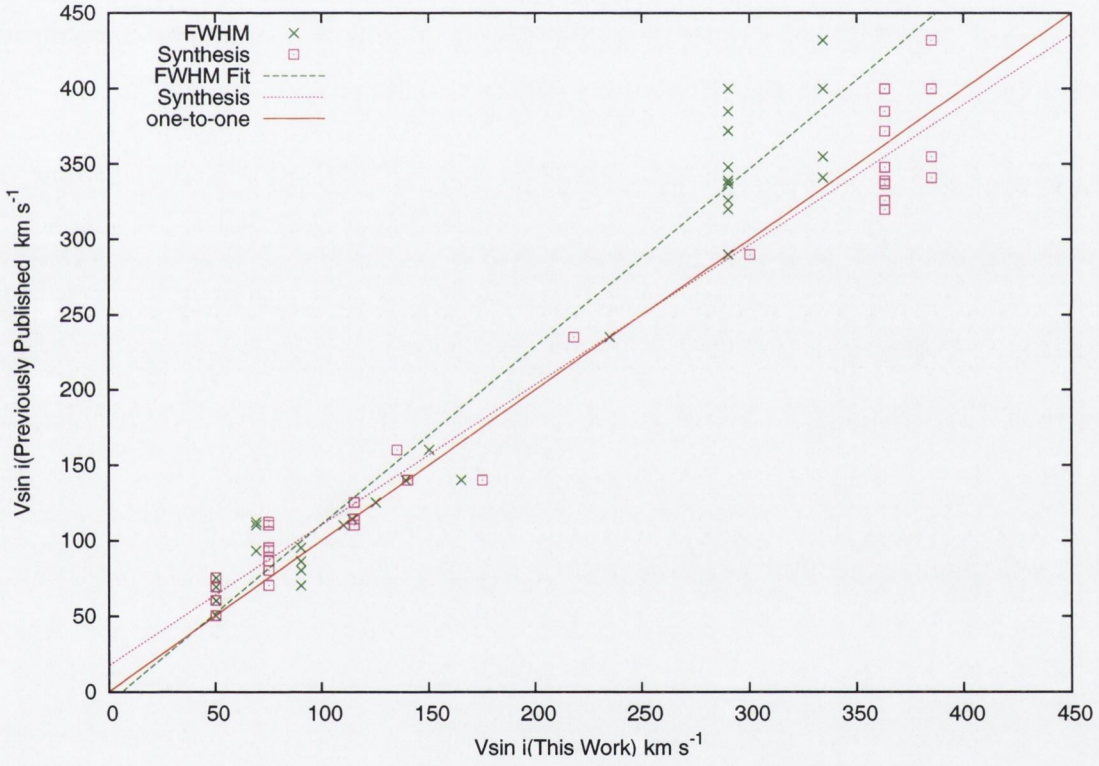


Table 6.3 shows the values of the vsin(i) estimates for our observed stars. Measurement errors vary among the stars as the strength of the lines of interest depend on the spectral class and type of star and the signal to noise ratio. A comparison of our calculated FWHM versus vsin(i) gives a mean scatter of 13.5km/s which represents the error for these estimates. Note that the resolution of the instrument puts constraints on the accuracy achievable for slow rotating stars. Stars with a vsin(i) <FWHM/2 are likely to have errors of approximately the same size ±FWHM/2 (Huang & Gies, 2006), which for these obser-

vations is 75km/s. At high rotation velocities line widths may be underestimated, as noted previously, because the fewer points characterising the curve at high rotation also leads to larger inaccuracies. By contrast the vsin(i) values from spectral synthesis fitting have errors of 5-10km/s. At higher rotation velocities these values are expected to be considerably more accurate than the FWHM derived values. At low rotation velocities the same limitation due to instrument resolution applies. Furthermore, stars which are thought to be part of binary systems also have larger errors. Where two components in a double system are resolvable then separate observations were made for each (e.g HD 191567, HD 227877). For the spectroscopic binary (HD 235807) the components were not separable hence the vsin(i) value is uncertain since the broadened spectral profile may be affected by the companion. For the eclipsing binary (HIP 5391) fits were made to both overlapping components. This too has a large uncertainty due to the difficulty in fitting each component.

Figure 6-5: *Comparison of measured vsin(i) values with FWHM and with Spectral Fitting. The solid line represents the ideal one-to-one relation. The dotted line represents a least square linear fit.*

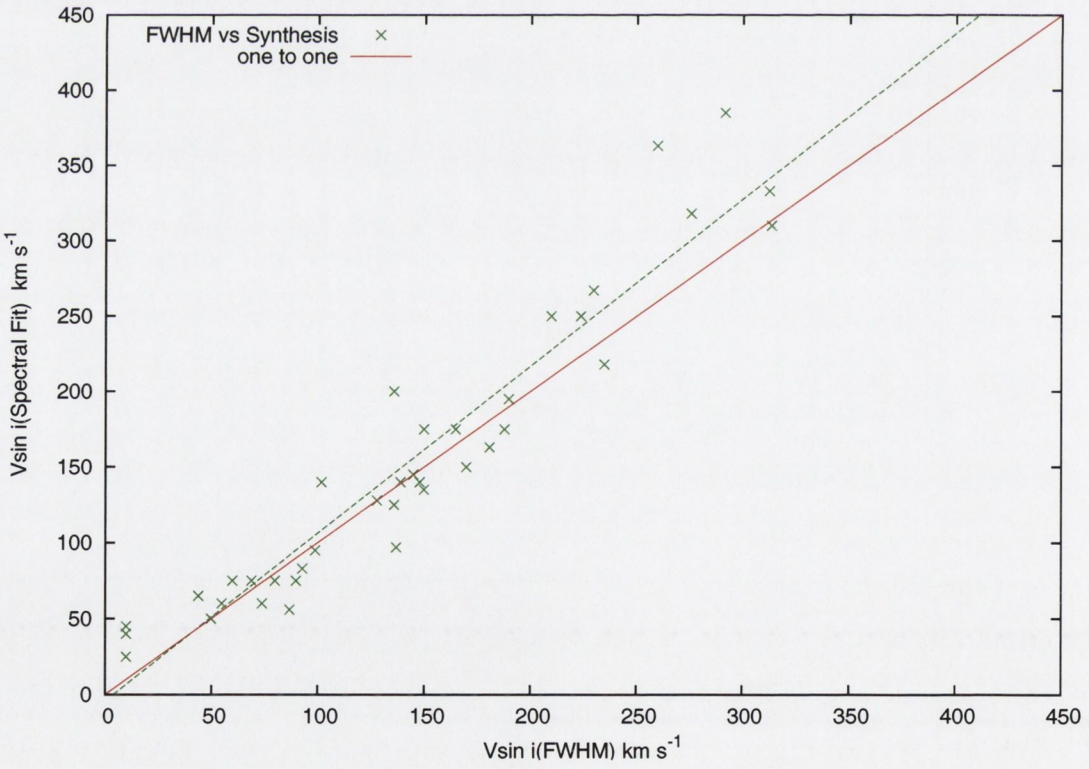


Table 6.3: *Table of estimated vsin(i) values for our runaway sample. The FWHM subscript indicates vsin(i) estimates using the FWHM method and Slettebak's standards. The Synth subscript, indicates vsin(i) estimates made from matching the observed line profile with the synthetic one. BS and RS for HIP 5391 eclipsing binary stand for Blue Shifted and Red Shifted lines relating to the individual components of the binary. NWC and SEC for HD 227877 indicate the observed North Western Component and South Eastern Components respectively. HD 191567a indicates the brightest of the two stars where HD 191567b is the companion. Recall that O stars earlier than O9 don't have a FWHM estimate as they are not listed in Slettebak's database. Stars with errors much larger than the mean as quoted in the text are noted with a colon (:).*

HIP	HD	vsin(i)$_{FWHM}$	vsin(i)$_{Synth}$	HIP	HD	vsin(i)$_{FWHM}$	vsin(i)$_{Synth}$
5316		44:	65:	85331	157857		128
5391$_{BS}$		161:	200	94934	181409	139	140
5391$_{RS}$		177:	175	97607	187567	165	175
8980	11606	276	318		188001	69	75
9498		10:	<40:	99580	192281		300
10849	14220	93	83		191567a	119:	128
13016	17114	148	140		191567b	58:	60
20330	26684	224	250	99435	192575	87:	56:
22061	30112	136	125	101350	195965	210	250
	30650	188	175	102274	197911	314:	310
27881	39478	230	267	102449		<10:	45:
30180	44172	80	75	104599	201910	235	218
33437	51477	313:	333	106896	206327	<10:	<50
45563	78584	99	95	115198	220057	137	97
51624	91316	<50	50:	115347	220172	74:	60:
52849	93521	292:	385		227877$_{NWC}$	181:	163
55051	97991	150	135		227877$_{SEC}$	170:	150
70275	125924	60	75	110362	235807	145:	145:
81153	149363	90	75	115566		102:	140:
81377	149757	260:	363	27683	248434	190	195

6.6 Discussion

From the analysis of the previous section we calculated the rotation rates for 38 runaway stars and have increased the database of known rotation velocities for runaways by about 20%. In order to compare these results with known values for stars of the same spectral type, the databases of Glebock et al. (2001) and Abt et al. (2002) are used. The former is simply a compilation of known rotational velocity estimates from various sources for ~12,000 stars. It contains ~3000 single OB star vsin(i) estimates. Where there was more than one estimate for vsin(i) the average was calculated. Table 6.4 gives the mean values by spectral type range and class for the OB stars in this database. This Table may be compared with that of Abt et al. (2002) who determined rotational velocities for $\sim$ 1000 B stars from the Bright Star Catalogue by measuring the FWHM and calibrating using Slettebak's standards. In general Glebocki's database yields mean value estimates that are larger by 30-40%. This is likely due to the fact that Glebocki's database is drawn from such a large and wide variety of sources from the literature by comparison to than that of Abt's (which was in fact the reason Abt made a large single evaluation so that their results would be more consistent) and that in many cases rotational velocities which comprise such a large database are upper limits.

Table 6.4: *Average rotational velocities (km/s) by spectral type range and class from the database of (Glebock et al., 2001). The error is the standard error of the mean and the numbers in parenthesis indicate the number of stars from which the mean was calculated*

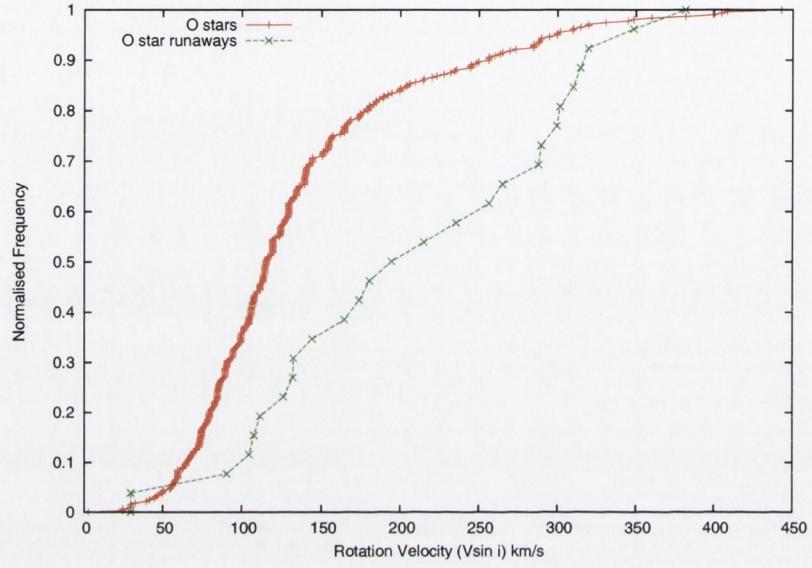
Spectral Type	V	IV	III	II	I
O3-O6	131 ± 15 (23)	0	127 ± 17 (10)	0	118 ± 18 (7)
O7-O9	151 ± 12 (65)	113 ± 14 (15)	149 ± 14 (39)	106 ± 9 (13)	110 ± 6 (45)
B0-B2	165 ± 5 (363)	137 ± 6 (218)	130 ± 7 (189)	108 ± 7 (65)	90 ± 3 (165)
B3-B5	165 ± 6 (269)	119 ± 8 (96)	106 ± 10 (66)	72 ± 14 (19)	63 ± 7 (32)
B5-B8	197 ± 7 (215)	142 ± 11 (65)	96 ± 7 (116)	37 ± 11 (6)	64 ± 16 (18)
B9-B9.5	143 ± 6 (276)	113 ± 11 (61)	91 ± 9 (70)	15 ± 4 (3)	48 ± 8 (11)

The evolutionary tracks in the Hertzsprung Russell diagram (HRD) are closely linked with rotation and it has been shown from simulations that the evolution of fast rotating stars, particularly massive stars, can be distinctly different from their slowly rotating coun-

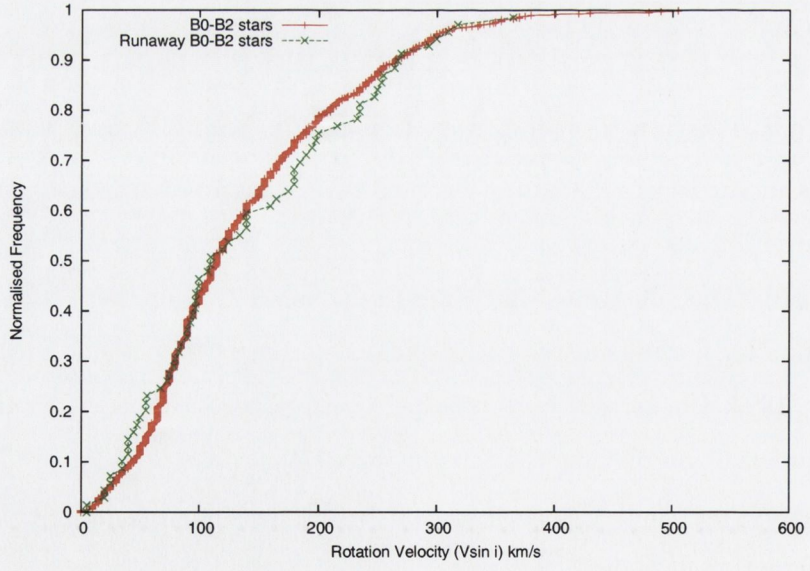
terparts (Heger & Langer, 2000; Meynet & Maeder, 2000). The fast rotation may result in strong mixing and change the chemical composition on the surface of the stars. Such rapidly rotating stars have been shown to spin down during the main sequence phase (Huang & Gies, 2006) due to angular momentum loss in the stellar wind and this spin down is also larger in massive stars. Furthermore, spin down may also occur in stars in massive close binaries as tidal locking brings the rotation of the stellar surface into synchronous rotation with orbital rotation rate (Abt et al., 2002). Conversely, spin-up may occur in lower mass stars (which generally rotate much more slowly than massive stars) from tidal locking. It may also result from the previously mentioned transfer of mass from the primary to the companion or it can even occur at the terminal age main sequence (TAMS) as a result of the overall contraction of the stellar core or by the physical collision of stars. These effects greatly complicate any interpretation of a relationship between rotation rates in runaways and average cluster stars.

However, from the distribution of cluster O star velocities it is possible to estimate if the runaway velocities are likely to be in excess for such a distribution. Table 6.4 gives the mean rotation velocities for all stars in the Glebock et al. (2001) database broken down into luminosity ranges. The 1σ standard deviation is typically large for this distribution ~90-100km/s and it is assumed here that stars with a rotation velocity greater than ($V_{Mean} + \sigma$; ~250km/s) are likely to be excess rotators. From the distribution of all O stars ~15% of them have rotation velocities above ~250km/s. By contrast, ~40% runaways have velocities in excess of ~250km/s for each of the luminosity classes (V,III,I), (Note that the distribution percentage above 250km/s didn't change drastically over the luminosity class range). This illustrates that the rotation velocities for these stars is in excess of the distribution for normal cluster stars which is consistent with the findings by other authors (Blaauw, 1993; Hoogerwerf et al., 2001). Considering all the O stars irrespective of their luminosity class and plotting the cumulative frequency distribution for all O stars and the O star runaways one can see that even with the relatively small numbers the distributions are very different (Figure 6-6a), offering further evidence that O type runaways are generally rapid rotators. The average for all known O star runaways, irrespective of luminosity class, is $205 \pm 22 km/s (28 stars)$ while the similar global average for all O stars, is $136 \pm 4 km/s (321)$. A student T-test shows that these means are significantly different and likely to come from different distributions. A χ^2 test confirms that the distributions are different with a

Figure 6-6: *Cumulative distribution function for OB stars and OB runaways.*



(a) O Stars



(b) B0-B2 Stars

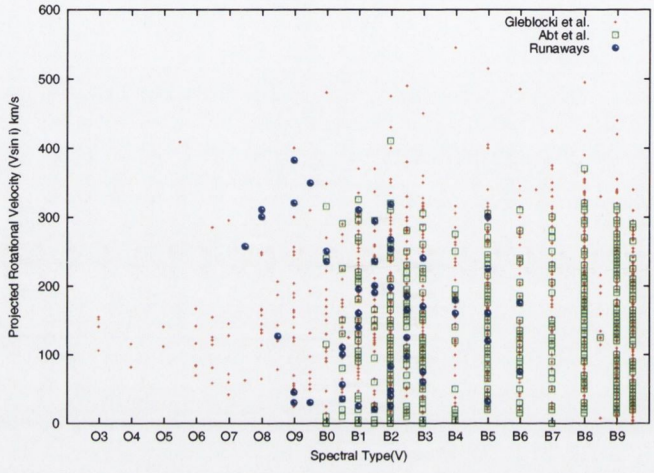
probability $p < 0.02$ that they vary due to chance.

Similarly, considering the distribution of B0-B2 star velocities it is expected that 20% of these stars have velocities above 250km/s. In this case 15-20% of the runaways have rotation velocities above 250km/s for luminosity classes (V,IV) indicating that these runaways would seem to have no rotation velocity excess. Again, looking over all luminosity classes and plotting the cumulative distribution frequency of all the B0-B2 stars against the runaway B0-B2 stars illustrates that the distributions are mostly the same. A χ^2 distribution test confirms this result with a probability, $p > 0.75$, that the two distributions are similar. This procedure was continued for the rest the B star range B3-B5 with the same conclusion, i.e. that B star runaways do not appear to be rapid rotators by contrast to B stars in general. Finally, note that the global average for all runaway B stars, irrespective of luminosity class, is $137 \pm 11 km/s(69)$ and the similar global average for all B stars is $135 \pm 2 km/s(2739)$

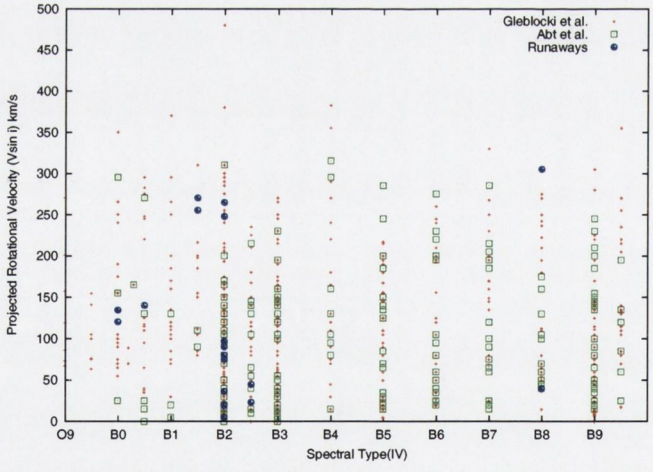
Figures 6-7a,b,c) give an illustration as to how the rotation velocities of runaways compare across spectral type and class to that of stars in general. It should be noted that the databases for rotation velocities all may have unknown runaways, unseen binaries which have experienced mass transfer and the low velocity group of stars disrupted by the supernova in a binary mechanism but which have experienced mass transfer and thus could also have high rotation velocities. However, considering that the B star runaways still appear to be distributed much in the same way as B stars in general, a number of them having elevated rotation velocities, it is difficult to say that they are particularly anomalous.

While the numbers within each spectral range and luminosity class are, in some cases, relatively low they do seem to suggest that there is certainly a distinct difference between the rotation properties of O star runaways and those of early B star runaways, which in turn suggests a change in the ejection mechanism ratio for both spectral types. This is consistent with the fact that the fraction are different for O and B-type runaways. Hoogerwerf et al. (2001) traced the paths of known runaways within 700pc, back in time in order to identify a possible birth association and estimate a probable ejection mechanism. His results give 14 SNB runaways and 6 DE runaways. The rotation rates of 10 SNB and all of the DE runaways are known, yielding that all of these SNB runaways have rotation rates above 200km/s and all these DE runaways have rotation rates below 120km/s. It is not likely that all DE runaways have lower rotation rates and it is reasonable to assume that at least some will have rotation rates above 200km/s. However, using 200km/s as a less strict criterion

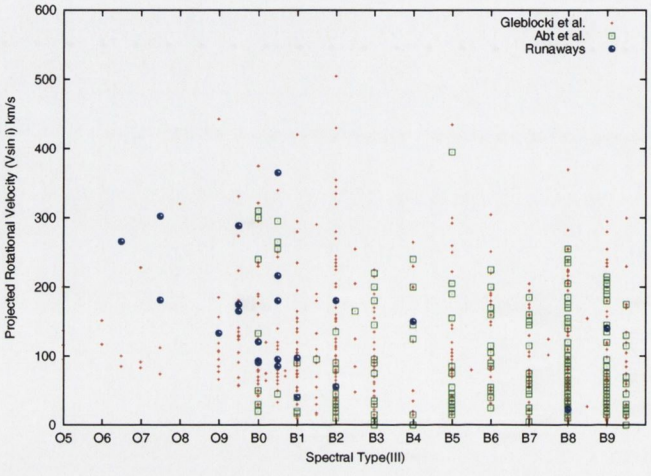
Figure 6-7: *Figures a,b and c (Top to Bottom - Luminosity Classes V,IV,III respectively) show rotation velocities of single stars from the databases of Glebock et al. (2001) (Crosses), Abt et al. (2002) (Squares), and those of runaway stars (filled circles). The figures are for illustrative purposes and show that there is some tendency for the O stars to sit at high rotation velocities while the B star runaways appear to be well distributed throughout the rotation velocity range.*



(a)



(b)



(c)

then the 250km/s previously, 22% of B star runaways and 46% of O star runaways have rotation rates above this value.

The difference between the two percentages of elevated rotation rates for O and B stars indicates a change in the dominant ejection mechanism for each of the populations; perhaps a reflection of the decrease in importance of collisions for DE runaways from O to B-type or that 100% of O star runaways and only ~60% of B star runaways experience mass transfer. The difficulty then is how this difference may be interpreted from the previously established framework. From the population synthesis simulations ~100% of O stars and ~60% of runaway B stars experience mass transfer if ejected via the supernova in a binary mechanism. The observational result suggests that ~40% of the O star runaways at least have a significant elevated rotation velocity above the expected distribution. This does not exclude that they all may have been spun-up at some point but are now indistinguishable from the normal population. If the remaining runaways are due to the dynamical ejection scenario then this is underestimating the population synthesis results which predict the percentage of observed O-type runaways from the supernova in a binary scenario to be around 70% of the total number of runaways. The B stars then remain more difficult to explain since an excess of rotation is not evident. This would indicate that the supernova in a binary mechanism is relatively less likely for these stars which is consistent with the high density simulations where the DE scenario is the dominant mechanism for the production of massive runaways. From the dynamical interaction results it was shown that a large percentage of dynamically ejected O stars experience a collision before they are ejected, 50-100% (so they may be spun-up) and that comparatively the number of B stars which experienced a collision and were ejected with high velocity is smaller ~10%. The high density simulations show that, less than 40% of B-type runaways may be ejected via the supernova in a binary scenario while the remainder is ejected via dynamical encounters.

Table 6.5 is a list of some basic data related to runaways stars from Table A in Appendix A. The relative percentage of stars within each luminosity class is shown along with the binary fraction and percentage of emission line stars. The O stars are referenced via Maiz-Apellaniz et al. (2004) 'Catalog of O stars" and the B star distribution is from the SIMBAD database. The O star binary percentage for cluster/association membership (Mason et al., 1998). The B star binary percentage from the analysis of Kouwenhoven et al. (2007) who suggest that the primordial population be close to 100%. Berger & Gies (2001) found that

about 7% of Be stars have high peculiar space velocities. From these statistics we see that a high fraction of both O and B stars are emission line stars. Specifically looking at spectral types B1-B2 then 36% of runaways are Be and 20% of spectral types B3-B5 runaways are Be. From Balona (2000) then ~15% of B1-B2 stars are expected to be Be and ~6% of B3-B5 stars. More significantly only ~2% of O stars are emission type. If we assume that the increase of Be stars is a direct result of the SNB scenario then this would imply that ~15% of B stars are ejected via this mechanism. While the errors and uncertainties on these estimates are large due to an incomplete database of runaways, the vastly different values offer further evidence that a large portion of runaways are rapidly rotating stars, particularly the O stars but also the B stars to some extent.

Table 6.5: *Statistics of OB known runaways from Table A, based on the well known sample of 133 runaways (i.e. excluding Mdzinarishvili & Chargeishvili (2005)). Luminosity Classes (V;IV;III;II;I) are relative percentages within each class. e, is the percentage of emission line stars. vsin(i) is the percentage of stars within a specific group with an estimated projected rotation velocity.*

Spectral Type	Binary %	V	IV	III	II	I	e	vsin(i)%
O runaways	15	33	0	22	8	37	20	73
B0-B5 runaway	13	56	21	7	7	9	23	75
Galactic O	75	61	4	22	8	27	3	N/A
Galactic B0-B5	>70%	42	13	27	8	11	7	N/A

6.7 Conclusions

From the above analysis we confirm the conclusions of both Blaauw (1993) and Hoogerwerf et al. (2001) that O star runaways are typically rapidly rotating objects. We show that at least 40% of them have rotation rates larger than 250km/s where the mean for rotation rate for O stars is typically ~150km/s. Rapid rotation may be further evidence by the fact that nearly 10 times as many O star runaways are emission stars by comparison to their cluster counterparts. Fast rotation in O stars may be indicative of both mechanisms either through mass transfer (SNB) or ejection of collided stars (DE). We suggest that ~40% of O star runaways are ejected due to the SNB scenario. Conversely we show that B star

runaways do not appear to be excessively rotating objects by comparison to B stars in general. However, there is evidence that at least some runaways are excess rotators due to the fact that B star runaways have 2-3 times more emission type stars then their cluster counterparts. If the excess in emission type stars is indicative of rapid rotation then this results in 15% of B star runaways being as a result of the SNB scenario. From our high density simulations we find that less than 40% of B stars may be ejected from the SNB scenario. Hence, we may estimate that between 15-40% of runaway B stars are ejected via the SNB mechanism.

7

Conclusions

In this thesis we have considered the ejection of high velocity massive stars via the two mechanisms which are thought to produce them: Dynamical gravitational interactions; A supernova occurring in a binary system. We have used sophisticated N-body stellar dynamic codes and advanced population synthesis algorithms in order to study ejections from both scenarios and how they react within different cluster environments. We use the observed frequency of 2-4% of B stars being runaways and 10-20% of O star runaways as constraints to our ejected fractions. We have combined these theoretical results with an observational study of the rotation rates of runaway stars. We have also included an exploratory study using the expected accuracies of the upcoming Gaia mission. Hence, we estimate the probability that companions to OB runaways could be detected astrometrically with such a satellite.

We have used an intermediate sized cluster of 450 stars, with masses between 1-120$M_{\odot}$ distributed with a typical IMF, stars as being representative of young clusters containing OB type stars from which the runaway population is ejected. In reality a wide variety of clusters exist with different populations. In the first instance we concentrated primarily

on dynamical ejections of OB runaways while giving only an estimate of the comparative supernova in a binary ejection rate. We considered a wide range of cluster parameters and estimated the corresponding OB runaway frequency for each of them. We studied low, medium and high density initial conditions and show that only at the medium and high densities do OB runaway ejections become significant. However, only at a cluster with a high initial density does the DE mechanism become a dominant mechanism for ejecting runaways. At this density DE ejections result in a B star runaway frequency of $\sim$4% and a $\sim$5% frequency for runaway O stars. We also find that at this density a significant runaway binary fraction results, with it being $\sim$25% for both and O and B runaways. This suggests that a stellar density similar to the high density cluster occurs, since DE runaway binaries are observed and it is only at this density that they are ejected. Furthermore, we find that a significant fraction of O stars, $\sim$50%, are ejected as collision products, where two lower mass stars have impacted and the merged star is subsequently ejected. Such stars may have high rotation rates due to this merger. By contrast the fraction of runaway B stars which are products of a collision is lower than approximately 20%.

We considered the initial primordial binary population and show that with a higher initial population the ejection of high velocity stars increases in general. However, the runaway binary fraction is similar if the initial binary fraction is above 50%. In addition, the initial separation distribution of binaries has an effect on the ejection rates of both scenarios with the overall result being that the increase in the rate of ejected runaways via the SNB mechanism is higher than that of the DE scenario. Significantly, with a more energetic distribution of binaries, O stars are dynamically ejected with greater frequency, $\sim$10%.

Since primordial mass segregation has been observed in some young clusters we investigate this possibility in our clusters. Primordial mass segregation may be a necessity for the formation of massive stars where elevated accretion and merger rates occur at the centre of pre-stellar clusters. We find that primordial mass segregation increases the dynamical ejection of massive stars by $\sim$30%. However, star formation efficiency in contracting molecular clouds which form clusters may not be very high. With low star formation efficiencies the cluster can rapidly expand and become unbound as the winds from the more massive stars in the cluster begin to blow the excess gas out. This has a dramatic effect on the dynamical ejection of stars, resulting in nearly no massive runaways being dynamically

ejected from such a system. We then consider a smaller cluster composed entirely of OB stars and liken this to a primordially mass segregated system where the central massive stars have remained bound, despite the ejection of gas, and the lower mass stars have left this central core in isolation. Due to the large number of OB stars present in the cluster the frequency of OB ejections is lower than for the system with greater population. However, by a combination of SNB and DE ejections the observed frequency of OB runaways may be attained and a high fraction of ejected runaway binaries is found. Nonetheless, the SNB scenario appears to be dominant in such a cluster. The fact that runaway binaries are ejected in a medium stellar density cluster suggests that the central potential plays a larger role in the ejection of massive single and binary stars with runaway velocities. The central potential in this small, medium stellar density cluster is comparable to that of the high, mass density cluster, from which high velocity massive binaries may be ejected. This smaller cluster represents an idealised simulation and all OB stars are not found in such low N systems. We also find that in a larger N system, N = 4500, the ejection rate via both mechanism is significantly reduced due to the difficulty in escaping from this clusters higher potential.

Due to the SNB scenario playing such an integral part in the ejection of OB runaways we investigated the consequences of such a scenario using a purely population synthesis code. We quantify a number of observational statistics for massive runaways ejected via this mechanism. We illustrate how the ejection percentages change with mean kick velocity and with initial binary separation. From the velocity distributions of ejected massive SNB binaries we suggest that the kick velocity dispersion is bimodal with lower velocity kicks selected from a Maxwellian with velocity dispersion of $\sim$95km/s occurring in Be/XRBs and higher velocity kicks selected from a Maxwellian with velocity dispersion of $\sim$190km/s for OB-supergiant XRBs. We determine that 100% of O star runaways have experienced mass transfer before ejection and that nearly all of them will be seen as Blue Stragglers with respect to their parent clusters for their entire lifetimes. By contrast only $\sim$60% of B-type runaways are expected to experience mass transfer before being ejected and only $\sim$50% of these are likely to be seen as Blue stragglers. We show that $\sim$15% of massive runaways may be Thorne-Zytkow objects which will be observed either as M-type red giant stars or WN8 Wolf Rayets. Further, with statistics for both SNB ejected binaries and DE ejected binaries we compare and contrast the characteristics distinctive to each scenario. This is

important for estimating the probable ejection mechanism for OB runaway binaries when the nature of the companion is unknown but some characteristics of its orbit are.

We also show that since mass transfer rejuvenates runaways, particularly O star runaways, then the frequency of SNB ejected O and B star runaways that is observed may be 12% and 0.5% respectively. This is significant for comparing simulation results with observational frequency and also on calculating the ratio of DE:SNB runaway ejections.

Using an N-body code which has a suite of binary evolution routines included we show that the cluster environment may alter the ejection rates of SNB runaways. This may occur in denser systems where dynamical interactions may harden the pre-runaway massive binary and exchange interactions may pair the stars with more massive companions. We also show that with very high densities, collisions are likely to reduce the SNB rate as the more massive close binaries, which are probable SNB runaway progenitors, are more likely to result in physical stellar collisions. We illustrate how the ratio of OB runaways from either mechanism, DE:SNB, changes with respect to cluster initial density. With the expectation that a medium to high density cluster seems to be required in order to produce massive binaries in high proportions then fractions of between 60-80% of B stars are likely to be produced via dynamical ejections, if the cluster begins with a high density, and 20-35% with a medium initial stellar density. However, these results don't include the probable observational effect discussed for SNB runaways which results in massive ejectees living longer than their typical cluster counterparts. This would result in 45-100% of B star runaways being dynamically ejected depending on the initial density between medium and high. The medium density clusters rarely produce massive O star runaways and the high density cluster produces $\sim$5%. If this is combined with the observed SNB O star runaway rate then we have a rate a DE percentage of O stars runaways, 30% .

We outline an exploratory method for using the known binary population of both SNB and DE mechanisms to infer the corresponding single star population using the statistics from the N-body and Population Synthesis calculations. From these preliminary estimates we suggest that 15-60% of O stars and 30-70% of B stars may be dynamically ejected. While there are a number of effects which are not accounted for in these estimates there is a broad suggestion that the DE scenario plays a smaller role in ejecting the more massive high velocity stars such as O type runaways and a larger role in the ejection of B-type runaways. This is consistent with the simulation findings but by no means conclusive.

Using the echelle spectrograph at Loiano we observe a number of runaway stars in order to determine their rotation velocities. We add these measurements to the database of runaways with known rotation velocities in order to improve the overall statistics. From the analysis of these statistics we seek to show if the O and B runaways show anomalous rotation velocities by comparison to O and B stars in general. We show that a large fraction of O stars have elevated rotation rates which fits well into our framework (i.e. Both the DE and SNB scenarios produce rapidly rotating O star runaways, the DE scenario through the collision and ejection of stars and the SNB scenario through the transfer of mass during RLOF prior to the supernova explosion of the primary). Nonetheless this favours the SNB mechanism for O star runaway ejection, since we have seen from the simulations that all O-type SNB runaways will have had mass transferred to them before ejection. By contrast only a fraction of DE O stars are collision products. We also find that there appears to be no distinct elevation in runaway B star rotation rates. This is also consistent with our results since we favour the DE scenario for the ejection of B stars and few B runaways are expected to be collision products. Nevertheless the observed runaway B stars have over twice as many Be stars as is typical for cluster stars which suggests that a portion of these runaways are spun-up and SNB ejected, which would be of the order of 15%.

From the previous considerations we suggest that the SNB scenario is the primary mechanism for producing O-type runaway stars. We estimate that $\sim$70% of O-type runaways are SNB ejections. By contrast we suggest that the DE scenario is the primary mechanism for the ejection of B-type runaways. We estimate that DE ejections constitute between 50-100% of the runaway population. However, we caution that these estimates suggest that a specific initial cluster environment is indicative of all young clusters which have OB stars present in them. This would suggest that disperse OB associations were once denser more compact systems which rapidly expanded.

8

Future Work

8.1 Cluster Analysis

Table 8.1 shows a number of OB associations and young clusters from Hoogerwerf et al. (2001) with values from de Zeeuw et al. (1999) and Brown et al. (2000) with distances less than 700pc. The stars Hoogerwerf et al. estimate to be ejected via DE are from the ONC and surrounding region. Specifically the stars AE Aurigae, μ Columbae are thought to be ejected from the Trapezia with an kinematic age of $\sim$ 2.5Myrs. The age of the ONC is estimated to be of this order. 80% of the stars being perhaps less than 2Myrs old (Scally 05). Naturally there are reasonably large errors on this estimate, however, it's likely that the dynamically ejected stars were then ejected when the cluster was near Zero Age Main Sequence (ZAMS) and perhaps embedded in gas. This may be the case for the majority of DE runaways and it is shown from the dynamical simulations that the vast majority of DE stars are ejected early on, $< 10 Myrs$. From the cluster ages then the majority have ages greater than 10Myrs and if DE occurs at early times then the stars travelling at velocities greater than 30km/s will travel distances greater than 300pc within 10Myrs. Such a bias is

accepted by Hoogerwerf in his analysis. Hoogerwerf traces orbits for no more than 10Myrs which means that stars with a runaway kinematical age greater times than this will be excluded. The supernova in binary scenario ejected stars by contrast will be much closer to their parent cluster and more easily traced back to their parents (considering that their parents are well evolved anyway i.e. $>$ 10Myrs). The large extent of these clusters also does not mean that they have begun with such sizes since even a small velocity dispersion, a few km/s, could bring them to their current sizes within their current ages (excluding a few cases like Cep OB2). It would be worth exploring further the possibility that very large sizes indicate high initial velocity dispersions and densities which would have likely led to mergers and ejections. This may lead to characteristically higher multiplicities, higher rotation rates and a skewed IMF towards higher masses as suggested by Bally & Zinnecker (2005). Note for example that of the 6 stars identified as probable dynamical ejections by Hoogerwerf: 2 come from the Trapezium in Orion; 2 from the λ Ori SFR; 1 from Orion OB1 b or c; 1 from Perseus OB2. From such a region as Orion a host of DE runaways have resulted. Within such a cluster analysis it would be of interest to try and characterise a likely DE and SNB runaway history based on the possible initial conditions. In this way one could use the suite of simulations presented in this thesis as a basis for determining such rates for a given cluster.

Table 8.1: *Age and diameters of a number of known OB associations*

Name	Age(Myrs)	Diameter (pc)
α Per	50	15
Per OB2	7	45
Vela OB2	15	45
Lac OB1	10	65
Cep OB2	5	105
Cep OB6	50	40
Upper Sco	5	30
Upper Centaurus Lupus	13	65
Lower Centaurus Crux	10	45
Collinder 69	11	89
Collinder 121	11	70
Collinder 135	12	50
Collinder 359	32	240
IC 346	44	7.0
IC 2391	45	60
IC 2602	32	100
IC 4665	43	70
NGC 1976	13	47
NGC 2232	53	45
Stephenson 1	54	20
Roslund 5	68	50
Pismis 4	34	25
Pismis 5	16	2.0
Stock 7	16	5.0

8.2 Radial Velocity Survey

The Hipparcos Input Catalogue has radial velocities for only $\sim 1/3$ of the massive stars in its database leaving a significant fraction as yet unexplored. Using the facilities at Loiano observatory in Italy it would be possible to take observational data of a large number of these bright objects and improve the general statistics for the motions of massive stars in the galaxy. Naturally once Gaia comes online then it will do a vastly superior job but this will not be till 2012 at the earliest. This would improve the simulation of star clusters by seeing how well the velocity dispersions for massive stars in general may be modelled. Note that the ejection of high mass O stars and binaries, even with low velocities is indicative of birthplaces of initially high density. Similarly, low mass, high velocity stars are also probes to the original state of the cluster.

8.3 Individual Analysis

A case by case analysis of the rotation rates of runaway stars, particularly the B star runaways, may yet yield the fraction that are excess rotators and have been thus spun-up. In this way one could take into account mechanisms which have affected the rotation, such as the expansion of star as it ages, slowing its rotation, making it indistinguishable from general cluster stars.

8.4 Further Simulations

From a simulation point of view it would be of use to consider gas expulsion and primordial mass segregation in more detail. It would be instructive to run simulations which have both factors included and to consider various star formation efficiencies and the impact they have on the runaway fraction.

A

OB runaways

Table A.1: Table of known OB runaways. Superscripts indicate where the runaways were identified in the literature. The list is then divided into four parts (Ordered by HIP,HD number): Runaways listed by Hoogerwerf et al. (2001) within 700pc; Runaways listed in other sources; Runaways listed by Moffat et al. (1998)(Wolf Rayets); New candidate runaways listed by Mdzinarishvili & Chargeishvili (2005). Superscripts above the HIP number indicate which main articles the runaways were identified or confirmed. (1)Hoogerwerf et al. (2001);(2) Gies & Bolton (1986);(3) Sayer et al. (1996);(4) Philp et al. (1995); (5) Blaauw (1961);(6) Gies (1987);(7)Moffat et al. (1998);(8) Mdzinarishvili & Chargeishvili (2005);(9) Kumar et al. (1983). In the Moffat list T() implies the transverse velocity as given by Moffat. Three superscript designations on the HD numbers indicate a binary system as indicated in the SIMBAD database. Bin - Binary ; DM - Double Multiple; SB1 - Single Lined Spectroscopic Binary; SB2 - Double Lined Spectroscopic Binary; EB - Eclipsing Binary; EBAt - Eclipsing Binary of Algol type;EBβLt - Eclipsing Binary of β Lyrae Type. $(V_t)_{pec}V_{tr}$ Mdzinarishvili & Chargeishvili (2005) are the estimated peculiar tangential velocities and the total transverse velocities respectively. Additional superscripts to the HD numbers indicate variability information given by SIMBAD, Var - Variable Star; CV - Cepheid Variable; VarBC - Variable of β Cep type; VarO - Variable of Orion type; SRPS - Semi-Regular Pulsating Star; PV - Pulsating Variable; EllipVar - Ellipsoidal Variable; EruptVar - Eruptive Variable. The red font indicates the runaways which were observed by us with the green font indicating the rotation velocity estimate we determined since in some cases there are the rotation velocity estimates by previous authors.

HIP	HD	NAME	$V_{rad}km.s^{-1}$	$V_{space}km.s^{-1}$	$vsin(i)km.s^{-1}$	SpT
$3478^{1,2,3,4,5}$	4142		-60	80.4	215;177,160	B5V
3881^{1}	4727^{SB2}	νAnd	-23.9±1.2	32.1	35;23;11;80;75;110;20	B5V+F8V
9549^{1}	12707		-21.9	107.9		B6V
$10849^{1,2,3,4}$	14220		-45.8	50.0	83	B2V
$14514^{1,2,4,5,8}$	19374^{VarBC}	53 Ari	21.2±1.2[c]	39.4	20,20,10,5,22,10	B1.5V
$18614^{1,2,4,5,6}$	24912	ξPer	58.8±5.0[e]	64.9	213	O7.5IIIe
20330^{1}	26684		6.0	34.7	250	B5
22061^{1}	30112		6.0± 5.0	86.5	125	B2.5V
$24575^{1,2,3,4,5,6,8}$	34078^{VarO}	AEAur	57.5 ± 1.2	113.3	25;40;30;25	O9.5Ve

Continued on Next Page...

Table A.1 – Continued

HIP	HD	NAME	$V_{rad(km.s^{-1})}$	$V_{space}(km.s^{-1})$	$vsin(i)(km.s^{-1})$	SpT
26241[1]	37043^{SB2}	ιOri	28.7 $\pm$1.1^{f}	8.0	121;125;120;116;68;80	O9III+B1III^{h}
27204[1,3,5,6,8]	38666^{Var}	μCol	109.0$\pm$2.5	107.8		O9.5V
28756[1,3,4,5]	41534^{DM}	72Col	93	196.6	115;80	B2.5V
29678[1,2,3,4,8]	43112^{Var}		10.65$\pm$0.49	63.0	10	B1V
30143[1]	44506		54	55.5	275;220;270	B1.5Ve
35951[1]	58343		-4.5	34.9	40;54;40	B2Vne (Be)
36246[1]	59215^{DM}		44	32.1		B6V
38455[1]	64503^{Ellipvar}		-31.0$\pm$5.0	41.4	180;150	B2V
38518[1]	64760		41.0$\pm$5.0	31.1	250;216	B0.5Iab
39429[1]	66811	ζPup	-23.9$\pm$1.2	62.4	230;210;219;203	O4I
40341[1]	69080^{Bin}		-49	61.7	200	B1.5V
42038[1]	73105		37.0$\pm$10.0	31.3		B3V
43158[1]	75222		66	57.2	95;80;96	B0Iab
45563[1,3,4]	78584		-125.2	125.9	95	B3
46928[1]	83979^{Var}	ζCha	10.0	45.3	120	B5V
46950[1]	83058		35.0$\pm$10.0	32.1	270	B1.5IV
48715[1,8]	86606		-30	34.5	55	B9Ib
49934[1]	88661		31.0$\pm$10.0	31.2	360;225;253;220	B2IVnpe
52161[1]	92464^{Var}		32	34.8	160	B4V
57669[1]	102776		29.0$\pm$2.5	31.1	270;210	B3Ve
59607[1]	106231		-43	78.8	150	B4IV
61602[1]		BD+25 2534	1.2	30.2	75	Bp
62322[1,8]	110879^{DM}		42	43.9	185	B2.5V

Continued on Next Page...

Table A.1 – Continued

HIP	HD	NAME	$V_{rad(km.s^{-1})}$	$V_{space}(km.s^{-1})$	$vsin(i)(km.s^{-1})$	SpT
66524[1,8]	118450			112.7		B5II
69491[1]	124195^{EBBLt}		66.0 ±10.0	77.2		B5Ve
70574[1]	126341^{CV}		-215	205.3	20;15	B2IV
76013[1]	137387	κ^1Aps	62.0 ±5.0	69.0	300	B1npe
81377[1,3,4,5,6]	149757*	ζOph	-9.0 ±5.5	23.5	353363	O9.5Vnn
82171[1,8]	150898		-53	62.9	120;95	B0.5Ia
82868[1]	152478		19.0±5.0	30.3		B3Vnpe
86768[1]	161056		26	30.1	230;240	B1.5V
91599[1]	172488		24S 34.1±1.2[a]	44.7	100	B0.5V
92609[1]	173948		9	31.0	217;170	B2II-IIIe
94899[1]	180183^{Bin}		151	162.8		B2V
94934[1]	181409		10	94.0	140;140	B2IVe
95818[1]	183537		-42.7	34.7	300	B5V
97774[1]	188252		-18.3	35.0	55	B2III
97845[1,2,4]	188439^{VarBC}		-65	70.3	400;330	B0.5IIIn
99435[1]	192575		-37.5	39.4	56	B0.5V
99580[1,4]	192281^{Var}	V2011Cyg	-60	55.6	290 ;300	05e
101350[1]	195965		10	36.4	250	B0V
102274[1]	197911		-3.8±5.0	46.1	310	B5
103206[1]	198766		-4	32.3		B5IV
105811[1]	204172		2.8	38.3	85;65;87	B0Ib
106620[1]	205618		-43	45.2	317	B2Vne

Continued on Next Page...

*HD 149757 - Additional rotation velocity estimates 659;372;348;400;320;337;339;385 (Average = 353)

Table A.1 – Continued

HIP	HD	NAME	$V_{rad(km.s^{-1})}$	$V_{space}(km.s^{-1})$	$vsin(i)(km.s^{-1})$	SpT
109556[1,2,4,5,6]	210839	λCep	-75.1±1.2	74.0	275;219;214	O6Iabe(N1)
3346[2]	3950^{SB2}	V486 Cas	-92		40	B2III + B1V
5316[4]		BD +59 186	21	V_p 56	65	B5II
5391[3]	^{EB}	V OX Cas	-102		200::175	B1V
8980[2]	11606^{SRPS}		12.5		318	B2Vne
9498[3]	^{DM}	SAO12092	-20		<40	B3II
10228[3]	13268		-126.8		320;309;302	O8Vnn (N5)
11099[3,6,7]	14633^{Bin}		-36		130;134;116	O8.5V (N6)
[6]	15137^{Bin}		-35			O9.5
12495[2,4]	16429^{VSBCt}		-62		165	O9.5III 5
13016[4]	17114		51		140:	B1V
15261[3,4]	20218		-57		180	B2
22034[2,4]	29866		41		305	B8IVne
22783[2,4,5,6]	30614	αCam	6.1	(Z >300pc)	80;129;115	O9.5Iae N2
[2,3,4]	30650		35		175	B6V
26064[2,3]	36576	120Tau		V_{pec} 34.7	285;210	B2IV-Ve
27683[4]	248434			Vp 83	195	B5Ie
26872[2]	37657		47.8		200;196	B3Ve
26889[2,4]	37737^{SB1}		-25		170;179	B0II
27881[3,4]	39478		-38		267	B2Ve
27941[2,3,4]	39680PV		18.4		170;218;197	O6:pe 5
28881[3]	41161^{Bin}		5		300;304;296	O8V
30180[2]	44172		-17		75	B6V

Continued on Next Page...

Table A.1 – Continued

HIP	HD	NAME	$V_{rad(km.s^{-1})}$	$V_{space}(km.s^{-1})$	$vsin(i)(km.s^{-1})$	SpT
31066[2]	45995				250;305;205	B2V:nne
33836[2,4]	52533^{SB1}		5.5	V_{pec} 47	310 UF	O9V
33437[9]	51477		-47		333:	B5Vn
51624[4]	91316^{Var}		42		60;75 50	B1Iab
52849[3,6]	93521		-16	Z > 500pc	432;355;400;341;385	09Vp
55051[2,3,4,5,8]	97991		24.5	Z 730pc	160;170;135	B1V
[6]	105056^{PV}		1	Z 483pc	85;68;97	ON9.7Iae
69892	124979		-68			O8
70275[4]	125924		252		75	B2IV
81153[2,3,4,5,8]	149363		146		95 75	B0.5III
82286[3,5]	151397		151		110	B0.5V
[6]	152408		-140			WN
82876[3]	152623		-7		190;106;102	O8
[6]	156212		-45.3s-3.4		40	O9.7Iab
85331[2,3,5,6,8]	157857		59		125;97;114;128	O7e (N8)
93118[3]	175876^{Bin}		14		265	O7/O8
[6]	188001		15.5	V_{pec}81.5	110;88;93;112;75	O7.5Iaf
97607[2,3]	187567		-30.1		140;175	B2.5IVe
98396[4]	333282		40			B7III
98530[2,4,6]	189957		43		92;89	B0III 5
[2,4,6]	191567^{SB2}	ADS13429	-29		60:: + 128::	B3 + B0.5IV
101411[2]	195907		-56		190	B1.5Ve
102195[2,3,4]	197419	V568 Cyg	-7.1		110;70	B2IV-Ve

Continued on Next Page...

Table A.1 – Continued

HIP	HD	NAME	$V_{rad(km.s^{-1})}$	$V_{space}(km.s^{-1})$	$vsin(i)(km.s^{-1})$	SpT
102999[2,3,5]	198846^{SB2}	ΓCyg	-56.8		145;121;137	BOIV-var+ B0IV
104316[2,3,4]	201345		20	(Z >300pc)	95;91;87	O9p 5
102449[3]		SAO 50033	-97		45	O9V
104599[2,3,4,5]	201910		-12.2	High V_{prop}	225;218	B5V
105186[2,3,4,5,6]	203064	68Cyg	1.0	High V_{prop}	315;305;295;280	08e 4(N4)
106896[3]	206327		-30		<50	B2V
110362[3]	235807^{SB1}		-118		145	B0.5IV:n
112022[2,3,4,5,8]	214930		-53		5	B2IV
112990[3,4,5]	216534		-77		75	B3V
[6]	218915		-72 -66.9		115;110;74;94	O9.5Iab
114690[2,4]	219188		48		235;197;280	B0.5III
115198[2]	220057^{SB2}		-41		97	B2IV + B3V
[4]	227877^{Bin}		-100		NWC 163::/SEC 150::	B1:IV:nn
111563[4,8]	214080^{Var}		0	V_{pec} 238.4	120;99	B1/B2Ib
115347[4]	220172		12.6		60	B3Vn
115566[4]		SAO 20610	26		140	B9III
[4]	276986			V_p 54		K2
[3]		BSD 8-1117	34			B5V
[7,8]	41997		-18	T(106)	257	O7.5V(n)
[7]	86161	WR16		T(124)		WN8
[7]	90657^{DM}	WR21		T(38)	85	WN4+O46(SB2)
[7]	92554		-38	T(46)	255;298;312	O9.5II
[7]	92740	WR22	33	T(242)		WN7+O6.5-8.5

Continued on Next Page...

Table A.1 – Continued

HIP	HD	NAME	$V_{rad(km.s^{-1})}$	$V_{space}(km.s^{-1})$	$vsin(i)(km.s^{-1})$	SpT
[7]		E305560	-37	T(65)		O9.5III
[7]	96548	WR40		T(95)		WN8
[7,8]	116852		-47		130;136	O9.5III
[7]		E329905	15	T(94)		O9I
[7]	143414*Erupvar*	WR71		T(240)		WN6
[7]		E328209		T(114)		O9.5Ia
[7]	160641	V 2076 Oph	106	T(326)		O9.5Ia
[7]	168941		105	T(212)	140;116;105	O9.5II
[7]		E227018	41	T(80)		O6.5III
[7]	197406			T(194)		WN7+B
				$(V_t)_{pec}$* V_{tr}†		
2702	3175		-16	95.05 62.57		B5III(B4V)
4384	5342		-2	56.60 43.04		B8II
5778	7374^{SpBin}		-15.5	62.38 59.47		B8III
13489	18100		72	131.68 111.01		B5II/III
26272	36879		17.6	81.47 89.12		O7.5III
29201	42259		27	85.91 90.20		B0V
29317	41689		38	95.29 91.02		B1Vn...
30071	44182			57.51 42.39		B8II
31365	259954			76.21 70.19		B2IV
34117	53269			145.43 143.53		B9III

Continued on Next Page...

*Peculiar Velocity

†Tangential Velocity

Table A.1 – Continued

HIP	HD	NAME	$V_{rad(km.s^{-1})}$	$V_{space}(km.s^{-1})$	$vsin(i)(km.s^{-1})$	SpT
35707	57682		23	98.81 96.97		O9V
36243	58683		54.7	69.61 82.63		B8III
36799	60930			150.70 198.75		B9II
38184	63655		-7	56.20 49.85		B8/B9II
41603	71833^{Bin}		7	109.38 92.307		B8II
46592	82011		31	86.16 93.91		B9III
47370	83866			91.20 149.51		B8II
48128	84971		68	73.15 43.17		B2V
54524				123.87 170.64		B6III
57870	103101^{Bin}			142.78 161.30		B4III
69640	124300			49.80 12.32		B2V
73720	133294			87.21 107.05		B8IIB
73778	132791			83.88 126.20		B9II/III
74660	134959		-36	82.22 98.33		B2Ia
75711	137595		-136	228.81 245.44		B2II/III
80338	147648			158.57 171.62		B8II
81362	$149881Cvar$		13	64.25 48.85	85	B0.5III
81696	150135^{Bin}		-39	87.34 84.67	315	O7V
81904	150608			66.67 81.17		B9II/III
82217	151346		24	104.01 116.06		B8II
82625	152160			95.83 113.49		B8/B9II
83509	153772^{Bin}			73.35 59.32		B2V
87164	161653		-21	59.53 54.83	35	B2II

Continued on Next Page...

Table A.1 – Continued

HIP	HD	NAME	$V_{rad(km.s^{-1})}$	$V_{space}(km.s^{-1})$	$vsin(i)(km.s^{-1})$	SpT
87287	162365		0	61.57 54.52		B2IV
89902	167806			80.85 80.42		B2V
90074	$168733Var$		-11.8	120.12 133.71	0	B7Ib/II
100170	192273			61.37 74.16	30;65	B2V
101729	453230			68.22 31.64		B0III
104361	201522		-5	63.74 33.20		B0Ve
106917	205805			935.12 952.91		B7III
110266	212043		-38	133.41 117.92		B6II
111086	213236		-27.6	213.87 225.26	30	B8II
111544	214168^{Bin}		-13.5	60.28 52.33	350;320	B2V
113735	217505			85.50 125.80		B2III/IV
114998	219639			98.93 106.94		B5II/III

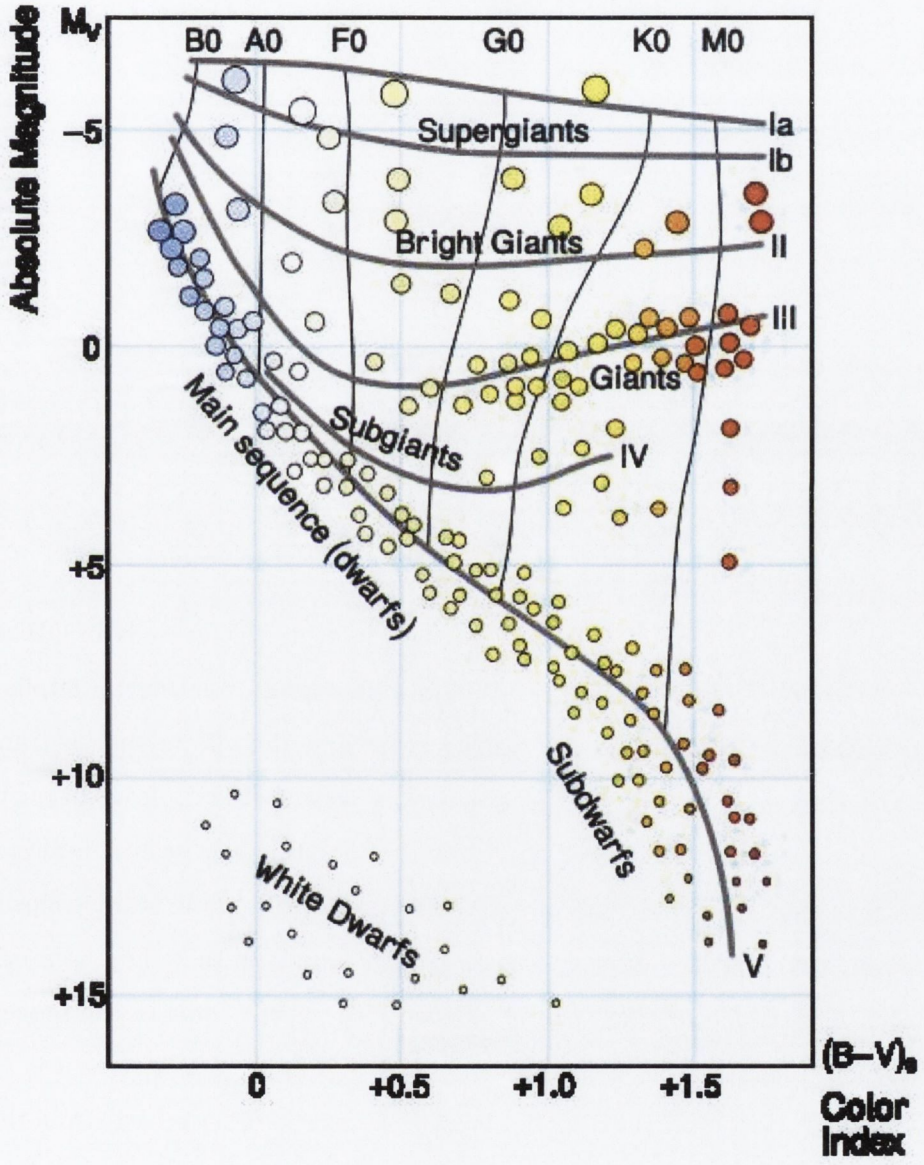
B

The Classification of Stars

We give here a brief overview of the classification system of stars for the non-astronomer. Spectral classification of stars is done via an in-depth look at specific spectral characteristics, in particular the photospheric temperature. Stars with similar characteristics are then grouped together and deemed to be of similar type. Broadly speaking there are six spectral types typically adopted O-B-A-F-G-K-M (the ordering and choice of letters is due to the historical evolution of the classification scheme). This divides stars into an order of temperature and colour in that: The O type stars are hottest ($\sim$ 30,000 K) and blue; The M-type are coolest ($\sim$ 2,000 K) and red. These are further divided by Arabic numerals (0-9) indicating the hottest within a specific type e.g. B0 being the hottest of the B-type and B9 being the coolest. Each of these types are then subdivided by luminosity class, indicated by a roman numeral e.g. I, II, III, IV, V. Luminosity classes suggest specific line features in the star's spectra are evident and are also indicative of specific stages of a star's life. A luminosity class V star indicates that it is a normal main sequence star, burning hydrogen. For example, the sun is a relatively average type main sequence star with a spectral classification G2V. As a star evolves it may change its luminosity class,

becoming a subgiant IV, a Giant III, a Bright Giant II, or a supergiant I, depending on its initial mass. Figure B-1 is known as a Hertzprung-Russell diagram, or specifically a colour-magnitude diagram, which shows the typical distribution of stars within a cluster by their magnitude (also, Luminosity, increasing from bottom to top on the y-axis) and colour index (also, Temperature decreasing from left to right on the x-axis) for the various classification points of stars. High mass stars occupy the top half of the diagram while the lower mass stars occupy the bottom half. Notice that the OB stars occupy the top left of the diagram indicating that they are blue, massive, luminous and hot. OB stars are relatively rare by comparison to stars of lower mass, however, due to their brightness they are much easier to detect. Finally note that O and B-type stars are often called early type stars, again due to historical reasons.

Figure B-1: *Hertzprung-Russell diagram showing the various classifications of stars and relating their colour index to their magnitude*



C

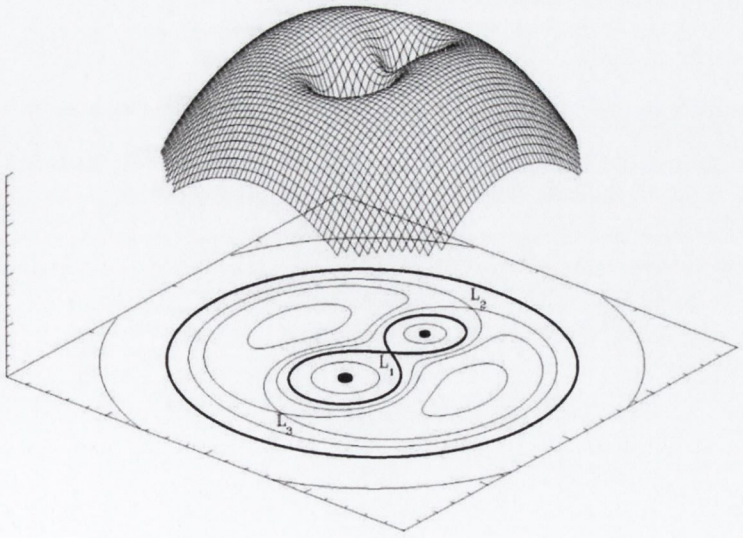
Binary Stellar Evolution - Roche Lobe Overflow

Binary stellar evolution is an important topic relating to the study of OB runaways. However, it is also leads to a wide range of complex issues relating to details specific to the transfer of matter from one star to the other and the effects such a transfer has. This results in many different types of systems in various stages of evolution being observed. Examples of such systems are X-ray Binaries (XRBs), double white dwarfs, double neutron stars/pulsars, cataclysmic variables, Algol systems, symbiotic stars, eclipsing binaries etc. However, what each of these systems have in common is that they were originally two ordinary main-sequence stars. In the following we outline some of the processes and effects concerning binary stellar evolution.

The stellar evolution of stars in binary systems can differ greatly from that of single star evolution. The equipotential surface within which matter is bound to a single star becomes deformed when the star is in a close binary system and this limits the size to which that star may expand to. Figure C-1 shows the equipotential surface being shaped like a figure of eight around stars in a binary system, these are called Roche Lobes. This means that if the one of the stars fills its Roche Lobe, matter may stream from it to its companion. This

process is called Roche Lobe Overflow (RLOF). The accreted material may then increase the size of the companion, rejuvenate it and increase its rotation velocity (as the angular momentum from the stream of accreted material is deposited on the stellar surface). At what evolutionary stage RLOF begins depends on the mass, mass ratio and separation of the stars in the binary system. Most commonly the companion star is still on the main sequence as the primary (the originally most massive star) moves off the main sequence, expands, and fills its Roche Lobe. In many calculations it is assumed that the total mass and angular momentum of the binary system is conserved. However, this may not be the case and in many cases non-conservative mass transfer occurs which can depend on the configuration of the system. For example, binaries in which the two stars have comparable mass and are closely bound are likely to undergo conservative mass transfer. By contrast, for binaries which have components with very different masses, most of the transferred mass is not captured by the small companion, but accumulates as a common envelope surrounding both stars. This envelope may then be cast away by the binary leaving a system which has lost most of its mass.

Figure C-1: *A three-dimensional representation of the Roche potential in a binary star with a mass ratio of 2, in the co-rotating frame. The droplet-shaped figures in the equipotential plot at the bottom of the figure are called the Roche lobes of each star. L1, L2 and L3 are the Lagrangian points where the forces cancel. Mass can then flow through the saddle point L1 from one star to its companion, if the star fills its Roche lobe.*



RLOF plays a major role in process the formation of objects such as X-ray Binaries, Blue stragglers and Thorne-Zytkow objects which are discussed in this thesis.

- **X-ray Binaries**

  If the primary star (the initially most massive star) erupts in a supernova and the system remains bound then a system with an ordinary main-sequence star with a compact object such as a Black Hole or Neutron Star typically remains. If the companion, main sequence star, evolves and fills its Roche Lobe, matter may stream to the compact object. The infalling matter releases gravitational energy in the form of X-rays. These systems are called X-ray Binaries.

- **Blue Stragglers**

  A Blue Straggler is a star in cluster which appears bluer then the rest of the cluster members. This is an indication that the star is more massive and younger then it should be. In a given cluster the age of the cluster may be referenced by the turn-off mass of the cluster. The turn-off mass is the mass of the most massive star which is still on the main sequence in a given cluster. If a star appears much more massive then the turn-off mass of the cluster then it is a blue straggler. One of the mechanisms by which it may become a blue straggler is to have mass transferred to it while it is in a close binary, this may make it more massive, rejuvenate it and thus make it appear bluer then the rest of the cluster members (see Section 4.3.2).

- **Thorne-Zytkow Objects**

  A Thorne-Zytkow Object is a star which has a Neutron Star in its core. After the supernova explosion of the primary and if the system has remained bound the remnant Neutron Star may spiral into the core of the ordinary companion star (see Section 4.3.3).

D

N-body Codes

In the following chapter we give an overview of the relevant details and use of the codes used in this thesis. Aarseth (2003) offers a comprehensive look at the details, development and use of N-body codes and is used as a reference for many details in the following chapter.

There are a number of methods for integrating the equations of motions in order to run simulations on a computer. The best methods are those which allow for a high degree of accuracy and are efficient such that the number of calculations the computer needs to do is reduced. We will discuss here some of the a few techniques used in the Nbody6 code for simulating realistic N-body systems: A fourth order predictor-corrector Hermite scheme; Ahmad-Cohen nearest neighbour method; Regularisation; Stellar Evolution.

D.1 Equations of Motion

For many applications the original Newton's Law of Gravity is sufficient. The equations of motion for N particles with index i are

$$\ddot{r} = -G \sum_{j=1, j\neq i}^{N} \frac{m_j(r_i - r_j)}{|r_i - r_j|^3} \tag{D.1}$$

where the left-hand side is defined as the force per unit mass, F_i. Given the initial mass (m_i), coordinates (r_i) and velocities (v_i) of each particle at some initial time, a set of 3N second-order differential equations may define the solutions $r_i(t)$. As an alternative (and what is adopted in practice) the complete solutions may be described by 6N first order differential equations which must be solved self-consistently. The energy (E) and angular momentum (J) of the system are

$$E = \frac{1}{2}\sum_{i=1}^{N} m_i v_i^2 - \sum_{i=1}^{N}\sum_{j>i}^{N} \frac{G m_i m_j}{|r_i - r_j|} \tag{D.2}$$

$$J = \sum_{i=1}^{N} r_i \times m_i v_i \tag{D.3}$$

The two terms in Equation D.2 are the kinetic and potential energy respectively.

In order create an N-body simulation the coordinates and velocities must then advance incrementally, where the accelerations are evaluated by the summation of Equation D.1 at each time-step. The solutions at time t may be related to the previous solution at time t_0 by a Taylor series expansion to lowest order as

$$v_i t = F_i \Delta t + v_i(t_0) \tag{D.4}$$

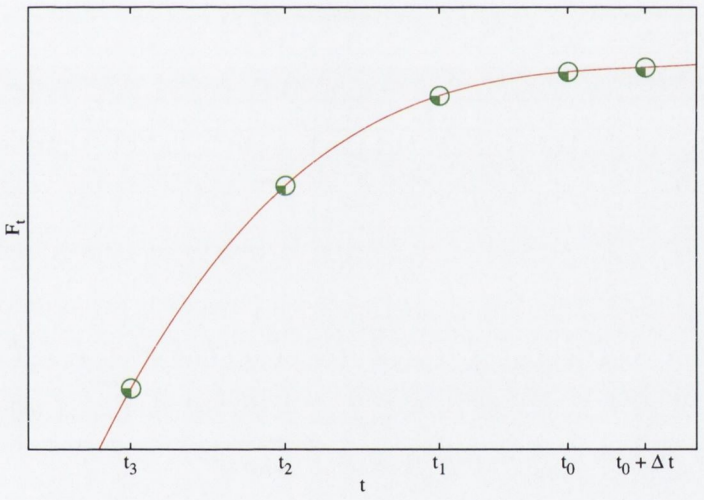
$$r_i t = \frac{1}{2} F_i \Delta t^2 + v_i(t_0)\Delta t + r_i(t_0) \tag{D.5}$$

where $\Delta t = t - t_0$. For a complete solution all the particles must be advanced simultaneously. This Euler method of step-by-step evaluation is computationally inefficient and requires a small time step to maintain reasonable accuracy. It is possible to improve accuracy significantly at little extra cost by making better use of existing information. The improved Euler method is such an example. First provisional coordinates are predicted in the usual way $\tilde{r}_i(t) = \frac{1}{2}F_i\Delta t^2 + v_i(t_0)\Delta t + r_i(t_0)$. An average force is then defined $\tilde{F}_i = \frac{1}{2}[F_i(t) + F_i(0)]$ and this is used to calculate the final values of $v_i(t)$ and $r_i(t)$ in Equations D.4 and D.5.

D.2 Force Polynomials and the Hermite Scheme

A predictor-corrector scheme is used in Nbody6 which refers to how the force acting on a particle is calculated over a given number of time steps. The idea is that the force acting on a particle/star typically varies in a smooth manner throughout an orbit. Hence one may fit a polynomial which relates the force over time through a number of past time steps (see Figure D-1). This allows one to extend the time interval for advancing the equations of motion and thereby reduce the number of force evaluations (making the scheme more efficient). In this way one can **predict** the future motion with greater confidence. For simplicity the details of how this is done is left out of this discussion. It is sufficient to realise that the predicted force evaluation has to be corrected at some stage before the next integration cycle and time-step, hence the name of the predictor corrector method.

Figure D-1: *Force polynomial fitting*



Experience has shown that there is some gain in increasing the order of the integration scheme but the law of diminishing returns applies and for practical purposes a fourth order scheme is sufficient for most purposes.

As shown in Figure D-1 the force on a particle/star can be approximated by a continuous function. If the previous values of the force **F** are known at four previous timesteps 't_3, t_2, t_1, t_0' (where t_0 is the most recent) one may then write a forth-order polynomial at time time t as

$$F_t = [(\mathbf{D}^4(t - t_3) + \mathbf{D}^3)(t - t_2) + \mathbf{D}^2](t - t_1) + \mathbf{D}^1(t - t_0) + F_0 \qquad \text{(D.6)}$$

using Sverre Aarseth's compact notation where

$$\mathbf{D}^k[t_0, t_k] = \frac{\mathbf{D}^{k-1}[t_0, t_{k-1}] - \mathbf{D}^{k-1}[t_1, t_k]}{t_0 - t_k}, \quad (k =, 1, 2, 3) \tag{D.7}$$

$\mathbf{D}^0 \equiv \mathbf{F}$ and square brackets refer to the appropriate time intervals, e.g. $\mathbf{D}^2[t_1, t_3]$ is evaluated at t_1. The term $\mathbf{D}^4$ is defined similarly by $\mathbf{D}^3[t, t_2]$ and $\mathbf{D}^3[t_0, t_3]$.

Converting the force polynomial into a Taylor series gives expressions for integrating the coordinates and velocities. Equating terms in the successive time derivatives of Equation D.6 with an equivalent Taylor series and setting $t = t_0$ yields the force derivatives.

$$\mathbf{F}^{(1)} = [(\mathbf{D}^4 t_3^{'} + \mathbf{D}^3) t_2^{'} + \mathbf{D}^2] t_1^{'} + \mathbf{D}^1 \tag{D.8}$$

$$\mathbf{F}^{(2)} = 2![\mathbf{D}^4(t_1^{'} t_2^{'} + t_2^{'} t_3^{'} + t_1^{'} t_3^{'}) + \mathbf{D}^3(t_1^{'} + t_2^{'}) + \mathbf{D}^2] \tag{D.9}$$

$$\mathbf{F}^{(3)} = 3![\mathbf{D}^4(t_1^{'} + t_2^{'} + t_3^{'}) + \mathbf{D}^3] \tag{D.10}$$

$$\mathbf{F}^{(4)} = 4!\mathbf{D}^4 \tag{D.11}$$

where $t_k^{'} = t_0 - t_k$. These equations are used to obtain the Taylor series derivatives at t = t_0, when the fourth difference is not yet known. thus the contribution from $\mathbf{D^4}$ to each order is only added at the end of an integration step, $t_0 + \Delta t$. This semi-iteration gives increased accuracy at little extra cost and no extra memory requirement.

In order for the simulation to progress each particle is given its own time-step which is related to the orbital timescale. Hence the integration cycle proceeds by determining the next particle i to be advanced (i.e. the particle j with the lowest value of $t_j + \Delta t_j$ where t_j is the time of the last time of the force evaluation.

The integration cycle may be summarised by the following algorithm as given by (Aarseth, 2003) page 22.

1. Determine the next particle: $i = min_j t_j + \Delta t_j$
2. Set the new global time by $t = t_i + \Delta t_i$
3. Predict all coordinates r_j to order $\mathbf{F}^{(1)}$
4. Form $\mathbf{F}^{(2)}$ by Equation D.9
5. Improve r_i and predict v_i to order $\mathbf{F}^{(3)}$
6. Obtain the new force $\mathbf{F}_i$

7. Update the times t_k and differences D^k

8. Apply the corrector D^4 to r_i and v_i

9. Specify the new timestep Δt_i

10. Return to step 1

The Hermite scheme is then an improvement on the standard predictor-corrector method. In order for an increased accuracy of integration based on the explicit values for $\mathbf{F}$ and $\mathbf{F^1}$ it is desirable to include a high-order corrector in the manner of the polynomial formulation. This is what the Hermite scheme aims to do. A Taylor series for the force and its first derivative to third order about the reference time t is

$$\mathbf{F} = \mathbf{F}_0 + \mathbf{F}_0^1 t + \frac{1}{2}\mathbf{F}_0^2 t^2 + \frac{1}{6}\mathbf{F}_0^3 t^3 \tag{D.12}$$

$$\mathbf{F^{(1)}} = \mathbf{F}_0^{(1)} + \mathbf{F}_0^2 t + \frac{1}{2}\mathbf{F}_0^3 t^2 \tag{D.13}$$

$$\mathbf{F}_0^{(2)} = 2[-3(\mathbf{F}_0 - \mathbf{F}) - (2\mathbf{F}_0^{(1)} + \mathbf{F}^{(1)})/t]t^2 \tag{D.14}$$

$$\mathbf{F}_0^{(3)} = 6[2(\mathbf{F}_0 - \mathbf{F}) + (\mathbf{F}_0^{(1)} + \mathbf{F}^{(1)})/t]t^3 \tag{D.15}$$

Using $\mathbf{F}$ and $\mathbf{F}^{(1)}$ evaluated at the beginning of a timestep, the coordinates and velocities are predicted to order $\mathbf{F}^{(1)}$ all particles by

$$r_i = [(\frac{1}{6}\mathbf{F}_0^{(1)}\delta t_i^{'} + \frac{1}{2}\mathbf{F}_0)\delta t_i^{'} + v_o]\delta t_i^{'} + r_0 \tag{D.16}$$

$$v_i = (\frac{1}{2}\mathbf{F}_0^{(1)}\delta t_i^{'} + \mathbf{F}_0)\delta t_i^{'} + v_0 \tag{D.17}$$

where $t_i^{'} = t - t_i$. A composite corrector is then evaluated by

$$\Delta r_i = \frac{1}{24}\mathbf{F}_0^{(2)}\Delta t_i^4 + \frac{1}{120}\mathbf{F}_0^{(3)}\Delta t_i^5 \tag{D.18}$$

$$\Delta v_i = \frac{1}{6}\mathbf{F}_0^{(2)}\Delta t_i^3 + \frac{1}{24}\mathbf{F}_0^{(3)}\Delta t_i^4 \tag{D.19}$$

for subsequent predictions an improved value of the second force derivative at the end of the current timestep is obtained as

$$\mathbf{F}_0 = \mathbf{F}_0^{(2)} + \mathbf{F}_0^{(3)}\Delta t_i \tag{D.20}$$

The name Hermite comes from its use in numerical analysis to denote a polynomial based on the function and its derivative. The Hermite scheme also employs block time-steps which allows for groups of particles to be advanced at the same time rather than

earlier schemes which employed individual time-steps for each of the stars. The further advantages of the Hermite scheme are:

- It is self-starting
- The corrector is significantly faster
- Hierarchical time-steps reduce predictions
- Special-purpose computers can obtain the explicit value for $\mathbf{F}$ and $\mathbf{F}^{(1)}$

D.3 Nearest Neighbours, Ahmad-Cohen (AC) Scheme

Most clusters have a large number of members which makes direct N-body simulations time consuming. The cpu cost of a direct N-body calculation scales $\propto N^3$. However, this large number of N can be used to our advantage in order to reduce the number of force evaluations. The idea of the AC scheme is to separate the force evaluation between distant particles and close particles. The force from distant particles changes over a longer timescale hence the total force on a given particle may be split into an **irregular**,F_I and **regular**,F_R component. The irregular force is evaluated over the short timestep and the regular force calculated over a longer timescale since it changes less rapidly.

$$F = F_I + F_R \tag{D.21}$$

This means that the summation for the irregular force at a given time-step is based on the sum of **n** nearest particles, together with a prediction of the more distance particle regular force contribution. Hence, a nearest neighbour sphere is created for each particle and the irregular force evaluation made only for these neighbours. Naturally particles which may move into the nearest neighbour sphere within a particular time-step are also accounted for. The size of the neighbour sphere is then modified at the end of each regular time-step. This scheme reduces the integration time significantly even for clusters with a small population.

D.4 Regularisation

Close encounters in N-body systems are inevitable and these close passages create systems that lead to difficulties or at the very least are so time-consuming that the entire simulation may slow to a crawl. Many short period binaries in a cluster simulation significantly increase

the simulation time due to the fact that thousands of orbits may occur while the overall cluster evolution advances little. Consider for example the difference in timescales for a short period binary of hundreds of days to years and the dynamical evolution of cluster of the order of millions of years. Not only can short period binaries slow the calculation but they are also configurations where systematic errors may be introduced. This indeed is still the limitation for now running simulations of 10^5 stars with a large binary fraction.

Regularisation itself is a mathematical transformation for treating the close approach of two point-mass particles in such a manner that the equations of motion are well behaved even as the inter-particle distance tends towards zero. This transformation is done not only for the particle coordinates but also for the time. The further advantages of regularisation are: A smaller number of integration steps per orbit is required; Distant contributors can be neglected since $F \propto 1/r^3$; Two-body elements can be used to study tidal interactions; Numerical stability is improved even for circular motion. Hence close encounters between two or more bodies can be handled effectively and efficiently allowing for systems which change on a short time-scale to be advanced quickly such that the entire cluster evolution can proceed.

D.5 Stellar Evolution

Stellar evolution plays an important role in the dynamical evolution of N-body systems due to the fact that as stars evolve they lose mass. Mass loss itself can change the dynamics of the system. Further, stellar evolution defines the timescale relevant to a particular N-body system, independent of its dynamically defined timescales such as cluster crossing time and half-mass relaxation time. It is currently unfeasible to combine hydrodynamic simulations for the evolution of specific stars along with a direct N-body simulation. The procedure that is adopted is to relate a star's current stage of evolution in a simulation to a set of previously determined functions based on factors such as its age, composition, mass etc. These functions were determined by fitting them to a suite of synthetic hydrodynamic stellar evolution simulations of stars with a large range of parameters. This allows for a fast method for determining the current stage and likely evolution of all the stars within a simulation. These fitting functions provide information on the stellar radius, luminosity, core mass, evolution type, rotation velocity as a function of time. Hence as the simulation progresses each star's stage of evolution is determined via a reference to these functions

making it an effective and efficient method for including stellar evolution in an N-body code.

D.6 Input Parameters

```
Input parameters
***************
-------------------------------------------------
NBODY6:
***************
KSTART  Control index (1: new run; >1: restart; 3, 4, 5: new params).
TCOMP   Maximum computing time in minutes (saved in CPU).

INPUT:
********
N       Total particle number (singles + binary c.m.; < NMAX - 2).
NFIX    Output frequency of data save or binaries (options 3 & 6).
NCRIT   Final particle number (alternative termination criterion).
NRAND   Random number sequence skip.
NNBMAX  Maximum number of neighbours (< LMAX - 2).
NRUN    Run identification index.

INPUT2:
********
ETAI    Time-step parameter for irregular force polynomial.
ETAR    Time-step parameter for regular force polynomial.
RS0     Initial radius of neighbour sphere.
DTADJ   Time interval for parameter adjustment (N-body units).
DELTAT  Output time interval (N-body units).
TCRIT   Termination time (N-body units).
QE      Energy tolerance (restart if DE/E > 5*QE & KZ(2) > 1).
RBAR    Virial cluster radius in pc (set = 1 for isolated cluster).
ZMBAR   Mean mass in solar units (1.0 assumed if 0).
********
KZ(J)   Non-zero options for alternative paths (see table).
********
DTMIN   Time-step criterion for regularization search.
RMIN    Distance criterion for regularization search.
ETAU    Regularized time-step parameter (6.28/ETAU steps/orbit).
ECLOSE  Binding energy per unit mass for hard binary (positive).
GMIN    Relative two-body perturbation for unperturbed motion.
GMAX    Secondary termination parameter for soft KS binaries.

INPUT: if (kz(4).gt.0)
********
DELTAS  Output interval for binary search (in TCR; #4, suppressed).
ORBITS  Minimum periods for binary output (level 1).
GPRINT  Perturbation thresholds for binary output (9 levels).

DATA:
********
ALPHAS  Power-law index for initial mass function (used if #20 < 2).
BODY1   Maximum particle mass before scaling (KZ(20): solar mass).
BODYN   Minimum particle mass before scaling.
NBIN0   Number of primordial binaries (for IMF2 with KZ(20) > 1).
ZMET    Metal abundance (in range 0.03 - 0.0001).
EPOCH0  Evolutionary epoch (in 10**6 yrs).

SCALE:
********
Q       Virial ratio (routine SCALE; Q = 0.5 for equilibrium).
VXROT   XY-velocity scaling factor (> 0 for solid-body rotation).
VZROT   Z-velocity scaling factor (not used if VXROT = 0).
RTIDE   Unscaled tidal radius (#14 >= 2; otherwise copied to RSPH2).
XTRNL0: if (kz(14).eq.2)
********
GMG     Point-mass galaxy (solar masses, linearized circular orbit).
RG0     Central distance (in kpc).
  if (kz(14).eq.3)
GMG     Point-mass galaxy (solar masses).
DISK    Mass of Miyamoto disk (solar masses).
A       Softening length in Miyamoto potential (in kpc).
B       Vertical softening length (kpc).
VCIRC   Galactic circular velocity (km/sec) at RCIRC (=0: no halo).
RCIRC   Central distance for VCIRC with logarithmic potential (kpc).
RG      Initial position; GMG+DISK=0, VG(3)=0: A(1+E)=RG(1), E=RG(2).
VG      Initial cluster velocity vector (km/sec).

  if (kz(14).eq.3.or.kz(14).eq.4)
MP      Total mass of Plummer sphere (in scaled units).
AP      Plummer scale factor (square saved in AP2).
MPDOT   Decay time for gas expulsion (MP = MP0/(1 + MPDOT*T).

HOTSYS: if (kz(29).gt.0)

SIGMA0  Hot initial velocities in km/sec (routine HOTSYS; option 29).

BINPOP: if (kz(8).eq.1.or.kz(8).gt.2)
********
NBIN    Number of primordial binaries (routine BINPOP; option 8).
SEMI    Semi-major axis in model units (all equal if RANGE = 0).
ECC     Initial eccentricity (< 0 for thermal distribution).
RATIO   Mass ratio M1/(M1 + M2); (= 1.0: M1 = M2 = <M>; not #20 > 1).
RANGE   Range in SEMI for uniform logarithmic distribution (> 0).
NSKIP   Binary frequency of mass spectrum (#20 < 2; body #1 first).
IDORM   Indicator for dormant binaries (>0: merged components).
ICIRC   Eigenevolution & period distribution (RANGE: minimum period).

HIPOP: if (kz(8).gt.0.and.kz(11).gt.1)
********
NHI     Number of primordial hierarchies (routine HIPOP; #11 > 1).
SEMI    Semi-major axis in model units (all equal if RANGE = 0).
ECC     Initial eccentricity (< 0 for thermal distribution).
RATIO   Mass ratio (= 1.0: M1 = M2; random in [0.5-0.9]).
RANGE   Range in SEMI for uniform logarithmic distribution (> 0).
ICIRC   Circularisation & collision check (not implemented yet).
```

```
INTIDE:
********
RSTAR   Size of typical star in A.U. (routine INTIDE; option 27).
IMS     # idealised main-sequence stars.
IEV     # idealised evolved stars.
RMS     Scale factor for main-sequence radii (>0: fudge factor).
REV     Scale factor for evolved radii (initial size RSTAR).

CLOUD0: if (kz(13).gt.0)
********
NCL     Number of interstellar clouds (routine CLOUD0; option 13).
RB2     Radius of cloud boundary in pc (square is saved).
VCL     Mean cloud velocity in km/sec.
SIGMA   Velocity dispersion (#13 > 1: Gaussian).
CLM     Individual cloud masses in solar masses (maximum MCL).
RCL2    Half-mass radii of clouds in pc (square is saved).
```

Table of Options KZ(J)
****

1	COMMON save on unit 1 at end of run (=2: every 100*NMAX steps).	21	Extra output line (MODEL #, TCOMP, DMIN, AMIN, RMAX & RSMIN).
2	COMMON save on unit 2 at output (=1); restart if DE/E > 5*QE (=2)	22	Initial m,r,v on #10 (=1: output; >=2: input; >2: no scaling).
3	Basic data on unit 3 at output time (unformatted, frequency NFIX) =1/2: standard and/or tail; =3: tail only; >3: cluster + tail.	23	Escaper removal (>1: diagnostics in file ESC; =2: angles unit #6; >=3: initialization of tidal tails).
4	Binary diagnostics on unit 4 (# threshold levels = KZ(4) < 10).	24	Initial conditions for subsystem (routine SCALE; KZ(24) = #).
5	Initial conditions (#22 =0; =0: uniform & isotropic; =1: Plummer)	25	Partial reflection of KS binary orbit (GAMMA < GMIN; suppressed).
6	Output of significant & regularized binaries (=1, 2, 3 & 4).	26	Slow-down of two-body motion (>=1: KS binary; =2: chain binary).
7	Lagrangian radii (>0: RSCALE; =2, 3, 4: output on unit 6 & 7).	27	Tidal circularisation & collisions (R_coll = 0.75*(R_1 + R_2)).
8	Primordial binaries (=1 & >=3; >0: BINOUT; >2: BINDAT; >3: HIDAT)	28	Magnetic braking and gravitational radiation (options 19 & 27).
9	Individual bodies printed at output time (MIN(5**KZ9,NTOT)).	29	Boundary reflection for hot system (suppressed).
10	Diagnostic KS output (>0: begin; >1: end; >=3: each step).	30	Chain regularization (>=2: main output; >2: diagnostic output).
11	Hierarchical systems (=1: diagnostics; =2: primordial; =3: both).	31	Centre of mass correction after energy check.
12	HR diagnostics of evolving stars (interval DTPLOT).	32	Increase of output intervals (based on single particle energy).
13	Interstellar clouds (=1: constant velocity; >1: Gaussian).	33	Block-step diagnostics at main output (>=1: STEP; =2: STEPR).
14	External force (=1: standard tidal field; =2: point-mass galaxy; =3: point-mass + disk + halo + Plummer; =4: Plummer sphere).	34	Roche-lobe overflow (not implemented yet).
15	Triple, quad, chain (#30 > 0) or merger search (>1: full output).	35	Time offset (global time from TTOT = TIME + TOFF).
16	Updating of regularization parameters (RMIN, DTMIN & ECLOSE).	36	Step reduction for hierarchical systems.
17	Modification of ETAI, ETAR (>=1) and ETAU (>1) by tolerance QE.	37	Fast time-step criterion (>0: STEP; >1: STEPR).
18	Neighbour additions in CHECKL (>0: high-velocity; >1: all types).	38	Force polynomial corrections (=0: I > N only).
19	Mass loss (=1: old supernova scheme; =3: Eggleton, Tout & Hurley)	39	No unique density centre (skips velocity modification of RS(I)).
20	Initial mass function (=1: Scalo; =2,4,6: Kroupa; =3,5: Eggleton).	40	Increase of neighbour numbers if <NNB> < NNBMAX/2.

E

Errata - Chapter 5

Two errors have been noted in the use of Gaia's astrometric accuracy. Since Chapter 5 is published more or less as is in this thesis we show here the effect these errors have on our results.

- The first error is a systematic error in the calculations which resulted in a lower astrometric accuracy for Gaia used for calculations of probability of detection of neutron star companions. The expected Gaia accuracy was quoted as 4μas, however the accuracy used in the calculations was $\sim$20mas.

- The second correction is due to the fact that the final mission accuracy of 4μas is not the angular positional accuracy that should have been used since this 4μas is expected accuracy averaged over the number of transits. For the determination of a positionally changing object (due to its orbital motion), the single measurement accuracy should be used which is on a factor $\sqrt{N_{transits}}$ worse then the average mission accuracy of 4μas. Furthermore, Casertano et al. (2008) note that a more recent estimate of the error budget may result in a 35-40% degradation in the single mea-

surement precision which would correspond to a final accuracy of 5-5.5μas. Hence for an expected $N_{transits}$ = 83 on average (de Bruijne, 2005), we conservatively adopt a single measurement accuracy of 50μas.

Using this new accuracy we re-evaluate the probability of detection for Neutron Star companions to OB runaways. Figures E-1 and E-2 correspond to Figures 5-1 and 5-4 in Chapter 5.

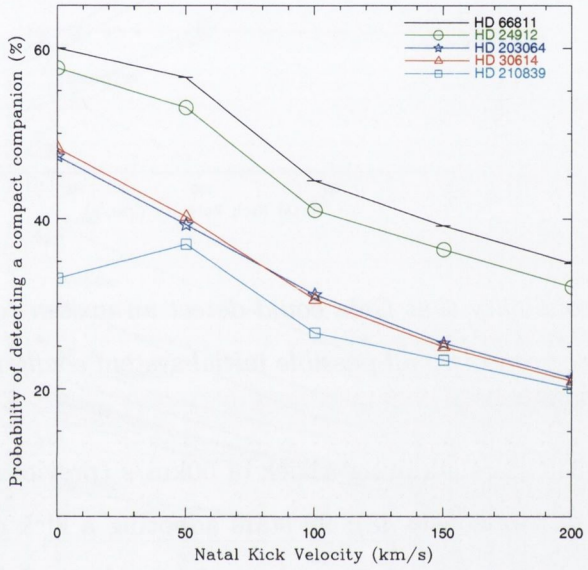


Figure E-1: *Percentage probability of Gaia detecting a neutron star companion for each of our sample stars, considering all theoretically possible system configurations that survive the supernova of the primary*

Since the corrected accuracy, 50μas, is actually higher then the one used in the previous calculations, 20mas, it is expected that the probability of detection increases. As noted in the discussion in section 5.6 there is a large spread in probabilities as shown in Figure E-1. These now range from ~20 to 60% (from 2-27% previously). Figure E-2 shows the likelihood of detecting a compact companion by factoring the number of binary systems likely to survive the supernova eruption of one of its components. Similarly, this now shows a significant increase in the likelihood of detecting a compact companion. In section 5.6.2 we make an estimate of the number of OB runaways that may be detected based on the space density of OB runaways in the local neighbourhood. With this new accuracy limit and from the *estimated* ~1890 OB runaways within 5kpc of the sun Gaia may then detect compact

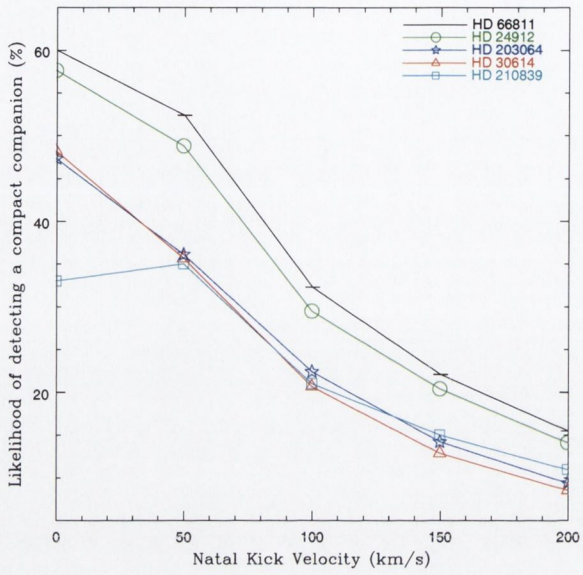


Figure E-2: *Probability that Gaia could detect an unseen companion to our illustrative sample stars, with respect to all possible initial system configurations*

companions to: 540 stars adopting a kick of 50km/s (previously 106); 266 stars adopting a kick of 100km/s (previously 48); 90 stars adopting a kick of 200km/s (previously 16). Hence the Gaia mission may detect a substantial number, ~5-30% of compact companions to OB runaways ejected as a result of the supernova in a binary mechanism.

The probability estimates for the HMXRBs in section 5.6.3 change in a similar fashion due to the different adopted accuracy level. We show a new figure here Figure E-3 which may be compared with Figure 5-5. With this accuracy we now expect from the known periods of the listed HMXRBs (Table 5.3) four astrometric detections of compact companions to the 13 HMXRBs listed (previously two detections were estimated). This implies that compact companions to ~30% (by comparison to the previous estimate of 15%) of HMXRBs may detected by Gaia through astrometric techniques.

Overall the difference due to the erroneous use of the accuracy capabilities of Gaia result in an approximate factor 2 to 3 improvement in our probability estimates. Our general conclusion that Gaia will do well in detecting compact companions to OB runaways therefore remains valid.

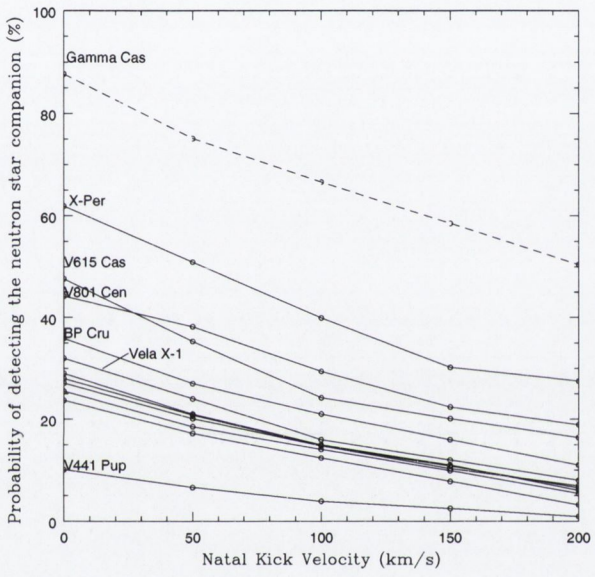


Figure E-3: *Percentage probability of Gaia detecting a neutron star companion to each of the HMXRB sample stars, considering all theoretically possible system configurations that survive the supernova of the primary. Five systems with a small probability of detection and without a label are V884 Sco, QV Nor, LS 55039, V725 Tau, V662 Cas in decreasing order of probability of detection, as shown in the figure taken from the left. Cen X-3 remains with a near zero probability of detection due to it's large distance. The result for γ Cas is dashed since the neutron star nature of its companion is not totally established (see text).*

F

Poisson Error

The Poisson function is given as

$$f(k, \lambda) = \frac{e^{-\lambda}\lambda^{k}}{k!} \tag{F.1}$$

where k is the number of occurrences of an event, λ is a positive real number, equal to the expected number of occurrences that happen during a given interval. λ is not only the mean number of occurrences (k), but also its variance. A Poisson or binomial error may then be applied to the results of our N-body and Population Synthesis calculations where each simulation is a trial and each ejected star is then an occurrences. The binomial distribution converges towards the Poisson as the number of trials tends to infinity provided that np remains fixed, where n is the number of trials and p the probability of an event. Then λ = np is a useful approximation for B(n,p), i.e. the binomial function. Two useful rules of thumb for a Poisson error to be a good approximation: if n $\geq$ 20 and p $\leq$0.05; n $\geq$ 100 and np $\leq$ 10. This typically leads to a 1 sigma error of between 3-10% for the runaway statistics that we compute. Since we determine a sigma error then the Standard Error may be estimated $SE = \frac{\sigma}{\sqrt{n}}$

Bibliography

Aarseth S.J., Lecar M., 1975, Annual Review A&A, 13, 1

Aarseth S.J., 2003, *Gravitational N-body Simulations*, Cambridge University Press

Aarseth S.J., Zare K., Celes. Mech., 10, 185

Abt H.A., Morrell N.I., 1995, ApJS, 99, 135

Abt H.A., Levato H., Grosso M., 2002, ApJ, 573, 359

Adams F.C., 2000, ApJ, 542, 964

Ahmad A., Cohen L., 1973, ' A numerical integration scheme for the N-body gravitational problem', J. Comput. Phys. 12, 389

Allen C., Poveda A., Hernandez-Alcantara A., 2006, MxAC, 25, 13

Ambartsumian V.A. 1947, Stellar Evolution and Astrophysics, Armenian Acad. Sci. [German translation:Abhandl. Sowjetischen Astron. 1951, 1, 33]

Amuél P.R., Guseinov O.Kh., Rakhamimov, Sh.Yu. 1975, SSVAL, Sov. Astron. Lett.,Vol. 1, No. 3, 99-100

Apparao K.M.V., 2002, A&A, 382, 554

Arzoumanian Z., Chernoff, D.F., Cordes J.M. 2002, ApJ, 568, 289-301

Aslanov A.A., Kornilova L.N., Cherepashchuk A.M. 1984, SvAL, 10, 278

Bacon D, Sigurdsson S., Davies M.B., MNRAS, 281, ,830

Balona L.A., 2000, ASPC, 214, 1B

Bally J., Zinnecker H., 2005, AJ, 129, 2281

Barai P., Gies D. R., Choi E., Das V., Deo R., Huang W., Marshall K., McSwain M. V., Ogden C., Osterman M. A., Riddle R. L., Seymour J. L., Jr., Wingert D. W., Kaye A. B., Peters G. J., ApJ, 608, 989

Bastian N., Goodwin S.P., MNRAS, 369, L9

Baumgardt H., Kroupa P., 2007, astro-ph, arXiv:0707.1944v1

Behrend R., Maeder A., 2001, A&A, 373, 190

Belczyński K., Bulik T., 1999, A&A, 346, 91

Berger D.H., Gies D.R., 2001, ApJ, 555, 364

Bethe H.A., Brown G.E., 1998, ApJ, 506, 780

Binney J., Tremaine S., 1987, Galactic Dynamics, ISBN 0-691-08445-9, Princeton University Press

Blaauw A., Morgan W.W. 1954, ApJ, 119, 625

Blaauw A. 1961, Bulletin of the Astronomical Institutes of the Netherlands, Vol 15, No. 505, pp 265-291

Blaauw A., 1991, The Physics of Star Formation and Early Stellar Evolution, NATO Advanced Science Institutes (ASI) Series C, Vol. 342, held in Agia Pelagia, Crete, Greece, May 27th - June 8th, Dordrecht: Kluwer, edited by Charles J. Lada and Nikolaos D. Kylafis., p.125

Blaauw A. 1993, Massive Stars: Their Lives in the Interstellar Medium, ASP Conference Series; Vol. 35; J.P. Cassinelli and E.B. Churchwell; Eds., p.207

Blaauw A., Ramachandran R., 1998, JApA, 19, 19

Boily C.M., Kroupa P., 2003a, MNRAS, 338, 673

Boily C.M., Kroupa P., 2003b, MNRAS, 338, 665

Bok B.J., 1934, Harvard College Observatory, Circular, 384, 1

Bonnell I.A., Bate, M.R., Zinnecker H., 1998,MNRAS, 298, 93

Bonnell I.A., Bate, M.R., 2002 ,MNRAS, 336, 659

Bonnell I. A., Clarke C. J., Bate M. R., Pringle J. E., 2001, MNRAS, 324, 573

Boyajian T.S, Beaulieu T.D., Gies D.R., Grundstrom E., Huang W.,McSwain M.V.,Riddle R.L., Wingert D.M., De Becker M., 2005, ApJ, 621, 978

Brandt N., Podsiadlowski P., 1995, MNRAS, 274, 461

Brown A. G. A., Verschueren W., 1997, 319, 811

Brown A. G. A., Dekker G., de Zeeuw P. T. 1997, MNRAS, 285, 479

Brown A. G. A., de Bruijne J.H.J., Hoogerwerf R., de Zeeuw P.T., Blaauw A., 2000, ESASP, 445, 293

Carpenter John M., Sanders D. B., 1998, AJ, 116, 1856

Casertano S., Lattanzi M.G., Sozzetti A., Spagna A., Jancart S., Morbidelli R., Pannunzio R., Pourbaix D., Queloz D., 2008, Astro-ph, arXiv:0802.0515v1

Casertano S., Hut P., 1985, ApJ, 298, 80

Chevalier C., Ilovaisky S.A., 1998 A&A, 330, 201

Chiosi C., Maeder A., 1986, Annual Review A&A, 24, 329

Clarke C.K., Pringle J.E., MNRAS, 225, 423

Clarke C.K., Bonnell I.A., Hillenbrand L.A., 2000, in Mannings V., Boss A.P., Russel S., eds, Protostars and Planets IV. Univ. Arizona Press, Tucson, p 151

Cordes J.M., Chernoff D.F. 1998, ApJ , 505, 315

Demerican O. Ozdemir S. Allakhverdiev A.O., Guseinov O.H., 1995, The Observatory, 115. 202

de Bruijne J.H.J., 2005, ESAASP, 576, 35

De Cuyper J.P., De Greve J.P., De Loore C.,van den Heuvel E.P.J., 1976 A&A, 52, 315

De Donder E., Vanbeveren D., Van Beer J., 1997, A&A, 318, 812

Duchêne G., 1999, A&A , 341, 547

Duquennoy A., Mayor M., 1991, A&A, 248, 485

Dray L.M., Dale J.E., Beer M.E., Napiwotzki R., King A.R., 2005, MNRAS, 364, 59

Eggleton P.P., 1983, ApJ, 268, 368

Eggleton P.P., Fitchett M.J., Tout C.A., 1989, ApJ, 347, 998

Fischer P., Pryor C., Murray, S., Mateo, M., Richtler T., 1998, AJ,115,592

Fellhauer M., Kroupa P., 2005, ApJ, 630, 879

Foellmi C., Moffat A.F.J., 2002, ASPC, 263, 123

Fliegner J, Langer N., Venn K.A., 1996, A&A, 308L, 13

Fryer C., Burrows A., Benz W., 1998, ApJ, 496, 333

de la Fuente Marcos R., 1996, A&A, 308, 141

Fukushige T., Heggie D.C., 2000, MNRAS, 318, 753

Fullerton L.W., Hills J.G., 1982, AJ, 87, 175

Garmany,C.D., Conti,P.S., Massey P., 1980, ApJ, 242, 1063

Geyer M.P., Burkert A., 2001, MNRAS, 323, 988

Giersz M., Heggie D. C., 1994, MNRAS, 267, 257

Giersz M., Heggie D. C., 1996, MNRAS, 279, 1037

Giannone G., Molteni D., 1985, A&A, 143, 321

Gies D.R., Bolton C.T., 1986, ApJ Supplemental, 61, 419

Gies D.R., 1987, Bulletin of the American Astronomical Society, Vol. 19, p.715

Gies D. R., Hartkopf W. I., Mason B. D., Bagnuolo W. G., Jr., Ten Brummelaar T., McAlister H. A., 1998, ASPC, 131, 382

Glebocki R., Gnacinski P., Stawikowski A., 2001, yCat, 3226, 0

Goodman J., Heggie D.C., Hut P., 1993, ApJ, 415, 715

Goodwin S.P., Kroupa P., 2005, A&A, 439, 565

Goodwin S.P., 1997, MNRAS, 284, 785

Gualandris A., Portegies Zwart S., Eggleton P.P., 2004, MNRAS, 350, 615

Haberl F., 1995, A&A, 296, 685

Hansen B.M.S., Phinney E.S. 1997, MNRAS, 291, 569

Harmanec P., Habuda P., Štefl S., Hadrava P., Korčáková D., Koubský P., Kritička J., Kubát J., Škoda P., Šlechta M., Wolf M., 2000, A&A, 364, 85

Hartmann J.W., 1997 A&A, 322, 127

Harrison P.A., Lyne A.G. 1993, MNRAS, 265, 778

Hayli A. 1971, Astrophysics & Space Science, 13, 309

Heger A., Langer N., Woosley S.E., 2000, ApJ, 528, 368

Heggie D.C., 1972, PhD Thesis (referenced from Mikkola 1983)

Heggie D.C., 1974, Celes. Mech., 10, 217

Heggie D.C., 1991, "Chaos in the N-body problem of stellar dynamics. [A. E. Roy, editor. Predictability, Stability, and Chaos in N-body Dynamical Systems.] pg 47=62

Heggie D.C., 1976, IAUS, 174, 131

Heggie D.C., Hut P., 2003, The Gravitational Million-Body Problem - A multidisciplinary approach to star cluster dynamics., Cambridge University Press.

van den Heuvel E.P.J. 1976, IAUS , 73, 35, Late Stages of Close Binary Systems, ed. P. Eggleton (Dordrecht:Reidel)

van den Heuvel E.P.J., van Paradijs J. 1997, ApJ , 483, 399

van den Heuvel E.P.J., 1985, in Birth and Evolution of Massive Stars and Stellar Groups, ed. W. Boland & H. van Woerden (Dordrecht:Reidel), 107

van den Heuvel E.P.J., Zwart P.S.F, Bhattacharya D., Kaper L. 2000 Astronomy and Astrophysics, 364, 563

van den Heuvel E.P.J., 2007, arXiv:0704.1215v2, astro-ph

Hills J.G., AJ, 80, 809

Hills J.G., ApJ, 235, 986

Hills J.G., Fullerton L.W., 1980, AJ, 85, 128

Hillenbrand L.A., 1997, AJ, 113, 1733

Hillenbrand L.A., Hartmann L.W., 1998, The ApJ, 492, 540

Hoffer J.B., 1983, 88, 14200

Hobbs G., Lorimer D. R., Lyne A. G., Kramer, M., 2005, MNRAS, 360, 974

Hoogerwerf R., de Bruijne J.H.J., de Zeeuw P.T., 2000, ApJ, 544, 133

Hoogerwerf R., de Bruijne J.H.J., de Zeeuw P.T., 2001, A&A, 365, 49

Howarth I.D., Siebert K.W., Hussain G.A.J., Prinja R.K., 1997, MNRAS, 284, 265

Huang W., Gies D.R., 2006, ApJ, 648, 591

van der Hucht K.A., 2001, New Astronomy, 45, 135

Hurley J.R., Pols O.R., Tout C.A., 2000, MNRAS, 315, 543

Hurley J.R., Tout C.A., Pols O.R., 2002, MNRAS, 329, 897

Hurley J.R., Shara M.M., 2003, ApJ, 589, 179

Hut P., Bahcall J.N., 1983, ApJ, 258, 319

Hut P., Inagaki S., 1985, ApJ, 298, 502

Jonker P.G., Nelemans G., 2004, MNRAS, 354, 355

Kaspi V.M., Bailes M., Manchester R.N., Stappers, B.W.,Bell, J.F 1996, Nature, 381, 584-586

King I.R., 1966, AJ, 71, 64

Kiseleva L.G., Colin J., Dauphole B., Eggleton P., 1998, MNRAS, 301, 759

Klessen R.S., 2001, ApJ, 550, 77

Kontizas M., Hatzidimitriou D., Bellas-Velidis I., Gouliermis D., Kontizas E., Cannon R. D., 1998, A&A, 336, 503

Kouwenhoven M.B.N., Brown A.G.A., Portegies Zwart S.F., Kaper L., A&A, 474, 77

Kroupa P., 1995, MNRAS, 277, 1491

Kroupa P., 1995, MNRAS, 277, 1507

Kroupa P., 1995, MNRAS, 277, 1522

Kroupa P., Aarseth S., Hurley J., 2001, MNRAS, 321, 699

Kroupa P., Tout C., Gilmore G., 1993, MNRAS, 262, 545

Kroupa P., Petr M.G., McCaughrean M.J., 1999, New Astronomy, 4, 495

Kroupa P., Burkert A., 2001, ApJ, 555, 945

Kubo S., Murakami T., Ishida M., 1998, PASJ, 500, 417

Kumar C.K., Wellman T.R., Thomas R.J. 1983, The ApJ, 272, 219

Kustaanheimo P., Stiefel E., 1965, 'Perturbation theory of Kepler motion based on spinor regularization', J. Reine Angew. Math. 218, 204

Kaper L., van Loon J.Th., Augusteijn T., Goudfrooij P., Patat F., Waters L.B.F.M., Zijlstra A.A., 1997, The Astrophyisical Journal Letters, 475, 37

Lada C.J., Margulis M., Dearborn D., 1984, ApJ, 285, 141

Lada C.J, Lada E.A. 1991, James K., ed., ASP Conference Series Volume 13, The Formation and Evolution of Star Clusters. Astronomical Society of the Pacific, San Franscico, pg.3

Lada C.J., Lada E.A., 2003, Annual Review A&A , 41, ,57

Lai D., Bildsten L., Kaspi V. M. 1995 ApJ, 452, 819

Lai D., 2003, ASP Conference Series, Radio Pulsars, 302, 307

Langer N., Yoon S.-C., Petrovic J., Heger A., IAUS 215, *Stellar Rotation*

Leonard P.J.T., Dewey R.J., 1993, in ASP Conference Series 45, Luminous High-Latitude Stars, ed. D.D. Sasselov(San Francisco:ASP 239)

Leonard P.J.T., Duncan M.J. 1988, The AJ, 96, 222

Leonard P.J.T., Duncan M.J. 1990, The AJ, 99, 608

Leonard P.J.T. 1995, MNRAS, 277, 1080

Liu Q.Z., van Paradijs J., van den Heuvel E.P.J., 2000, A&AS, 147, 25

Liu Q.Z., van Paradijs J., van den Heuvel E.P.J., 2001, A&A, 368, 1021

Lorimer D.R., Bailes M., Harrison, P.A. 1997, MNRAS, 289,592-604

Lucy L. B., Ricco E., 1979, AJ, 84, 401

Lyne A.G., Lorimer D.R., 1994, Nature, 369, 127

Mackey A.D., Wilkinson M.I., Davies M.B., Gilmore G.F., 2007, submitted

Madau P., Blaes O., 1994, ApJ, 423, 748

Makino J., Aarseth S.J., 'On a Hermite integrator with Ahmad-Cohen scheme for gravitational many-body problems', 1992, Publ. Astron. Soc. Japan 44, 141

Maiz-Apellaniz J., Walborn N.R., Galue H.A., Wei L.H., 2004, ApJS, 151, 103

Mason B.D., Gies D.R., Hartkopf W.I., Bagnuolo W.G., Jr., ten Brummelaar T., McAlister, H.A., AJ, 115, 821

Massey P., Lang C.C., DeGioia-Eastwood K., Garmany C.D., 1995, ApJ, 438, 188

Massey P., 1997, A User's Guide to CCD Reductions with IRAF

Mathieu R.D., 1994, ,ARA&A, 32, 465

McCaughrean M.J., Stauffer J.R., 1994, The AJ, 104, 1382

McSwain M.V., Gies D.R., Huang W., Wiita P.J., Wingert D.W., 2004, ApJ, 600, 927

McSwain M.V., Boyajian T.S., Grundstrom E.D., Gies D.R., 2007, ApJ, 655, 473

Mdzinarishvili T.G., Chargeishvili K.B., 2005, A&A, 431, L1

Meynet G., Maeder A. 2000, A&A, 361,101

Melioli C., de Gouveia Dal Pino E.M., 2006, A&A, 445, L23

Meurs E.J.A., Fennell G., Norci L., 2001, An X-ray examination of runaway stars, in "The influence of binaries on stellar population studies", D. Vanbeveren (Ed.), Kluwer, pg. 165

Meurs E.J.A., Fennell G., Norci L., 2005, The ApJ, 624, 307

Mikkola S. 1983, MNRAS, 203, 1107

Mikkola S., 1984, MNRAS, 208, 75

Mikkola S., 1985, MNRAS, 215, 171

Mikkola S., Aarseth S.J., 1990, Celes. Mech. Dyn. Ast., 47, 375

Mikkola S., Aarseth S.J., 1993, Celes. Mech. Dyn. Ast., 57, 439

Mikkola S., Aarseth S.J., 1996, Celes. Mech. Dyn. Ast., 64, 197

Mikkola S., Aarseth S.J., 1998, New Astron., 3, 309

Miyamoto M., Nagai R., 1975, Publications of the Astronomical Society of Japan, 27, 533

Moeckel N., Bally J., ApJ, 661, 183

Moffat A.F.J., 1989, ApJ, 347, 373

Moffat A.F.J., Marchenko S.V., Seggewiss W., van der Hucht K.A., Schrijver H., Stenholm B., Lundstrom I., Steia Gunawan D.Y.A., Sutantyo W., van den Heuvel E.P.J., De Cuyper J.-P., Gomez A.E., 1998, A&A, 331, 949

Monaghan J.J.,1976,MNRAS,177,583

Murakami T., Koyama K., Inque H., 1986, ApJ, 310, 31

Nelemans G., Tauris T.M., van den Heuvel E.P.J., 1999,A&A ,352, 87

van Oijen J.G.J., 1989, A&A, 217, 115

Packet W., 1981, A&A, 102, 17

Paczynski B., 1990, ApJ, 348, 485

Pfahl E., Rappaport S. 2002, The ApJ, 574, 364

Pflamm-Altenburg J., Kroupa P., 2006, MNRAS, 373, 295

Philp C.J., Evans C.R.,Leonard P.J.T., Frail D.A. 1995, American Astronomical Society, 187, 3303

Plummer H.C., 1911, MNRAS, 71,460

Podsiadlowski, Ph., Langer N., Poelardens A.J.T., Rapport S., Heger A., Pfahl E., 2004, ApJ, 612, 1044

Pols O.R., Marinus M., 1994, A&A, 288, 475

Portegies Zwart S.F., 2000, Astrophyiscal Journal, 544, 437

Poveda A., Ruiz J., Allen C. 1967, Boletín de los observatorios de tonantzintla y tacubaya, vol 4, No. 28, pp. 86-90

Pourbaix D., Tokovinin A.A., Batten A.H., Fekel F.C., Hartkopf W.I., Levato H., Morell N.I., Torres G., Udry S., 2005, 9th Catalogue of Spectroscopic Binary Orbits, yCat, 5122,0

Quist C.F., 2001, A&A, 370, 672

Ross D.J., Mennim A., Heggie D.C., MNRAS, 284, 811

Sayer R.W., Nice D.J., Kaspi V.M., 1996, ApJ, 461, 357

Scally A., Clarke C., McCaughrean M.J., 2005, MNRAS, 358, 742

Schaller G., Schaerer D., Meynet G.,Maeder A., 1992, A&A Suppl. Ser., 96, 269

Schmidt-Kaler Th., 1982, Numerical Data and Functional Relationships in Science and Technology, Landolt-Bornstein, Vol.2, Stars and Star Clusters, pp 15,18,453-455

Sigurdsson S., Phinney E.S., 1993, ApJ, 415, 613

Shklovskii I.S. 1970, Soviet Astronomy, 13, 562

Ŝimon V., 1999, A&AS, 134, 1

Slettebak A., 1954, ApJ, 119, 146

Slettebak A., Howard, R.F., 1955, ApJ, 121, 102

Slettebak A., 1954, ApJ, 124, 173

Slettebak A., Collins G.W. II, Parkinson T.D., Boyce P.B., White N.M., 1975, ,ApJS, 29, 137

Spitzer L. 1958, ApJ, 127, 17

Spitzer L., 1969, AJ Lett., 158, L139

Sterzik M.F., Durisen R.H., A&A. 304, L9

Sterzik M.F., Durisen R.H., Pickett B.K., 2001, ASPC, Vol. 244, Young Stars Near Earth: Progress and Prospects. ed. Jayawardhana R., Green T.P.

Stetson P.B., 1983, BAAS, 15, 684

Stone R.C., 1982, AJ, 87, 90

Stone R.C., 1991, AJ, 102, 333

Taam R.E.,1996, IAUS, 165, 3

Tassoul J.L., Tassoul M., 1992, ApJ, 395, 259

Tauris T.M., Takens R.J., 1998, A&A, 330, 1047

Terman J.L., Taam R.E., Hernquist L., 1995, The ApJ, 445, 367

Terlevich E., MNRAS, 1987, 224, 193

Thorne K.S., Zytkow A.N., ApJ, 199, 19

Tout C.A., Aarseth S.J., Pols O.R., Eggleton P.P., 1997, MNRAS, 291, 732

Valtonen M.J., 1974, I.A.U.S., 62, 211

Van Oijen J.G.J., 1989, A&A, 217, 115

Van Rensbergen W., Vanbeveren, D., de Loore, C., 1996, A&A, 305, 825

Vine S.G., Bonnell I.A., 2003, MNRAS, 342, 314

Vrancken M., De Greve J.P., Yungelson L., Tutukov A., 1991, A&A, 249, 411

Willmarth D., Barnes J., 1994,A User's Guide to Reducing Echelle Spectroscopy

de Wit W.J., Testi L., Palla F., Zinnecker H., 2004, ASPC, 322, 447

de Wit W.J., Testi L., Palla F., Zinnecker H., 2005, A&A, 437, 247

de Zeeuw P.T., Hoogerwerf R., de Bruijne J.H.J, Brown A.G.A., Blaauw A., 1999, AJ, 117, 354

Zinnecker H., McCaughrean M. J., Rayner J. T., Wilking B. A., Moneti A., 1993, RvMA, 6, 191